Application of Flow Cytometry and Fluorescence Spectroscopy to Monitor and Predict the Fermentation Activity in a Vaccine Manufacturing Process

by

Vanessa Zavatti

A thesis
presented to the University of Waterloo
in fulfillment of the
thesis requirement for the degree of
Doctor of Philosophy
in
Chemical Engineering

Waterloo, Ontario, Canada, 2018

Examining Committee Membership

The following served on the Examining Committee for this thesis. The decision of the Examining Committee is by majority vote.

External Examiner	M. Denis Groleau Professor and Canada Research Chair, Université de Sherbrooke
Supervisor	Hector Budman Professor, University of Waterloo
Supervisor	Raymond L. Legge Professor, University of Waterloo
Internal Member	William A. Anderson, Professor, University of Waterloo
Internal Member	Ali Elkamel Professor, University of Waterloo
Internal-external Member	Maud Gorbet Associate Professor, University of Waterloo

AUTHOR'S DECLARATION

This thesis consists of material all of which I authored or co-authored: see Statement of Contributions included in the thesis. This is a true copy of the thesis, including any required final revisions, as accepted by my examiners.

I understand that my thesis may be made electronically available to the public.

Statement of Contributions

Chapters 5 and 6 are journal submissions. Hector Budman, Raymond Legge and Melih Tamer contributed to the conceptualization of the work, analysis of the results and editing of the manuscripts.

Abstract

Bordetella pertussis is a Gram-negative coccobacillus, pathogenic and aerobic bacterium responsible for causing whooping cough, which is an upper respiratory tract infection in humans. To prevent this disease whole cellular and acellular vaccines have been developed. Acellular vaccines are generally preferred since they are less reactogenic. For these vaccines, different antigenic compositions are currently available in the market where some of them are based on one antigen (pertussis toxin or PT), two antigens (PT and filamentous hemagglutinin (FHA)) or five antigens. The latter is referred to as five component pertussis (5CP) composed of PT, FHA, pertactin (PRN) and two fimbriae units (FIM2 and FIM3).

This research was motivated by preliminary results found in the analysis of the upstream fermentation and downstream purification of PRN in the manufacturing process of whooping cough vaccine at Sanofi Pasteur (Toronto, Canada). By combining fluorescence measurements and multivariate statistical analysis it was found that the levels of NADPH present in the supernatant were negatively correlated to productivity of PRN, and that downstream purification protocols can be dismissed as a cause for low productivity. The importance of these results is that accumulation of NADPH is known to be related to oxidative stress. These initial results led to the hypothesis that low productivity may be related to the occurrence of oxidative stress during fermentation. For this reason, this research focused on the effect of oxidative stress on growth of *B. pertussis* and PRN productivity.

The research plan involved a parallel investigation that included analyses of samples collected from the large scale train of fermenters at Sanofi Pasteur, and samples from lab scale fermentations performed to mimic the observed behavior in large scale fermentations.

Because the fermenters are tightly controlled in terms of dissolved oxygen (DO), pH and temperature, it was hypothesized that the observed variability in PRN may be related to the heterogeneity of the cell population in the fermenters. To investigate this hypothesis flow cytometry was used to quantify the heterogeneity in the cell population and its effect on growth and productivity. The data acquired was processed using multivariate statistical methods, such as Principal Component Analysis (PCA), and Partial Least Squares (PLS) to compress data and eliminate noise.

Bench-scale experiments were conducted in flasks, 2 L and 20 L bioreactors. Oxidative stress was induced either by the addition of H_2O_2 or by the use of small size inoculum. These experiments served to confirm the correlation between high NADPH in the supernatant and high reactive oxygen species (ROS), the effect of oxidative stress on PRN, growth, and a mechanism of adaptation to stress. A mathematical model considering elements of the *B. pertussis* metabolic network was built to explain this observed adaptation.

The comparisons of the flask and bioreactor cultures indicated that closed-loop DO control appears to exacerbate oxidative stress compared to open-loop (e.g. in shake flasks fermentations). In the bioreactors, DO is controlled by a closed-loop mechanism through manipulation of agitation or aeration rates. When H_2O_2 was added to the culture, it was converted to oxygen by the action of catalase and thus the agitation decreased to maintain the oxygen at set point, likely resulting in a decrease in mass transfer, and reduction of metabolism and growth.

Following these arguments, samples from the entire train of production fermenters of increasing volume (20 L, 200 L, and 2000 L) were analyzed by means of flow cytometry. The PCA model showed clear correlations with the distributions of ROS and scattering from samples at different time points from each fermentation to the corresponding PRN yield at the end of the purification. As a result of this

study, it was concluded that oxidative stress is correlated with productivity similar to the observations made for the lab scale experiments. A possible source of oxidative stress might be variability in media and growth factor composition, or length of time for media sterilization. This conclusion was reached after investigating the effect of media sterilization cell growth after external imposition of stress. Furthermore, growth in fermenters with low productivity showed a slower biomass evolution compared to fermenters with high productivity, even though the final optical density was the same for all cultures. These differences in growth are similar to the ones observed for small scale experiments where adaptation to stress was clearly observed.

By means of PLS, it was possible to build regression models for predicting the final concentration of PRN from distributions of cells at different time points for the 2000 L fermentation. The PLS regression model between the weighted average of the ROS cytometry distribution and the final productivity had a smaller correlation as compared to the model that used the entire distribution. These results appear to demonstrate that measurements of population distributions are a better indicator of fermentation state rather than average measurements as per the original hypothesis.

Due to the central role that NADPH plays in this system, the nature and origin of NADPH in the supernatant was further investigated. It is believed that NADPH observed in the supernatant is bound to catalase. Bench scale experiments showed that fluorescence excitation/emission spectra of catalase has similar fingerprints to those observed for fluorescence spectra acquired from the supernatant of production samples.

The proposed flow cytometric method was found to be a suitable indicator of the state of the fermentation and as a method to predict productivity. Future work will be required to identify the exact source of variability in the production of PRN.

Acknowledgements

I would like to express my deep gratitude to my supervisors Prof. Hector Budman and Prof. Raymond Legge for their huge patience, encouragement and useful critiques of this research work. I would also like to extend my thanks to Melih Tamer for his continuous support, encouragement and advice.

Financial support provided by Mitacs Accelerate, and Sanofi Pasteur is greatly appreciated.

I appreciate the help offered by George Georgiou, Javier Menendez, Carlos Aragon, Liwei He, Al Simpson, Alex Petrovic, Vadim Vitosky, George Samuel, Olga Simakova, Yevheniya Chabanyuk, Leo Sauvaget, Ricardo Matínez, Steve George, Andrew Chiappetta, Fabien Lux, and Fabien Barbirato.

I am also thankful to my friends and colleagues specially Ali Nikdel, and Hengameh Mohseni for their kind help and support.

I am truly indebted and thankful to Rogelio Hernandez for accompanying me during this long journey and encouraging me to write this thesis. Thanks to Chilli for being my writing partner.

Finally, I would like to express my gratitude to my family, my parents Gabriele and Bruna, my siblings Elvis and Gabriela, and brother-in-law Vladimiro Mujica for their support and encouragement throughout my study.

Dedication

To my parents.

Table of Contents

List of Figures

List of Tables

Nomenclature

5cP- five component pertussis vaccine

7-AAD- 7-aminoactinomycin D

Å- Angstrom

Al- aluminum

Ac-Hly –adenylate cyclase-hemolysin

AT- autotransporter

A.U. – arbitrary units

carboxy- DCFHDA – carboxy-2’,7’-Dichlorohydrofluorescin diacetate

carboxy- H_2DCFDA – carboxy-2’,7’-Dichlorodihydrofluorescin diacetate

CCA- coumarin-3-carboxylic acid

CFDA- carboxyfluorescein diacetate

CO_2- carbon dioxide

CTC- 5-cyano-2,3-ditolyl tetrazolium chloride

BCECF-AM- 2’,7’-bis-carboxyethyl-5,6-carboxyfluorescein

BOX- refers to DiBAC4(3)

BrdU- 5-bromo-2’-deoxyuridine

DAPI- 4',6-diamidino-2-phenylindole dihydrochloride

DCF- 2’,7’-dichlorofluorescein

DCFDA- 2’,7’-dichlorofluorescein diacetate

DCFH- 2’,7’-Dichlorohydrofluorescin

DCFHDA - 2’,7’-Dichlorohydrofluorescin diacetate

DiBAC4(3)- bis-(1,3-dibarbituric acid)-trimetine oxanol)

DHR123- dihydroethidium, dihydrororhodamine 123

DMFB- dynamic metabolic flux balance model

DNA- deoxyribonucleic acid

DMAX- 9-[2-(3-carboxy-9,10-dimethyl) anthryl]-6-hydroxy-3H-xanthen-3-one

DPAX- 9-[2-(3-carboxy-9,10-diphenyl) anthryl]-6-hydroxy-3H-xanthen-3-one

DTP- diphtheria, tetanus and pertussis

EB- ethidium bromide

EC- Enzyme Commission

EdU- ethynyl deoxyuridine

EEM- excitation-emission matrix

ELISA- enzyme linked immunosorbent assay

ETC- electron transport chain

FACS- fluorescence-activated cell sorting

FAD- adenine dinucleotide

FDA- fluorescein diacetate

FMN- adenine mononucleotide

Fe- iron

Fe_2^+ - ferrous ion

Fe_3^+ - ferric ion

$Fe(NH_4)_2(SO_4)_2$- ammonium iron (II) sulfate

FeSOD- iron superoxide dismutase

FHA- filamentous hemagglutinin

FCM- flow cytometry

FIM2/FIM3- fimbriae units

FITC- fluorescein isothiocyanate

FL1- fluorescence channel 1

FL3- fluorescence channel 3

FORS- first order Rayleigh scattering

FSC- forward scattering

G1- gap 1 phase

G2- gap 2 phase

G6P- glucose-6-phosphate

Ga- gallium

GAP- glyceraldehyde 3-phosphate

GDH- glutamate dehydrogenase

GLU- glutamate

H_2DCF- 2',7'-Dichlorodihydrofluorescein

H_2DCFDA- 2',7'-Dichlorodihydrofluorescein diacetate

H_2O_2 – hydrogen peroxide

HO^-- hydroxide

$HO^{\cdot}$- hydroxyl radical

HPLC- high performance liquid chromatography

IDH- isocitrate dehydrogenase

K- Monod constant

Kj- Kjeldahl

kDa- kilo dalton

KGDH- α-ketoglutarate dehydrogenase

LPS- lipo-polysaccharide

MFI- median fluorescence intensity

Mn- manganese

MnSOD- manganese superoxide dismutase

MS- mass spectroscopy

MW- molecular weight

NAD^{+}- oxidized nicotinamide adenine dinucleotide

NADH- reduced nicotinamide adenine dinucleotide

NADK- NAD kinase

$NADP^+$- oxidized nicotinamide adenine dinucleotide phosphate

NADPH- reduced nicotinamide adenine dinucleotide phosphate

NAD(P)H- refers to NADH and/or NADPH

NADP-ICDH- NADP dependent isocitrate dehydrogenase

NaOH- sodium hydroxide

NO- nitric oxide

$^1O_2$- singlet oxygen

$O_2^{\cdot -}$ - superoxide radical

OD- optical density

ODE- ordinary differential equation

PBS- phosphate buffered saline

PC- principal component

PCA- principal component analysis

PEP- phosphoenolpyruvate

PFI- Peroxyfluor-1

Phe- phenylalanine

PI- propidium iodide

PLS- partial least squares

PMT- photomultiplier tube

(p)ppGpp- guanosine pentaphosphate or tetraphosphate

PRN- Pertactin

PT- *Pertussis* toxin

RNA- ribonucleic acid

RNS- reactive nitrogen species

ROOH- hydroperoxides

ROOR'- peroxides

ROS- reactive oxygen species

SDS-PAGE- sodium dodecyl sulphate polyacrylamide gel

Se- selenium

SFDA- sulfofluorescein diacetate

SOD- superoxide dismutase

SORS- second order Rayleigh scatering

SSC- side scattering

Supp- supplement

SYBR- N',N'-dimethyl-N-[4-[(E)-(3-methyl-1,3-benzothiazol-2-ylidene)methyl]-1-phenylquinolin-1-ium-2-yl]-N-propylpropane-1,3-diamine

TA- terephthalic acid

Trp- tryptophan

Trxs- oxidized thioredoxins

TrxRs- Thioredoxin reductases

Tyr- tyrosine

Greek Letters

α-KG- α-ketoglutarate

λ- wavelength (nm)

Chapter 1
Introduction

1.1 Research Motivation

Whooping cough is an infectious bacterial disease that affects the respiratory tract of the host, and is caused by the Gram-negative bacteria *Bordetella pertussis*. Prevention of this disease relies on early immunization. Whole-cellular and acellular vaccines have been developed, but due to the side effects associated with whole-cellular vaccines, acellular vaccines are preferred even though they are less effective (Thalen, 2008).

Some acellular vaccines contain five antigens or virulence factors while some others are based on just two factors. The five component pertussis vaccine (5CP) is based on pertussis toxin (PT), filamentous hemagglutinin (FHA), pertactin (PRN), and two fimbriae units (FIM2 and FIM3).

In the manufacturing process of an acellular pertussis vaccine, the five antigens are separated, purified and gathered for the final formulation. The process is mainly divided into two main groups of manufacturing steps: the upstream, which comprises two parallel trains of three consecutive reactors of increasing volume where the bacteria are grown, and the downstream where the five target antigens are purified. In the next section, a description of the process is presented.

In a previous study (Zavatti *et al*., 2016), samples from different stages of this manufacturing process at Sanofi Pasteur were analyzed by means of fluorescence spectroscopy. The collected data was then treated with multivariate techniques (Principal Component Analysis (PCA) and Partial Least Squares (PLS)) in order to localize the origin of the variability present observed in the final yield of pertactin (PRN). In that preliminary study, it was concluded that the source of variability is located in the

upstream portion of the process. We have recently hypothesized that oxidative stress occurring during fermentation is affecting antigen production, but still the causatives of the oxidative stress are not clear. The research pointed to the presence of oxidative stress based on the accumulation of a NADPH-enzyme complex in batches with low productivity. Under oxidative stress, cells attempt to increase the amount of NADPH because this pyridine is known to be involved in detoxification reactions required to fight oxidative stress (Puri, 2011).

Although we have found the above indication of possible oxidative stress, the actual source of variability among batches has not been identified. Moreover, since the basic operating conditions that are frequently monitored in the fermenter such as dissolved oxygen, aeration rates and media composition are consistent among batches, it was hypothesized that the observed variability may correspond to heterogeneity of the cell status within the fermenters. Thus, while on average the dissolved oxygen or aeration rate may be similar, in reality the cell population is heterogeneous and the distributions describing this heterogeneity in terms of oxidative stress or other indicators may explain the observed variations. For this reason, this research aimed to investigate the distributions in the cell population in the fermenters in terms of different indicators such as ROS (Reactive Oxidative Species), forward and side scattering, which are related to size and granularity of cells respectively, and to correlate these distributions with the observed variations in productivity. Flow cytometry (FCM) was chosen to monitor the culture since FCM can be used to determine the different parameters and how they are distributed within a cell population. In this manner, a population can be described more accurately as compared to monitoring average cell culture parameters since the measurements are done on each individual cell (Rieserberg *et al*., 2001). This feature in conjunction with the rapid processing time and identification of mixed populations are the virtues of flow cytometric analysis (Álvarez-Barrientos *et al*., 2000).

Within a population, cells can be quite different from one another. Heterogeneities arise from modifications in the microenvironment of single cells, alterations in the cell cycle or some other genetic mutations. Hence, the productivity in a bioprocess is also expected to be variable within the population (Broger, 2011).

1.2 Upstream and downstream PRN purification

The upstream process starts by thawing a frozen Component Pertussis seed. Subsequently, the thawed culture is transferred to seed flasks containing liquid medium which are incubated for 39 to 48 hours. Following incubation, the cultures are added to two parallel seed 20 L fermenters (initial fermentation stage) containing mainly Component Pertussis broth and growth factors. The seed fermenter cultures are grown for 22 to 25 hours. Subsequently, the cultures are transferred to two parallel 200 L fermenters (intermediate fermentation stage) for 22 to 25 hours, and then to two parallel 2000 L fermenters (production fermentation stage) that are operated for up to 56 hours. All fermenters work under the same operating conditions in terms of temperature (36°C), dissolved oxygen (35%) and pH (7.2) levels, which are continuously monitored and controlled in closed-loop. In the production fermenters, supplement feed media is added when the initial supply of the key nutrients is exhausted. The depletion of nutrients is detected by a significant sudden decrease in oxygen consumption which is accompanied by a corresponding spike in dissolved oxygen.

These fermentation steps are followed by harvesting, which involves centrifugation of the fermentation culture. The cell paste coming from the centrifugation, is collected into a tank for further fimbria (FIM) purification, and the supernatant, to be referred as centrate, is filtered to ensure the complete removal of the live cells.

In the downstream process, the filtered centrate, which contains PT, FHA and PRN, is further concentrated by using 10-kDa cellulose membranes. Following this, a perlite fractionation is used in the initial separation of three antigens which are needed for the acellular vaccine formulation in addition to FIM: Pertactin (PRN), Filamentous Haemogglutinin (FHA) and Pertussis Toxin (PT). PRN is collected in the run-through of the column used in this separation step, while PT and FHA are eluted from the column. Since the production bottleneck has been identified as the productivity of PRN, the description that follows and the general analysis are targeted to this particular antigen.

After the separation column, PRN is precipitated in three consecutive precipitation steps using ammonium sulphate at three different concentrations. In the first and third precipitation, the pellet is the fraction of interest while in the second precipitation the supernatant is used. The final pellet collected by centrifugation is dissolved in 10 mM HCl Tris buffer and loaded onto a chromatography column. Finally, the product is ultrafiltered and diafiltered before being subjected to a final chromatography step. The final filtration involves a pre-filtration step and a sterile filtration (0.2 μm filter) prior to quantification.

A flow-diagram of the downstream and PRN purification is shown in Figure 1-1.

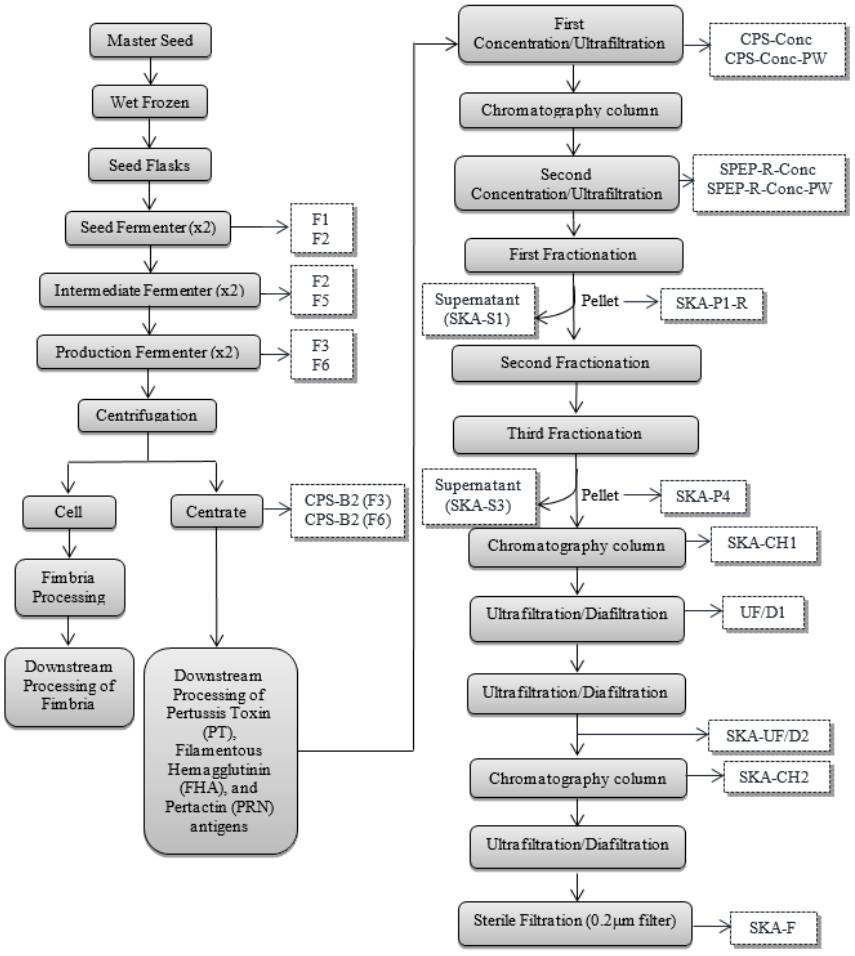

Figure 1-1 Flow-diagram of the downstream and PRN purification.

1.3 Objectives and Hypotheses

The main objective of this research is to identify the source of oxidative stress during fed-batch fermentations by mapping intracellular conditions within the cells as well as the extracellular operating

conditions by means of flow cytometry and fluorescence analysis in conjunction with multivariate statistical methods, such as PCA and PLS. The specific objectives are the following:

1- Flow cytometry based cell viability analysis.

2- Flow cytometry and spectrofluorescence based detection of reactive oxygen species (ROS).

3- Multivariate statistical analyses (PCA and PLS) to find correlations between production samples and PRN yield.

4- Small scale experiments to mimic the behavior observed in production to find possible explanations to variability in productivity.

5- Development of a mathematical model to explain evolution of NADPH and ROS along the fermentations.

These objectives are based in the following hypotheses:

1- The measured distributions of properties such as ROS (reactive oxidative species) forward scattering (FSC) and side scattering (SSC), in conjunction with PCA and PLS, can explain the observed variability among batches.

2- Oxidative stress has a significant impact on protein production thus explaining the observed reduction in antigen productivity.

1.4 Novelty

1- To gain an understanding of the variability over time that develops in a train of industrial-scale bioreactors during a vaccine manufacturing process.

2- To investigate the correlation between cell populations heterogeneity to variability in productivity by using flow cytometry is novel for *B. pertussis*.

3- The detection of ROS species as a stress indicator and their correlation with production of antigens by *B. pertussis* is novel. Monitoring ROS will allow the assessment of the behavior of these species during different stages of the fermentation and their impact on growth, viability and production of antigens.

4- Applicability of NADPH and ROS measurements as diagnostic tools for lab scale and industrial fermenters.

5- Gaining understanding of oxidative stress in *B. pertussis* and its effect on growth and productivity.

1.5 Thesis Structure

This thesis consists of nine chapters that contain the following information:

- The current chapter contains the description of the process, hypothesis, research objectives and novelty.
- Chapter 2 presents the theoretical background about whooping cough and vaccines, fluorescence, instrumentation, uses of flow cytometry and fluorescence spectroscopy in biological processes, and multivariate statistical methods such as PCA and PLS.
- Chapter 3 explains the materials and methods employed in the main analyses that were performed in this thesis: flow cytometric analysis, spectrofluorometric analysis, and product quantification and data treatment for both small scale experiments and analysis of the upstream fermentation process.
- Chapter 4 presents a comparison of flow cytometry and spectrofluorometry for the analysis of ROS. Three different fluorescein derivatives were tested for the analysis of ROS using both techniques.

- Chapter 5 and 6 are presented in manuscript format and for this reason they both show introduction and materials and methods sections, and some information from these chapters' duplicates what appears in the previous chapters. The data in the plots for these manuscripts were normalized since numerical data must remain confidential to Sanofi Pasteur.

- Chapter 5 refers to the impact of oxidative stress externally induced by the addition of H_2O_2 on growth and protein production by *B. pertussis*, at different fermentation scales: 250 mL, 2 L and 20 L. This chapter has been submitted for publication in the journal Vaccine.

- Chapter 6 also explains the impact of stress on *B. pertussis* growth, but with stress induced by means of addition of rotenone (experiments in 250 mL flasks), by reducing the inoculum size (experiments done in 250 mL flasks, and 2 L and 20 L fermenters) and by increasing the dissolved oxygen (DO) set-point in 2 L fermenters. Also, the effect of using autoclaved media or filtered media on growth and productivity was assessed with the imposition of stress with addition of H_2O_2.

- Chapter 7 presents a mathematical model that describes the adaptation observed in the growth profiles of *B. pertussis* after the imposition of stress either with H_2O_2 or by decreasing the inoculum size. Also, NADPH fluorescence measurements were NADPH is presumably bound to an enzyme (catalase) were done with the spectrofluorometer. For this test, bovine liver catalase (BLC) was used. The goal of this measurement was to assess the possibility of detecting NADPH fluorescent emission in catalase and relate this observation with what is observed in production samples. Calculations of intracellular and extracellular NADPH through fluorescence in combination with a mass balance showed that NADPH might be secreted.

- Chapter 8 shows the flow cytometric results obtained from the analysis of the train of fermentations in the manufacturing process: two seed fermenters (20 L), two intermediate fermenters (200 L), two production fermenters (2000 L). The main goal of this analysis was to correlate the observed distributions of the measured parameters (ROS quantities, forward and side scattering) in the samples with the final PRN yield, by means of multivariate statistical methods (PCA and PLS).
- Chapter 9 highlights final conclusions and recommendations for future work.
- Appendix A presents a manuscript published in Bioprocess and Biosystems Engineering: Zavatti, V., Budman, H., Legge, R., & Tamer, M. (2016). Monitoring of an antigen manufacturing process. *Bioprocess and Biosystems Engineering*, 39(6), 855-869.

Chapter 2

Literature Review

2.1 Whooping Cough

Whooping cough, also referred to as pertussis, is an infectious respiratory tract disease. In humans, one of the causative agents of this illness is the Gram-negative bacterium *Bordetella pertussis*, which was first isolated by Bordet and Gengou in 1906. The name pertussis means “violent cough” (Hijnen, 2008). This disease occurs ubiquitously in the world at any time of the year. Annually, an average of 30 million people contract whooping cough worldwide, where approximately 2,000 cases occur in Canada. The reported deaths are around 400,000 per year. Early symptoms resemble the common cold, and then evolve into intense coughing fits, distinguishable by the "whoop" sound produced while inhaling the air. Without treatment, the duration of the disease can range from several weeks to several months, and severe complications can lead to pneumonia, seizures, brain damage, or death. Children less than one year old are more likely to suffer severe symptoms. (Public Health Agency of Canada, Pertussis (whooping cough), Canada. Last Date Modified: 21 February 2014).

Aside from *Bordetella pertussis*, there are several other pathogenic species in the genus *Bordetella* that can cause upper respiratory tract infections. *B. parapertussis* causes a mild whooping cough-like syndrome, whereas *B. bronchiseptica*, an animal pathogen, is isolated rarely from humans (Locht, 1999). Since *B. parapertussis* causes less severe symptoms as compared to *B. pertussis*, all vaccines are based on the latter (Thalen, 2008). The production of whooping cough vaccines started immediately after the isolation of *B. pertussis*. In the early 1930s, the first mono component whole-cell pertussis vaccines were prepared (Hijnen, 2006), and in 1947 the production of combined vaccines started, which

contained components for diphtheria, tetanus and pertussis (DTP). Mortality was reduced by 10-fold following the introduction of these vaccines (Hijnen, 2006).

Although the whole cell vaccines were highly effective, they had drawbacks related to their side-effects (Hijnen, 2006; Thalen, 2008). Symptoms such as fever and more serious events such as convulsions were believed to be caused by the lipo-polysaccharide (LPS) existing in the external membrane of *B. pertussis*. For this reason, acellular vaccines that only consist of one or more *B. pertussis* antigens were sought. During the 80's and 90's, the development of acellular vaccines started, which replaced the previous whole-cell vaccines (Thalen, 2008). Even though whole-cell vaccines are more efficient against bacteria, acellular vaccines are desirable because of the minor side effects (Thalen, 2008). Typically acellular pertussis vaccines contain at least two of four purified and detoxified *B. pertussis* antigens: pertussis toxin (PT), filamentous hemagglutinin (FHA), fimbriae (FIM types 2 and 3) and pertactin (PRN). The selection of these antigens was based on the strong immune response that they elicit in both human and animal models (Locht, 1999; Noofeli, 2008).

Antigens or virulence factors are proteins used by a pathogen to enter the host and allow interaction with a specific target cell. Ultimately the pathogen must evade the host defenses to survive, damage the cell host and propagate either by itself or by its by-products to cause disease (Noofeli, 2008). Virulence factors such as fimbriae (FIM), filamentous hemagglutinin (FHA), and pertactin (PRN) are held in common among different species of Bordetella: *B. parapertussis*, *B. pertussis*, and *B. bronchiseptica*. However, some factors such as pertussis toxin are only released by *B. pertussis* (Noofeli, 2008). Pertussis toxin (PT) is one of the major protein toxins secreted by *B. pertussis*. It is released into the extracellular milieu and remains cell-bound. PT is a 105 kDa hexamer consisting of five subunits which are responsible for the interaction of the toxin with the target cell receptors (Locht, 1999). Fimbriae are submicroscopic proteinaceous appendages that protrude from the cell surface. They are comprised of

two major subunits: FIM2 with molecular weight (MW) of 22.5 kDa and FIM3 with MW equal to 22 kDa (Noofeli, 2008) that bind to sulphanated sugars existing in the respiratory tract (Babu *et al.*, 2001). Filamentous hemagglutinin (FHA) is a main appendage of *B. pertussis* and facilitates adherence of the cells to the respiratory epithelial cells. It is a filamentous structure about 2 nm wide and 50 nm long, and has a molecular weight of 220 kDa (Babu *et al*., 2001).

Pertactin (PRN) is an outer membrane protein partly responsible for adhesion of the bacterium to the host cell. By means of sodium dodecyl sulphate polyacrylamide gels (SDS-PAGE), the molecular weight of this antigen was found to be 69 kDa, however, when other methods such as mass spectroscopy (MS) have been used, estimates are close to 60 kDa (Charles *et al*., 1994; Noofeli, 2008). PRN belongs to the family of extracellular proteins called autotransporters (AT) found in various Gram-negative bacteria. The autotransporter secretion, or type V secretion, is one of the mechanisms developed by Gram-negative bacteria to achieve their physiological goals, i.e. surface motility and host invasion (Henderson *et al*., 1998). This type of secretion is called "autotransporter" because the protein is able to transport the passenger domain (stable units of protein structure that could fold autonomously) by itself through the outer membrane present only in Gram-negative bacteria. The autotransporter structure consists of three domains: the amino-terminal (N-terminal), the passenger domain or mature protein and a carboxyl terminal (C-terminal) (Henderson *et al*., 1998) as depicted in Figure 2-1. Virulence factors production and their interaction with the cell, as well as bacteria growth rate, are influenced by the cultivation conditions for the bacterium and the composition media employed in the fermentation (Thalen, 2008). Changes in culture conditions, such as changes in media composition, pH, temperature, and pressure can alter cell metabolism and have a significant impact on the subsequent purification steps and therefore, in productivity of the protein product (Vojinović *et al*., 2006).

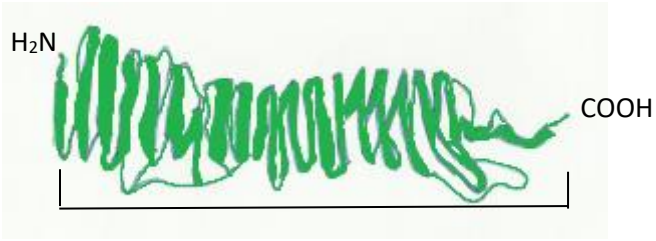

Figure 2-1 Autotransporter structure (adopted with modifications from Junker *et al*., 2006)

2.1.1 Oxidative stress and mechanisms of defense

To overcome fluctuations in environmental conditions, microorganisms have evolved adaptive mechanisms and defense systems (Schweder *et al*., 2004). Under stress conditions such as amino-acid starvation, iron and fatty acid limitation and oxidative stress, bacteria synthesize intracellular signal molecules, called alarmones, to produce a stringent response (Sugisaki *et al*., 2013). There is evidence that the alarmone (p)ppGpp is produced by *B. pertussis* to regulate the formation of biofilms and the expression of filamentous antigens for auto-aggregation (Sugisaki *et al*., 2013). Bacteria have also developed antioxidant systems to fight oxidative stress. Oxidative stress starts when the capacity to scavenge and neutralize ROS is not sufficient to counteract the generation of reactive oxygen species (ROS) (Shacter, 2000). ROS are continuously produced during the course of the aerobic metabolism. These species include free radicals such as singlet oxygen ($^1O_2$), hydroxyl radical ($HO^{\cdot}$), superoxide radical ($O_2^{\cdot -}$), peroxides (ROOR'), hydroperoxides (ROOH) and the non-radical hydrogen peroxide (H_2O_2) (Eruslanov *et al*., 2010). ROS are paramount in the defense system of the cell but overproduction of these species can have a deleterious effect on proteins, lipids and DNA, accelerating the aging process (Eruslanov *et al*., 2010; Frisard *et al*., 2006).

Superoxide radical (O_2^-) is formed when oxygen is reduced in the electron transport chain. This radical is responsible for the oxidation of $[4Fe\text{-}4S]^{2+}$ clusters present in iron-sulfur proteins with consequent release of ferrous ions (Fe^{2+}). Fe^{2+} can react with hydrogen peroxide (H_2O_2) via the Fenton reaction to produce the harmful hydroxyl radical ($OH^{\cdot}$) (Raghavan *et al*., 2011). It is believed that Fe^{2+} might also settle in the DNA surface and serve as catalyst in the generation of DNA oxidants (Keyer *et al*., 1996).

Superoxide dismutases are metalloenzymes that are able to catalytically convert superoxide radical to oxygen and hydrogen peroxide. Reactive oxygen intermediates are toxic to cells so SOD transforms superoxide radicals ($O_2^{\cdot -}$) into H_2O_2 and O_2 and catalase detoxifies H_2O_2. SOD enzymes have been found in all respiring organisms and appear to be critical in minimizing the toxicity of oxygen (Pile *et al*., 1977). Oxidative stress maybe mitigated by SOD as per the following reactions:

$$2O_2^{\cdot -} + 2H^+ + SOD \rightarrow O_2 + H_2O_2 \quad (2.1)$$

$$O_2^{\cdot -} + Fe^{3+} \rightarrow O_2 + Fe^{2+} \quad (2.2)$$

$$Fe^{2+} + H_2O_2 \rightarrow Fe^{3+} + OH^{\cdot} + OH^- \quad (2.3)$$

Reactions 2.2 and 2.3 are called the Haber-Weiss reactions. An important function of SODs is to prevent the oxidation of the iron-sulfur clusters in some enzymes (Lynch *et al*., 2000).

Depending on the metal co-factor, there are four types of dismutases, but only two are present in prokaryotic cells: FeSOD and MnSOD (Guo *et al*., 2008). FeSOD (SOD^B) is believe to confer protection from environmental stress while MnSOD (SOD^A) protects against internal stress (Miller, 2001).

Within the host, intracellular survival of *B. pertussis* is at least partly dependent on several enzymes to encountering reactive oxygen metabolites which could damage the microorganism's DNA. The enzymes which tackle them are SOD, catalase, glutathione synthase, and glutathione reductase (Graeff-Wohlleben *et al*., 1997).

SOD has been found in all respiring organisms and plays a critical role in minimizing the toxicity of oxygen. Exposure of *E. coli* to oxygen causes an increase in MnSOD (SOD^A) but not in FeSOD (SOD^B) which suggests that SOD^B is periplasmic and is primarily targeted to providing protection against exogenous $O_2^{\cdot -}$ (Pile *et al*., 1977).

It is known that inactivation of SOD can provoke mutagenesis, defects in the synthesis of amino acids and in the cell structure (Lynch *et al*., 2000). Oxidative stress might develop at particular subcellular locations, while the neighborhood of that location remains intact. Also, oxidative stress can be selective in relation to a particular radical species, since the antioxidant defenses are also specific to various radical species. For instance, SOD scavenges superoxide while catalase scavenges hydrogen peroxide (Dugan *et al*., 1999).

Lipid peroxidation results from the addition of hydroxyl or peroxyl groups to unsaturated fatty acids or from the attachment of a fatty carbon chain to an aldehyde when reacting with free electrons to produce a fatty acid aldehyde. Fatty aldehydes might react with free thiol groups in proteins, such as in the amino acid cysteine, producing thioesters, which can affect protein stability and function (Dugan *et al*., 1999).

It is believed that DNA is damaged indirectly by $O_2^{\cdot -}$ when participating in the generation of hydroxyl radicals (OH^-). Iron molecules bound to DNA are reduced by $O_2^{\cdot -}$. Consecutive oxidation of H_2O_2 by iron, produces hydroxyl radicals, which in turn attacks DNA. However, it has been also proposed that

superoxide promotes leaching of iron from [4Fe-4S] clusters. The leached iron deposits on the DNA surface and catalyzes the formation of oxidants, accepting electrons from surrounding donors (Keyer *et al*., 1995; Keyer *et al*., 1996).

Inorganic elements could also impact TCA cycle functioning. It has been reported that when *P. fluorescens* is exposed to gallium (Ga), aluminum (Al) and iron (Fe), elements known to create an oxidative environment, the activity of NADP-ICDH (NADP dependent isocitrate dehydrogenase) is increased while the activities of KGDH (α-ketoglutarate dehydrogenase) and NAD-ICDH (NAD dependent isocitrate dehydrogenase) are markedly decreased (Mailloux *et al*., 2007).

According to Graeff-Woelleben *et al*. (1995), different environmental stimuli have different effects on transcript stability. Their data suggest that the regulation of virulence in *B. pertussis* as a response to variations in the growth conditions is regulated differentially by several mechanisms, involving not only the action of additional transcription factors, but also the participation of general mechanisms such as changes in DNA topology or transcript stability (Graeff-Wohlleben *et al*., 1995).

The protection that SOD confers against DNA damage is a major role of this enzyme. It has been reported that the probability to survive the stationary phase is less for SOD deficient *B. pertussis* mutants than for the wild types (Lynch *et al*., 2000) because of the accumulation of oxidized proteins susceptible to proteolysis (Benov *et al*., 2001).

Catalases are another group of enzymes that help in the detoxification of reactive oxygen metabolites generated during growth under aerobic conditions (Graeff-Wohlleben *et al*., 1997). However, the inactivation of these enzymes does not cause severe effects on bacterial phenotype, probably due to redundant oxidoreductase activities present in most bacteria which can compensate for lost function. Graeff-Wohlleben *et al.* (1997) were able to delete the gene encoding Mn containing enzyme without obvious effects on the bacteria. In contrast, they were unable to suppress the SOD^B gene. They reported

that Fe containing SOD^B is essential for normal growth of *B. pertussis*. Inactivation of the SOD^B gene caused a decrease (about 35%) of the viable counts after 45 min, whereas the viability of SOD^A deletion mutant was only slightly (<5%) impaired (Graeff-Wohlleben *et al*., 1997).

The relationship between SOD activity and the conditions under which bacteria are cultured is not yet fully understood, although some studies indicate that SOD activity is influenced by various growth conditions such as O_2 concentration or pH level. NADH oxidase, an enzyme that regulates the production of superoxide radicals might be linked with SOD (Kimoto-Nira *et al.*, 2014). The detrimental effect of oxygen might start prevailing as the cells age. It has been reported that the ability to consume oxygen is strongly dependent on the age of the cells. Even though SOD's specific activities are in general directly proportional to the availability of oxygen in the broth, SOD can be present at significant levels under anaerobic conditions (Smart *et al.,* 1987). Hansson *et al.* (1984) showed that when *Streptococcus lactis* is cultivated at elevated partial pressures of oxygen, the SOD activity increases. They also reported an incremental increase in SOD activity when Fe^{+3} was present, possible due to the generation of reactions such as the ones participating in the Haber-Weiss mechanism.

Thioredoxin reductases (TrxRs) are oxidoreductases, which contain pyridine, selenium and reactive disulfide bonds. As the name implies they have the capacity to reduce oxidized thioredoxins (Trxs) utilizing NADPH as a catalyst (Mustacich *et al*., 2000; Eruslanov *et al*., 2010). TrxRs defend cells against H_2O_2 by providing reducing equivalents to Trx peroxidase, which converts H_2O_2 into water (Eruslanov *et al*., 2010). Selenium (Se) has a crucial role in the proper functioning of TrxR. It has been reported that the activity of TrxR increases by adding Se to the growth medium of a cell culture (Mustacich *et al.,* 2000).

Complex I (NADH:ubiquinone oxidoreductase or NADH dehydrogenase), which is the first membrane-bound enzyme in the electron transport chain (ETC), is known to be a major source of

electrons that can generate radicals and oxidative stress (Esterházy *et al*., 2008). Complex I acts as catalyst in the oxidation of NADH to NAD^+, where coenzyme Q is reduced. Different complexes (I, III and IV) located in the inner membrane along with cytochrome c and coenzyme Q, participate in the transfer of electrons from NADH to oxygen (Diwan, J. J., Electron Transfer Chain. Biochemistry of Metabolism. Retrieved from https://www.rpi.edu/dept/bcbp/molbiochem/MBWeb/mb1/part2/redox.htm).

Studies with *Escherichia coli* showed that NADH dehydrogenase II (one of the three dehydrogenases found in bacteria, also called NADH:quinone oxidoreductase II (Heikal *et al*., 2014)), sulfite reductase, succinate dehydrogenase and fumarate reductase formed superoxide and hydrogen peroxide after exposure to O_2 (Messner *et al*., 2002).

NADPH is important for aerobic organisms to survive since it is a source of reducing equivalents that serves to protect against ROS (Singh *et al*., 2007). Some of the enzymes that catalyzes the reactions involve in the production of NADPH are 6-phosphogluconate dehydrogenase, malic enzyme, glucose-6-phosphate dehydrogenase, glutamate dehydrogenase-$NADP^+$, and $NADP^+$-isocitrate dehydrogenase (Singh *et al*., 2007). Another important enzyme in the production of $NADP^+$ from which NADPH is synthesized, is NAD kinase (NADK) (Grose *et al*., 2006). An imbalance between the reduction and oxidation of pyridine nucleotides can affect important cellular functions compromising cell survival (Nakamura *et al*., 2012). It is thought that one of the contributors of the reduction of Fe^{3+} during oxidative stress is NADH. The reduced iron would then react to produce hydroxyl radicals via Fenton reaction. On the other hand, NADPH contributes to diminish oxidative stress by helping reactions to create a reductive environment (Grose *et al*., 2006). NADPH also contributes in the proper functioning of enzymes such as SOD, glutathione peroxidase and catalase. ATP production via oxidative phosphorylation is not effective in the absence of NADPH (Singh *et al*., 2007).

The oxidation of isocitrate catalyzed by isocitrate dehydrogenase generates α-ketoglutarate (α- KG), CO_2 and NADPH. It is believed that prokaryotes only have $NADP^+$ dependent isocitrate dehydrogenase (IDH). In *E.coli* grown under conditions of limited ammonia or glucose most of the production of NADPH comes from IDH-related reactions (Spaans *et al*., 2015).

Singh *et al*. (2007) found that under oxidative stress conditions, *Pseudomonas fluorescens* decreases NADH production, which in turn diminishes ROS generation and ATP synthesis. This is a strategy for increasing the generation of NADPH, and decreasing the functioning of the TCA cycle and the production of NADH (Singh *et al*., 2007).

ROS production is directly impacted by the concentration of NAD^+. In the presence of α-ketoglutarate dehydrogenase (α-KGDH), NAD^+ accelerates the catalysis of the conversion of α-ketoglutarate (α-KG) in succinyl-CoA releasing CO_2 and NADH (Tretter *et al*., 2004). Inhibition of α-KGDH can be critical in the progress of the metabolic pathway of the TCA cycle (Mailloux *et al*., 2009; Tretter *et al*., 2005).

Aconitase is one enzyme that is easily attacked by ROS, but if α-KGDH remains functional in the case of aconitase inactivation, NADH can still be generated. The supply of NADH to the Krebs cycle is restricted when α-KGDH is impaired (Tretter *et al*., 2005). Aconitase is also affected by cellular iron status. Middaugh *et al*. (2005) reported that the activity of aconitase in aluminum stressed *Pseudomonas fluorescens* was recovered after the addition of $Fe(NH_4)_2(SO_4)_2$.

Glutamate dehydrogenase (GDH) and α-KGDH are instrumental for the production of α-KG. Mailloux *et al*. (2009) showed that α-KG is of important in order for *P. fluorescens* to fight oxidative stress. In their studies they observed that a decrease in α-KGDH restricts the access of α-KG in the Krebs cycle, creating a pool that would help to alleviate oxidative stress through the scavenging of

ROS. GDH, α-KGDH and α-KG seemed to work together to lessen oxidative stress (Mailloux *et al*., 2009).

2.2 Process Monitoring and Control

The monitoring and control of processes has a crucial role in all industries in maintaining the highest productivity and required product quality. For instance, in pharmaceutical processes such as vaccine production, productivity and product quality are highly dependent on bioreactor design, composition of media and control of several upstream and downstream process conditions. Efforts in sensor design, data management, and sampling planning have been made to improve process monitoring and control (Pohlscheidt *et al.*, 2013).

2.2.1 Methods of Monitoring

Based on where the sampling points are located, process monitoring methods can be categorized into the following types:

2.2.1.1 In-Line or In Situ Monitoring

In this type of monitoring, sensors are directly located within the piece of equipment or along a pipeline, and no withdrawal of sample is needed. Chemical and physical parameters, such as pH, redox potential, O_2, CO_2, conductivity, and turbidity, are usually monitored in situ. The advantage of in situ monitoring over offline monitoring is the rapid measurement and direct control (Pohlscheidt *et al*., 2013).

This type of monitoring is sometimes referred to as on-line monitoring. Some authors make a differentiation between these two terms, naming on-line monitoring the process in which the withdrawal and analysis of the sample is automated.

2.2.1.2 Off-Line Monitoring

In this type of monitoring, samples are analyzed in an appropriate device once they are withdrawn from the process (Elshereef, 2009; Pohlscheidt *et al*., 2013). By doing sampling, it is possible to evaluate the overall state of the process at a certain time. Even though this approach allows high precision measurements, off-line analytics always results in a delay between the sampling and the measurements (Vojinović *et al*., 2006). Handling and preparation of the sample can have a significant impact on the accuracy of the measurement. For instance, aseptic treatment and mixing after sampling are important aspects to be considered before analysis (Pohlscheidt *et al*., 2013).

Traditional laboratory techniques are usually implemented off-line (Elshereef, 2009). For example, the measurement of metabolites that is essential for maintaining, characterizing and further improving fermentation processes is implemented off-line. Enzyme linked immunosorbent assay (ELISA) and high performance liquid chromatography (HPLC) are techniques conventionally employed in the analysis of specific proteins and substrates. Enzyme-based biosensors, e.g. bioprofiles, are usually employed to measure glucose, lactate, glutamine, and glutamate as off-line (Pohlscheidt *et al*., 2013).

2.3 Principles of Fluorescence

Fluorescence is a type of luminescence, which occurs when molecules emit light after being physically, mechanically or chemically excited. When visible or ultraviolet light is used as source of excitation, the phenomenon is called photoluminescence, and based on the electronic configuration of

the excited states it can be categorized as either fluorescence or phosphorescence. In fluorescence, light is re-emitted immediately after absorption. In contrast, when molecules phosphoresce the emission of light occurs slowly and it can be seen with naked eye (Lakowicz, 2006; Wehry, 1997).

2.3.1 Fluorophores

Fluorophores (or fluorochromes) are compounds that can re-emit light upon excitation. Fluorescent compounds are characterized by their excitation (light absorbed) and emission (light emitted) spectra.

Fluorophores can be classified in two groups: intrinsic and extrinsic. Fluorophores are intrinsic when they are naturally present in the sample. This group comprises amino acids such as phenylalanine, tyrosine and tryptophan, and co-factors such as pyridines mainly reduced nicotinamide adenine dinucleotide phosphate (NADPH), reduced nicotinamide adenine dinucleotide (NADH), and the oxidized flavins: adenine dinucleotide (FAD) and the mononucleotide (FMN) (Hairston *et al*., 1997; Lakowickz, 2006).

Extrinsic fluorophores are molecules that are incorporated into the sample and depending on how they react to the environment, a characteristic fluorescent emission is produced. Based on this interaction, extrinsic fluorophores can be divided as follows: i- fluorophores that exhibit an increase in the fluorescence intensity after binding to a particular compound such as nucleic acids (SYTOX or propidium iodide PI), proteins (some fluorescein derivatives such as FITC) and lipids (Rhodamine 123, Nile Red, FSL-fluorescein), ii- fluorophores that fluoresce based on physiological state variables such as pH and membrane potential and iii- fluorophores whose fluorescence is subject to enzymatic activity (Álvarez-Barrientos *et al*., 2000).

2.3.2 Theory of Fluorescence

When a fluorophore is irradiated by a light source with a wide spectrum of wavelengths, it will absorb light and reach different vibrational and electronic states. The probability, in which these states can occur, depends on the electronic configuration of the molecule. This configuration is unique to each fluorophore, making each fluorescence spectra also unique.

The Jablonski diagram is a graphical representation of the absorption-emission process. Figure 2-2 shows a simplified Jablonski diagram. S0 represents the ground state, S1 the first electronic state and S2 the second electronic state. The vibrational energy levels, in which a fluorophore might exist, are indicated by 0, 1, 2, 3, and 4. The vertical lines represent the transitions among states during absorption (green lines) and fluorescence emission (blue lines).

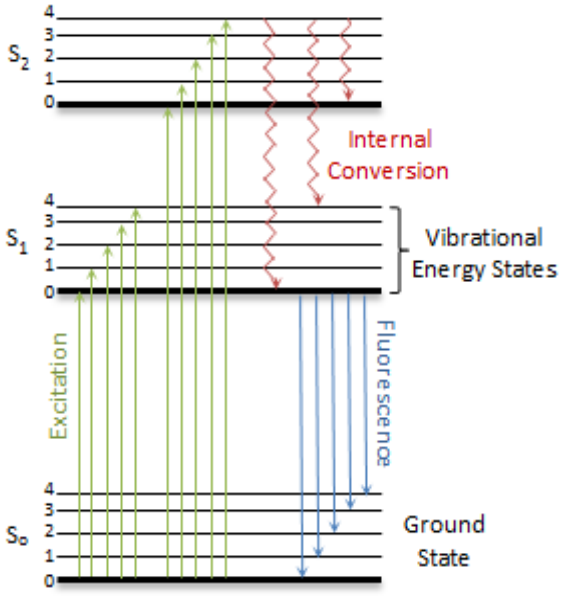

Figure 2-2 Jablonski diagram; B: Simplified operating diagram for a spectrofluorometer (adopted with modifications from Peiris, 2010).

2.3.3 Fluorescence Instrumentation

Fluorescence instruments share common features for fluorescence detection: (i) a source of excitation, (ii) filters to segregate photons depending on the excitation emission wavelength, (iii) detectors to record output signal (Wiederschain, 2011). Some types of fluorescence instruments include:

- Fluorescence microscopes which take advantage of fluorescence to generate a magnified image of the sample.
- Spectrofluorometers and microplate readers which estimate the average fluorescence signal of the whole sample.
- Flow cytometers which measure fluorescence signal per cell.

2.4 Principles of Flow Cytometry

Flow cytometry (from "cyto" = cells and "metry" = measurement) is a robust technique for the analysis of single cells within a heterogeneous population, employing fluorescence and light scattering (Davey *et al*., 1996; Biosciences, 2000; Rieseberg *et al*., 2001; Díaz *et al*., 2010). The simultaneous quantification of a broad range of parameters, either structural or functional, and the acquisition of data related to the distribution of these parameters in a cell population are the key characteristics that is increasingly making this technology an effective tool for the design and control of industrial bioprocesses (Rieseberg *et al*., 2001; Díaz *et al*., 2010).

The flow cytometer operates by passing single cells through a laser beam at rates from 100 to 1,000 cells/s. The light emitted is then captured with suitable detectors (Davey *et al*., 1996; Givan, 2000). Low cell rates result in a tedious analysis, and high rates can have detrimental effects on the intensity

resolution and the accuracy of the measurement since two cells passing fast and close together through the laser can be mistakenly detected as a single event (Givan, 2000). An event is the data that represents one particle or cell (Díaz *et al.*, 2010).

The collected data can be processed by software to statistically account for characteristics such as complexity, cell size, and health. Since size and complexity can be detected without staining, they are considered intrinsic parameters (Álvarez-Barrientos *et al*., 2000).

2.4.1 Instrumentation

2.4.1.1 Types of flow cytometers

There are two generic types of flow cytometers: i- the analyzers, which simply analyze and discard the samples, and ii- the cell sorters, which are more sophisticated and can arrange individual cells according to the scattered light and fluorescence emission. The latter type is usually called fluorescence-activated cell sorting (FACS), and permits the collection of cells at any combination of fluorescence emission and scattering (Veal *et al*., 2000; Birtwistle, 2014).

Cell sorting can be done by means of two main methods: droplet deflection and mechanical sorting. In droplet depletion sorters, an electric charge is applied to droplets that contain the cells prior to transporting them through an electric field. In this manner, cells are separated based on their electric charge. In mechanical sorters, cells are deflected by moving a tube which collects the cells once they are passed through the interrogation point (Veal *et al*., 2000; Wulff *et al*., 2006).

2.4.1.2 Principal components of a flow cytometer

A flow cytometry is composed of several operating units: i- the hydraulic fluidic system, which transports the sample to the interrogation point, ii- the light source, iii- the optical system that gathers and directs the light, iv- the detectors that capture the emitted light, v- the electronic system that

transforms the signal from the detector into digital data and vi- the data acquisition and processing system that performs the necessary analysis (Álvarez-Barrientos *et al.,* 2000; Díaz *et al*., 2010).

2.4.1.2.1 The hydraulic fluidic system

The main goal of the hydraulic fluid system is to transport the sample to the interrogation point, where the sample is excited by the laser and the resulting emission of fluorescence and scattering is collected. For obtaining accurate results, it is important to reduce the nozzle obstruction and to pass the cells through the interrogation point one by one. To achieve this, flow cytometers employ hydrodynamic focusing, which consists in confining the core fluid (or sample) to the central portion of a sheath fluid (e.g. water or saline solution). In this manner, the diameter of the flow stream squeezes to practically the diameter of one cell (Álvarez-Barrientos *et al*., 2000; Biosciences, 2000; Shapiro, 2005).

Flow cytometers can accommodate cells that span roughly three orders of magnitude in size. In most cases, the cell diameter detected by cytometers ranges from one to 15 microns, although, through the use of specialized systems, the detection of particles with sizes outside this range can be accomplished (Álvarez-Barrientos *et al*., 2000; Biosciences, 2000; Shapiro, 2005).

2.4.1.2.2 The light source

Flow cytometers can employ arc lamps (e.g. mercury arc lamps) or lasers as light source. The choice of the source depends on the type of desired analysis. It has been reported that arc lamps have greater resolution for scatter signal and for this reason it is preferred for microbiological testing. On the other hand, lasers are chosen in fields such as immunology because the range of wavelength desired to excite fluorophores relevant to the analysis of the cells (Álvarez-Barrientos *et al.,* 2000).

The signal is produced when the light source hits the cells at the interrogation point. When this occurs, part of the light is re-emitted as fluorescence signal, and another portion is scattered in different directions. The light scattered in the forward direction, is called forward scatter and it is equivalent to the cell size. The light scatter at 90° from the incident light is called side scatter, and it is proportional to the granularity or complexity of the cell (Díaz *et al*., 2010).

2.4.1.2.3 The optical system

The optical system comprises a series of filters that allow the absorption of particular wavelengths, while letting pass others. The types of filters are three: short pass filters that impede the pass of light above certain wavelength (e.g. 600 nm <), long pass filters that impede the transmission of light below a particular wavelength (e.g. <600 nm), and band pass filters that allow the pass of light between two certain wavelength values (e.g. 550 nm < λ < 570 nm) (Díaz *et al*., 2010).

2.4.1.2.4 The detectors

The detectors are photomultiplier tubes (PMTs) and photodiodes. PMTs are usually use to collect side scatter and fluorescence signals, and photodiodes for forward scatter (Shapiro, 2005).

2.4.1.2.5 The electronic system

The scattered light received by the detector is transformed into electric (voltage) pulse. As a result, the magnitude of the voltage is proportional to the signal. When plotted as a histogram, forward scatter data represents the size distribution within the population where small particles appear towards the left and large particles locate towards the right. The same happens for the side scatter and fluorescence. High voltages for side scatter implies more cell granularity, and high voltages for fluorescence signal indicates high intensity and amount of the fluorophore being analyzed.

2.4.1.2.6 The data acquisition

The data acquisition is referred to the statistical information and graphical representation that can be subtracted by means of software. The data can be visualized as histograms, density distributions, dot plots, contour plots among others (Álvarez-Barrientos *et al*., 2000; Díaz *et al*., 2010). Figure 2-3 shows a schematic representation of a flow cytometer.

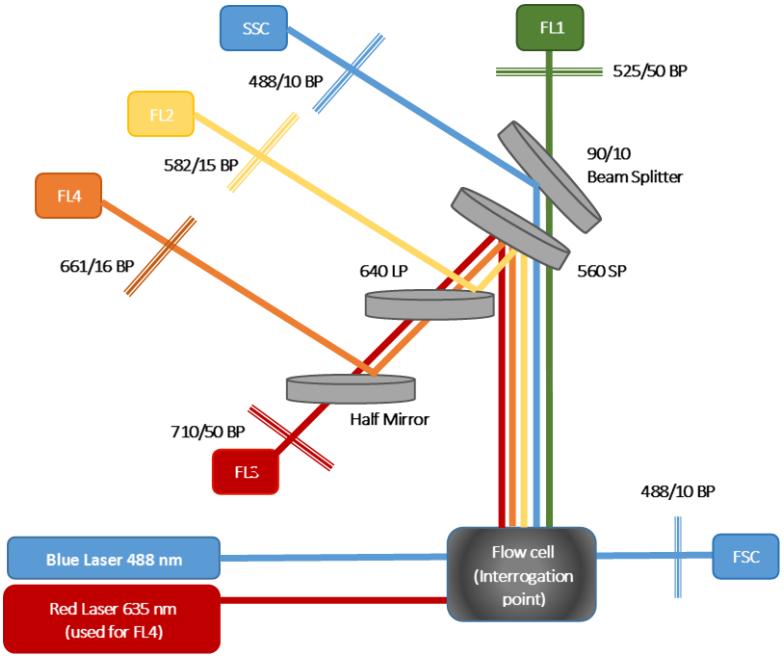

Figure 2-3 Schematic representation of a flow cytometer. BP: band pass, LP: long pass, SP: short pass. Half mirror (or beam splitter) passes 50% and reflects 50% of the light. 90/10 beam splitter reflects 90% and passes 10% of the light (taken with modifications from http://www.bdbiosciences.com/sg/instruments/facscalibur/features/index.jsp)

2.4.2 Fluorophores used in flow cytometry

Flow cytometers can use the auto-fluorescence properties of molecules to measure intrinsic parameters or added fluorescent reagents for the measurement of extrinsic parameters (Dartnell *et al*., 2013; Shapiro, 2005), even though many scientists have also studied intrinsic fluorescence just as a source of noise for low fluorescent signals to avoid interferences in the measurements (Shapiro, 2005).

Autofluorescence of bacteria and mammalian cells is due to amino acids such as phenylalanine, tyrosine and tryptophan, and co-factors such as NAD(P)H and oxidized flavins (FAD and FMN) (Hairston *et al.*, 1997; Lakowickz, 2006). Since the fluorescence of pyridines and flavins change within the course of oxidation-reduction reactions, these co-factors are employed to monitor redox states in cells (Shapiro, 2005). Bacterial viability can be assessed by the presence NAD(P)H since this molecule is associated with the metabolic state of cells (Hairston *et al*., 1997; Ho *et al*., 1999). Intrinsic fluorescence can be useful to discriminate among species of bacteria (Winson *et al*., 2000).

Besides intrinsic fluorescence, cell viability is also assessed by extrinsic fluorophores. The novelty of flow cytometric analysis in viability assessment is that through this technique different physiological states, e.g. live or dead cells, have been identified (Berney *et al*., 2007; Czechowska *et al*., 2008). For example, Nielsen *et al*. (2009) quantified the population of *Pseudomonas fluorescens* DR54 and distinguish four sub-populations: i- "intact cells" which are healthy cells without any membrane damage, ii- "de-energized cells" where the electron transport activity is compromised, iii- "depolarized cells" where membrane potential has been reduced, and iv- "permeabilized cells" which are cells with an injured membrane. The evaluation of the survival of pathogens is one of the reasons that motivate the identification of physiological states (Czechowska *et al*., 2008).

Nielsen *et al.* (2009) utilized SYBR Green for detecting "intact cells", which is a membrane permeable dye that stains both DNA and RNA in all cells, but it only accumulates in healthy cells

leaving the rest unstained. For detecting the de-energized cells, ethidium bromide (EB) was employed as it penetrates the cytoplasmic membrane and reaches DNA if it is not exported by a proton gradient. This binding gives a strong red fluorescent signal. The depolarized phase was detected with the BOX stain bis-(1,3-dibarbituric acid)-trimetine oxanol) abbreviated DiBAC4(3). Cells at this state also bind SYBR and EB, but the further binding of DiBAC4(3) to the membrane or intracellular proteins, gives a strong green signal greater than that resulting from SYBR emission. Permeabilized cells were detected by means of propidium iodide (PI), which is not a able to penetrate through intact membranes and it only binds to DNA and RNA when it enters the cell such as in case of cell damage (Shapiro, 2005).

A widely used kit commercialized by Molecular Probes for viability assessment is the LIVE/DEAD BacLight bacterial kit, which is a two-color fluorescence assay that utilizes a mixture of SYTO9 and PI. SYTO9 is cell-permeable and stains both live and dead bacteria, and emits a strong green fluorescent signal. PI is impermeable to the cell membrane and thus it only stains cells with membrane damage (Spence *et al*., 2010). Since the affinity of PI for DNA and RNA is higher than the affinity of SYTO9 to nucleic acids, the latter is displaced in the presence of PI (Stocks, 2004). Special care has to be taken in order to avoid the simultaneous labeling of DNA by SYTO9 and PI. It has been reported that when DNA is in excess, double staining might occur. Stocks (2004) found that PI must be in excess of the DNA concentration in order to avoid double staining. They also reported that the concentration of SYTO9 is not crucial for determining bacterial viability and its optimal concentration can be set based on the fluorescence brightness. In this work, the estimated association constants for PI and SYTO9 were 3.7×10^5 /M and 1.8×10^5 /M, respectively.

Even though many scientists have succeeded in detecting dead cells using PI in bacteria (Boulos *et al*., 1999; Gant *et al.*, 1993; Stiefel *et al*., 2015; Williams *et al*., 1998), some investigations have reported that PI is less useful for this analysis. Shi *et al*. (2007) have shown that PI can stain growing

cells of *Sphingomonas sp*. and *M. frederiksbergense*. Also, it has been claimed that intermediate cellular states can be observed when using SYTO9 and PI (Berney *et al*., 2007). Another dye used for staining dead bacteria is SYTOX Green, which is not permeant to live cells and have higher fluorescence than PI (Breeuwer *et al*., 2000). This dye is useful in cases where the DNA content is low, and a probe with a high quantum yield is necessary (Rieseberg *et al*., 2001).

Besides the aforementioned probes that have been used for analyzing viability based on membrane integrity and membrane potential, other probes have been developed based on enzymatic activity and cellular respiration (Sincock *et al*., 2001). The enzymatic activity approach consists of using lipophilic and non-fluorescent molecules that can cross the cell membrane, and remain trapped inside the cell once they are hydrolyzed by esterases and converted into fluorescent compounds. Since the hydrolyzed forms are polar, they cannot diffuse outside the cell unless the membrane is compromised. In this manner, intact and dead cells can be detected. Fluorescein diacetate (FDA), carboxyfluorescein diacetate (CFDA) and sulfofluorescein diacetate (SFDA) are probes that can serve in this type of analysis. The drawback of these fluorescing derivatives is that sometimes they cannot efficiently permeate through the cell membrane (Sincock *et al*., 2001).

In the cell respiration approach, a non-fluorescent probe is converted into a fluorescent probe following electron transport activity. The salt 5-cyano-2,3-ditolyl tetrazolium chloride (CTC) used for this analysis, is reduced to the fluorescent CTC-formazan that remains trapped inside intact cells. The disadvantages of this probe are that some bacteria are unable to reduce tetrazolium salts and also it is believed that CTC could inhibit the metabolism of some microorganisms (Sincock *et al*., 2001).

Intracellular pH measurements have also been employed to test cell viability, since it is an indicator of metabolic activity and physiological state. Fluorescent substrates such as Calcein-AM and 2',7'- bis-

carboxyethyl-5,6-carboxyfluorescein (BCECF-AM) have been used in this type of analysis (Rieseberg *et al*., 2001).

Another important flow cytometric target in bioprocesses studies is the measurement of DNA content (Rieseberg *et al.*, 2001). The goal of this analysis is mainly the assessment of cell proliferation and the determination of the fraction of cells in distinct phases of growth (Jacobberger *et al*., 2011). For cell cycle analysis are also employed fluorescent dyes that are common in viability tests, but prior to their use, the elimination of the RNA by means of RNase is required, since these types of dyes have affinity for both DNA and RNA (Rieseberg *et al*., 2001). PI, the Hoechst dyes, 4',6-diamidino-2-phenylindole dihydrochloride (DAPI) and 7-aminoactinomycin D (7-AAD) are commonly used for the analysis in cells that have been previously permeabilized in order to allow the complete diffusion of the probe through the cell membrane (Gordon *et al*., 2003; Rieseberg *et al*., 2001). These fluorescent probes are sometimes not sufficiently efficient for distinguishing among the different phases of the cell cycle. The simplest way to overcome this difficulty is to add an additional marker that is specific to the phase of interest. The most common probes are 5-bromo-2'- deoxyuridine (BrdU) or ethynyl deoxyuridine (EdU) that can be used to identify cells in S phase (Darzynkiewicz *et al*., 2001; Kotogány *et al*., 2010).

Fluorescent probes are also employed in the detection of ROS. ROS are natural products of cellular respiration of all aerobic species. Even though ROS have been considered as toxic molecules that can lead to oxidative stress, new roles have been identified for these species such as biological messengers. Hence, there is active research on ROS and their effects (Soh *et al*., 2006).

A traditional probe employed in ROS detection is 2',7'-dichlorodihydrofluorescin (DCFH). When DCFH is oxidized by ROS, the highly fluorescent 2',7'-dichlorofluorescein (DCF) is formed, which emits fluorescence at an excitation-emission wavelength combination of Ex/Em = 498 nm/522 nm (Gomes *et al*., 2005). The diacetate form DCFH-DA is widely used in this analysis since it can permeate

through the cell membrane. DCFH-DA is hydrolyzed by intracellular esterases, and converted into the non-fluorescent and cell-membrane impermeable H_2DCF, which is then oxidized by ROS into DCF (Gomes *et al*., 2005; Eruslanov *et al*., 2010; Soh *et al*., 2006). This probe was initially thought to be selective in the detection H_2O_2, but it has been reported that it also reacts with other ROS and with some reactive nitrogen species (RNS). For this reason, this probe is considered more appropriate to be employed in the detection of total oxidative activity (Gomes *et al*., 2005; Soh *et al*., 2006).

Dihydro-compounds such as dihydroethidium, dihydrororhodamine 123 (DHR123), dihydrororhodamine 6G and dihydrocalcein, can be used also as general probes for ROS detection since they are not specific to a particular molecule (Soh *et al*., 2006).

Among fluorescent probes used to detect $^1O_2$ is the 9-[2-(3-carboxy-9,10-diphenyl) anthryl]-6-hydroxy-3H-xanthen-3-one (DPAX). From the reaction of this molecule with $^1O_2$ a fluorescent endoperoxide is formed (Gomes *et al*., 2005; Soh *et al*., 2006). An additional probe used in this analysis is 9-[2-(3-carboxy-9,10-dimethyl) anthryl]-6-hydroxy-3H-xanthen-3-one (DMAX), which also produces a fluorescent endoperoxide after reaction with $^1O_2$ (Soh *et al*., 2006).

For the detection of H_2O_2, specific probes have emerged in recent years (Soh *et al*., 2006). The pentafluorobenzenesulfonyl fluoresceins are probes that react with H_2O_2 to generate fluorescein. Even though those probes have a high selectivity to H_2O_2, they are also able to react to some degree with nitric oxide (NO). Peroxyfluor-1 (PFI) is an excellent probe for this analysis since it has much higher reactivity to H_2O_2 compare to other ROS, producing a highly fluorescent fluorescein (Soh *et al*., 2006).

The detection of $^{\cdot}OH$ is challenging because of its short lifetime. However, many probes have been reported for its detection. Terephthalic acid (TA) is converted into the stable fluorescent product 2-

hydroxy-TA after hydroxylation with ·OH. The coumarin-3-carboxylic acid (CCA) reacts with ·OH producing the fluorescent compound 7-hydroxycoumarin (Soh *et al*., 2006).

A probe that has been widely used in the detection of $O_2^{\cdot -}$ is dihydroethidium (hydroethidine) despite its low selectivity. The bis(2,4-dinitrobenzenesulfonyl) fluoresceins are probes that have been reported to be selective for $O_2^{\cdot -}$. These chemicals react with superoxide radicals to produce a molecule with a fluorescein moiety and two equivalents of 2,4-dinitrobenzenesulfonic acid. Another reagent developed for this ROS is 2-(2-pyridyl)-benzothiazoline, which is oxidized to the fluorescent product 2-(2-pyridyl)-benzothiazole (Soh *et al*., 2006).

2.4.3 Advantages and disadvantages of flow cytometry

In addition to the ability to classify individual cells, there are additional features that make flow cytometric analysis a powerful technique (Davey *et al*., 1996). In contrasts with other methods, flow cytometry allows the measurement of multiple parameters for each single cell permitting to distinguish different cells types or different cell variables within a population. Another advantage is the high-speed of the flow cytometry analysis. Most flow cytometers can analyze from 100 to 1,000 cells per second with a high level of precision. Thus, modern flow cytometers have the exceptional capacity to rapidly segregate cell populations based on biological characteristics (Davey *et al*., 1996; Wulff *et al*., 2006).

In spite of the unique features that confer important advantages of flow cytometry over other techniques, there are still some disadvantages associated to this technique such as the high cost of acquisition, and the need for skilled operators to obtain meaningful results (Davey *et al*., 1996).

2.4.4 Applications of flow cytometry in biotechnology

Flow cytometric analyses of biological samples were accomplished during the 40's, even though the first description of this technique dates from the earliest 30's (Shapiro, 2005). Through the following years, efforts have been made to improve the sensitivity in the identification and isolation of microorganisms (Díaz *et al*., 2010). During World War II, the U.S. Army sponsored successful research on the rapid detection of bacteria in aerosols used as biological weapons by means of flow cytometry (Shapiro, 2005). From then on, strengthened by improvements in electro-optical technologies and the development of fluorescent probes, flow cytometry has found a wide range of applications in research and routine analysis in distinct fields (Díaz *et al*., 2010; Shapiro, 2005).

Areas such as the food and drink industries, alcoholic beverage production, pharmaceutical industry, medicine and environmental microbiology are some examples where flow cytometry has played an important role in quality and process control (Díaz *et al*., 2010; Sincock, 2001). In general, some of the common functional and structural parameters detected in the analyses are membrane integrity, membrane potential, metabolic activity, labeled antigens, esterase activity and nucleic acids (Díaz *et al*., 2010).

In the food and drink industries, the rapid detection of pathogenic microorganisms and control of spoilage microorganisms in raw materials and final products that can compromise food safety, and the assessment of food preservation process through cell viability analysis have been accomplished through flow cytometry (Díaz *et al*., 2010; Sincock, 2001). Pathogens such as *Listeria monocytogenes*, *Samonella typhimurium* and *Escherichia coli* O157:H7 can be identified with flow cytometry using specific monoclonal antibodies (Sincock, 2001).

In beer, wine and cider production, flow cytometry has been employed to control fermentation processes. Selection of yeast starting cultures, discrimination between viable and non-viable cells,

assessment of process and storage conditions (e.g. temperature, preservatives) are routine analyses that can be obtained from flow cytometry for obtaining good quality products (Díaz *et al*., 2010).

Flow cytometry has also arisen as a powerful tool in water systems and environmental microbiology as a method for characterization of physiological states that is important for assessing the survival of pathogens under certain environmental conditions (Czechowska *et al*., 2008) and the efficacy of treatments for disinfection of water (Díaz *et al*., 2010).

In the pharmaceutical industry, flow cytometry has been applied in identification of species, evaluation of drug effects on cell viability, clinical diagnosis as well as at industrial scale in process monitoring (Díaz *et al*., 2010). The spread of some diseases such as AIDS played a crucial role in the advancement of flow cytometry. The earliest flow cytometers were capable of detecting just one fluorescence signal, and it was not until the end of the 80s when four-color experiments could be performed. At that time, the necessity to employ multicolor measurements in flow cytometric analysis was unclear. During that decade, many analyses were done in T cells from an HIV-infected population, and through the employment of multicolor flow cytometric analysis, it was possible to simultaneously detect CD4 and CD8 co-factors levels that appear to be lower in patients with this infection. These analyses paved the path for new applications and developments using multiple markers in flow cytometry (Sklar, 2015).

In the development of vaccines, flow cytometry has been employed to evaluate the immune response evoked by an immunogen. This has been achieved through the detection of antigens and immune cells, and measurements of cytokines' production (Nolan *et al*., 2007; Roederer *et al*., 2004). Vaughan *et al*. (2014), employed flow cytometry for the detection of the two fimbrial subunits, Fim2 and Fim3, among isolated *B. pertussis* cells. The analysis was performed using fimbrial specific monoclonal antibodies in order to distinguish among the viable serotypes of fimbria. As a result, they found that the expression

of these antigens is more variable than previously reported. From the point of view of vaccine manufacturing process, this presents a motivation to perform a selection of specific serotypes for production of antigens during a fermentation process.

2.5 Multivariate Statistics Analysis

2.5.1 Data pre-processing

Before starting any analysis using multivariate statistics methods, it is necessary to pre-process the data to avoid uneven distributions. Among the frequently used methods are the following:

- Median centering: in this procedure, the median of each variable of the data set is calculated and subtracted from the variable. In this manner, the median of the resulting data set will be equal to zero.
- Mean centering: similar to median centering, but mean is used instead of median.
- Auto-scaling: this method uses the mean-centering approach follow by the division of each variable by the standard deviation. The mean and standard deviation of each variable will be zero and one respectively (Wise *et al*., 2007).

2.5.2 Principal Component Analysis

One of the common methods employed to extract information from a data set with a large number of variables is Principal Component Analysis (PCA). PCA compresses the data to reduce the original variables into a lower number of orthogonal (non-correlated) variables called principal components (PCs) (Abdi *et al*., 2010; Wise *et al*., 2007).

PCA finds linear combinations of original variables that captures the major tendencies of the data. A certain number of components are considerate for the analysis since they describe the highest percentage of the variance, and the rest are inferred to be related to noise.

In Figure 2-4 there is a graphic example of how PCA works. Data points of three variables (X_1, X_2 and X_3) measured from a group of samples are shown in a three dimensional (3D) space. The objective is to find a vector that describes the greatest variation in the data with minimum loss of information (e.g. **u** in Figure 2-4).

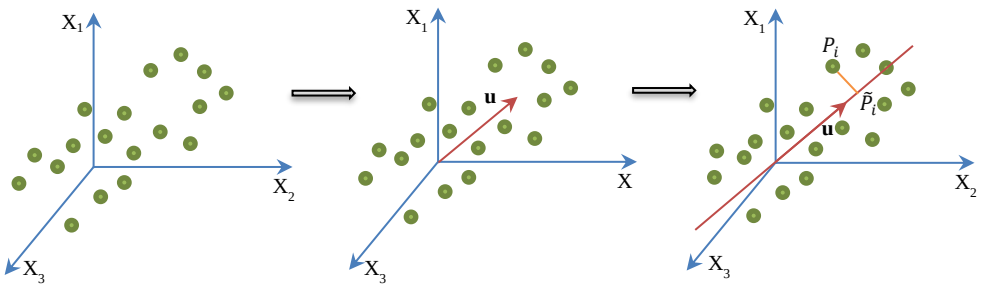

Figure 2-4 Projection of a point on an axis

Any point of the data set (e.g. P_i) can be projected by multiplying per the normalized vector **u**. The result is the reduction of a three dimensional point to one dimension. The idea is to retain the distance between the data point and the PC at minimum (equation 2.4)

$$\sum_i \left(P_i - \tilde{P}_i\right)^2 = min \tag{2.4}$$

Once the first PC is found, the method finds another PC orthogonal to the previous one that captures the remaining variability (Figure 2-5).

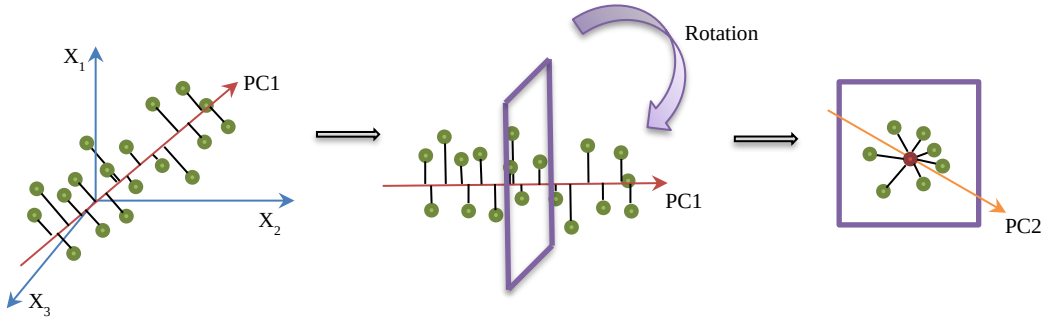

Figure 2-5 Plane rotations in PCA

As depicted in Figure 2-5, PCA rotates the axes of the first found PC to situate an orthogonal plane where the second PC is going to be located.

Equation 2.5 shows the general equation of PCA, where a set of data (matrix *X*) is decomposed as the summation of the products of s_i and p_i, and a residual matrix E that contains the unexplained variables.

$$X = \sum_{i=1}^{n} s_i * p_i + E \tag{2.5}$$

where *n* represents the number of samples, s_i represents the scores that contain information about the relation between the original samples and the principal components, and p_i are the loadings that contain information about the relation among original variables in a principal component.

While PCA attempts to find factors or components that captures most of the variability, there are other methods that also find correlation between variables. Partial Least Squares (PLS) is another multivariate method that maximizes covariance. PLS is used to find a correlation between to matrices, so that the new regression model can be used to predict a new response from a given data set.

2.5.3 Partial Least Squares

Partial Least Squares is a statistical method that not only compresses data, but also retrieves a number of latent variables (LVs) that describe the original data. The LVs correlates the scores in a given matrix X with the scores from a different matrix Y, and maximize the covariance.

Equations 2.6 and 2.7 describe the decomposition of matrices *X* and *Y*:

$$X = TQ + E = \sum_{i=1}^{m} t_i * q_i + E \tag{2.6}$$

$$Y = UC + F = \sum_{i=1}^{m} u_i * c_i + F \tag{2.7}$$

where m is the number of latent variables. The t_i and u_i vectors represent the scores that contain information about the relation between the original samples (X and U respectively) and the latent variables. The q_i and c_i vectors are called *loadings* and contain information on how T relates to X, and U relates to Y. E and F contain the variables that cannot be explain by the model.

The inner relation between U and T is given by the following equation:

$$U = WT \tag{2.8}$$

where W is the weight matrix. From equation 2.8, scores in Y can be predicted from scores in X, and from equation 2.7 the new response data.

Chapter 3

Materials and Methods

The materials and methods are organized according to the main analyses performed: flow cytometric analysis, fluorometric analysis, and product quantification and data treatment.

3.1 Samples

3.1.1 Small scale studies

The small scales studies were performed in the laboratory facilities of Sanofi Pasteur (Toronto, Ontario, Canada). *B. pertussis* fermentations were run at three different scales: 250 mL shake flasks, 2 L and 20 L fermenters.

Shake Flask Experiments: Flasks were run in duplicate with a working volume of 100 mL, incubated at 36°C, 200 rpm for 48 hrs. Three different analyses were conducted: i- assessment of the effect of the external imposition of stress on growth and production of PRN by adding 600 μM of H_2O_2 either at 4 h or at 24 h, and with 600 μM of rotenone either at 4 h or at 24 h (initial optical density (OD at 600 nm) was 0.3, which is the value used in the control fermentations); ii- assessment of the impact of low inoculum size (OD 0.03, ten times smaller than the control) in growth and production of PRN; and iii- assessment of the effect on growth and production of PRN by external imposition of stress with 600 μM of H_2O_2 at 4 h in autoclaved and filtered media. Media composition is not given for commercial reasons.

2 L Fermentations: Four fermentations were performed in 2 L BiosStat Bplus (Sartorius Stedim) bioreactors. The working volume was 1.3 L. All fermenters operated at 36°C, pH 7.2, agitation from 100-678 rpm, and airflow 0.5 lpm (maintained constant). The dissolved oxygen (DO) was maintained

constant by means of cascade control by firstly manipulating the airflow rate followed by the agitation rate. The various experimental conditions tested were the following: i- 35% DO and OD 0.3 for the control reactor; ii- 35% DO, OD 0.3 and 600 μM H_2O_2 added at 4 h; iii- 70% DO and OD 0.3; and iv- 35% DO and OD 0.03. These experiments were done to assess the effect of the external imposition of stress by H_2O_2 and increased DO, and to assess the impact of low inoculum size on growth and production of PRN.

20 L Fermentations: Three fermentations were performed in 20 L BiosStat Bplus (Sartorius Stedim) bioreactors. The working volume was 13 L. Temperature and pH were 36°C and 7.2, respectively. The airflow was 0.6 lpm and the agitation rate from 100-700 rpm. The DO was maintained constant employing cascade control like the 2L fermentations. The various experimental conditions tested were the following: i- 35% DO and OD 0.3 for the control reactor; ii- 35% DO, OD 0.3 and 600 μM H_2O_2 added at 4 h; and iii- 35% DO and OD 0.03.

For all experiments, sampling was done at several times during the fermentation. OD was measured at 600 nm. Samples collected were centrifuged (10,000 xg, 3 min, 4°C). Cells were resuspended with 10 mM PBS for flow cytometric analyses and the supernatant was used for fluorometric analyses.

OD measurements were done diluting the sample in 10 mM PBS buffer to reach an OD not higher than 0.3. All measurements were done in triplicates.

3.1.2 Production fermentation studies

Samples were provided by Sanofi Pasteur (Toronto, Ontario, Canada) from upstream steps for different batches. For the upstream portion of the process, there are two parallel fermenter trains of increasing volume: 20 L, 200 L and 2000 L that are combined together before downstream processing. One fermentation batch is composed by two trains of fermenters, and each PRN batch is composed by two batch fermentations (Figure 3-1).

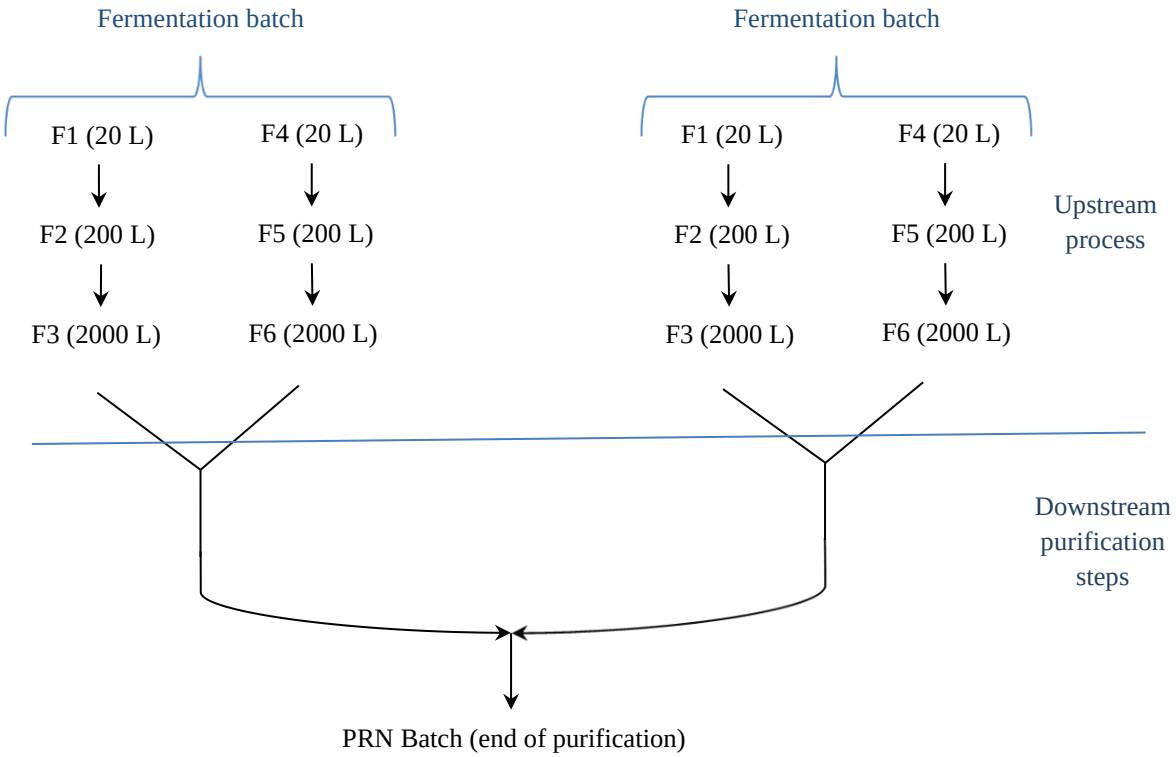

Figure 3-1 Schematic of the process showing the fermentation steps analyzed.

For the 20 L fermenters (F1 and F4) and the 200 L fermenters (F2 and F5), sampling was done at 0 h, 7 h, and 24 h. For the 2000 L fermenters (F3 and F6), sampling was done at 0 h, 7 h, 24 h, 36 h, 52 h. Thus, a total of 44 samples were collected for every PRN batch.

Table 3-1 provides the batches analyzed and the final PRN content measured by means of Kjeldahl analysis (Kj).

Fermenter batch	PRN batch	Kj (g/batch)
A1	A	1.00
A2		
B1	B	0.88
B2		
C1	C	0.81
C2		
D1	D	0.76
D2		
E1	F	0.65
E2		

Table 3-1 Fermentation batches analyzed from the upstream process. PRN quantification was done by Kjeldahl analysis (Kj). Kj values were normalized for confidentiality.

3.2 Flow cytometry analysis

3.2.1 Cell staining for viability

For cell viability two fluorescent dyes were used in combination: SYTO9 (Invitrogen) a green fluorescent nucleic acid stain which stains live and dead cells, and PI (propidium iodide) (Invitrogen) which is a red-fluorescent stain that stains dead cells. SYTO9 is cell permeable and PI cannot penetrate the cells unless there is membrane damage.

The optical density (OD) at 600 nm for each sample was adjusted to 0.05 with 10 mM PBS. The concentrations of SYTO9 and PI in 1 mL of resuspended cells was 0.12 µM and 3 µM, respectively. Fluorescence emission for SYTO9 was measured using the green fluorescence FL1 detector and PI the

red fluorescence FL3 detector. SYTO9 and PI have an excitation/emission maxima at 483/503 nm and 530/625 nm, respectively. Samples were incubated in the dark for 10 min prior to measurement.

3.2.2 Detection of reactive oxygen species (ROS)

Oxidative stress was assessed by means of measuring three fluorescein derivatives. The three fluorescein derivatives tested were: 2',7'-dichlorofluorescein diacetate (DCF-DA), 2',7'-dichlorodihydrofluorescein diacetate (H_2DCFDA), and carboxy-2',7'-dichlorodihydrofluorescein diacetate (carboxy-H_2DCFDA) from Sigma-Aldrich (Canada).

The protocol followed for the reagents was the same: 1 mM of the reagent was prepared dissolving it in DMSO and the final concentration per sample was 50 μM. Cells were incubated for 1 h at room temperature. The reagents are non-fluorescent and cell permeable, but once in the cell they are deacetylated by esterases and converted to the fluorescent DCF when they react with H_2O_2 and other oxygen derivatives (Halliwell *et al*. 2004). DCF fluoresces at Ex/Em 503/523 nm.

3.2.3 Equipment

Flow cytometric analysis was performed using a S3e Cell Sorter (Bio Rad). The instrument has 2 excitation lasers at 488 nm (primary) and 640 nm (secondary), and emission filters for forward scattering (FSC) and side scattering (SSC) detection (488/10 band width filters), and fluorescence emission detection: 526/48 (FL1), 593/40 (FL2), 670/30 (FL3) and 700 LP (FL4). In this analysis, the FL1 detector was used for green fluorescence (SYTO9), the FL3 detector for red fluorescence (PI) and the primary excitation laser (488 nm). In the ROS detection analyses, the FL1 diode was used for DCF detection (green fluorescence). The total number of events per sample was 10,000 at a rate of 1,600-1,800 events/sec.

3.2.4 Flow cytometric data analysis

3.2.4.1 Weighted Average

The average level of ROS in the cell population was determined using a weighted average (*WA*) as per the following equation:

$$WA = \sum_i^f \frac{C_i}{C_t} * I_i \quad (3.1)$$

Where C_i is the number of cells that have fluorescence intensity I_i, and C_t is the total number of cells analyzed.

3.2.4.2 ANOVA

Statistical significance was assessed using one-way ANOVA $p < 0.05$ conducted using Minitab 17.1 (Minitab, Inc.) statistical software.

3.2.4.3 PCA and PLS analysis

The fluorescence signal from cDCF and the forward (FSC) and side scattering (SSC) signal were acquired for 10,000 cells in each sample. The signal was converted into a voltage pulse. The height of the voltage pulse was used in all cases to build the histograms that were later used in the PCA and PLS analysis. So, for each height there were a certain number of cells that have the same height, or that fall in a range of heights. Those numbers of cells were rearranged in a single row for each distribution (cDCF, FSC, and SSC), and gathered in one row. The rows for each sample were stacked together as described in Figure 3-2.

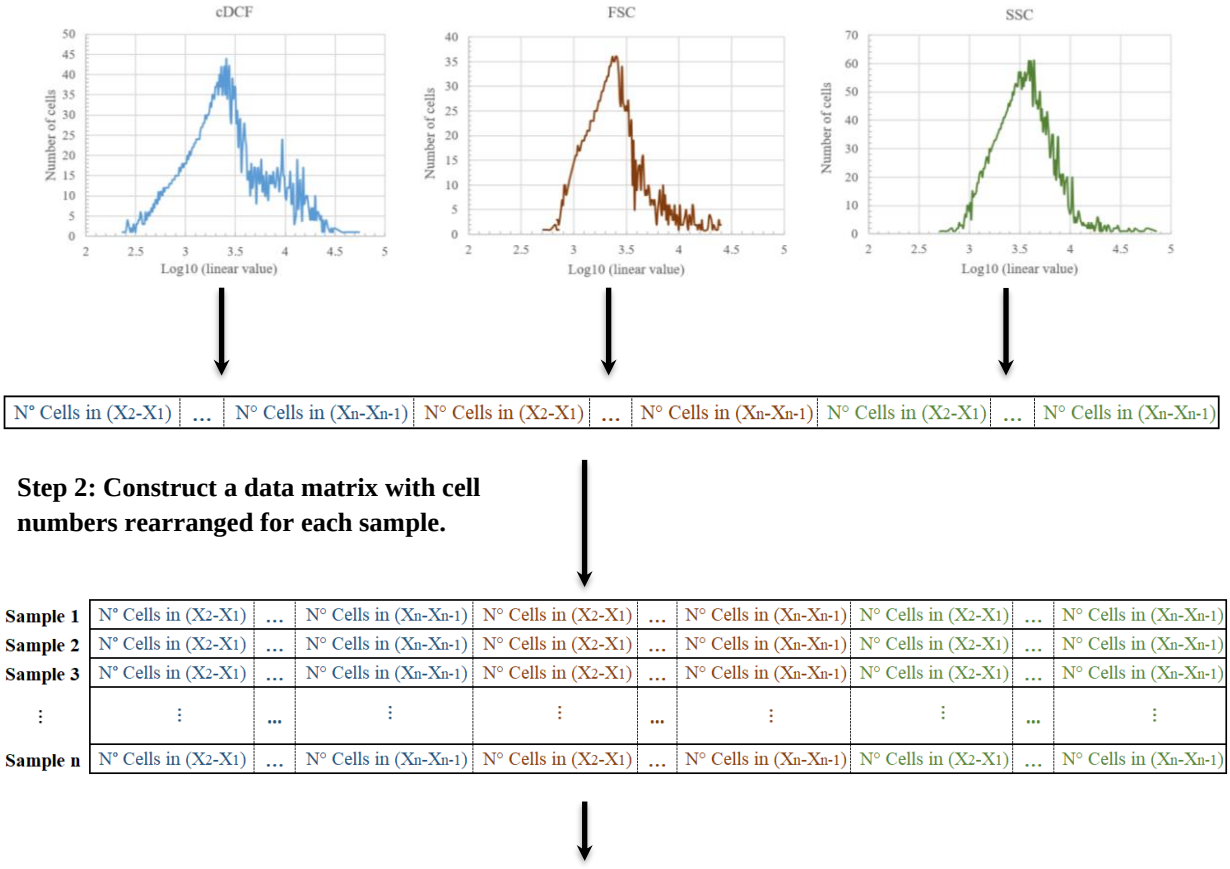

Figure 3-2 Steps involved in generating data rows of numbers of cells for PCA and PLS analysis.

Cell counting was done in intervals of the logarithmic values of the voltage pulse (e.g. from 2 to 2.5, from 2.5 to 3). In Figure 3-2, each column of the final matrix represents the variables that were processed with PCA and PLS. In total there were 33 variables: 11 variables for each parameter measured (cDCF, FSC, SSC). These intervals were selected based on a trial and error procedure where

different values were tested, and the interval that resulted in a PCA model that captured the greatest variance in the data was chosen for the analysis.

Three matrices were built for PCA: i- a matrix with samples from the 20 L fermenters; ii- a matrix with samples from the 200 L fermenters; and iii- a matrix with the 2000 L fermenters. The time points for the 20 L and 200 L fermenters were t= 0 h, 7 h, and 24 h, and for the 2000 L were t= 0 h, 7 h, 24 h, 36, and 52 h. For PLS, the matrices were separated according to the time points, so there were five matrices in total. Also, to evaluate the sensitivity of the regression method to the data in the form of the distribution of the population and in the form of the average (treating the signal as a bulk), it was calculated as a weighted average for each distribution using equation 3.1 So, five extra matrices for each time point were constructed using the weighted average.

The goal of performing PCA is to reduce the numbers of variables in a data set, to several non-correlated variables. The new variables are called principal components (PC) (Wise *et al*., 2007). For the case under study the actual variables are the number of cells in each column of the final matrix obtained with the procedure described in Figure 3-2. The linear combination of those variables are the PC's, and they collect most of the variance in the data. Just a limited number of PC's describes the variability of the data and the remaining PC's are considered being related to noise and are discarded.

The original data matrix (X) is decomposed by PCA in the summation of a product of two vectors: $\boldsymbol{s_i}$ and $\boldsymbol{p_i}$ (called scores and residuals respectively) and residual matrix E (Equation 3.2)

$$X = \sum_{i=1}^{n} s_i * p_i + E \tag{3.2}$$

Where n is the number of samples. The scores (s_i) represent the relationship between the original variables and the principal components. The loadings (p_i) represents the connection among the original variables along the principal component.

Data pre-treatment is necessary before a multivariate statistical analysis. In this case, two methods were used: i- mean centering, where the mean of each variable is subtracted from each element of the variable in order to obtain a mean equal to zero; and ii- autoscaling, where each element of the variable is divided by the standard deviation of the variable in order to scale to unit variance. Without normalization by the variance, the PCA model could wrongly focus on few variables with the largest absolute variances (Wise *et al*., 2007)

Cross-validation was done to select the numbers of PC's that better describe the model. The method used was the so-called random subset (Wise *et al*., 2007), which consists of dividing the data matrix into N sets in a random fashion. Based on the N-1 remaining sets, PCA builds a model leaving one set out. Subsequently, the set left out is calculated by the model. The resulting error between the original and the calculated set for the left-out, is the plotted against the number of components. The number of components that resulted in less error is the chosen one. The error is presented as the Root Mean Square Error of Cross-Validation (*RMSECV*), which is defined as:

$$RMSECV = \sqrt{\frac{\sum_{i=1}^{n}(y_i - \hat{y}_i)^2}{n}} \tag{3.3}$$

Where y_i is the measured value, $\hat{y}_i$ is the predicted variable and n is the number of calibration samples (Wise *et al*., 2007).

The second multivariate statistical method used to process the data was Partial Least Squares (PLS). PLS find correlation between two set of data matrices (e.g. *X* and *Y*). The goal is to obtain a regression between *X* and *Y* matrices that can be used to predict a new *Y* matrix from a new acquired *X* data matrix.

PLS was used to obtain a regression model between the distributions of cells in the samples and the PRN yield of the batch of those samples. Also, PLS was used to perform a regression between the average value of the signal obtained with the flow cytometry and PRN yield. Before performing PLS, it was also necessary to pre-process the data as explained for PCA.

PLS not only compresses the data and finds major variations between the two matrices, but also identifies a number of latent variables (LV) that correlates the scores of both matrices to have maximum covariance.

In this sense, PLS decomposes the two matrices (X and Y) as follows:

$$X = TQ + E = \sum_{i=1}^{m} t_i * q_i + E \tag{3.4}$$

$$Y = UC + F = \sum_{i=1}^{m} u_i * c_i + F \tag{3.5}$$

Where m is the number of latent variables. The scores (t_i and u_i) represent the relationship between the original variables and the latent variables. Scores in *T* are the projections of the input data *X* (e.g. number of cells with certain fluorescence or scattering signal to a LV in the *X*-space), and scores in *U* are the projections of the response data (e.g. PRN yield to a LV in the *Y*-space). The loadings (q_i and c_i) represent the connection between *T* and *X*-space, and *U* and *Y*-space respectively. *E* and *F* contain the variables that are not explained by the model.

The inner relation between *U* and *T* is given by the following equation

$$U = WT \tag{3.6}$$

Where *W* is the weight matrix. Using Equation 3.6, one can calculated the scores *U*, using the scores *T*, and then calculate the new response matrix using Equation 3.5.

PCA and PLS analysis were performed using the PLS_ Matlab Toolbox (Eigenvector Research Inc., Manson,WA). Data collection, analysis and plotting were conducted using MATLAB R2016b software (The Mathworks Inc., Natick, MA).

3.3 Fluorometric analysis

3.3.1 Reagents

For catalase fluorescent analysis NaOH was used to denature the enzyme. Bovine liver catalase (BLC) was purchased from Sigma-Aldrich (Canada) and 35% w/w H_2O_2 was purchased from Sigma-Aldrich (USA).

3.3.2 Catalase fluorescence measurements

Catalase fluorescence was measured under different conditions: i- a solution made with 100 μL of catalase as supplied by the manufacturer was added to 3.2 mL of 10 mM PBS; ii- 100 μL of pure catalase was treated with 3.2 mL of a 5 N NaOH solution in order to denature the enzyme and fluorescence was measured at different time points: 30 min, 2 h, and 6 h; iii- a solution made of 100 μL of catalase as supplied by the manufacturer in 3.1 mL of 10 mM PBS spiked with 100 μL of 35% H_2O_2; and iv- 40 μL of 35% H_2O_2 was added to 3 mL of media with growth factors (as used in the

fermentations) and then this solution was spiked with a 40 μL of a catalase solution (10 μL catalase as supplied by the manufacturer in 1 mL 10 mM PBS).

3.3.3 NADPH Measurements

NADPH intrinsic fluorescence was measured at Ex/Em 340/460 nm. The NADPH measurement in the broth was reported per OD of the original sample (NADPH/OD) since NADPH accumulates along of the fermentation, it was necessary to standardize this value to compare each time point.

3.3.4 Equipment

Fluorescence excitation-emission spectra were acquired with a Cary Eclipse Fluorescence Spectrophotometer (Agilent Technologies). The samples were analyzed using polymethylmethacrylate cuvettes at a slit width of 5 nm and PMT of 700 V (for NADPH measurements) or PMT of 800 V (for catalase measurements). The excitation and emission ranges were 250-400 nm and 360-500 nm, respectively. A wide range of Ex/Em values were used to ensure that all possible emissions were captured. Phosphate buffered saline (PBS) 10 mM (pH 7.2) was used as a blank.

3.4 Product quantification

3.4.1 ELISA

The final quantity of PRN released by the bacteria at the end of the fermentation was determined using ELISA. Microplates were coated with 50 μL/well of 1.5 μg/mL PRN polyclonal antibodies purified from guinea pig blood. Plates were incubated at room temperature for 20 h. After incubation, plates were washed three times with 200 μL/well of a solution containing 10 mM PBS, 0.1% Tween 20 and 0.1% BSA, and blocked for 30 min at room temperature with 100 μL/well of 10 mM PBS and

0.1% BSA. After blocking, the plates were washed again two times with 200 μL/well of a solution containing 10 mM PBS, 0.1% Tween 20 and 0.1% BSA. Samples were centrifuged and filtered with a 0.2 μm filter. The filtered supernatants were diluted, added to the wells and incubated for 1 h at room temperature. After incubation, the plates were washed with the PBS-Tween 20-BSA solution. 100 μL of guinea pig anti-PRN antibody conjugated to horseradish peroxidase was added to each well and plates were incubated for 1 h at room temperature. Plates were washed again and 100 μL/well of a mixture of 1 mL of 10 mM tetramethylbenzidine and 9 mL of 0.004% (v/v) H_2O_2 was added and incubated for 30 min at room temperature. The reaction was stopped with 50 μL/well of 2 N H_2SO_4 and absorbance was measured at 450 nm. The absorbance was proportional to PRN content. The concentration was calculated based on a standard curve.

3.4.2 Kjeldahl Method

The Kjeldahl method was used to quantify the protein content at the end of the purification process of PRN based on the quantity of nitrogen present in the antigen. This method consists of three steps: digestion, distillation and titration. An aliquot of the sample (10-75 mL) was precipitated with trichloroacetic acid 30% w/v (TCA) in excess (1 mL of TCA precipitates approximately 200 μg of protein) and incubated for 3.5 h at room temperature. After incubation, the sample was centrifuged for 1 h, at 2100 rpm. The supernatant was discarded and 2 mL of sulfuric acid (H_2SO_4) were added, heated gently to dissolve pellet, and let to cool for 5 min. Digestion: The dissolved pellet was transferred into a 30 mL Kjeldahl digestion flask containing selenized granules (catalyst). For the blank, 2 mL of high purity water were added into two digestion flasks containing the catalyst. For the protein standard, 1 mL of a protein standard solution was added into two digestion flasks containing the catalyst. As a positive control, a nitrogen standard solution was made with 1 g of ammonium sulfate in 1000 mL with high purity water. The nitrogen standard does not need digestion. 2 mL of H_2SO_4 were added to the

blank and the protein standard, and incubated with an initial low temperature that was gradually increased to avoid excessive foaming. The solution was heated for an additional 1 ½ h starting from the moment when a white-grey color appeared. Distillation: The digested solutions were cooled to room temperature before digestion. 125 mL flasks were prepared adding 5 mL of 4% w/v of boric acid and 4 drops of a mixed indicator made with 5 volumes of 0.1% w/v bromocresol green with 1 volume of 0.1% w/v methyl red in 95% ethyl alcohol. This will serve as the receiving solution. The digested solutions were reconstituted with 3 mL of high purify water, mixed and poured into the distilling flasks (without the granules). The digestion flasks were rinsed three times with high purity water and the rinsing was added to the distilling flask. 8 mL of 50% w/w NaOH was added slowly to the distilling flasks. The set up for distillation was prepared. The distillation was started until a change of color from pink to pale blue was perceived in the boric acid solution and neutral pH is obtained. Titration: the receiving solution containing boric acid and the absorbed ammonia is titrated with 0.01 N HCl. The quantity of nitrogen present in the sample was calculated from the volume of HCl consumed: 1 mL 0.01 N HCl = 0.14 mg nitrogen.

3.4.3 Treatment of biomass and productivity data

To quantify the gradual accumulation over time of cells and PRN, population growth and protein productivity was done by means of a "cumulative volumetric cell-hours" approach, which quantifies biomass on a cumulative basis (Dutton *et al*., 1998). The cumulative volumetric cell-hours (CH_{VOL}) is defined as:

$$CH_{VOL} = \sum_{i=0}^{f} \frac{(x_{i+1} - x_i)}{ln\,(x_{i+1}/x_i)} (t_{i+1} - t_i) \qquad (3.7)$$

where x_i is the cell concentration at t_i hours of the culture. The specific productivity is estimated by the ratio of the final product concentration (PRN) divided by the cumulative volumetric cell-hours. In this work, "cells" are measured as optical density (x in equation 3.7):

$$sPRN = \frac{[PRN]}{CH_{VOL}} \tag{3.8}$$

where *sPRN* is the specific productivity of PRN in μg/mL/OD-hour, *[PRN]* is concentration of PRN in μg/mL measured by ELISA, CH_{VOL} is calculated from equation 3.7.

3.5 Glutamate determination

Glutamate concentrations were measured using a BioProfile-FLEX Analyzer (Nova Biomedical). Samples were centrifuged at 15,000 *xg* for 10 min. 1 mL of the supernatant was taken and analyzed.

3.6 Catalase activity

Catalase activity was determined according to Iwase *et al.* (2013). Reagents were 35% w/w H_2O_2 (Sigma-Aldrich, USA), 1% Triton X-100 (EMD Millipore Corporation, USA) and 10 mM phosphate buffer saline (PBS) at pH 7.4. Sodium azide (Sigma-Aldrich, Canada) at a concentration of 10 μM was used as inhibitor of catalase activity. Samples were incubated at 37°C in 10mm x 75mm culture tubes (Fisher Scientific, Canada). Each tube contained 100 μL of sample, 100 μL of Triton X-100 and 100 μL of 35% H_2O_2. The method is based on the detection of molecular oxygen (O_2), produced after the dismutation of H_2O_2 that remains trapped in the surfactant (Triton X-100). The foam produced is proportional to the amount of active catalase present in the sample. The assay was done with a negative

control (10 μM sodium azide as a catalase inhibitor Iwase *et al.* (2013)) that did not show any foam formation confirming the specificity of the assay under the conditions employed.

For catalase activity in NaOH, two solutions were compared: one tube with 10 μL of a solution of catalase in 10 mM PBS and one tube with 10 μL of a solution of catalase in 5 N NaOH. In each tube, 90 μL of 10mM of PBS was added to reach a final volume of 100 μL. Secondly, 100 μL of 1% Triton-X were added and finally, 100 μL of 35% H_2O_2.

Chapter 4

Comparison of Flow Cytometry and Spectrofluorometry for the Analysis of ROS

4.1 Introduction

The central role that the measurements of ROS play in the current work motivated a study to assess their reliability. In this chapter, a comparison is conducted between flow cytometric and fluorometric measurements of ROS using DCFDA, H_2DCFDA and carboxy-H_2DCFDA, which are three dichlorofluorescein variants used for ROS detection. The aim of this analysis was to investigate whether both methods provide consistent results. It should be remembered that while spectrofluorometry provides a dominant fluorescence peak that correspond to an average ROS level in the cells, flow cytometry provides a distribution of ROS levels across the cell population. Thus, to compare both measurements it was required to obtain a lumped quantity that is representative of the flow cytometry distribution that can be used for comparison to the spectrofluorescence measurements. Two different lumped quantities are investigated in this chapter: the median and the weighted average of the flow cytometry distribution. The experiments for comparing spectrofluorometry and flow cytometry were done in control flasks and flasks that were treated with H_2O_2 at different concentrations.

4.2 Preliminary results with DCFDA

The first dye that was tested for ROS detection was 2′,7′-dichlorofluorescein diacetate (DCFDA). DCFDA penetrates the cell membrane and is deacetylated by esterases to dichlorofluorescin (DCFH).

This non-fluorescent product is converted by reactive oxygen species (ROS) into fluorescent DCF which remains trapped in the cells. An experiment with shake flasks was done to test DCFDA measurements with both methods. 7 flasks were run, and H_2O_2 was added at different concentrations at 24 h: 350 μM, 400 μM, 450 μM, 500 μM, 550 μM, 600 μM, and control (no addition of H_2O_2). Samples were taken at 0 h, 24 h, 31 h, and 48 h for flow cytometric and spectrofluorometric analysis.

The DCF signal was detected at an excitation/emission of 500/520 nm. In the flow cytometer, the signal was detected in the green channel (FL1) with a band filter of 526/48.

Figure 4-1 shows the results obtained with both techniques where the DCF intensity at 500/520 nm is used for spectrofluorescence and the median of the distribution is used to quantify the flow cytometry results.

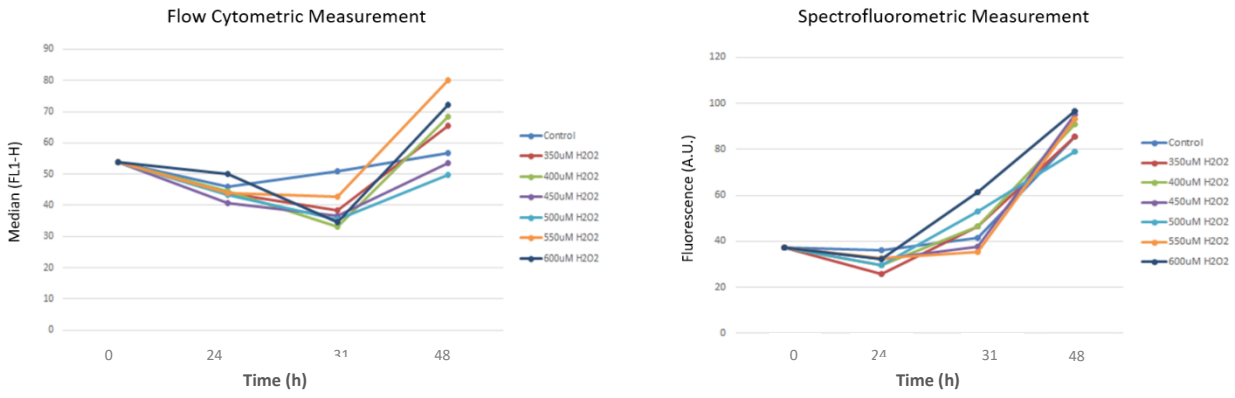

Figure 4-1 Flow cytometric and spectrofluorometric results for flasks with addition of different concentrations of H_2O_2.

From these plots it was observed that the correlation between both results was not clear, especially at time 31 h where it seems to be an inverse correlation between both techniques. It was hypothesized that discrepancies between both techniques are possibly related to the effect of fluorescence quenching.

The term "quenching" refers to factors that reduce intensities, such as:

- High concentration of the sample: when cell concentration is too high, the light cannot pass through the sample to cause excitation, thus highly concentrated samples exhibit very low fluorescence.
- Collisions among molecules: it results in a loss of excitation energy in the form of heat instead of as emitted light.
- Formation of a complex between the fluorophore and the quencher (static quenching): a special case of static quenching is self-quenching, where the fluorophore and the quencher are the same species. Self-quenching is particularly evident in concentrated solutions.
- Resonance energy transfer: In this case, the two participating molecules do not have to collide and the interaction can occur over distances of 100Å. When a molecule is excited, this excitation is transferred to another molecule, without emitting light. As a result, the acceptor molecule remains excited while the donor stays in the ground state (Elshereef, 2009).

4.3 Experiment to test quenching

For assessing the effect of quenching, a fluorescence experiment was done. A sample was taken at the end of the fermentation and centrifuged (15,000 xg, 3 min) to discard the supernatant. Cells were washed and resuspended in 10 mM PBS to an OD 0.1. Cells were incubated with DCFDA at a concentration 50 μM for 1 h at room temperature, protected from light. After the fluorescence was

recorded for the first time, the same sample was progressively diluted and the corresponding fluorescence was recorded again. The results are shown in Figure 4-2

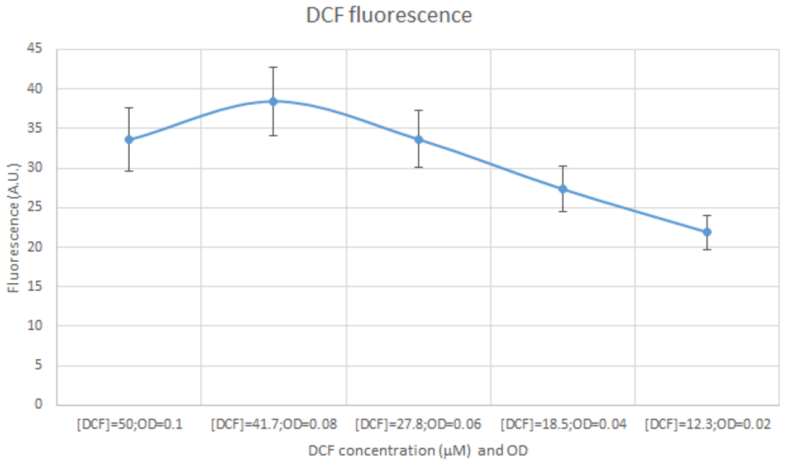

Figure 4-2 DCF Fluorescence emission at different concentrations. In the x-axis is shown the concentration of DCF and OD of cells, and in the y-axis is shown the fluorescence of cells measured at 600 nm.

In Figure 4-2, it is clear that from OD 0.1 to OD 0.08 there was quenching because the fluorescence intensity increased even though the dilution increased and thus there was a smaller quantity of cells. Beyond an OD 0.08 there was no quenching since the fluorescence started to decrease proportional to the dilution.

On the other hand, inspecting the graphs (Figure 4-3 A) for the flow cytometric data for control and 600 µM H_2O_2, it appears that the cells in the control sample have more ROS since the distribution is shifted to the right. To explain this, a correlation between the number of cells in the region located before of the peak of the distribution (marked in red) and the behavior seen in the fluorometer (Figure 4-3 A and B) was found. It is possible that intensities beyond this peak were quenched.

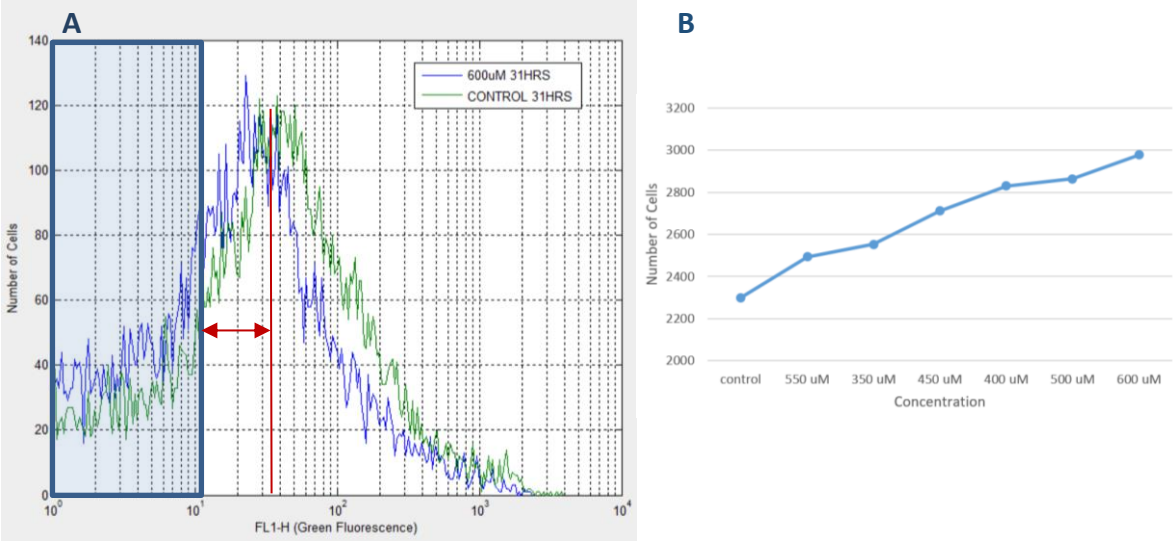

Figure 4-3 A- Histogram graphs for samples from flasks at 31 h from control and with H_2O_2 addition. B- Number of cells before the intersection point between the two curves vs concentration of H_2O_2 added. The blue region in A represents the unstained cells, and the double red arrow indicates the region of the distribution taken before the intersection of both curves and used for figure B.

Since the measurements obtained from the spectrofluorometer are an average of the fluorescence emission of all fluorophores in the sample it was hypothesized that the median may not be a representative averaging of the flow cytometry distribution for comparison with the fluorescence results. Thus, to find a better correlation between flow cytometry and fluorescence results, the use of a "weighted average" for the distributions obtained from the flow cytometry was investigated as a possible better lumped quantification of cytometry for comparison to fluorescence.

The weighted average was calculated using Equation 4.1

$$WA = \sum_i^f \frac{C_i}{C_t} * I_i \tag{4.1}$$

Where C_i is the number of cells that have fluorescence intensity I_i, and C_t is the total number of cells analyzed.

The results are shown in Figure 4-4

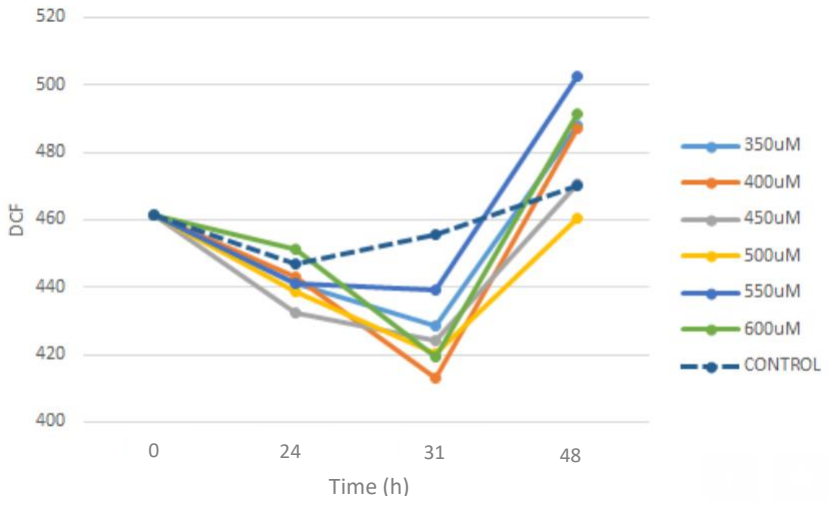

Figure 4-4 Weighted average for flasks treated with different H_2O_2 concentrations.

From Figure 4-4, one can appreciate that the trending for the weighted average is similar to the trend obtained with the median of the distributions and it is still not correlated with the fluorescence measurements.

At this point another set of experiments were done with other types of reagents in an attempt to eliminate quenching and find a better correlation between fluorescence and flow cytometry. Different dilutions were tried with H_2DCFDA, carboxy-H_2DCFDA and again with DCFDA, for cells sampled at time 50 h (harvest), and fluorescence. The results are shown in Figure 4-5.

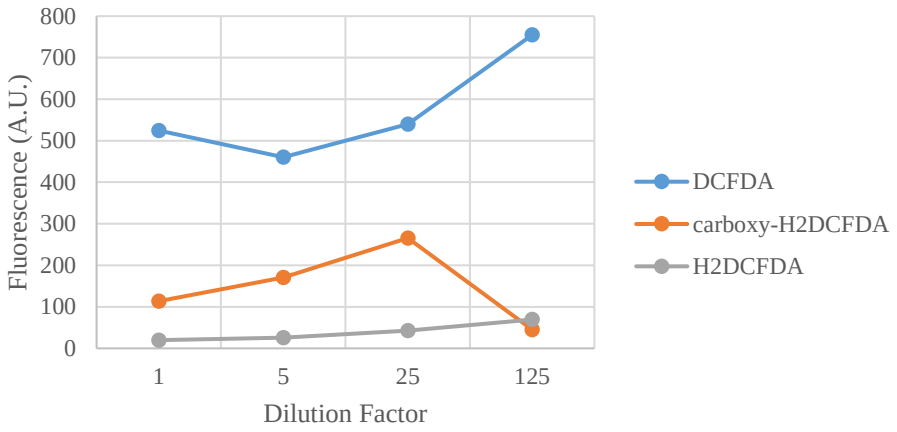

Figure 4-5 Fluorescence for cells treated with DCFDA, carboxy-H_2DCFDA and H_2DCFDA. Dilution factor equal to 1, refers to concentration of dye of 50 μM and OD 0.1.

Among the three dyes tested, the expected reduction of the fluorescence as a function of increasing dilution was only observed for carboxy-H_2DCFDA. Hence, this dye was chosen for further use since it was the only one that exhibited the correct behavior as a function of increasing dilutions. Figure 4-6 shows other dilutions tested for carboxy-H_2DCFDA, and a dilution factor DF 80 was chosen for the flasks experiments because it seems that for that dilution there is no quenching.

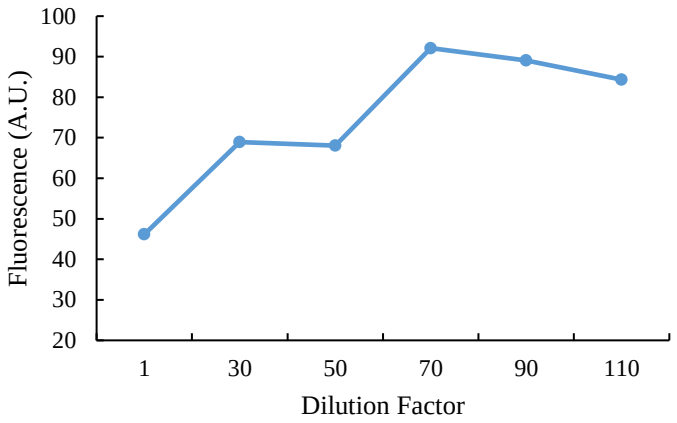

Figure 4-6 Fluorescence of cells treated with carboxy-H_2DCFDA at different dilutions.

Figure 4-7 shows the flow cytometry weighted averages and the spectrofluorometer intensities results for samples from the flasks treated with 600 μM of H_2O_2 at 4 h and 24 h.

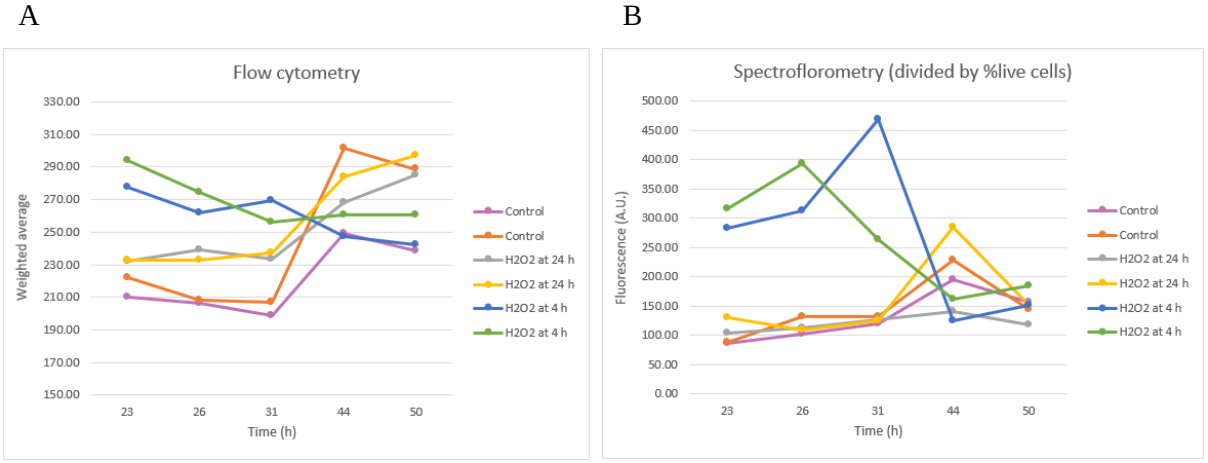

Figure 4-7 Flow cytometry (A) and fluorescence (B) results for flasks treated with 600 μM H_2O_2 at 4 h and 24 h. For these measurement, carboxy-H_2DCFDA was used to detect intracellular ROS.

In Figure 4-7 B, the values were divided per % of live cells because carboxy-H_2DCFDA should react only in live cells.

The results with carboxy-H_2DCFDA for both techniques appeared to be well correlated with each other since the trends are very similar. This is evident from the coinciding ordering of the measurements at each time point during the batches. For this reason, the rest of the analyses were done using the aforementioned dye. It has been reported that carboxy-H_2DCFDA is better retained inside the cells compared to non-carboxylated forms (ThermoFisher (2006). *Reactive Oxygen Species (ROS) Detection Reagents*. Retrieved from https://assets.thermofisher.com/TFS-Assets/LSG/manuals/mp36103.pdf).

Chapter 5

Impact of Oxidative Stress on Protein Production by *Bordetella pertussis* for Vaccine Production

5.1 Abstract

Fluorescence spectroscopy and flow cytometry were employed to assess the response of *Bordetella pertussis* to induced oxidative stress during fermentation. *B. pertussis* is the causal agent of whooping cough in humans and purified pertactin (PRN) is used as one of the components in the production of acellular pertussis vaccines. When grown in bioreactors, bacteria adapt to environmental conditions which may include high levels of reactive oxidative species (ROS) that stress cells and can have detrimental effects on growth and protein production. By employing fluorescence spectroscopy and flow cytometry, it was possible to track ROS that are commonly attributed to oxidative stress and relate these measurements to PRN production. Oxidative stress was imposed using hydrogen peroxide addition in both flask and bioreactor studies. The results indicate a clear detrimental effect of oxidative stress on PRN productivity and cell growth, and also a significant correlation between oxidative stress and the level of extracellular NADPH. The results also showed long term adaptation of cells to stress whereby the growth rate increases after the cells are exposed to oxidative stress for a sufficiently long time. Furthermore, differences in this adaptation behavior between flask and bioreactor operations are identified and explained.

Keywords: *Bordetella pertussis*, flow cytometry, fluorescence spectroscopy, oxidative stress, pertactin.

Abbreviations: 5CP, five component pertussis; AKGDH, alpha-ketoglutarate dehydrogenase; cDCFDA, carboxy-2′,7′-dichlorofluorescein diacetate; CH_{VOL}, volumetric cell-hour; DMSO, dimethyl sulfoxide ; DO, dissolved oxygen; Ex, excitation; Em, emission; FAD, flavin adenine dinucleotide; FCM, flow cytometry; FHA, filamentous hemagglutinin; FIM2 and FIM3, fimbriae units; LP, long pass filter; lpm, liters per minute; FSC, forward scattering; MSG, monosodium glutamate; NADH, nicotinamide adenine dinucleotide; NADPH, nicotinamide adenine dinucleotide phosphate; OD, optical density; PBS, phosphate buffer saline; PCA, principal component analysis; PLS, partial least squares; PMT, photomultiplier tube; PRN, pertactin; PT, pertussis toxin; rpm, revolutions per minute; ROS, reactive oxygen species; sPRN, specific productivity of PRN in μg/mL/OD-hours; SSC, side scattering.

5.2 Introduction

Bordetella pertussis is a Gram-negative bacterium responsible for causing whooping cough in humans; a respiratory tract disease characterized by strong coughing fits. Cellular and acellular vaccines have been developed to control this infection but acellular vaccines are preferred due to fewer side effects. Acellular vaccines are composed of antigens, or virulence factors, but no whole cells. Existing pertussis vaccines are based on one antigen (pertussis toxin or PT), two antigens (PT and filamentous hemagglutinin (FHA)) or five antigens, called five component pertussis (5CP): PT, FHA, pertactin (PRN) and two fimbriae units (FIM2 and FIM3) (Warfel *et al.*, 2015).

The production of the 5CP acellular vaccines involves two main processing steps: i- upstream fermentation where bacteria are grown in a train of reactors of increasing volume; and ii- downstream purification where the five antigens are purified in a series of centrifugation and filtration steps and combined into the final product after being processed for quality control.

Different monitoring approaches have emerged in the field of bioprocessing (Lourenço *et al.*, 2012; Oh *et al*., 2013; Carrondo *et al*., 2012). In a previous work by the authors (Zavatti *et al.*, 2016), the entire manufacturing process of a 5CP acellular vaccine process was monitored by means of fluorescence spectroscopy combined with multivariate statistical methods to detect possible sources of the variability observed in the final PRN yield. This approach takes advantage of the intrinsic fluorescent properties of molecules to enable the detection of different compounds along the process train. Among these compounds were amino acids such as phenylalanine, tyrosine and tryptophan, and cofactors such as NADPH and FAD. The presence of NADPH-enzyme complexes could be detected as a shift in excitation-emission (Ex/Em) of NADPH from its adenine moiety (Gazzotti *et al.*, 1974). The main source of variability for PRN was attributed to the upstream fermentation steps based on the observed accumulation of an NADPH-enzyme complex in batches with low PRN yield. It was hypothesized that under oxidative stress cells attempt to increase the amount of NADPH as this co-factor is key in creating the reductive environment to minimize this stress (Puri, 2011).

Oxidative stress begins when cells are not sufficiently capable of scavenging reactive oxygen species (ROS) or counterbalance their production (Betteridge, 2000). The ROS intermediates are inevitable by-products of aerobic metabolism. Specifically, the use of oxygen to oxidize nutrients for obtaining energy through respiration generates superoxide (O_2^-), hydroxyl radicals (OH^-), and hydrogen peroxide (H_2O_2). At low concentrations, these radicals are beneficial as they serve as a defense against external agents that can be detrimental to the cells, and play an important role in cell signaling and energy metabolism (Li, 2013). At concentrations where antioxidant defenses are overwhelmed, ROS are harmful to cells causing damage to proteins, DNA and lipids (Rui *et al.*, 2010). In general, ROS can damage all types of biological molecules (Dalle-Donne *et al*., 2003).

Superoxide promotes hydroxyl-radical formation, which would accelerate DNA and protein damage by leaching iron from storage proteins or enzymatic clusters (Keyer *et al.*, 1996). *B. pertussis* uses

several enzymes to offset ROS such as superoxide dismutase, catalase, glutathione synthase, and glutathione reductase (Graeff-Wohlleben *et al*., 1997). Since ROS is generated in response to different factors occurring during batch/fed-batch operation, it is important to control the level of oxidative stress to better understand and quantify its impact on growth and productivity. Previous research has considered externally triggered oxidative stress so that impact could be studied under relatively controlled conditions (Zheng *et al*., 2009; Abrashev *et al*., 2011). H_2O_2 is a mild means of triggering oxidative stress that can elicit inhibitory responses of certain key enzymes in the TCA cycle such as aconitase and α-ketoglutarate dehydrogenase (Miller *et al*., 2001).

Confirmation of cell degradation by oxidative stress is important not only because it affects the quantity of biomass, but also proteolysis within and possibly outside the cells due protein modification through oxidation (Miller *et al.*, 2001; Rolfe *et al*., 2012). An understanding of the effect of oxidative stress is expected to explain the observed variability in the protein yield and to suggest ways to reduce this variability. Furthermore, experiments with *a priori* known oxidative stress conditions serve to validate the measurements that correlate with this stress. The measurements used to assess stress were: NADPH, catalase, and ROS. The impact of oxidative stress on productivity of pertactin was also assessed.

B. pertussis is a resilient organism that can persist in the human body for at least 4 weeks and has the ability to adapt and survive harsh conditions for prolonged periods (Nakamura *et al.*, 2006). However, in comparison to other pathogens like *Escherichia coli*, it is neither a fast nor efficient grower *in vitro*. It exhibits low tolerance to conditions occurring during the stationary growth phase thus resulting in low yield of some of the proteins that are used in acellular vaccine formulations (Nakamura *et al.*, 2006). Following our previous research (Zavatti *et al.*, 2016) which found low productivity in batches with high extracellular concentrations of NADPH, it was hypothesized that oxidative stress known to be correlated to NADPH production (Singh *et al.*, 2007; Grose *et al.*, 2006), is a possible source of

variability in productivity of pertactin during the vaccine manufacturing process. To investigate this hypothesis, the current study focuses on the impact of externally imposed oxidative stress with two main goals: i- to quantify the resulting oxidative stress with appropriate indicators; and ii- to determine if the response to imposed oxidative stress was similar under different culturing conditions to address productivity issues at industrial scale.

The results of this study indicate that oxidative stress along the course of a fermentation train significantly affect the yield of pertactin and thus could partially explain the observed batch to batch variability in the production environment. Moreover, it was found that the culture can adapt over time to oxidative stress. It was also found that this adaptation mechanism has different dynamics depending on whether growth occurs in shake flasks without oxygen control versus bioreactors operated with closed-loop oxygen control. The mechanistic basis of these differences is discussed.

5.3 Materials and Methods

5.3.1 Samples

Samples were collected from fermentations performed at the laboratory facilities of Sanofi Pasteur (Toronto, Ontario, Canada). Fermentations were run in 250 mL shake flasks, 2 L and 20 L fermenters. For shake flasks experiments, flasks were run with a working volume of 100 mL, incubated at 36°C, 200 rpm for 50 h. Each flask was run in duplicate. Oxidative stress was imposed with 600 μM of H_2O_2 (final concentration in the culture) introduced at either 4 h or 24 h from the start of the culture. For the 2 L fermentations, two fermentations were run in separate 2 L BiosStat Bplus (Sartorius Stedim) bioreactors with a working volume of 1.3 L. All fermentations were conducted at 36°C, pH 7.2, agitation from 100-678 rpm (Rushton impeller) and a constant airflow of 0.5 lpm. The dissolved oxygen (DO) was constantly maintained by a sequential control strategy that manipulated the agitation rates

against a constant aeration rate to a DO set-point. The operating conditions for each reactor were: i- 35% DO and initial OD 0.3 for the control reactor; and ii- 35% DO, initial OD 0.3 and 600 μM H_2O_2 added at 4 h. For the 20 L fermentations, two fermentations were performed in 20 L BiosStat Cplus (Sartorius Stedim) bioreactors with a working volume of 13 L. All fermentations were conducted at 36 °C, pH 7.2, agitation from 100-700 rpm and a constant airflow of 0.6 lpm. The DO was constant employing a cascade control as for the 2 L fermentations. The operating conditions for each reactor were: i- 35% DO and initial OD 0.3 for the control reactor; ii- 35% DO, initial OD 0.3 and 600 μM H_2O_2 added at 4 h.

For all experiments, sampling was performed during the course of the fermentation. OD was measured at 600 nm. Samples collected were centrifuged (10,000 *x g*, 3 min, 4°C), the pellet was resuspended to OD 0.05 in 10 mM PBS and used for flow cytometric analysis. The supernatant was used in fluorometric analysis. The final antigen PRN yield was measured by ELISA test. Analyses were done in triplicates.

5.3.2 Pertactin determination

The final quantity of PRN released by bacteria at the end of fermentation was determined by ELISA test. Microplates were coated with 50 μL/well of 1.5 μg/mL PRN polyclonal antibodies purified from guinea pig. Plates were incubated at room temperature for 20 h. After incubation, plates were washed three times with 200 μL/well of a solution containing 10 mM PBS, 0.1% Tween 20 and 0.1% BSA, and blocked for 30 min at room temperature with 100 μL/well of 10 mM PBS and 0.1% BSA. After blocking, the plates were washed again two times with 200 μL/well of a solution containing 10 mM PBS, 0.1% Tween 20 and 0.1% BSA. Samples were centrifuged and filtered with a 0.2 μm filter. The filtered supernatants were diluted, added to the wells and incubated for 1 h at room temperature. After incubation, the plates were washed with the PBS-Tween 20-BSA solution. 100 μL of guinea pig anti-

PRN antibody conjugated to horseradish peroxidase was added to each well and plates were incubated for 1 h at room temperature. Plates were washed again and 100 μL/well of a mixture of 1 mL of 10 mM tetramethylbenzidine and 9 mL of 0.004% (v/v) H_2O_2 was added and incubated for 30 min at room temperature. The reaction was stopped with 50 μL/well of 2 N H_2SO_4 and absorbance was measured at 450 nm. The amount of absorbance was proportional to PRN content. The concentration was calculated based on a standard curve.

5.3.3 Biomass and productivity data treatment

To quantify the gradual accumulation over time of cells and pertactin, population growth and protein productivity was done by means of a "cumulative volumetric cell-hours" approach, which quantifies biomass on a cumulative basis (Dutton *et al.*, 1998). The cumulative volumetric cell-hours (CH_{VOL}) is defined as:

$$CH_{VOL} = \sum_{i=0}^{f} \frac{(x_{i+1} - x_i)}{ln\,(x_{i+1}/x_i)} (t_{i+1} - t_i) \tag{5.1}$$

where x_i is the cell concentration at t_i hours of the culture. The specific productivity is estimated by the ratio of the final product concentration (PRN) divided by the cumulative volumetric cell-hours. In this work, "cells" are measured as optical density (x in equation 5.1):

$$sPRN = \frac{[PRN]}{CH_{VOL}} \tag{5.2}$$

where *sPRN* is the specific productivity of PRN in μg/mL/OD-hour, *[PRN]* is concentration of PRN in μg/mL measured by ELISA, CH_{VOL} is calculated from equation (5.1).

5.3.4 Glutamate Determination

Glutamate concentration was measured with a BioProfile-FLEX Analyzer (Nova Biomedical). Samples were centrifuged at 15,000 *xg* for 10 min. 1 mL of the supernatant was taken and analyzed.

5.3.5 Fluorometric Analyses

Fluorometric analyses were performed to track the appearance of NADPH during fermentation. Fluorescence excitation-emission spectra were acquired using a Cary Eclipse Fluorescence Spectrophotometer (Agilent Technologies) in polymethylmethacrylate cuvettes. The PMT voltage was 700V and the slit width for both excitation and emission was 5 nm. These parameters were optimized to obtain good signal, reproducibility, and to avoid quenching. The excitation and emission ranges were 250-400 nm and 360-500 nm, respectively.

5.3.6 Catalase Activity

Catalase activity was determined according to Iwase *et al*. (2013). Reagents were 35% w/w H_2O_2 (Sigma-Aldrich, USA), 1% Triton X-100 (EMD Millipore Corporation, USA) and 10 mM phosphate buffer saline (PBS) at pH 7.4. Sodium azide (Sigma-Aldrich, Canada) at a concentration of 10 μM was used as inhibitor of catalase activity. Samples were incubated at 37°C in 10 mm x 75 mm culture tubes (Fisher Scientific, Canada). Each tube contained 100 μL of sample, 100 μL of Triton X-100 and 100 μL of 35% H_2O_2. The method is based on the detection of molecular oxygen (O_2), produced after the dismutation of H_2O_2 that remains trapped in the surfactant (Triton X-100). The foam produced is proportional to the amount of active catalase present in the sample. The assay was done with a negative control (10 μM sodium azide as a catalase inhibitor (Iwase *et al.*, 2013; Chelikani *et al.*, 2004)) did not show any foam formation confirming the specificity of the assay under the conditions employed.

5.3.7 Flow cytometric analyses

5.3.7.1 Reagents

Oxidative stress was assessed by means of ROS detection. Carboxy-2′,7′-dichlorofluorescein diacetate (cDCFDA) was from Sigma-Aldrich (Canada). A 10 mM of cDCFDA stock solution was prepared dissolving it in dimethyl sulfoxide (DMSO) to a final concentration per sample of 50 μM. The incubation time was 1h at room temperature and protected from light. After incubation, cells were analyzed and the fluorescence signal was detected using the FL1 green fluorescence channel in the flow cytometer.

5.3.7.2 Equipment

Flow cytometric analyses were performed using an S3e Cell Sorter (Bio-Rad). The instrument was equipped with two excitation lasers 488 nm (primary) and 640 nm (secondary), and emission filters for forward scattering (FSC) and side scattering (SSC) detection (488/6 band width filters), and fluorescence emission detection: 526/48 (FL1), 593/40 (FL2), 670/30 (FL3) and 700 LP (FL4). The voltages and gates were set using an unstained control. The total number of events per sample were 10,000 at a rate of 1,600-2,000 events/sec.

5.3.7.3 Flow cytometric data analysis

The average level of ROS in the cell population was determined using a weighted average (*WA*) as per the following equation:

$$WA = \sum_i^f \frac{C_i}{C_t} * I_i \tag{5.3}$$

Where C_i is the number of cells that have fluorescence intensity I_i, and C_t is the total number of cells analyzed.

5.3.8 Statistical analysis

Statistical significance was assessed using one-way ANOVA $p < 0.05$ conducted using Minitab 17.1 (Minitab, Inc.) statistical software.

5.4 Results and Discussion

5.4.1 Hydrogen peroxide addition and impact on viability, and NADPH in flasks

The impact of H_2O_2 on oxidative stress, growth (based on OD) and productivity (based on PRN yield) was investigated in batch cultures (flasks) by measuring NADPH, ROS and PRN production. Flask experiments were conducted in duplicate adding 600 μM H_2O_2 (final concentration) either at 4 h or 24 h. The growth measured in terms of OD is shown in Figure 5-1

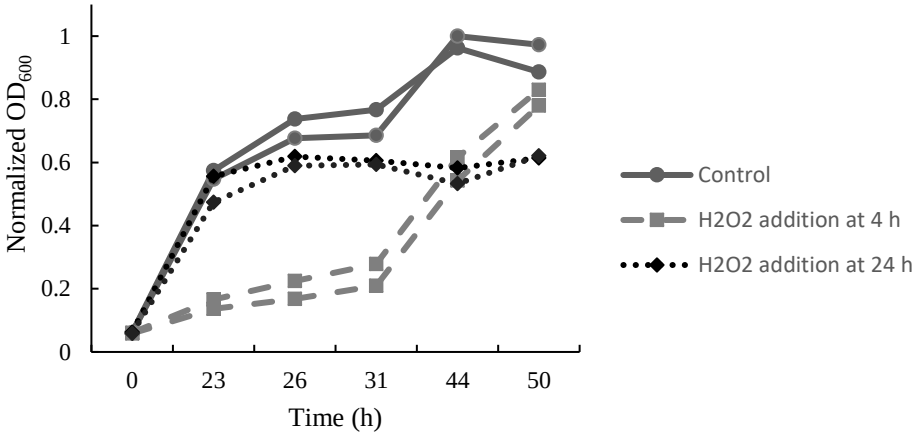

Figure 5-1 Growth of *B. pertussis*. Lines of same pattern show two distinct flasks for each condition. Values were scaled with respect to maximum observed OD.

As shown in Figure 5-1 H_2O_2 addition for all cultures resulted in an immediate decrease in growth rate compared to the control cultures. A noticeable difference was observed according to the time when the addition occurred. For flasks where H_2O_2 was added at 4 h, there was a significant recovery in growth rate after approximately 31 h. This corroborates the occurrence of adaptation to oxidative stress after some time elapsed after the introduction of a stressor a previously reported for *E. coli* (Rui *et al.*, 2010; Farr *et al*., 1991; Lushchak, 2011). It can be argued that the earlier addition of peroxide at 4 h occur within the lag phase. It has been reported that during the lag phase, the necessary enzymes needed for survival in the new environment are built (Barrière *et al.*, 2002) and that, following the imposition of a new stressor, bacteria develop mechanisms to cope with the new environment. On the other hand when H_2O_2 was added at 24 h, cells were at the exponential phase and they were more sensitive to stress as reported in Aldsworth *et al*. (1999). In the current work it was observed that growth was arrested after the addition of H_2O_2 (Figure 5-1) at 24h that might signify that cells cannot adapt to the new environment.

Beyond the observed differences in growth and the differences in cumulative cell hours between the different batches, there were corresponding differences in productivity. For example, the specific productivity of PRN (*sPRN*) released from bacteria treated with H_2O_2 at 4 h was 0.0366 μg/mL/OD-hour compared to 0.0421 μg/mL/OD-hour for the control culture. Thus, *sPRN* value in control flasks was higher than the flasks treated with H_2O_2. The total quantity of PRN released in the flasks treated at 24 h was 22% less than the control culture.

Another marked difference between the control and the peroxide treated cultures is that for the latter cultures high levels of extracellular NADPH per OD unit were observed as shown in Figure 5-2 A.

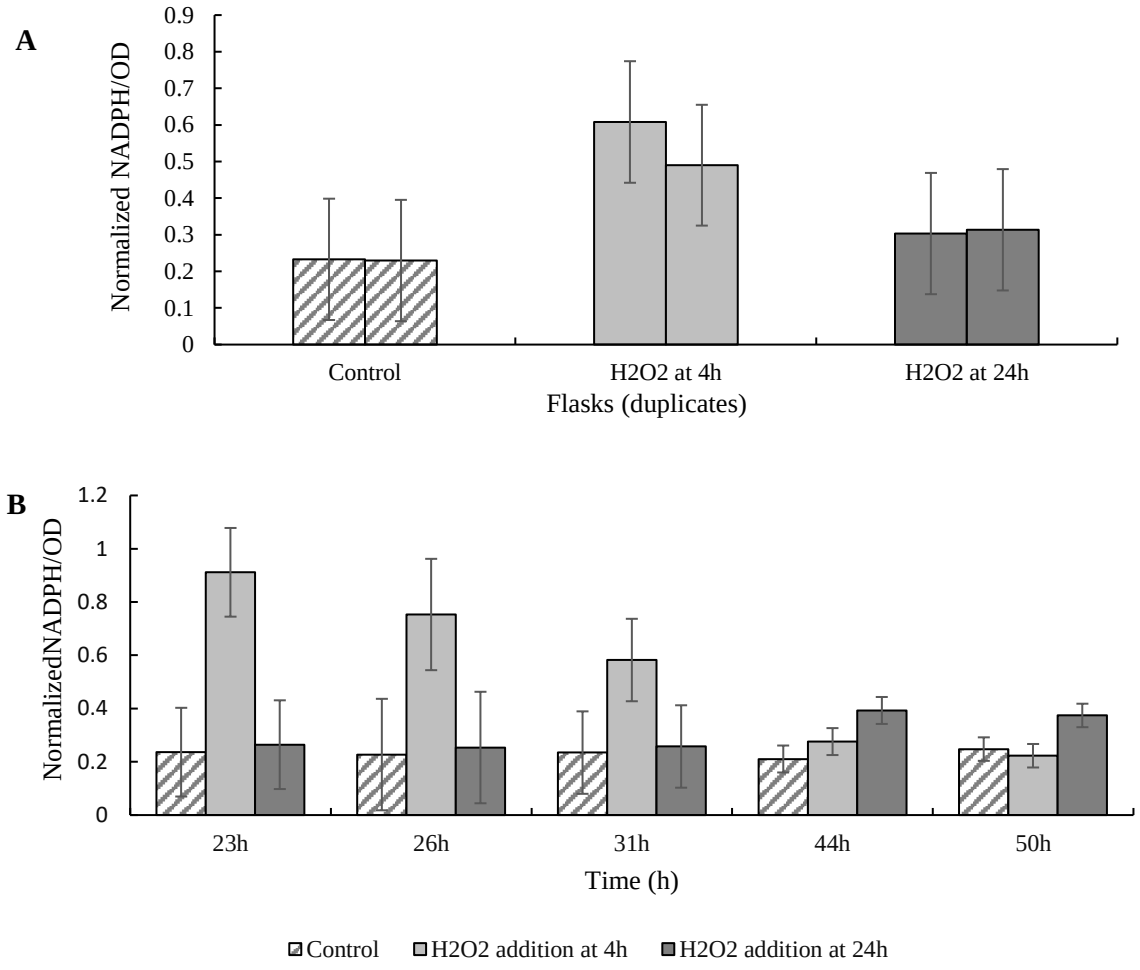

Figure 5-2 ANOVA of NADPH per OD unit for control flask and cells exposed to 600μM H_2O_2 at 4 h and 24 h ($p<0.05$). A- Average of measurements collected at different times for each flask. B- Average of measurements at 23 h, 26 h, 31 h, 44 h and 50 h from the start of the cultures. Bars show 95% confidence intervals. Values were scaled with respect to the maximum value in the data set.

As showed in Figure 5-2 B, in response to the addition of peroxide at 4 h within the time interval of 23 h through 36 h the NADPH production per OD unit was statistically significantly higher ($p<0.05$) as compared to the control culture and the culture spiked with H_2O_2 at 24 h. Cells treated with H_2O_2 at 4 h show a clear decrease of NADPH per OD unit towards the end of the culture which correspond to

the observed recovery in growth rate for that culture indicating the ability of the cells to cope with the oxidative stress imposed earlier. This fact is again attributed to a mechanism of adaptation that was not observed in cells treated with the H_2O_2 at 24 h.

These experiments verified that increased levels of NADPH are observed under conditions of increased oxidative stress. NADPH synthesis increases in an attempt to reduce the levels of ROS, since NADPH provides a reductive environment necessary to scavenge these species (Singh *et al*. 2007; Bériault *et al*., 2007) as opposed to NADH production that is geared to ATP generation. It has been previously found by the authors of this work (Zavatti *et al*., 2016) that high levels of NADPH correlated with low PRN production by *B. pertussis*. NADPH fluorescence occurred at an emission of 460 nm and excitation of 280 nm with the latter is slightly shifted with respect to the commonly reported excitation of 260 nm for NADPH free in solution. NADPH absorbs at two excitation wavelengths, 260 nm and 340 nm, with an emission at 460 nm. The excitation at 260 nm is due to the adenine group and the peak at 340 nm corresponds to the absorption by the pyridine ring (Rover *et al*., 1998). Also, NADPH has the same Ex/Em as NADH (Lakowicz, 2006). When bound to a protein, the excitation at 260 nm is shifted to 280 nm (Gazzotti *et al*., 1974) similar to what was observed in the current study.

NADH and NADPH fluorescence has been employed to study binding to proteins. When bound to a protein, NAD(P)H exhibits an extended conformation, which prevents quenching of the pyridine ring by the adenine group. As a result, the emission intensity is higher compared to NADPH in its free form. Also, due to the binding, there can be quenching of tryptophan present in the protein (Lakowicz, 2006).

Certain anti-oxidative enzymes utilize NADPH as cofactor, such as catalase and thioredoxin reductase (Kirkman *et al*., 1984; Pannala *et al.*, 2015). There are three types of catalase: i- monofunctional catalase; ii- bifunctional catalase-peroxidase; and iii- Mn-containing catalase (Barrière *et al.*, 2002). The protective function of catalase is a result of the heme moieties that detoxify H_2O_2 producing oxygen and water (Chelikani *et al*., 2004; Barrière *et al.*, 2002). NADPH has a protective

effect on the enzyme, but the lack of this cofactor renders the enzyme less effective but without inactivating it (Kirkman *et al.*, 1984). *B. pertussis* has a gene encoding catalase (*katA*) that is believed to confer protection against ROS produced during respiratory bursts (DeShazer *et al*., 1994).

It is hypothesized that for cells exposed to H_2O_2 at 4 h, a reductive environment is created by *B. pertussis* through increased catalase production as the fermentation proceeds. There is evidence that Gram-negative bacteria, such as enterohemorrhagic *Escherichia coli*, can secrete catalase into the environment to fight host ROS once they are phagocytized by a macrophage (Wan *et al*., 2017). For example, the Gram-positive bacterium *Bacillus subtilis* can secrete catalase into the broth milieu when it is under oxidative stress triggered by the addition of ethanol and H_2O_2 (Yao *et al*., 2009). Although following the injection of H_2O_2 at 4 h the cell growth is very low, it eventually recovers towards the latter stages of the culture while NADPH decreases likely due to reactions with oxidative species (Figure 5-1).

To determine if the observed shift in NADPH stems from the binding of NADPH to catalase, the latter was measured. Using this, it was possible to verify the presence of catalase that has been released by the cells into the supernatant while a small quantity or almost imperceptible amount of the enzyme was detected in the cells (the amount of foam observed in the supernatant was 4 times higher than the amount observed in the cells).

To further quantify the level of ROS intracellular cDCF measurements were conducted by cytometry and the corresponding weighted averages for the different cultures are shown in Figure 5-3. cDCFDA is permeable to the cell. It has been reported that once in the cell, cDCFDA is hydrolyzed to cDCFH and trapped within the cells. The non-fluorescent cDCFH is then converted to the fluorescent cDCF after oxidation by H_2O_2 and other oxygen derivatives (Halliwell *et al*., 2004). For cells treated at 4 h, cDCF intensities were higher during the first 31 h, where cells started to show some recovery reflected

in the OD measurements. Conversely, cells treated with peroxide at 24 h, showed an increase in the level of ROS until the end of the fermentation.

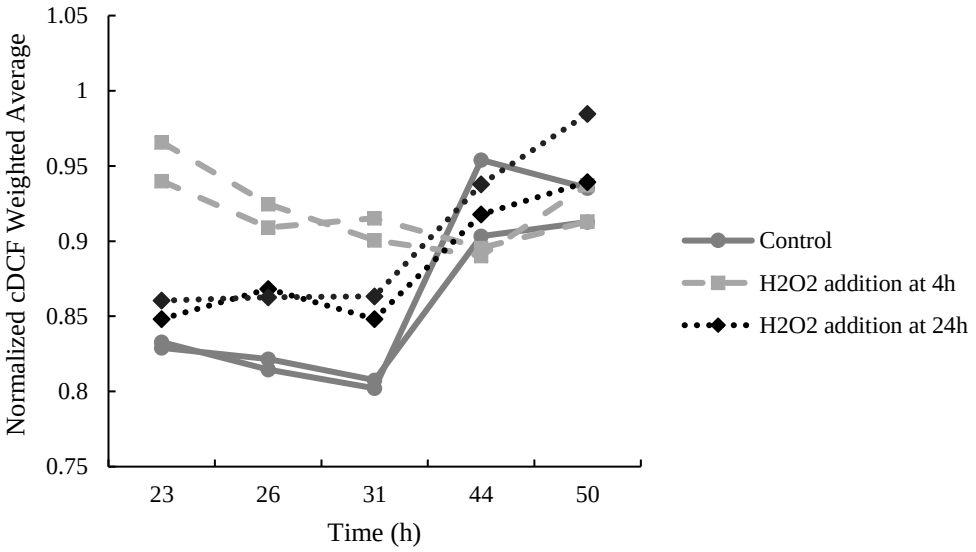

Figure 5-3 Weighted average of cDCF in cells. Values were scaled with respect to the maximum value in the data set.

Figure 5-4 shows ANOVA results for the average of the total measurements at different times of the culture for each flask (Figure 5-4 A) and time point (Figure 5-4 B). There is a significant difference ($p<0.05$) among the averages, where cells treated at 4 h appeared more affected by the peroxide addition.

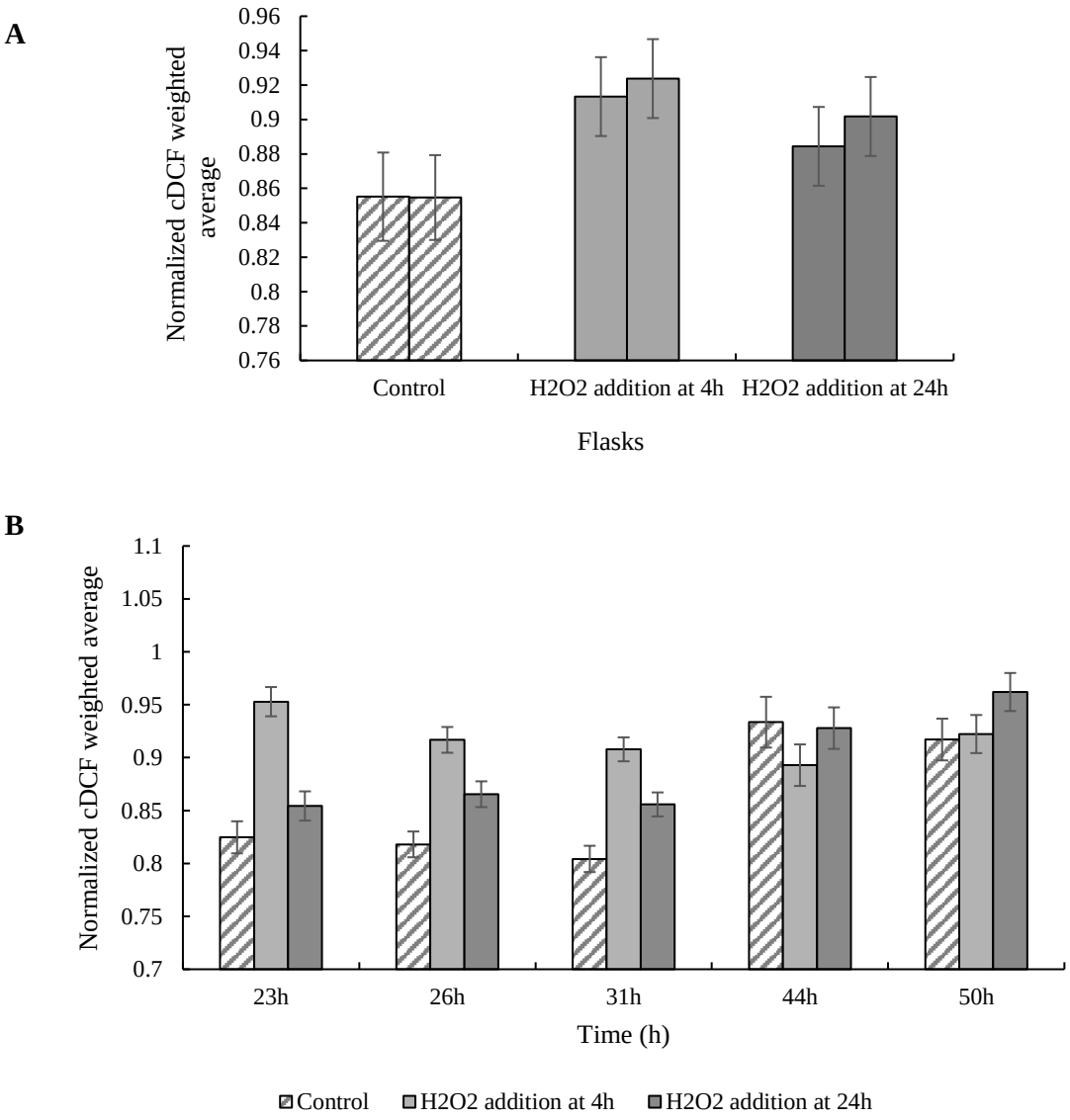

Figure 5-4 ANOVA of cDCF weighted average for fermentation times for control flask and cells exposed to 600 μM H_2O_2 at 4 h and 24 h ($p<0.05$). A- Average of measurements for all samples at different times for each flask. B- Average of measurements at 23 h, 26 h, 31 h, 44 h and 50 h from the start of the culture. Bars show 95% confidence intervals. Values were scaled with respect to the maximum value in the data set.

As seen in the NADPH results, cells treated at 4 h showed high levels of ROS compared to the other cultures until 31 h when cells start to recover as observed based on biomass measurements. However,

late in the fermentation, the levels of ROS decreased compared to the culture treated at 24 h, possibly due to an adaptive response as mentioned above.

5.4.2 Hydrogen peroxide addition and impact on ROS and NADPH production in bioreactors

Similar experiments to the ones described for flasks were repeated for 2 L and 20 L bioreactors to better emulate manufacturing operating conditions. The key differences between flask and bioreactor operation are that the latter are operated under closed loop control of dissolved oxygen, pH and temperature as in the industrial scale operation. In the 2 L fermentation, cells were treated with 600 μM H_2O_2 at 4 h. The biomass growth is showed is Figure 5-5 A.

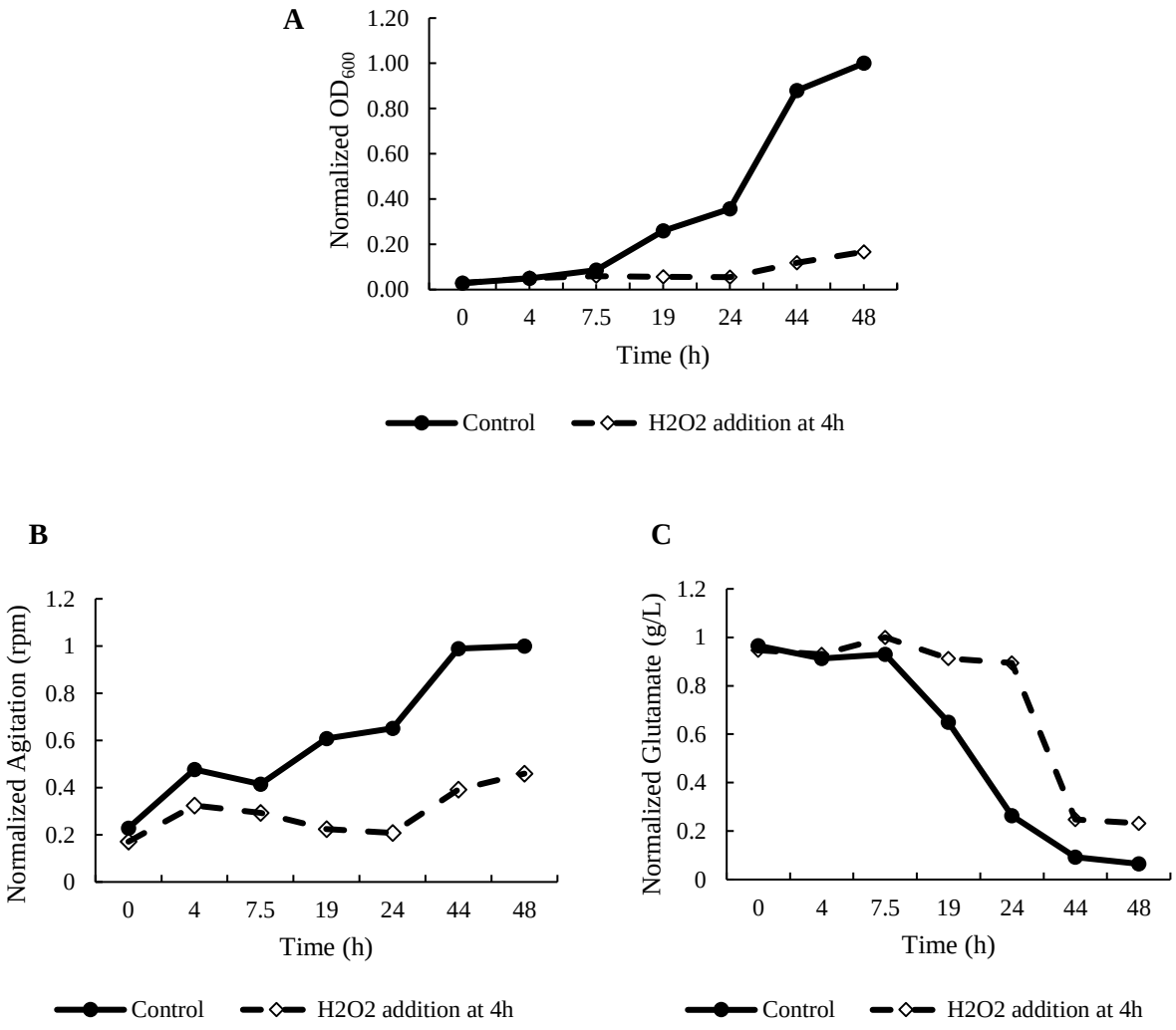

Figure 5-5 A- Bacterial growth of *B. pertussis* in 2 L fermenter. B- Agitation regime for (rpm) in 2 L fermenter. C- Glutamate concentration (g/L) in 2 L fermenter. Values were scaled with respect to the maximum value in the data set.

Compared to the flask, the main difference is that for the 2 L fermenter treated with H_2O_2 at 4 h did not fully recover at 44 h as occurred in flask and only a slightly increase of biomass was observed towards the end. It is believed that the difference observed in the adaptive behavior of flask and

bioreactor cultures to oxidative stress directly stems from the aforementioned closed loop control of DO in the bioreactor. In fact, these experiments show that the presence of this control significantly exacerbates the stress as follows. Under oxidative stress the catalase detected in all these experiments produces large amounts of molecular oxygen from the H_2O_2 introduced into the system. Following the generation of oxygen, the controller in the bioreactor reduces the agitation and airflow in order to maintain the DO at its 35% target while in the flasks, in the absence of oxygen control, no such reduction of agitation occurs, and the flask culture continues to take-up oxygen available through the cap.

This reduction in agitation rate to maintain the oxygen target is clearly observed in Figure 5-5 B which shows the agitation profile for the 2 L fermenters. Thus, in spite of the oxidative stress induced by H_2O_2, the addition of this peroxide also has an indirect effect on how oxygen is supplied to the system. For example, other studies have reported that hydrogen peroxide can serve as an alternative source of oxygen in cell culture (Lee *et al*., 2004). Then, as a result of the significant reduction in agitation rate in the culture treated at 4 h with H_2O_2 (due to indirect supply of oxygen), it is expected that the mass transfer coefficient significantly decreased thus resulting in slower metabolism a minimal glutamate depletion up to 44 h of operation (Figure 5-5 C) with resulting further reduction in growth rate as shown in Figure 5-5 A. This slower growth results in an overall smaller consumption of the ROS species by the anti-oxidative reactions, e.g. those using NADPH, thus extending the exposure to stress of the cells for a longer duration.

To verify the occurrence of oxidative stress in the 2 L bioreactor, NADPH in the supernatant was measured by fluorescence. The results shown in Figure 5-6 A confirm that the culture treated with H_2O_2 at 4 h exhibited a much larger concentration of NADPH/OD as compared to the control which is indicative of a much prolonged anti-oxidative response. The fact that NADPH/OD levels remain high until the end of the culture as compared to the NADPH/OD in the flask at 44 h for the culture treated

with peroxide (Figure 5-2 B) also correlates well with the fact that stress was present through the duration of the culture and thus the growth rate did not recover in contrast with flasks.

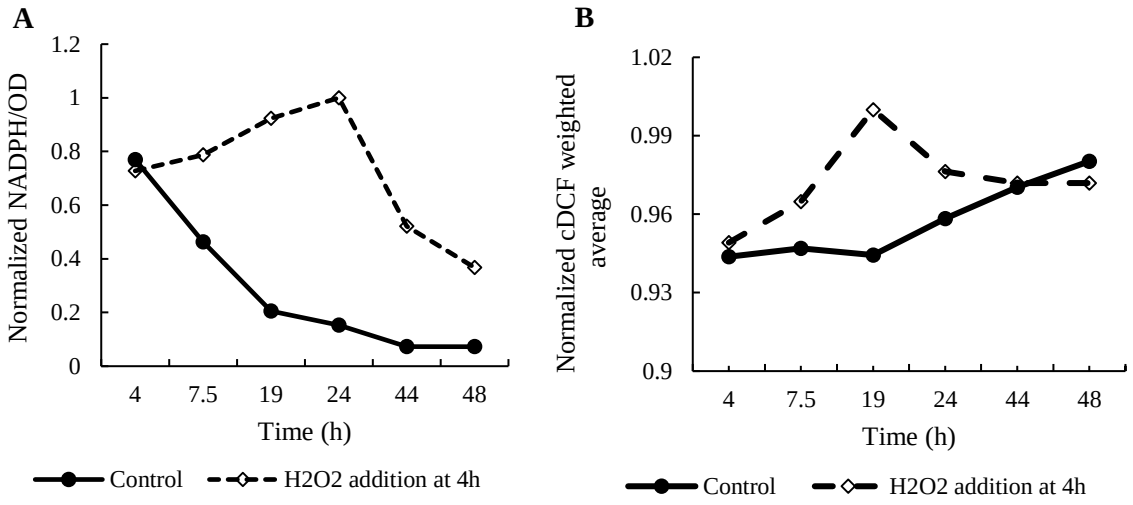

Figure 5-6 A- NADPH fluorescence intensity (Ex/Em 340/460 nm) per OD in 2 L fermenters. B- Weighted average of cDCF in cells (2 L fermentation). Values were scaled with respect to the maximum value in the data set.

Figure 5-6 B shows the results of cDCF measurements for the 2 L fermenters.

Up until 24 h, there is significant difference ($p<0.05$) among the averages of ROS, and no significant difference at the final ages of the fermentations. As evident from the biomass concentration, cells treated with H_2O_2 started to recover after 24 h. Also, there was a decrease in NADPH/OD (Figure 5-6 A) after 24 h, possibly because of the late consumption of NADPH as a means of defense.

The specific productivity of PRN for the 2 L bioreactor culture treated with H_2O_2 was 15% less than the control culture (0.0235 compare to 0.0199 μg/mL/OD-hour).

To further confirm the effect of oxidative stress in bioreactors, 20 L reactors were used with addition of H_2O_2. These experiments were prolonged to 72 h to allow cells to recover and reach the same biomass concentration as the control reactor. Biomass evolution with time is shown in Figure 5-7 A for the control and H_2O_2 treated.

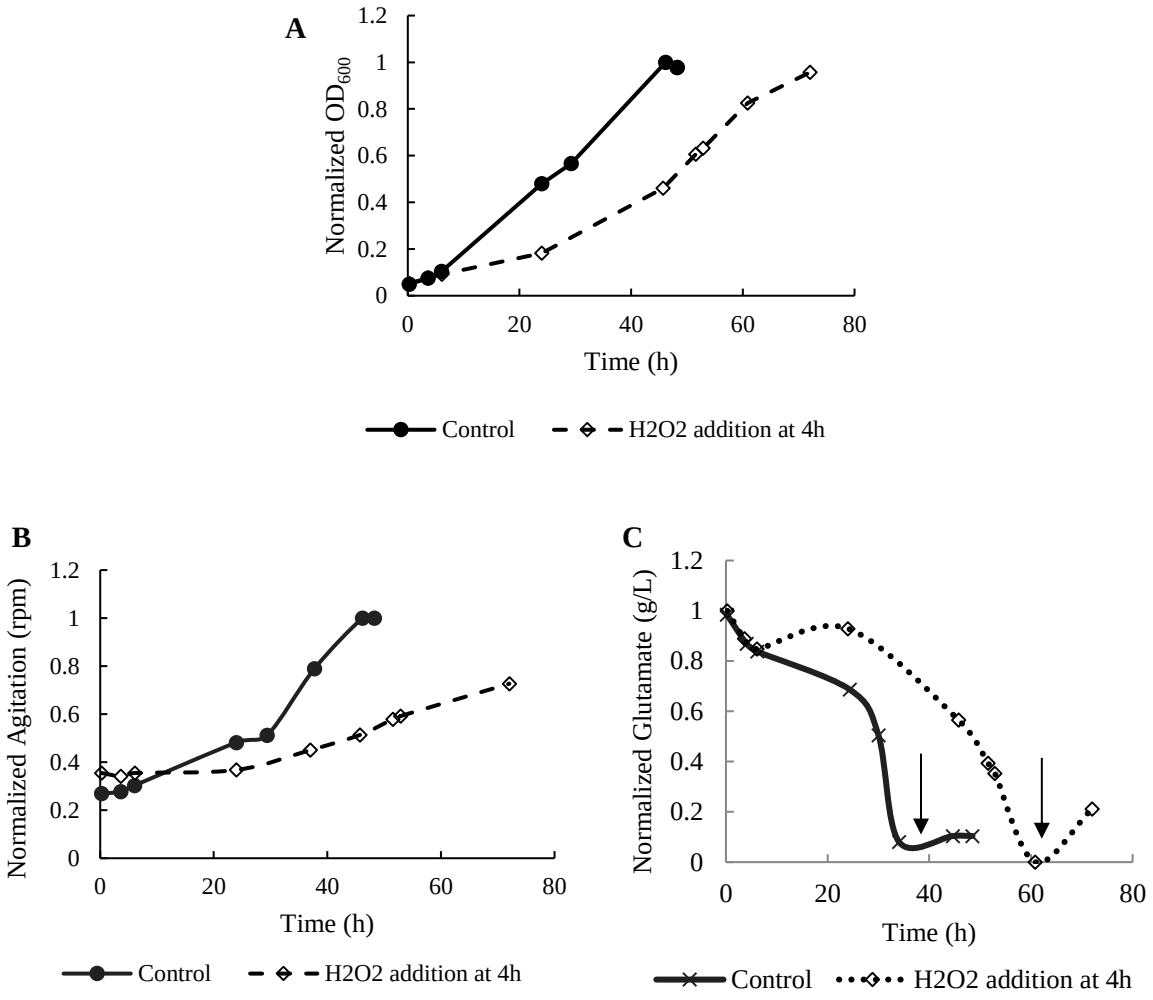

Figure 5-7 A- Biomass in 20 L fermentations. B- Agitation profile for 20 L fermenter. C- Glutamate consumption in 20 L fermentations (arrows show supplementation time). Values were scaled with respect to the maximum value in the data set.

In contrast to experiments run in the 2 L bioreactors, the H_2O_2 treated cells started to recover earlier. This is possibly due to the fact that agitation did not decrease significantly as shown in Figure 5-7 B as compared to the 2 L bioreactor (Figure 5-5 B) following H_2O_2 addition. It should be remembered that in 20 L the amount of air per working volume in the fermenter is smaller than in the 2 L (0.05 vvm and 0.38 vvm respectively) and following the introduction of peroxide and its dismutation to oxygen by catalase, it is not required for the controller to reduce the agitation rate to maintain the DO set point as much as needed in the 2 L bioreactors. Since the agitation is not reduced significantly, there is not a reduction of mass transfer in the 20 L bioreactor as compared to the 2 L reactor.

As for the 2 L bioreactor experiments the introduction of H_2O_2 also had an impact on glutamate consumption resulting from the slowing down of the metabolism. A decrease in consumption rate was observed for cells under stress and a delay in the supplementation time was observed (supplementation was done at 62 h compared to the control fermentation that was done at 38 h). Supplementation started when the initial nutrient supply was exhausted. At 24 h, the NADPH per OD unit was higher for cells treated with H_2O_2 (significance, $p<<0.05$). At the end of the fermentation, these differences continued to be significant ($p<0.05$) even though the NADPH/OD ratio decreased significantly in the stressed culture. As also seen in the flasks experiments, the NADPH per OD unit decreased as cells adapted to stress.

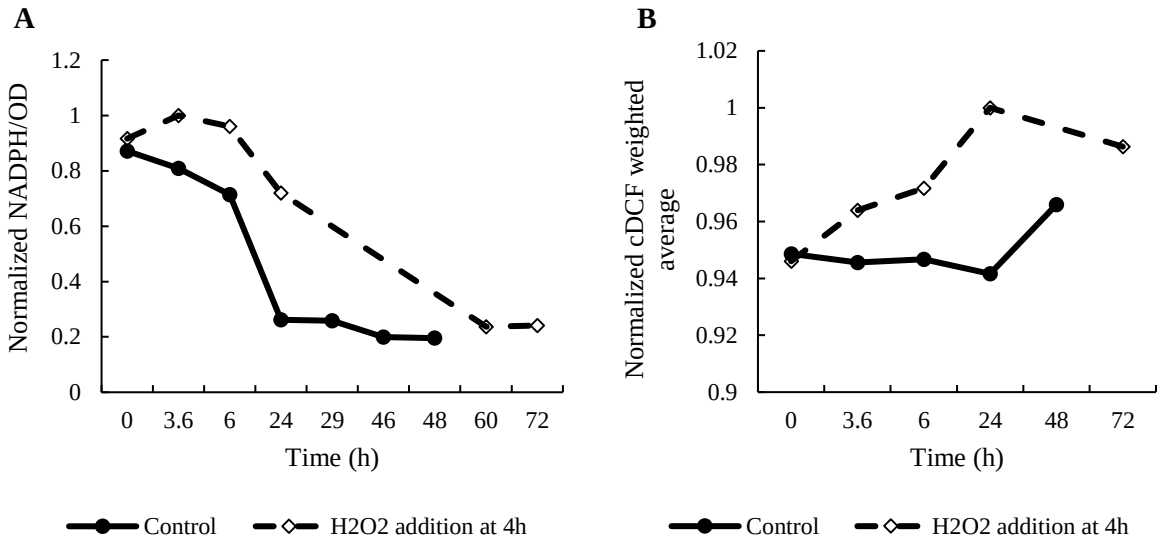

Figure 5-8 NADPH fluorescence intensity (Ex/Em 340/460 nm) per OD in 20 L fermenter. B-Weighted average of cDCF in cells (20 L fermenters). Values were scaled with respect to the maximum value of the data.

Cells treated with peroxide showed an increase in ROS amounts until 24 h and a decrease until the last hours of the fermentation that correlated with the NADPH results ($p<0.05$). The same behavior was observed in the 2 L fermentations.

The specific productivity for PRN in the culture treated with H_2O_2 was 18% percent less than the control culture (0.0218 compared to 0.0177 μg/mL/OD-hours) thus confirming the significant impact of oxidative stress on PRN productivity.

5.5 Conclusions

Externally administered hydrogen peroxide adversely affects the PRN production from the cells regardless of the timing of administration in the shake flasks. The oxidative stress has a significant

inhibitory effect on growth but adaptation to stress and recovery in cell growth are observed after a certain period of time from peroxide exposure. This adaptation mechanism is found to be correlated with NADPH which is known to be a key reactant in anti-oxidative reactions. Thus, after the exposure to stress the NADPH initially increases but, after some time, NADPH is consumed towards anti-oxidative reactions and this consumption is found to be correlated with a recovery in cell growth.

Average NADPH and ROS values were found to be negatively correlated with PRN yield thus corroborating the hypothesis that oxidative stress with the resulting increase in NADPH has significant adverse effect on antigen production and also confirming the correlation of NADPH and productivity found in previous work.

The specific productivity of PRN for cells treated with H_2O_2 at 4 h for flasks, 2 L fermenter and 20 L fermenter were 0.0366, 0.0199, 0.0177 μg/mL/OD-hour respectively. The differences in productivity can be explained in that for the bioreactors, closed loop control of DO intensifies the oxidative stress. Once H_2O_2 is added to the culture, the action of catalase converting the peroxide to O_2 results in the oxygen controller to decreasing the agitation rate to maintain the DO at target (35%), with the possible concomitant decrease of mass transfer. Due to this decrease, the metabolism of nutrients and the growth rate are considerably reduced resulting in slower consumption of ROS species with resulting exposure of the culture to high ROS levels for a longer period of time.

Since in flasks there is no DO control, agitation remains constant, and mass transfer is expected to be less affected as compared to closed loop controlled bioreactors. The early adaptation in the cultures is attributed to this fact. Catalase activity was qualitatively detected in the supernatant. NADPH is tightly bound to catalase and the NADPH secreted seems to be associated with this enzyme. Catalase has four NADPH moieties that are not detectable with fluorescence unless there is denaturation or a conformational change in the protein that allows the exposure of NADPH to the environment. In this

case, if the NADPH fluorescence emission detected comes mostly from catalase that might signify that there is a change in the protein caused by the oxidative stress itself (Kneeshaw *et al.*, 2017).

Chapter 6

Investigation of the Effects of Oxidative Stress Inducing Factors on Culturing and Productivity of *Bordetella Pertussis*

6.1 Abstract

The stress response of *Bordetella pertussis* during fermentation was assessed by means of fluorescence-based techniques. During the manufacturing of vaccines, *B. pertussis* is subjected to stress during the adaptation to a new environment and operating conditions in the bioreactor, which can have harmful consequences on growth and protein yield. In this study, stress was imposed by varying the percentage of dissolved oxygen and inoculum size, by adding rotenone and by the addition of hydrogen peroxide. High levels of dissolved oxygen during fed-batch operation had no detrimental effect on growth but the specific productivity of pertactin (PRN) decreased. Low inoculum cultures resulted in significantly less PRN as compared to controls where reduction was more significant in flasks as compared to bioreactors. A comparison of filtered media to heat sterilized revealed that filtered media offered a protective effect against H_2O_2. Heat sterilization of the media might result in the destruction of components that offer protection against oxidative stress. The effect of these stressors, while investigated for other microorganisms, have not been studied as yet for *B. pertussis*

6.2 Introduction

Whooping cough disease, also called pertussis, is an acute bacterial infection of the respiratory tract. In humans, the principal causative agent is the Gram-negative bacterium *Bordetella pertussis*.

Bordetella parapertussis can also cause the disease but with milder symptoms (Galliard, 2009). The best strategy for prevention is through vaccination. Cellular and acellular vaccines based on *B. pertussis* have been developed over the past few decades. In spite of being less effective, acellular vaccines have been demonstrated to be safe and less reactogenic than cellular vaccines, and for this reason acellular vaccines are preferred (Galliard, 2009; Thalen, 2008).

Acellular pertussis vaccines are based on virulent factors or antigens secreted by the bacterium. Formulations can range from one to five antigens (Meade *et al*., 2014; Warfel *et al*., 2015). The five-component pertussis vaccine (5cP) is composed of pertussis toxin (PT), filamentous hemagglutinin (FHA), two fimbriae subunits (FIM2, FIM3), and pertactin (PRN) (Warfel *et al*., 2015).

B. pertussis is a slow-growing bacterium, and cultivation on solid medium it might last 7 days. The development of liquid media with the essential requirements has helped to shorten the time of cultivation and improve vaccine production (Cohen *et al.*, 1946). However, some factors affect the growth of *B. pertussis* in culture media. For instance, it has been reported that heat sterilized cysteine inhibits the growth because of the formation of colloidal sulphur and sulphides, and this inhibition is avoided by filter sterilization of the cysteine (Rowatt, 1957). Casamino acids contains a small amount of cysteine, which could provoke inhibition of growth when heat sterilized. Peroxide and fatty acids have also been reported to cause growth inhibition (Rowatt, 1957; Imaizumi *et al.*, 1983).

Rowatt (1957) found that the size of the inoculum plays a role in the growth of *B. pertussis*, where a larger final population is obtained with a large inoculum in the presence of an iron source. It has been reported that the history of the inoculum has an important effect in the adaptation to a new environment (Robinson *et al*., 2001). For example, it has been observed in *Listeria monocytogenes* that the lag phase duration is longer in stressed cells when the size of the inoculum is small (Augustin *et al.* 2000; Gay *et al.*, 1996). Robinson *et al.* (2001) found for *L. monocytogenes* growing under optimum conditions the

lag times were generally unaffected by inoculum size but in the case where an inhibitory concentration of salt was present, the lag phase duration increased inversely to the inoculum size.

Nutrient excess has also been attributed to causing oxidative stress in mammalian cells and bacteria, thus affecting growth (Wellen *et al.*, 2010; Wang *et al.*, 2009). Oxidative stress occurs when there is an imbalance between the production of reactive oxygen species (ROS) and the capacity of the system to detoxify these compounds (Zheng *et al*., 2009; Yao *et al*., 2009). In the tricarboxylic acid cycle (TCA), nutrients are oxidized and the resulting electrons are fed to the electron transport chain (ETC). When nutrients are in excess, the capacity of the ETC to assimilate the surplus of electrons is compromised and ROS production increases (Wellen *et al.*, 2010).

The understanding of ROS production and generation of oxidative stress during cell culture is paramount for bioprocess control due to its impact on growth and protein production. To study the impact mechanisms of oxidative stress, it is a common practice to externally induce stress (Zheng *et al*., 2009; Abrashev *et al*., 2011; Munna, 2013). For example, addition of hydrogen peroxide (H_2O_2) is a mild means of triggering oxidative stress that can elicit inhibitory responses of certain key enzymes in the TCA cycle such as aconitase and alpha-ketoglutarate dehydrogenase (α-KGDH) (Miller *et al*., 2001). Another means of triggering oxidative stress is by the addition of rotenone. Rotenone is a form of isoflavonoid that is used as a pesticide, and is known to inhibit complex I in the respiratory chain (Bai *et al.*, 2003; Li e*t al.*, 2011), without interfering with other complexes (Bai *et al*., 2003). Complex I, also named NADH:ubiquinone oxidoreductase, is an enzyme that participates in the first step of the respiratory chain of bacteria (Ross *et al*., 2000). It is a membrane-bound molecule that facilitates the transport of electrons between NADH and ubiquinone, and also the transport of protons out of bacterial cytosol (Ross *et al*., 2000). It is known that the inhibitory effect of rotenone in complex I causes oxidative stress and cell death (Li *et al.*, 2003; Gupta *et al.*, 2014).

High concentrations of molecular oxygen have also been employed to induce stress to study cell behavior and product release (Baez *et al.*, 2014). It has been demonstrated that at a high extracellular concentration, molecular oxygen can penetrate inside the cells and oxidize flavoenzymes to produce superoxide and H_2O_2 (Baez *et al.*, 2014). Korshunov *et al*. (2006) reported that the formation rate of superoxide in *Escherichia coli* is proportional to the amount of molecular oxygen. Excessive ROS production has been related to lipid peroxidation, and DNA damage (Keyer *et al.*, 1996; Keyer *et al.*, 1995).

To avoid the deleterious effects of oxidative stress, bacteria employ enzymes such as superoxide dismutases, catalase, and glutathione reductase to detoxify ROS (Munna, 2013; Munna *et al*., 2014). Khelef *et al.*, (1996) reported that in Fe-superoxide dismutase (Fe-SOD) *B. pertussis* mutants, the production of the toxin adenylate cyclase-hemolysin (AC-Hly) and PRN were affected due to DNA damage. Also, they pointed out that these virulence factors could be damaged by the direct exposure to superoxide free radicals. NADPH helps enzymes to detoxify the system and, under high oxidative stress, it appears in high quantities and its detection can be used to quantify the amount of stress (Singh, *et al.*, 2007).

To monitor a 5cP acellular pertussis vaccine manufacturing process, an approach using fluorescent spectroscopy and multivariate statistical methods was developed (Zavatti *et al.*, 2016) with the aim to find the origin of the fluctuations in the final yield of PRN. By taking advantage of naturally fluorescent molecules, such as NADPH, it was found that there was an inverse correlation between the production of PRN and the quantity of NADPH. The goals of the current work were to corroborate the ability of NADPH to serve as a broad-spectrum indicator of oxidative stress and to verify the observed negative correlation between NADPH and stress with lower PRN productivity. NADPH formation was measured by fluorescence spectroscopy while flow cytometry was used to detect the formation of ROS in cells using an extrinsic probe.

First, experiments with rotenone were used as a mean to corroborate the correlation between NADPH formation and ROS, and the impact of the latter on growth and PRN productivity. Then, experiments were conducted to investigate the response to oxidative stress for different factors that are relevant to the actual manufacturing environment as follows: i-variation of the dissolved oxygen set-point; ii-variation in inoculum size; and iii- use of heat sterilized or filtered media (in response to stress externally induced by hydrogen peroxide).

6.3 Materials and Methods

6.3.1 Samples

Fermentations were run in 250 mL flasks, 2 L and 20 L bioreactors and samples taken at different stages of the culture. By investigating these different experimental systems, the objective was to investigate the effect of the closed loop control of DO, available in the bioreactors but not in flasks, in response to different conditions of oxidative stress.

Shake flasks experiments: 250 ml flasks with a working volume of 100 mL were incubated at 36°C, 200 rpm for 50 h. Each flask was run in duplicate. In one set of flasks, stress was induced with a onetime addition of 600 μM of rotenone at either 4 h or 24 h (initial OD was 0.3). In another pair of flasks, an inoculum ten times smaller than the control (OD 0.03) was used. Two additional controls were run with an initial OD 0.3. A different set of experiments was done to assess the difference between heat sterilized media (121°C, 30 min) and filtered media (0.2 μm filter) on the growth of *B. pertussis* following the external imposition of oxidative stress with 600 μM of hydrogen peroxide (H_2O_2) at 4 h.

All control cultures in shake flasks and bioreactors had an initial inoculum with OD 0.3.

Three fermentations were conducted in 2 L bioreactors BiosStat Bplus (Sartorius Stedim) with a working volume of 1.3 L at 36°C, pH 7.2, agitation from 100-678 rpm, and constant airflow of 0.5 lpm. The dissolved oxygen (DO) was maintained constant by means of a sequential control strategy that manipulated first the aeration and then the agitation rate to maintain the DO set-point. The operating conditions for each reactor were as follows: i- 35% DO and initial OD=0.3 for the control reactor, ii- 35% DO, initial OD 0.03 and iii- 70% DO and initial OD 0.3.

Two fermentations were conducted in 20 L bioreactors (BiosStat Bplus, Sartorius Stedim) to test the effect of inoculum size. The working volume was 13 L at 36°C, pH of 7.2, and airflow was 0.6 lpm with the agitation rate varied in the range of 100-700 rpm. The DO was maintained constant employing the same cascade control strategy as used in the 2 L fermentations. The operating conditions for each reactor were the following: i- 35% DO and initial OD 0.3 for the control reactor; ii- 35% DO, initial OD 0.03.

For all experiments, sampling was done at various times during the fermentation. The OD was measured at 600 nm. Samples collected were centrifuged (10,000 xg, 3 min, 4°C).

The final PRN yield was measured by an ELISA test as explained below.

6.3.2 Pertactin determination (ELISA)

ELISA tests were performed to quantify the final PRN concentration in the broth. PRN polyclonal antibodies from guinea pigs were used to coat the 96 well microplates at a concentration of 1.5 μg/ml and 50 μl/well. Each well contained 50 μL at a concentration of 1.5 μg/mL. Plates were washed three times after incubation at room temperature for 20-24 h. The washing solution contained 10 mM PBS, 0.1% Tween 20 and 0.1% BSA. Following washing, a blocking solution containing 10 mM PBS and 0.1% BSA was added and plates were incubated at room temperature for 30 min. Subsequently, the microplates were washed with the aforementioned washing solution two times. Samples were filtered

to separate supernatant from the pellet. Supernatants were added to the wells (100 µl/well), incubated at room temperature, and washed after 1 h incubation. 100 µL of guinea pig anti-PRN antibody conjugated to horseradish-peroxidase was added to each well. Plates were left for incubation at room temperature for 1 h. A wash was done following incubation. 100 µL of a solution containing 9 mL of 0.004% (v/v) H_2O_2 and 1 mL of 10 mM tetramethylbenzidine was added to each well. Plates were incubated at room temperature for 30 min. The reaction was stopped with a solution of 2 N sulfuric acid (H_2SO_4). Absorbance was measured at 450 nm. The concentration of PRN was calculated based on a standard curve relating concentration to absorbance.

6.3.3 Biomass and productivity data treatment

Since the final quantity of protein and cells is the result of a continuous accumulation over time, the evaluation of cell growth and protein yield was done by normalizing with respect to "cumulative volumetric cell-hours" to transform the biomass data to a cumulative basis (Dutton *et al.*, 1998). Equation (6.1) defines the cumulative volumetric cell-hours (CH_{VOL}):

$$\boldsymbol{CH_{VOL}} = \sum_{\boldsymbol{i=0}}^{\boldsymbol{f}} \frac{(\boldsymbol{x_{i+1}} - \boldsymbol{x_i})}{\boldsymbol{ln}\,(\boldsymbol{x_{i+1}}/\boldsymbol{x_i})} (\boldsymbol{t_{i+1}} - \boldsymbol{t_i}) \tag{6.1}$$

Where x_i is the cell concentration (in this work, quantify by means of optical density) at t_i hours that elapsed from the start of the culture. The specific productivity (*sPRN*) in µg/mL/OD-hour is defined by Equation 6.2 where *[PRN]* is the PRN concentration and the end of the fermentation in µg/mL.

$$\boldsymbol{sPRN} = \frac{\boldsymbol{[PRN]}}{\boldsymbol{CH_{VOL}}} \tag{6.2}$$

6.3.4 Glutamate Determination

The concentration of glutamate, which is the primary carbohydrate source used by *B. pertussis*, was determined using a BioProfile-FLEX Analyzer (Nova Biomedical). The measurements were done on supernatant obtained following centrifugation of the samples.

6.3.5 NADPH Analysis

The NADPH was measured by spectrofluorometry. The fluorescence excitation-emission spectra were acquired using a Cary Eclipse Fluorescence Spectrophotometer (Agilent Technologies). Samples were analyzed using polymethylmethacrylate cuvettes. The PMT voltage was 700 V and the slit width for both excitation and emission was 5 nm. These parameters were optimized in earlier studies to result in good signal, reproducibility, and to avoid quenching due to high concentration of the sample. The excitation and emission (Ex/Em) ranges for acquiring spectra were 300-400 nm and 360-500 nm respectively. NADPH fluoresces at Ex/Em = 340/460 nm (Lakowicz, 2006).

6.3.6 Flow cytometric analyses

6.3.6.1 Reagents

Carboxy-2′,7′-dichlorofluorescein diacetate (cDCFDA) from Sigma-Aldrich (Canada) was employed to detect the production of ROS in cells. A 10 mM stock solution of cDCFDA was prepared using dimethyl sulfoxide (DMSO) as solvent. cDCFDA was added to each sample to a final concentration of 50 μM. Samples were incubated for 1 h at room temperature and then analyzed in the flow cytometer. The FL1 green fluorescence channel was used to detect the fluorescence emission.

6.3.6.2 Equipment

Flow cytometric analyses were performed using an S3e Cell Sorter (Bio-Rad). The instrument has two excitation lasers 488 nm (primary) and 640 nm (secondary), and emission filters for detecting forward scattering (FSC) and side scattering (SSC) (488/6 band width filters), and for fluorescence emission detection: 526/48 (FL1), 593/40 (FL2), 670/30 (FL3) and 700 LP (FL4).

The total number of events per sample was 10,000 acquired at a rate of 1,600-2,000 events/sec.

6.3.6.3 Flow cytometric data analysis

To compare flow cytometric data to fluorometric data, it was necessary to calculate an average of ROS for the entire cell population in each sample. This was achieved by the calculation of a weighted average (*WA*) defined in Equation 6.3:

$$\boldsymbol{WA} = \sum_{\boldsymbol{i}}^{\boldsymbol{f}} \frac{\boldsymbol{C_i}}{\boldsymbol{C_t}} * \boldsymbol{I_i} \tag{6.3}$$

Where C_i is the number of cells that have fluorescence intensity I_i, and C_t is the total number of cells analyzed.

6.3.7 Statistical analysis

Statistical significance of the experimental results was assessed using one-way ANOVA $p < 0.05$. The statistical software employed for these calculations was Minitab 17.1.

6.4 Results and discussion

6.4.1 Rotenone addition

Rotenone is a well-established cause of oxidative stress. Therefore initial experiments were done with rotenone in order to corroborate that increased production of NADPH is an anti-oxidative response to stress and the impact of stress on specific growth rate and specific antigen productivity. Two sets of experiments were conducted where rotenone was introduced after 4 h or 23 h from the start of the culture. The objective of testing two times for addition was to assess the response during the lag phase of growth where the culture is expected to build antioxidative defenses, and during the exponential phase.

The addition of rotenone (600 μM) at an early stage (4 h) appears to cause a permanent detrimental effect on the *B. pertussis* growth without any signs of recovery towards the end of the culture (Figure 6-1 A). Also, there is a clear increase in NADPH production per unit OD, which is also significantly higher ($p<0.05$) as compared to the control following rotenone addition (Figure 6-1 A). Conversely, rotenone added in the middle at a later stage of the fermentation (23 h) did not elicit a significant anti-oxidative response in terms of NADPH production and it did not have any considerable impact on the growth during the span of the experiment (Figure 6-1 B). The mechanism of oxidative damage from rotenone is related to its ability to inhibit the transfer of electrons to ubiquinone in Complex I of the electron transport chain. This results in oxidative stress due to superoxide that will be mitigated by the action of superoxide dismutase (SOD). SOD catalyzes the dismutation of superoxide to O_2 and H_2O_2. Subsequently, catalase and NADPH are needed for H_2O_2 detoxification to O_2 and H_2O. The fact that the impact of rotenone on growth and productivity is negligible when the rotenone is introduced later in the culture could indicate that sufficient SOD might be available to counteract the stress. This can further explain the formation of NADPH following late addition of rotenone since in this case, ROS

production is expected to be low thus not necessitating production of NADPH as compared to the case where rotenone was introduced at 4 h.

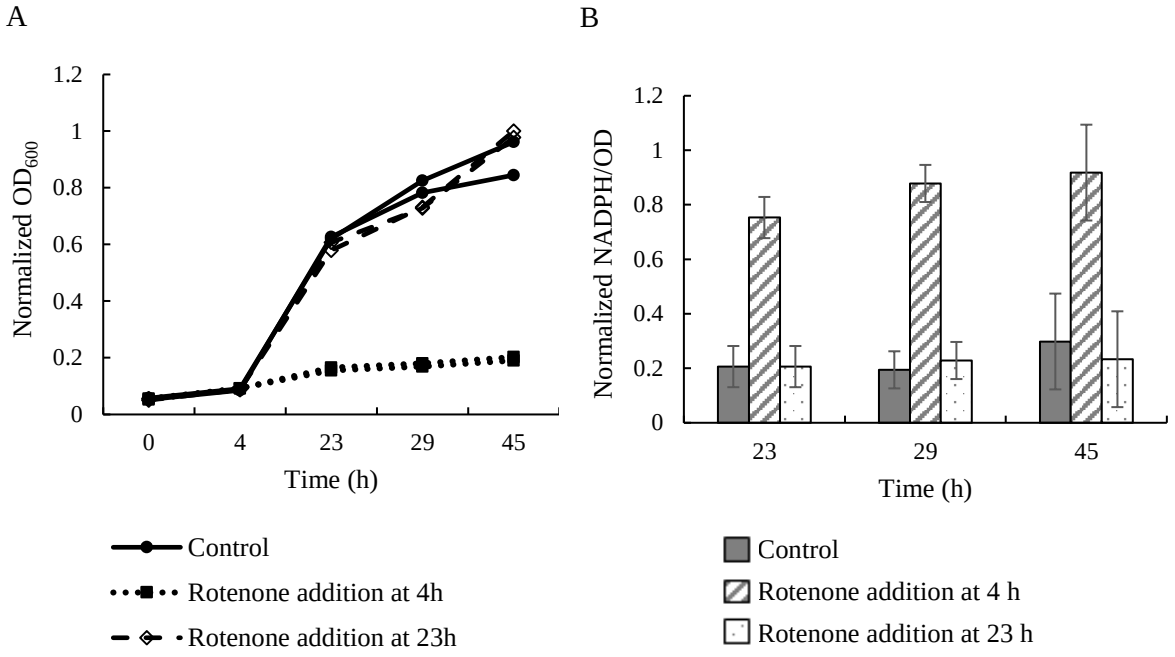

Figure 6-1 A- OD_{600} for control flasks and rotenone addition at 4 h and 23 h. B- NADPH/OD for flasks control and rotenone addition at 4 h and 23 h. Values were scaled with respect to the maximum value of the data.

Conversely, there are studies for yeast (Light, 1968) that demonstrate loss of rotenone sensitivity in cells when growth is switched to iron-limited conditions. This has not been tested in this study, but might explain the loss of sensitivity to rotenone at 23 h since iron supplied with the growth factors can be depleted to a sufficiently low concentration to cause this effect (Storey, 1980).

The averages of the specific productivity for pertactin were 0.0635, 0.0819, and 0.0561 μg/mL/OD-hour, for control and for rotenone added at 4 h and 23 h, respectively.

6.4.2 Effect of dissolved oxygen (DO)

Hyperoxia has been reported as a source of oxidative stress that may have a significant impact on the culture (Imlay, 2013; Lushchak *et al*., 2005). The effect of a change in DO set-point to induce oxidative stress was investigated in 2 L fermenters with set-points 35% (control) and 70%. In Figure 6-2 the growth of *B. pertussis* at 35% and 70% DO is presented. As seen in Figure 6-2 there was not significant difference in the evolution of the biomass under the two DO concentrations. It was reported (Baez *et al.*, 2013) that *E. coli* can evade stress caused by elevated molecular oxygen by activation of SoxRS and SOD. For *E. coli* it has also been reported that the evolution of biomass at elevated DO concentrations does not differ from growth at 30% DO, but the volumetric oxygen uptake and carbon dioxide formation decreases (Baez *et al.*, 2013).

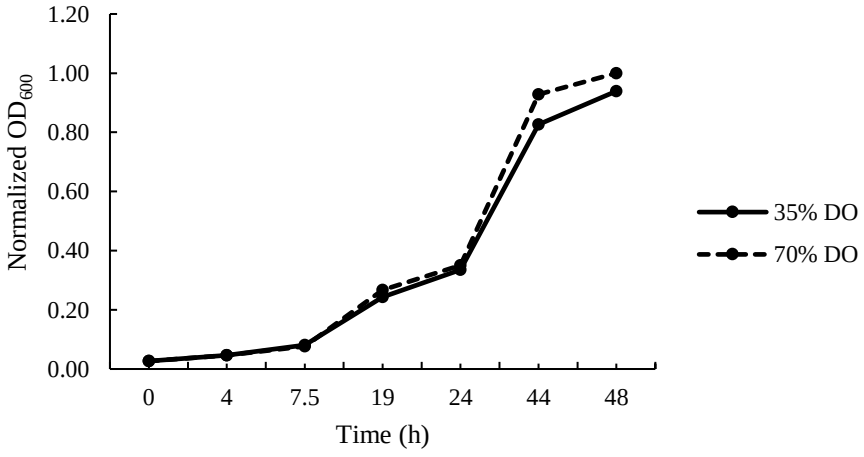

Figure 6-2 Biomass in 2 L fermentations. Values were scaled with respect to maximum OD

The results are similar to those found by (Baez *et al.*, 2013). Also, the NADPH and cDCF plots (Figure 6-4) show no significant difference between both DO set points. cDCFDA is a non-fluorescent compound that is permeable to cells. Once in the cell, cDCFDA is hydrolyzed to cDCFH and remains

trapped within the cells. cDCFH reacts with ROS to form the fluorescent cDCF. In this manner, the measurement of cDCF fluorescence is a way to detect ROS production in cells (Halliwell *et al.*, 2004).

Conversely, the effect of increased DO was a slight reduction on the specific productivity of PRN: 0.0235 μg/mL/OD-hour for control and 0.0193 μg/mL/OD-hour for 70% DO. Since the cDCF level was not significantly different for the different DO set-point values it appears that this reduced productivity is not directly related to oxidative stress. Instead, it may be related to the higher agitation rate that was imposed by the control strategy in the high DO experiment. The productivity of FHA (Filamentous hemagglutinin), one of the five antigens of *B. pertussis* components in the acellular vaccine, has been reported to be reduced when there is increased shear stress caused by high agitation (Rodriguez *et al.*, 1993). Figure 6-3 B presents the agitation profiles for the reactors under both conditions. The agitation profile for the 70% DO was higher in order to maintain the DO at set point, which might have caused more shear stress. The sudden decreased peak observed in the control reactor coincides with the supplementation time.

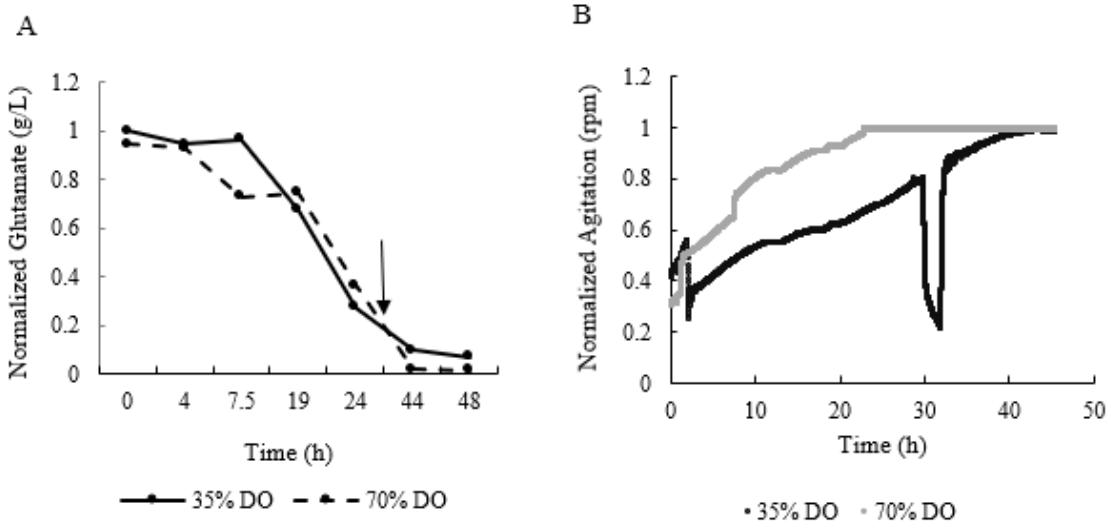

Figure 6-3 A- Glutamate (g/L) in 2 L fermentation. B- Normalized agitation (rpm) in 2 L fermentation. The arrow indicates the start of the supplementation.

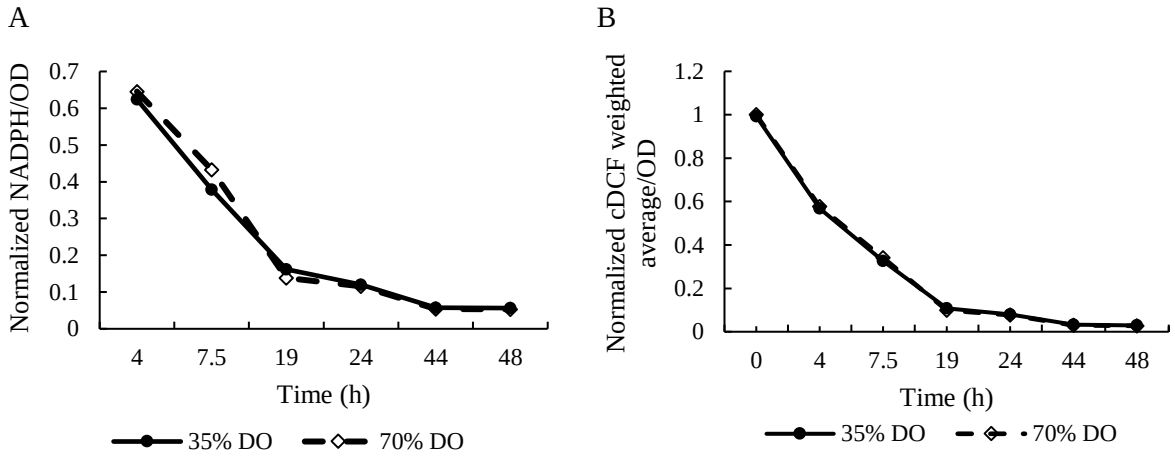

Figure 6-4 A- NADPH per OD unit for 2 L fermentations at different DO set points. B- cDCF weighted average per OD unit for 2 L fermentations at different DO set point. Values were normalized with respect to maximum value of the data.

In addition to shear stress, another factor that could affect productivity is the fact that cells redirect energy to produce anti-oxidative enzymes to minimize oxidative stress instead of producing PRN.

6.4.3 Low inoculum

6.4.3.1 Low inoculum in flasks

The inoculum was prepared by adding a volume of cells obtained from a previous passage to a volume of fresh media to obtain OD values of 0.03 or 0.3. Figure 6-5 shows the biomass time profiles of *B. pertussis* in flasks with different initial OD's.

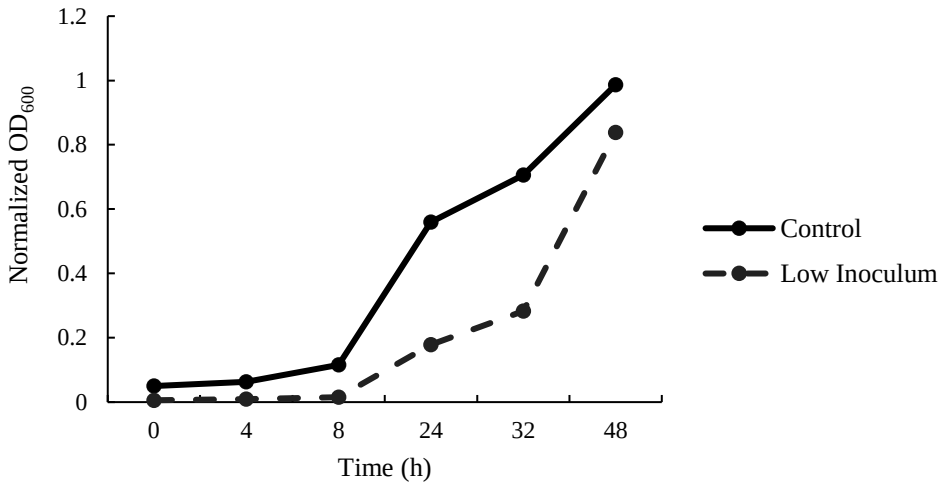

Figure 6-5. Growth of *B. pertussis*. Values were scaled with respect to maximum OD.

Accordingly, the low inoculum fermentation are exposed to a slightly larger concentrations of media components constituents. The low inoculum cultures have glutamate concentrations that remain higher for a longer period of time as compared to the control culture due to lower consumption of nutrient by the smaller number of cells. Thus, the exposure to high nutrient concentration persists for a longer period of time for the low inoculum culture as compared to the control culture. It has been reported that exposure to high nutrient concentrations often results in high production of electrons that are diverted to the production of biomass and NADPH (Naviaux, 2012). As shown in Figure 6-6 the specific growth rate for the flasks that started with a low inoculum appears to be higher than the control cultures. These differences appeared to be significant ($p<0.05$), except at 8 h, where the differences was not significant ($p>0.05$).

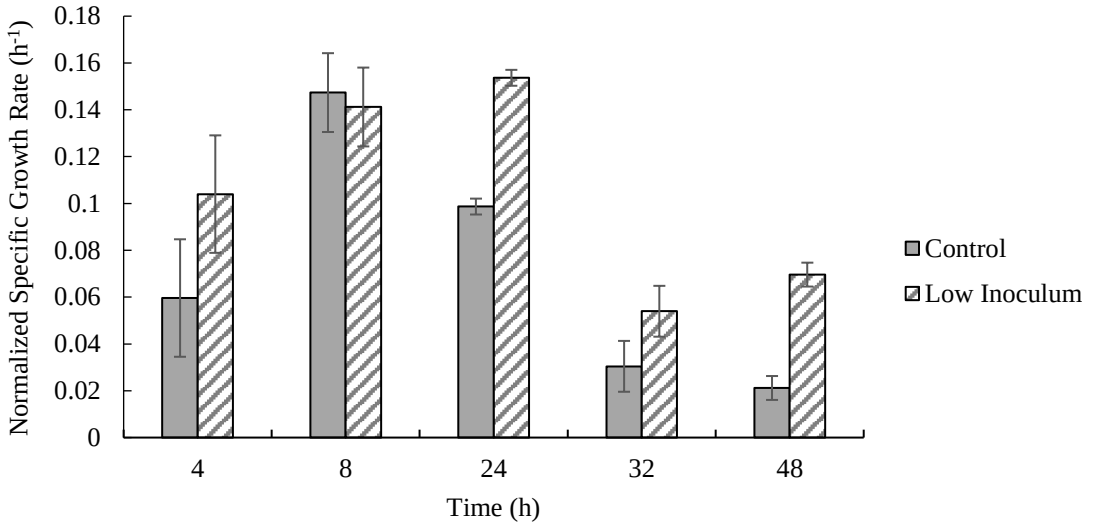

Figure 6-6 Specific growth rate (h^{-1}) for flasks. Values represent the averages for the replicates of flasks. Bars show 95% confidence intervals.

The NADPH per OD unit appeared to be increased in both flasks that started with low inoculum compared to the control flasks (Figure 6-7 A).

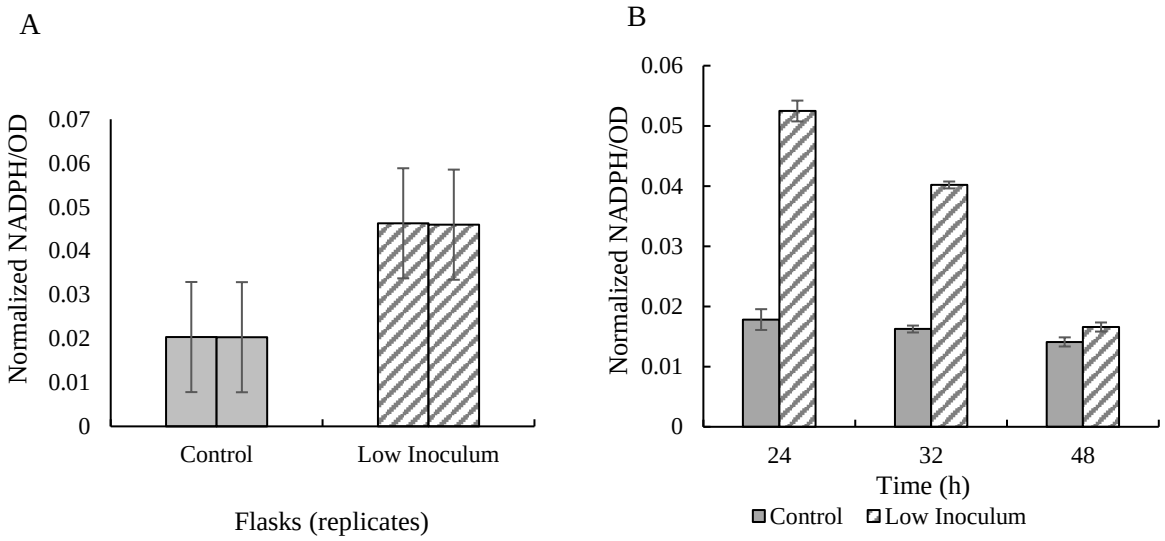

Figure 6-7 A- Average for NADPH/OD in flasks (for 24 h, 32 h, and 48 h). B- Average NADPH/OD in flasks vs time. Values were scaled with respect to the maximum value of the data. Bars show 95% confidence intervals.

The greater production of electrons and NADPH is also accompanied by higher oxidative stress for the low inoculum culture as compared to the control. In fact, higher NADPH production has been reported as correlated to oxidative stress (Singh *et al.*, 2007). Correspondingly, it can be seen that the amount of ROS increases at the earlier stages of the fermentation compared to the control (Figure 6-8). Only towards the later stages of the fermentation (48 h in Figure 6-8) is the ROS lower compared to the control culture. The recovery of both cultures in terms of significant increase in specific growth rate after 24 h (Figure 6-6) and mitigation of oxidative stress (Figure 6-8) of the low inoculum as compared to the control culture is due to the action of antioxidative enzymes such as glutathione peroxidase and catalase that result in higher NADPH consumption (Łukaszewicz-Hussain *et al.*, 2004) (Figure 6-7). This recovery for cultures that are exposed to oxidative stress, such as the low inoculum culture at 24 h, has been reported previously for *E. coli* and has been referred to as an adaptation mechanism to high oxidative stress (Lushchak, 2011; Crawford *et al.*, 1994).

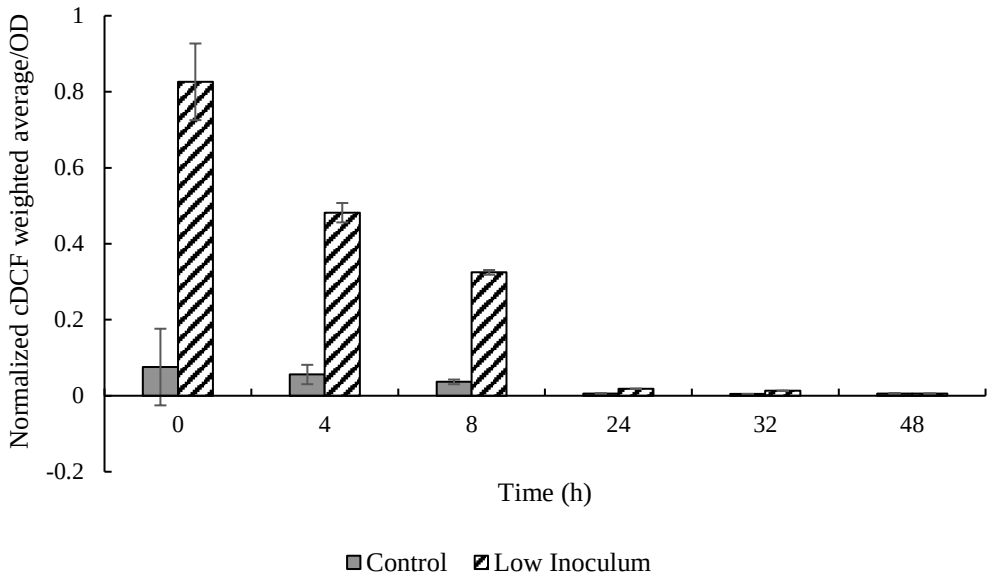

Figure 6-8 cDCF weighted average per OD unit in flasks. Values were scaled with respect to the maximum value of the data. Bars show 95% confidence intervals.

The specific productivities of PRN were on average 0.0421 μg/mL/OD-hour and 0.0224 μg/mL/OD-hour for control and low inoculum flasks, respectively. This corroborates the fact that the low OD culture that was exposed to higher oxidative stress (Figure 6-8) for a longer duration as compared to the control culture, exhibited a lower specific productivity.

6.4.3.2 Low inoculum in 2 L and 20 L fermentations

Figure 6-9 shows the biomass concentration for 2 L fermentations under control and low inoculum conditions.

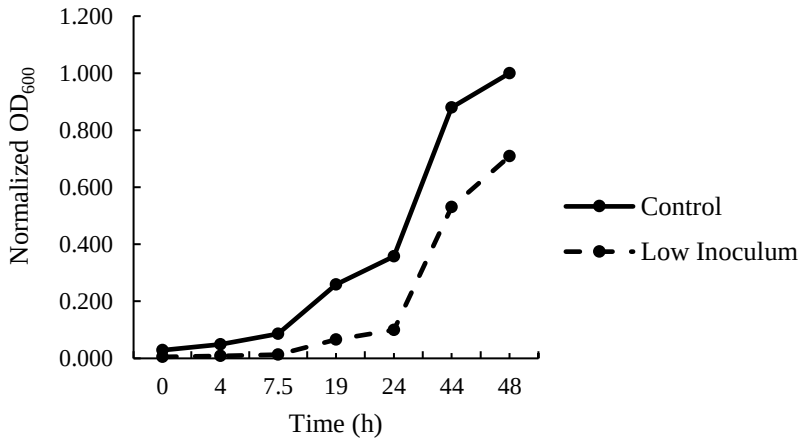

Figure 6-9 Biomass in 2 L fermentations. Values were scaled with respect to the maximum value of the data.

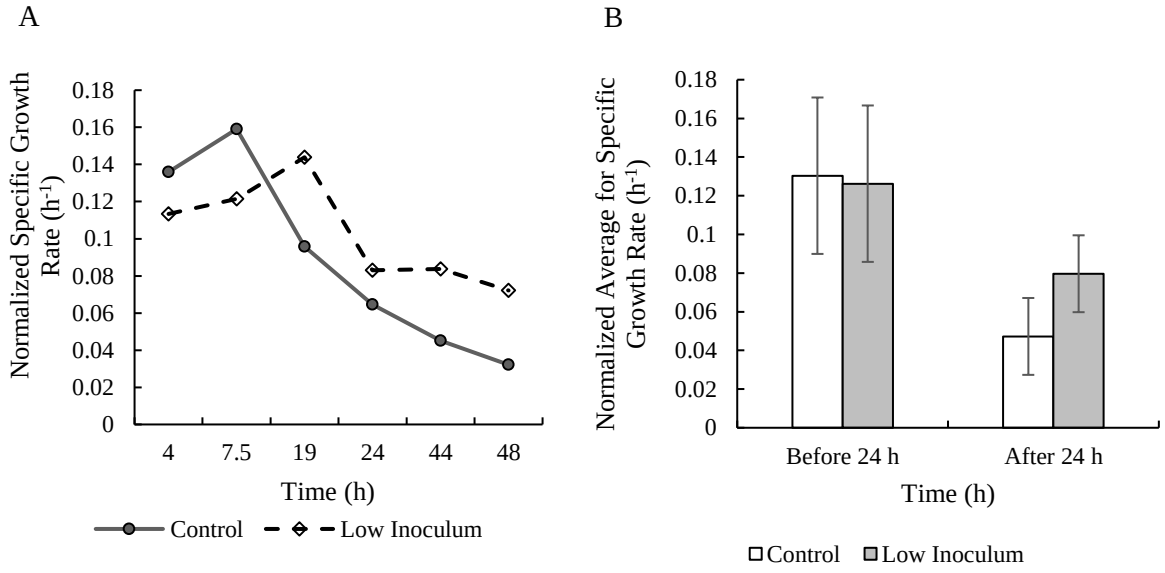

Figure 6-10 A- Specific growth rate (h^{-1}) in 2 L fermentations. B- ANOVA for specific growth rate (h^{-1}). Values were scaled with respect to the maximum value of the data. Bars show 95% confidence intervals.

As observed for flasks, the specific growth rate for the 2 L fermentation with lower inoculum was significantly higher ($p<0.05$) than the control after 24 h. The specific growth rate before 24 h was not found to be significantly different ($p>0.05$) (Figure 6-10 A).

Glutamate depletion (Figure 6-11 A) is consistent with the increased specific growth rate since after 24 h cells started to consume more glutamate compared to the control. The agitation profile (Figure 6-11 B) show a decrease at the beginning of the fermentation due to the small number of cells and the dissolved oxygen (DO) available. As the fermentation proceeded, the low agitation rate compared to control can be attributed to the combined effect of the DO closed loop control with the initial larger oxidative stress occurring in the low inoculum culture. In the bioreactor, in contrast with the flask experiment, DO is controlled by manipulating the aeration and agitation rates. This strategy is implemented in a sequential fashion where the aeration rate is increased first until it reaches its upper bound and subsequently the agitation rate is manipulated to maintain the DO at its set-point.

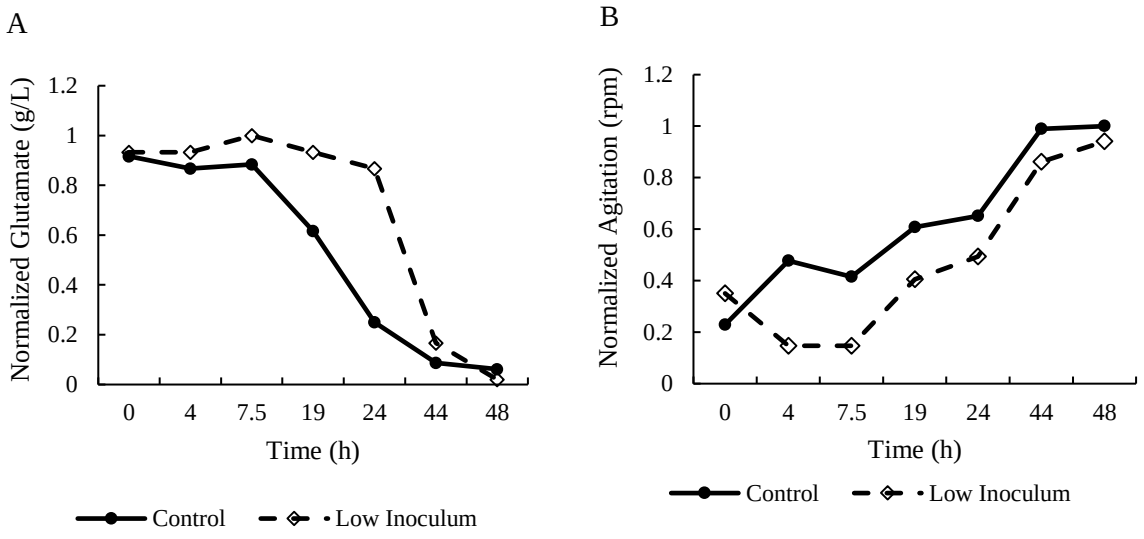

Figure 6-11 A- Glutamate consumption and B- Agitation in 2 L. Values were scaled with respect to the maximum value of the data.

The low inoculum culture is exposed for a longer time to high concentrations of glutamate as compared to the control. Figure 6-11 A shows that the low inoculum culture is exposed to the higher glutamate concentration until ~24 h after the start of the fermentation. A further corroboration that the oxidative stress is higher as evident from the levels of NADPH and cDCF observed during the initial stages of the fermentation shown (Figure 6-12). NADPH/OD values for the low inoculum cultures are higher during the first 24 h of the fermentation as compared to the control culture and only decrease towards the end of the fermentation.

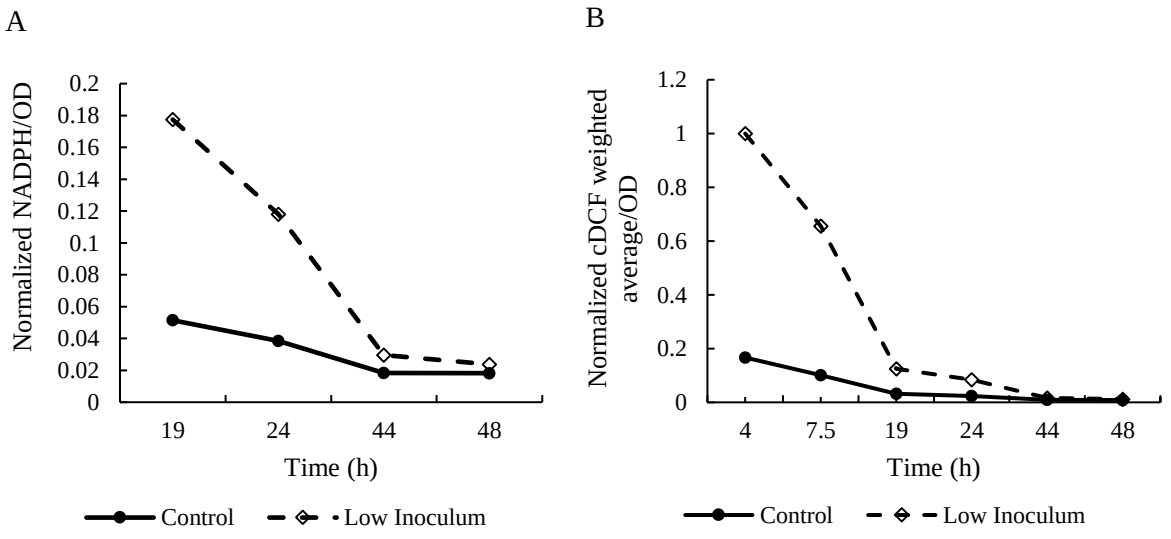

Figure 6-12 A- NADPH fluorescence intensity (Ex/Em 340/460 nm) per OD in 2 L fermenters. B- Weighted average of cDCF per OD unit in cells (2 L fermentation). Values were scaled with respect to the maximum value in the data set.

The cDCF values are also higher for the low inoculum culture thus corroborating the occurrence of higher oxidative stress. Since a small number of cells are present, there is less consumption of oxygen

and it is not necessary to increase agitation to maintain the DO at target. The reduced agitation observed during the initial 4 h period (Figure 6-11 B) will be accompanied by a reduction of mass transfer that may explain the very slow depletion of nutrients (Figure 6-11 A). This slow depletion results in the glutamate concentration remaining high for a longer period thus further increasing the exposure of cells to stress. Furthermore, when agitation starts to increase (from 7.5 h to 19 h), there was a decrease in ROS values coinciding with the period where oxidative stress has been already reduced as shown in Figure 6-12 B.

The specific productivity of the antigen PRN was similar for both experiments: 0.0224 μg/mL/OD-hour and 0.0211 μg/mL/OD-hour for control and low inoculum respectively. The higher oxidative stress in the initial period of the fermentation in the low OD experiment may explain the slightly lower productivity in this experiment.

The trends for the 20 L fermentation are similar as for the observed trends in the 2 L experiments. As shown in Figure 6-13 A the low inoculum is able to recover and to almost equate by the end of the fermentation the biomass level achieved in the high OD experiment. The specific growth rates shown in Figure 6-13 B are significantly higher for the low inoculum as compared to the control over the entire duration of the fermentation. Figure 6-14 A shows that the low inoculum culture was exposed for a longer period of time to high glutamate concentration as compared to the control thus resulting in stressful conditions for a longer period. As observed in the plot for glutamate consumption (Figure 6-14 A) the depletion of nutrients took longer, but at the final stage of fermentation, the culture reached at higher OD than the control, which demonstrates a better adaptation to the initial stress (Figure 6-13 A).

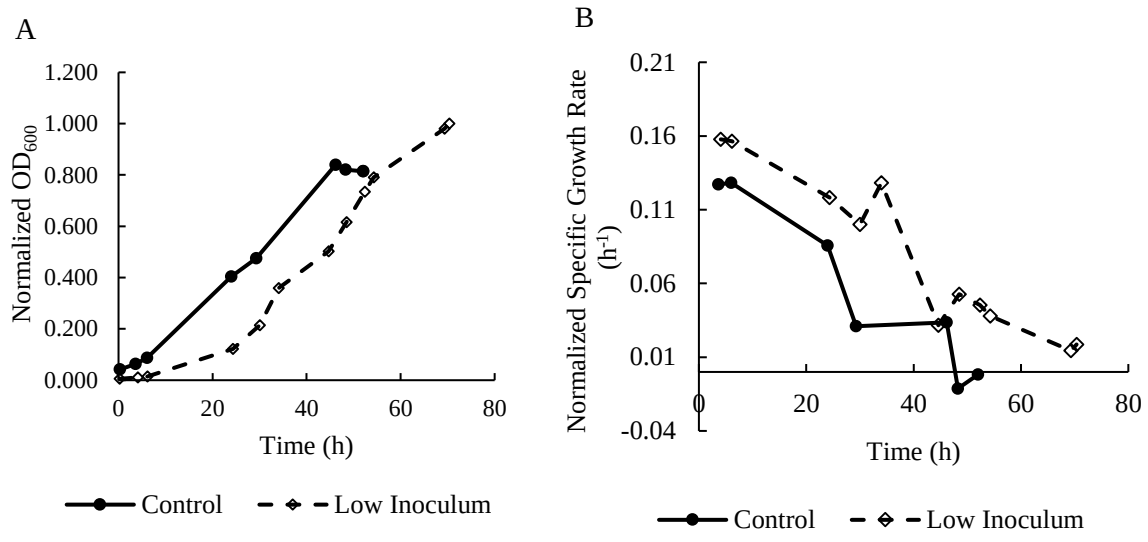

Figure 6-13 A- Biomass in 20 L fermentations B- Specific growth rate (h^{-1}) in 20 L fermentations. Values were scaled with respect to the maximum value of the data.

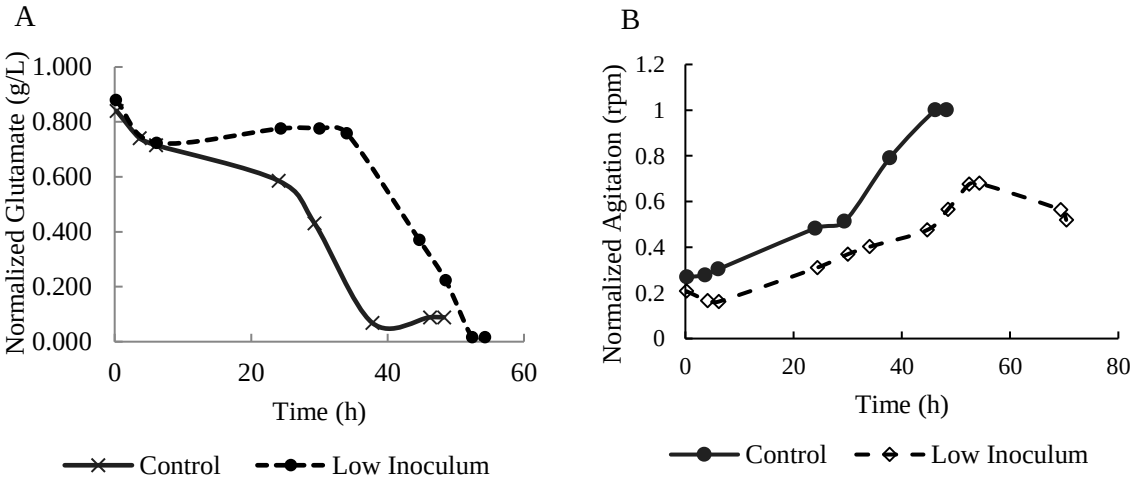

Figure 6-14 A- Glutamate consumption in 20 L fermentation. B- Agitation in 20 L fermenter. Values were scaled with respect to the maximum value of the data.

Similar to the 2 L fermentation, the agitation rate decreases initially due to the controller response to maintain DO at its set-point in the presence of oxidative stress. The occurrence of higher oxidative stress in the low inoculum culture is evidenced by the higher NADPH/OD values for the low inoculum culture that is high at the first 24 h as compared to the control culture and then starts to decrease towards the end (Figure 6-15 A). ROS values are also higher at early hours of the fermentation (as in the 2 L fermentation) for the low inoculum culture thus corroborating higher stress and then decreases corresponding to the ability of the culture to deal with the initial stress. At the end of the fermentation, there is a decrease in ROS that coincides with the final growth observed in this culture as compared to the control culture (Figure 6-13 A).

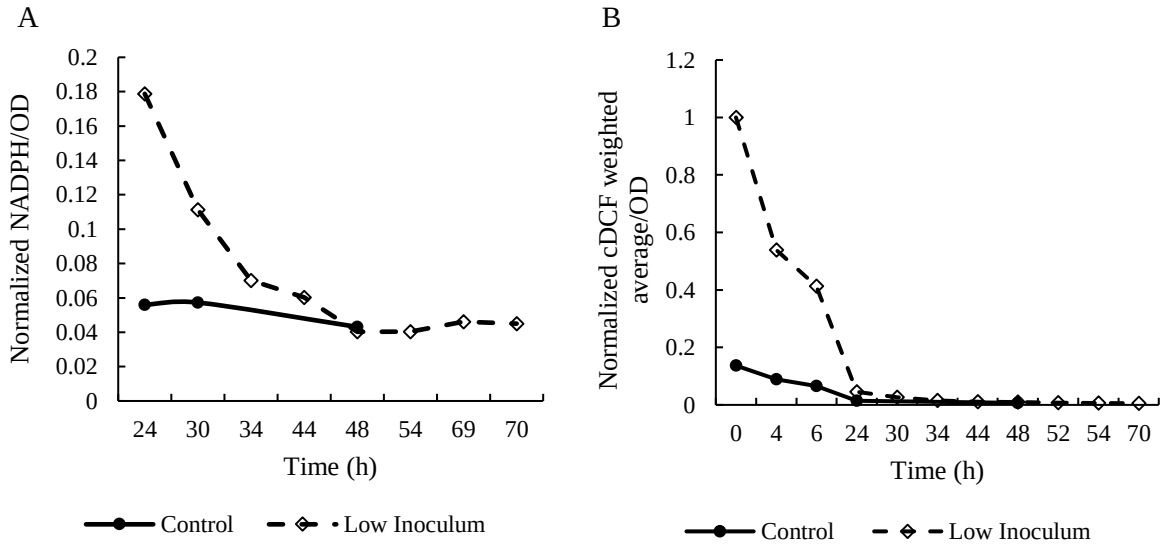

Figure 6-15 A-NADPH/OD values for 20 L fermenters. B- cDCF weighted average per OD unit for 20 L fermentation.

The specific productivities of PRN were 0.0218 μg/mL/OD-hour and 0.0127 μg/mL/OD-hour for control and low inoculum cultures respectively in correspondence with the occurrence of higher oxidative stress occurring in the low inoculum culture.

6.4.4 Impact of filtered and heat sterilized media for flasks fermentations

These experiments were done in duplicate in 250 mL flasks with the aim of assessing the impact of externally imposed oxidative stress using H_2O_2 with heat sterilized and filtered media. The H_2O_2 was introduced at 4 h after the start of the fermentations.

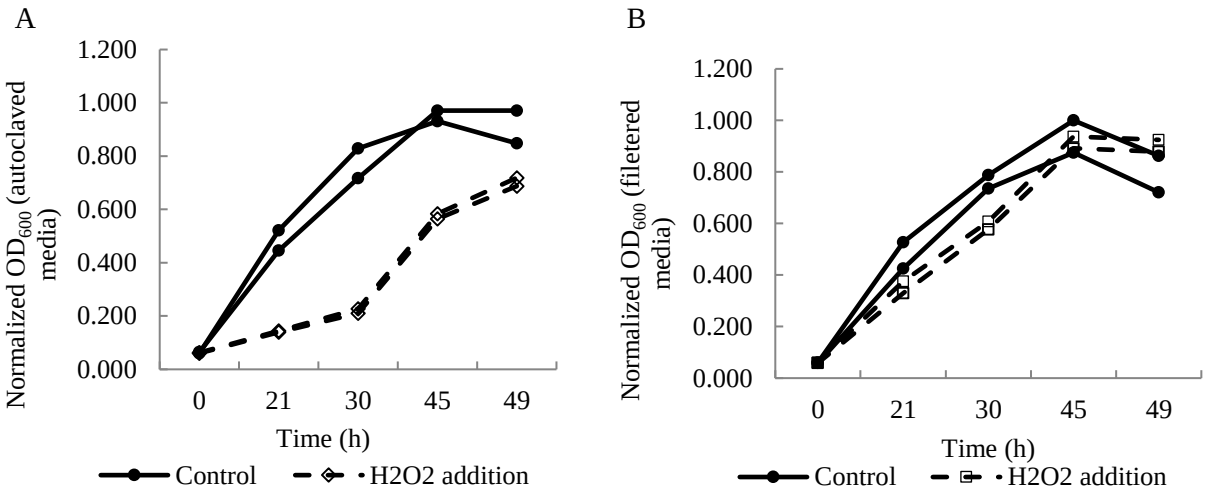

Figure 6-16 A- Flask cultures in heat sterilized media (121°C, 30 min). B- Flask cultures in filtered media (0.2 μm filter). Values were scaled with respect to the maximum value of the data.

From Figure 6-16 it is clear that the filtered media confers better protection against the oxidative stress induced by H_2O_2 as compared to the filtered media. There is no significant difference among the values of NADPH/OD for heat sterilized and filtered media in the control cultures ($p>0.05$), but there

is a statistical difference when comparing cultures stressed with 600 μM H_2O_2 at 4 h (Figure 6-17). It is likely that compounds that confer protection against oxidative stress, are damaged during heat sterilization or, components that are more oxidizable by H_2O_2 are degraded during heat sterilization (the reactivity of the medium might play a role in determining how much H_2O_2 actually remains over time). Cysteine, which is present in casaminoacids, is known to cause detrimental impact on the growth of *B. pertussis* when autoclaved (Rowatt, 1957).

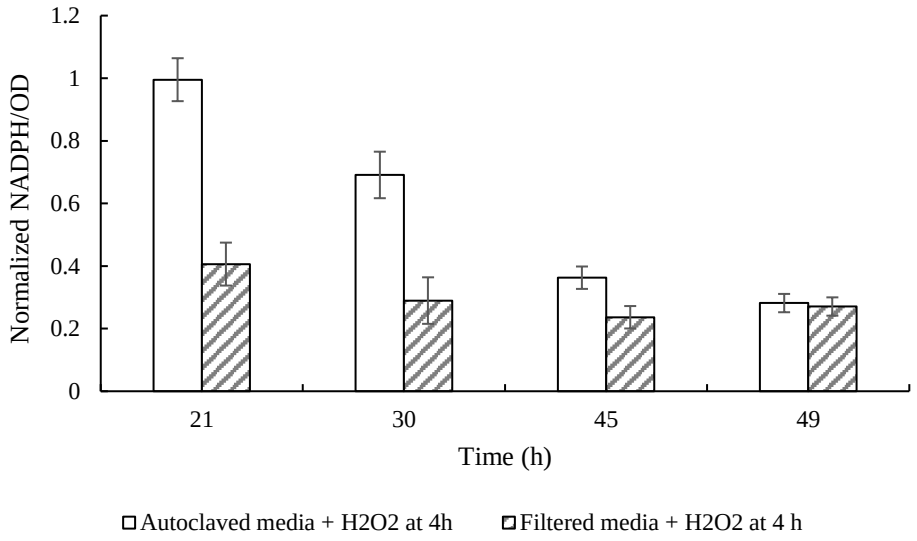

Figure 6-17 NADPH/OD in flasks cultures with heat sterilized and filtered media. Values were normalized with respect to maximum value in the data. Bars show 95% confidence interval

The NADPH content for the heat sterilized media was significantly higher than for the filtered media ($p<0.05$). These values are statistically different ($p<0.05$) until 45 h. At 49 h, the difference is not significant ($p>0.05$). The higher values of NADPH indicate that anti-oxidative reactions that require consumption of NADPH to mitigate the stress, e.g. catalase and glutathione mediated reactions, were

less active in the heat sterilized media as compared to the filtered media thus explaining the effect of stress on growth for the former as compared to the latter (Figure 6-16).

In accordance with the higher impact of oxidative stress when using heat sterilized media as compared to filtered media, the specific productivities of PRN for the heat sterilized media were the following: 0.0759 μL/mL/OD-hour and 0.0680 μL/mL/OD-hour for control and H_2O_2 addition in autoclaved media, and 0.0748 μL/mL/OD-hour and 0.0713 μL/mL/OD-hour for control and H_2O_2 addition in filtered media.

6.4.5 Specific productivities for each experiment

In Table 6-1, specific productivities of PRN for each set of experiments are shown. It should be noticed that control values are different because different inocula were used in each experiment, even though the strain was the same. Also, in the 20 L fermentations the volume of air per working volume per minute (vvm) in the reactor was smaller than in the 2 L fermentation (0.05 vvm compared to 0.38 vvm).

Experiment	Condition	µl/ml/OD-hour
Rotenone	Control Flask	0.0635
	Addition at 4 h	0.0819
	Addition at 24 h	0.0561
Dissolved oxygen	Control (35%)	0.0235
	70%	0.0193
Low Inoculum	Control Flask	0.0421
	Low Inoculum Flask	0.0224
	Control 2 L	0.0224
	Low Inoculum 2 L	0.0211
	Control 20 L	0.0218
	Low Inoculum 20 L	0.0127
Autoclaved media	Control autoclaved media	0.0759
	Autoclaved media + H_2O_2	0.0680
Filtered media	Control filtered media	0.0748
	Filtered media + H_2O_2	0.0713

Table 6-1 Specific productivities for PRN obtained for different conditions.

6.5 Conclusions

Addition of rotenone at 4 h adversely affected PRN production/release. Figure 6-1 shows that rotenone elicits significantly higher NADPH production as compared to the control. This is in agreement with the earlier observations (Zavatti *et al.*, 2016) for samples collected from an actual vaccine production train.

High levels of dissolved oxygen during fed-batch fermentation seem to have no detrimental effect on growth, since a similar behavior was obtain for control cultures (70% DO compared to 35% DO), but the specific productivity of PRN decreased (22% less PRN was released compare to control cultures). In view that the oxidative stress levels measured by flow cytometry were not higher for the high DO culture, it is argued that the decrease in PRN productivity is due to higher agitation rates that may fragment the PRN secreted into the extracellular environment as previously reported for another *B. pertussis* protein in (Rodriguez *et al*., 1993).

Low inoculum cultures in shake flasks also resulted in less specific PRN compared to the control. Measurement of oxidative stress with flow cytometry showed higher oxidative stress for the low inoculum culture as compared to the control culture that may explain the reduced productivity. The NADPH/OD is also significantly higher for the low inoculum culture thus corroborating previous observations of a negative correlation between NADPH and specific productivity due to stress.

A similar occurrence of higher oxidative stress was observed for low inoculum in the 2 L bioreactor with a corresponding lower specific productivity due to closed-loop control. However, the oxidative stress in 2 L appears to be more significant compared to the flask especially during the initial stages of the fermentation. It is argued that the closed-loop control, available in the bioreactor but not in flasks, serves to further exacerbate the detrimental effect of stress. It was observed that in response to the initial stress the agitation rate initially decreased so as the controller attempts to maintain the DO target in the presence of molecular oxygen generated by the anti-oxidative mechanisms. Because of this decrease

the mass transfer is expected to decrease thus resulting in slower glutamate consumption and longer exposure to higher concentrations of nutrient. The specific productivity of PRN in flasks was higher than those obtained in bioreactors.

Filtered media appears to have a protective effect against H_2O_2 addition compare to heat sterilized media. It is argued that heat sterilization results in inactivation/destruction of compounds that could serve to ameliorate oxidative stress.

We postulate that the culprit of deceleration of growth as well as significant reduction of PRN yield could be oxidative stress. Based on the heterogeneity of the cell populations, the degree of endurance against oxidative stress varies which probably as the result of fluctuations in protein yields, especially those which are susceptible to oxidative stress, such as PRN and AC-Hly (adenylate cyclase hemolysin). These proteins are likely to be harmed by superoxide (Khelef *et al*., 1996) which would turn out to become quantitatively diminished at the end of the purification process.

Chapter 7

The Role of NADPH in Anti-oxidative Mechanisms in *B. Pertussis*: Experimental and Modelling Studies

7.1 Introduction

In an earlier study (Zavatti *et al.*, 2016) it was found that the levels of NADPH in the supernatant of the production fermenters was negatively correlated with PRN levels at the end of the purification process. Since that correlation was relatively high at the fermentation stage as compared to the downstream processing stages, it was hypothesized that the fermentation step is the main source of variability in productivity of the PRN. NADPH has been identified as playing a role in anti-oxidative reactions for bacteria. For example, Carbiscol *et al.*, (2000) have found that in response to increased levels of reactive oxygen species (ROS) several reactions producing NADPH are upregulated. It was claimed that natural evolution has promoted such regulatory responses since NADPH is a key reactant in anti-oxidative reactions.

For example, Carbiscol *et al.*, (2000) (Figure 7-1) identifies anti-oxidative responses to oxidative stress involving the induction of two enzymes, catalase and peroxidase, that regulate glutathione related reactions and that require NADPH as a key reactant. Thus, in these reactions NADPH provides the reductive power to quench stress and regenerates enzymes such as catalase once they are oxidized after detoxification of ROS.

The key role of NADPH in anti-oxidative reactions and in view that NADPH is not present in fresh media led to the hypothesis that the observed increase in NADPH in the supernatant is related to increased oxidative stress. This hypothesis was further reinforced as oxidative stress has been reported

to negatively impact both cell growth and protein production and causes protein damage (Keyer *et al.*, 1996). Thus, the observed negative correlation between NADPH levels and productivity can be assumed to be related to increase ROS during fermentation.

However, NADPH is generated within the cells while the observed NADPH was measured in the supernatant leading to a number of questions: i- Is there a mechanism for transport of NADPH from the cell?; ii- How are the intracellular levels of NADPH related to the observed extracellular levels of NADPH?; and iii- How are the observed levels of extracellular NADPH related to the measured concentration of ROS, glutamate (main nutrient) and biomass?

This chapter addresses these questions through experimental and modelling studies. Since NADPH has been reported to be secreted when bound to catalase, the possibility that the observed NADPH is bound to this enzyme was investigated. Secondly, a simple mass balance was used to relate intracellular to extracellular NADPH. Finally, a simple metabolic model was formulated to explain the observed levels of nutrient, biomass, NADPH and ROS. This model also served to explain the observed adaptation mechanism of the culture to oxidative stress as supported by the late recovery in growth rate sometime after the culture was exposed to induced oxidative stress. Model predictions were compared to lab scale experiments reported in Chapter 5 and 6 corresponding to early exposure of the cell cultures to H_2O_2 or initiated with low inoculum size.

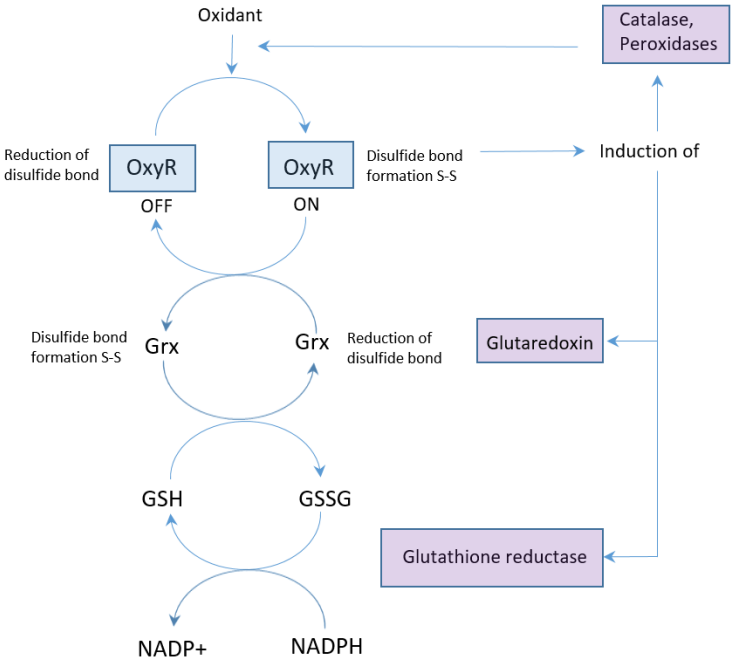

Figure 7-1 "On-off" mechanism of OxyR regulation (adapted from Cabiscol *et al.*, 2000).

7.2 Catalase fluorescence

In previous work (Zavatti *et al.*, 2016) it was found that the fluorescence peak associated with NADPH was shifted slightly in terms of emission/excitation values with respect to the values reported for pure NADPH (Rover *et al.*, 1998; Lakowicz, 2006). NADPH binding has been reported to be a possible cause for such shift in fluorescence (Gazzotti *et al.*, 1974). In addition, NADPH has been reported to be bind to catalase for protective purposes and the secretion of NADPH bound with catalase has also been reported (Kirkman *et al.*, 1987; Wan *et al.*, 2017). Following these considerations it was hypothesized that the NADPH peak found in the culture supernatant is related to catalase bound to NADPH that is secreted by the bacteria. Catalase has four tightly bound NADPH moieties (Kirkman

et al., 1984). In order to assess the fluorescence emission of NADPH from catalase, a series of experiments were done with bovine liver catalase (BLC).

It has been reported that NADPH binding sites in bovine liver catalase (BLC) are conserved in KatA (Barrière *et al.*, 2002), which is the gene encoding catalase in *B. pertussis* (DeShazer *et al.*, 1994). The sites Arg-202 and His-234 in BLC, appear in KatA as Arg-181 and His-213. Changes in other residues of KatA in comparison to BLC, are reported to not influence the enzyme activity or the interaction with NADPH (Barrière *et al.*, 2002). For this reason, both enzymes are comparable and BLC was chosen for this test.

The fluorescence emission-excitation matrix for catalase in 10 mM PBS (pH 7.2) is shown in Figure 7-2.

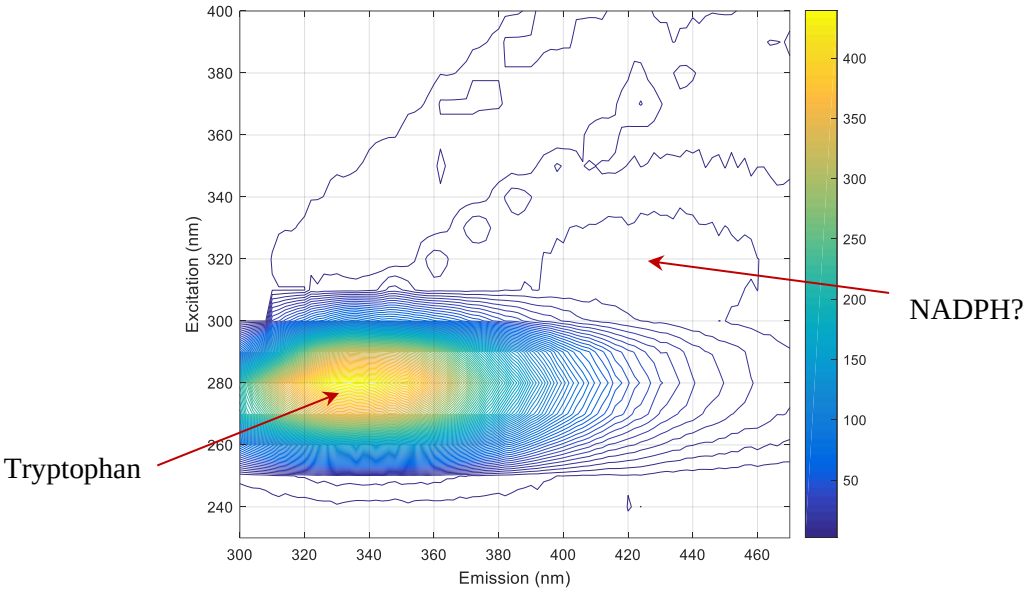

Figure 7-2 Fluorescence excitation-emission matrix for bovine liver catalase (BLC) in 10 mM PBS (pH 7.2).

In the fluorescence spectrum of BLC, a strong peak related to tryptophan (Trp) occurs at Ex/Em=280/330 nm, and a second weaker peak appears around Ex/Em=320/430 nm, which it is not exactly at the expected Ex/Em of NADPH (340/460 nm). Since NADPH is embedded in the protein, it was necessary to denature the enzyme to observe the NADPH emission. It is known that reduced forms of pyridine (NADH, NADPH) survive in strong alkali, while the oxidized forms (NAD^+, $NADP^+$) are destroyed (Lowry *et al*., 1972). 100 μL of BLC was treated with 3.2 mL of 5 N NaOH in an attempt to capture the emission of NADPH embedded in the molecule.

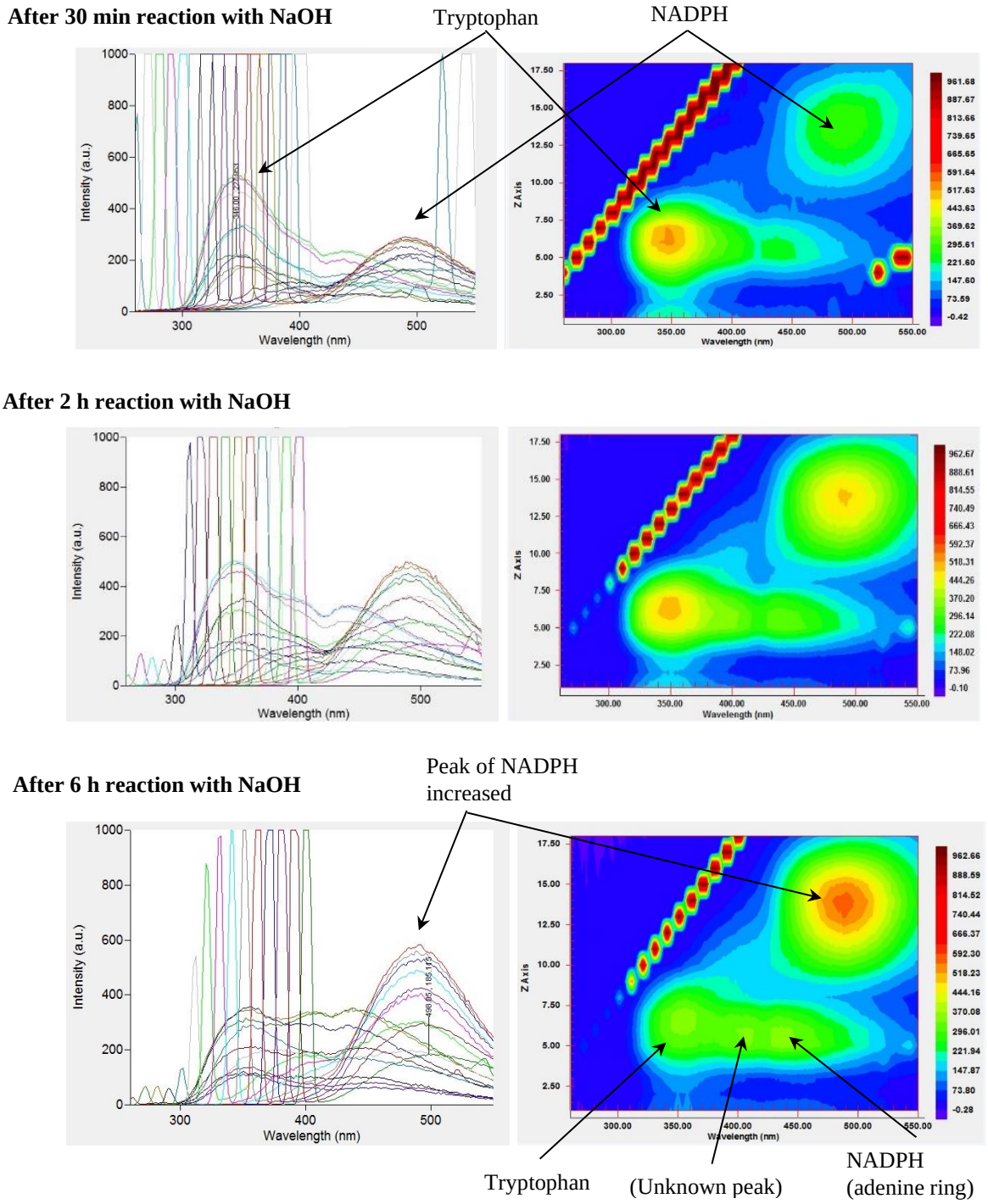

Figure 7-3 Catalase fluorescence at various time intervals following treatment with NaOH.

Figure 7-3 shows the excitation-emission matrix for catalase at different time intervals following treatment with 5N NaOH. Lines in the graphs in the LHS are the emissions for each different excitation value; graphs in the RHS are the contour representations of these values. After treatment with NaOH, there is a progressive increase in the visibility of NADPH (Figure 7-3). Prajapati *et al.* (1998) found that at pH 11.5, BLC loses enzymatic activity and dissociates into monomers, and that the protein can refold after treatment with a salt (KCl or Na_2SO_4) but with a different structure. It has been reported that the prosthetic group, ferriprotoporphyrin IX, present in heme-catalases can catalyze the same enzymatic reaction as its holoenzyme, but in a less efficient fashion (Zámocký *et al.*, 1999).

To verify whether the catalase present in the sample was still active, the activity of the catalase was measured. The test involves assessing the presence of active catalase by observing the amount of foam formed after the introduction of H_2O_2 into the sample. In Figure 7-4 provides a picture of the catalase assay with and without NaOH.

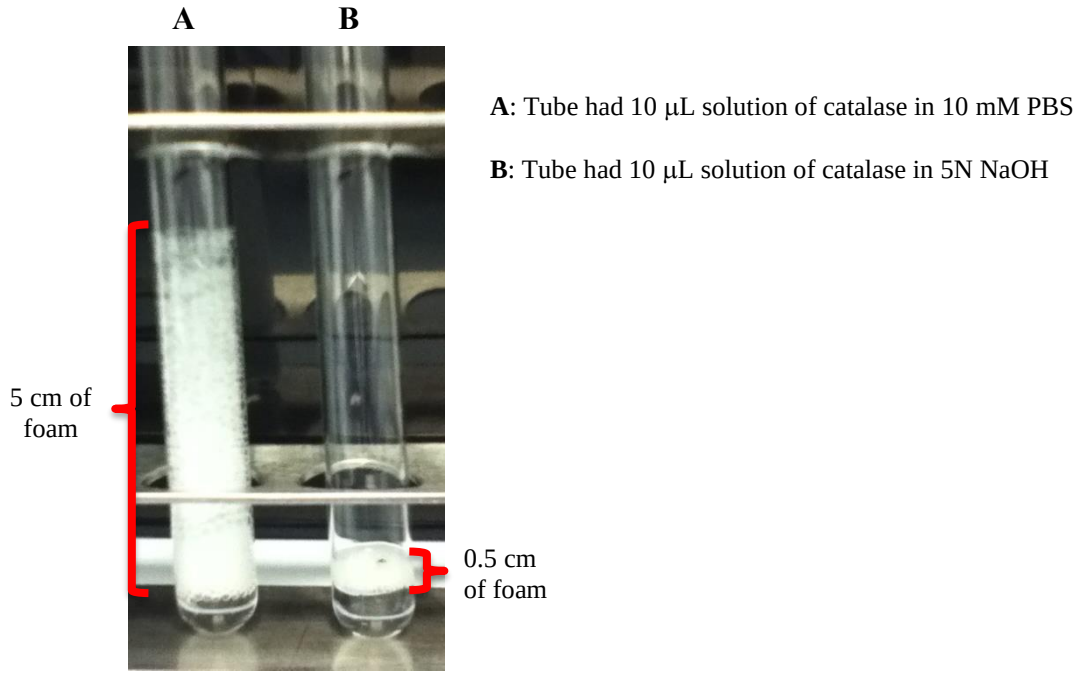

Figure 7-4 Catalase test for BLC in 10 mM PBS and treated with NaOH.

The catalase catalyzes the decomposition of H_2O_2, to produce O_2 and H_2O. In the presence of the surfactant (Triton-X) the O_2 bubbles are stabilized in the surfactant resulting in foam formation. For the catalase in buffer, a column of foam 10 times greater than the one formed for catalase treated with NaOH was observed. The minor formation of foam in the latter indicates that the catalase is still active. This same test was done on the supernatant of flask cultures of *B. pertussis* and formation of foam was also observed. Also, to test the specificity of the method, a negative control experiment was conducted with sodium azide, which is a catalase inhibitor (Iwase *et al.*, 2013).

An additional experiment was performed to determine if changes in the fluorescent emission of catalase occur in the presence of H_2O_2. Kirkman *et al*. (1987) reported that NADPH prevents inactivation of catalase by H_2O_2. The spectra obtained are shown in Figure 7-5. To correlate this observation with the particular fluorescence fingerprint, samples were treated with H_2O_2 and spectra collected.

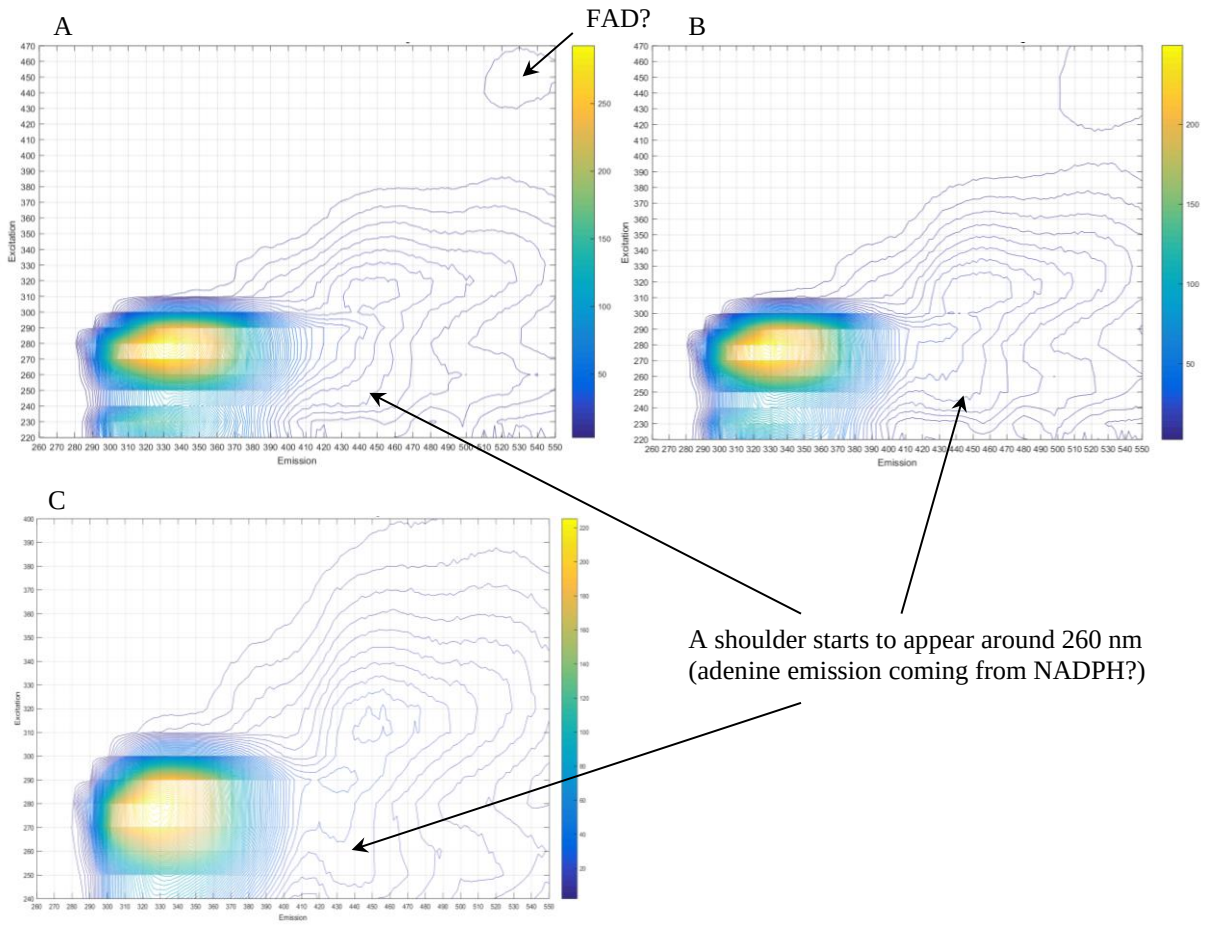

Figure 7-5 Catalase fluorescence after reaction with 35% H_2O_2: A- after 5 min, B- after 40 min, and C- after 4 h.

After H_2O_2 addition, a shoulder at an emission of 260 nm started to appear. This emission can be largely be attributed to the NADPH and its adenine moiety.

To further investigate whether the observed NADPH emission can be attributed to catalase, another experiment was done using media with growth factors. Results of this experiment are presented in Figure 7-6. 40 µL of 35% H_2O_2 was added to 3 mL of media with growth factors. The objective was to

show that the presence of growth factors that may influence the spectra. The observed shift in NADPH fingerprint is similar to the one observed from samples collected from the production reactor train.

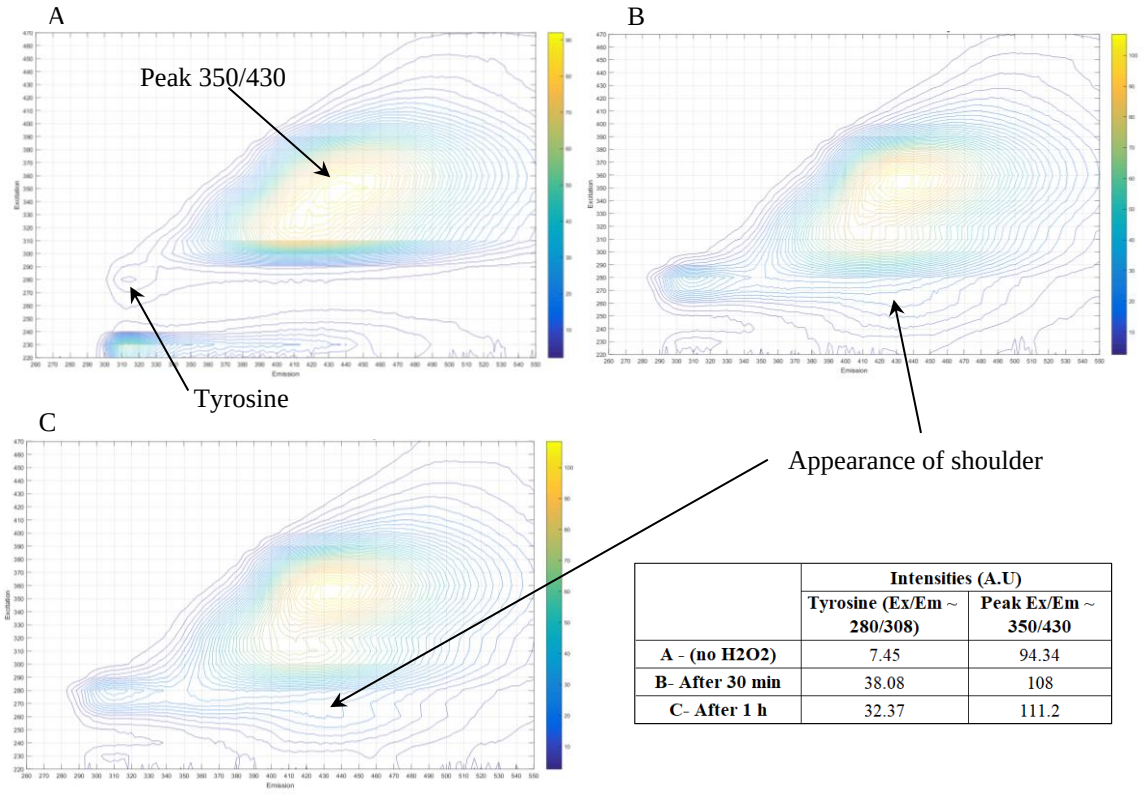

	Intensities (A.U)	
	Tyrosine (Ex/Em ~ 280/308)	Peak Ex/Em ~ 350/430
A - (no H2O2)	7.45	94.34
B- After 30 min	38.08	108
C- After 1 h	32.37	111.2

Figure 7-6 Fluorescence for media, growth factors and 35% H_2O_2. A- without H_2O_2, B- after 30 min from the addition of H_2O_2, C- after 1 h from the addition of H_2O_2**.**

After 1 h reaction of media and growth factors with H_2O_2, 40 µL of a solution of catalase (10 µL pure catalase in 1 mL 10 mM PBS) were added.

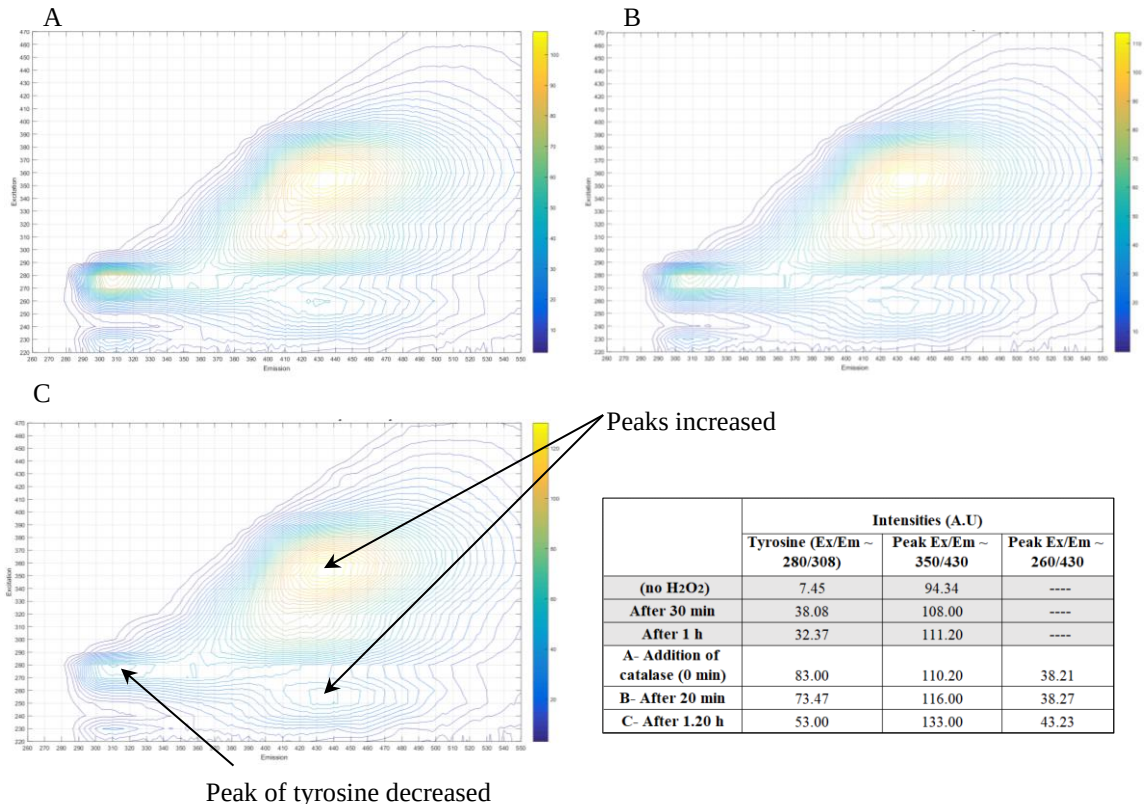

	Intensities (A.U)		
	Tyrosine (Ex/Em ~ 280/308)	Peak Ex/Em ~ 350/430	Peak Ex/Em ~ 260/430
(no H_2O_2)	7.45	94.34	----
After 30 min	38.08	108.00	----
After 1 h	32.37	111.20	----
A- Addition of catalase (0 min)	83.00	110.20	38.21
B- After 20 min	73.47	116.00	38.27
C- After 1.20 h	53.00	133.00	43.23

Figure 7-7 Fluorescence for media, growth factors, 35% H_2O_2 and addition of catalase after 1 h from the addition of H_2O_2. A- At 0 min, B- After 20 min from the addition of catalase, and C- After 1.2 h from the addition of catalase

The resulting fluorescence spectra in Figure 7-7 following the addition of hydrogen peroxide, are very similar to the ones obtained for supernatant *B. pertussis* cultures from the production train (Figure 7-8). For *B. pertussis* supernatant, there is a peak that appears around Ex/Em 280/460 nm, which is attributed to NADPH bound to an enzyme that has been hypothesized to be catalase. This peak appears 24 h into the fermentation (Figure 7-8)

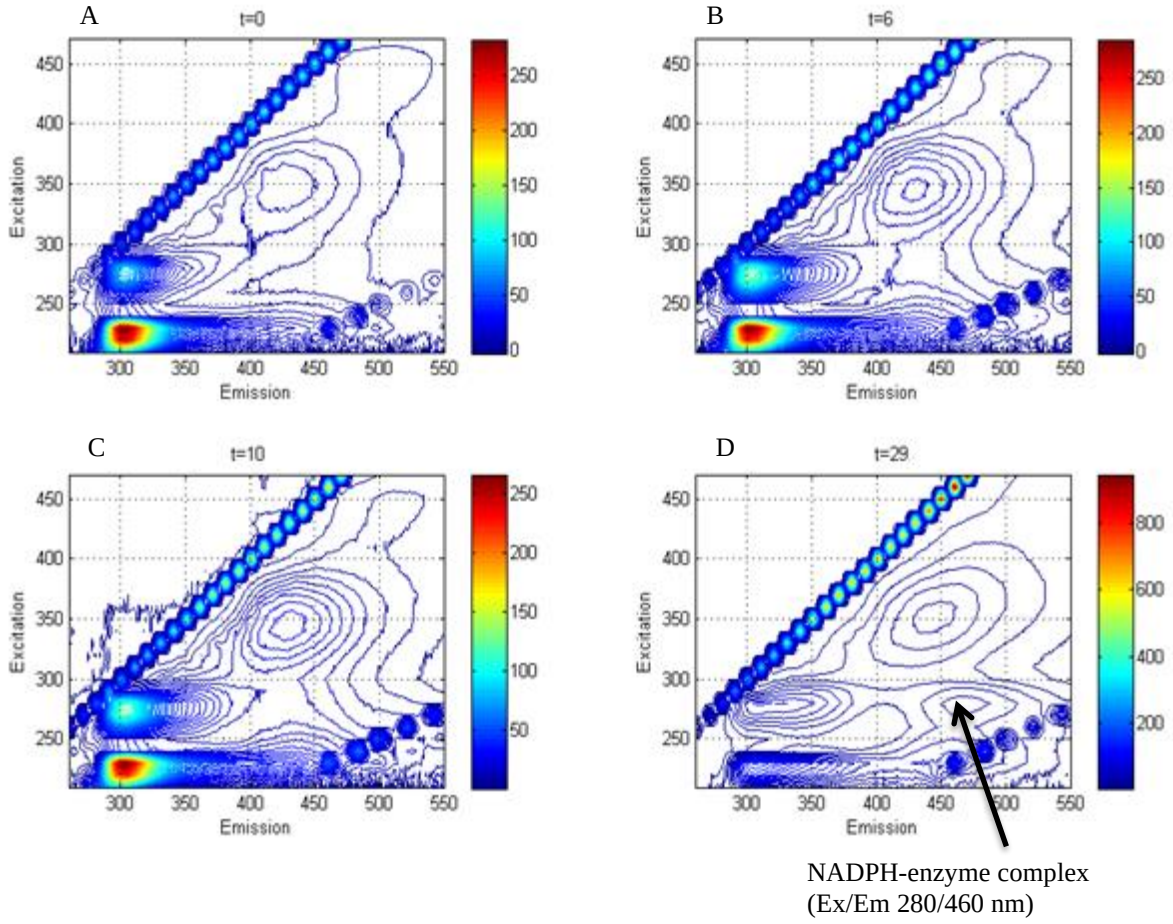

Figure 7-8 Fluorescence spectra for 2000 L fermentation supernatant samples for A- t= 0 h, B- t=6 h, C- t= 10 h, D- t= 29 h.

The results in this section may indicate that the observed shift of NADPH in the fluorescence spectra appears to be related to its binding to an enzyme. Since the catalase activity experiments indicate that there is an enzyme that catalyzes a reaction involving peroxide, it is proposed that enzyme bound to NADPH is catalase. It cannot be categorically attributed to catalase since other enzymes, such as glutathione peroxidase, can also catalyze the consumption of hydrogen peroxide. However, since there

isn't any evidence in the literature that glutathione peroxidase binds to NADPH, catalase is the most plausible candidate for binding of the NADPH in the supernatant.

Although a mechanism for secretion of catalase has been reported in the literature for *E. coli* (Wan *et al*., 2017), it was not evident whether for *B. pertussis* the presence of a NADPH-catalase complex in the supernatant was due to a continuous secretion of the intracellular NADPH or a result of release due to cell death. To investigate this a mass balance of the intracellular and extracellular levels of NADPH as quantified by fluorescence in samples from flask studies was conducted and presented in the following section.

7.3 Intracellular and Extracellular NADPH

Equation 7.1 describes the mass balance for intracellular and extracellular NADPH in a sample. The accumulation of extracellular NADPH in the culture volume is assumed to be equal to the summation of the NADPH secreted plus the NADPH released to the supernatant due to cell death (lysis) as follows:

$$V_{sample}\frac{dNADPH_{ext}}{dt} = K_s * NADPH_{int} * V_{cell} + V_{dead}\frac{dNADPH_{int}}{dt} + NADPH_{int}\frac{dV_{dead}}{dt} \quad (7.1)$$

Where V_{sample} is the volume of the sample, $NADPH_{ext}$ and $NADPH_{int}$ are extracellular and intracellular NADPH concentrations respectively, K_s is a kinetic constant of secretion, V_{cell} is the volume of cells in the sample and V_{dead} is the volume of dead cells in the sample. The term in the left hand side represents the accumulation of extracellular NADPH in the supernatant. The first term in the right hand side represents the NADPH secreted and the last two right hand side terms are related to cell

death. There are many mechanisms for enzyme transport across biological membranes (Kostakioti *et al.*, 2005) but since the particular mechanism for catalase transport in *B. pertussis* has not been investigated, it was assumed for simplicity that the secretion is proportional to the intracellular concentration of NADPH where the latter is bound to catalase as discussed above (first term in the right hand side of equation 7.1). The last two terms in the right hand side of equation 7.1 describing the release of the NADPH-catalase complex from dead cells is obtained from the time derivative of the product of $V_{dead} * NADPH_{int}$ that is the amount of NADPH contained inside the dying cells, that might be secreted because of membrane damage.

The NADPH fluorescence (intracellular and extracellular) were measured, and by means of a standard calibration curve (Figure 7-9) the concentration of NADPH was calculated

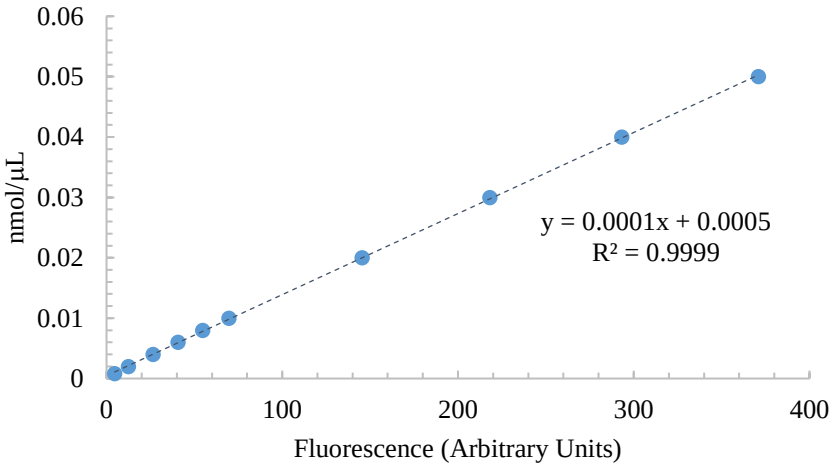

Figure 7-9 NADPH standard calibration curve.

The volume of live and dead cells were inferred from the percentage of live and dead cells measured by means of a flow cytometric viability test (using SYTO9 for live cells and PI for dead cells). The

total volume of cells was calculated using a calibration curve between OD_{600} and colony forming units per mL (CFU/mL) for *B. pertussis*. A volume of a single cell was calculated assuming that the cell has spherical shape with diameter 0.5 μm.

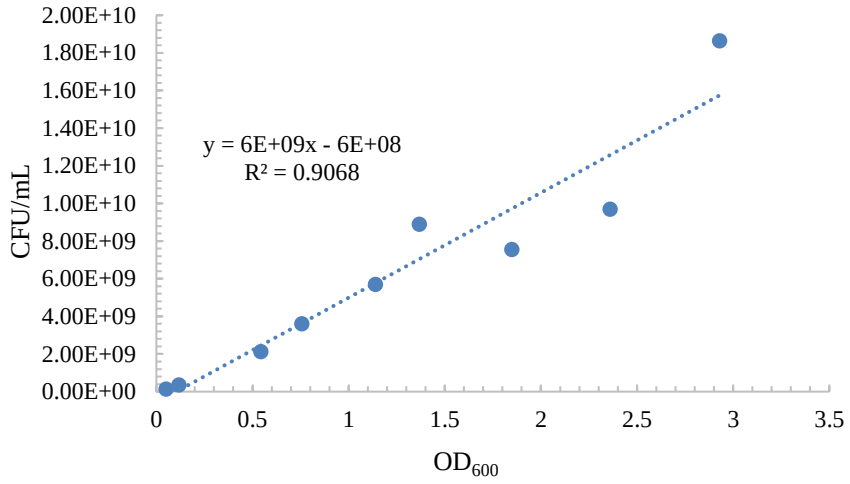

Figure 7-10 Calibration curve between OD_{600} and colony forming units per mL (CFU/mL) for *B. pertussis*

In Table 7-1, discretized calculations for samples from two control flasks are shown for time 24 h and 32 h.

				"Extracellular NADPH" (term)	"secretion" term		"Loss by dead cells" term	
Flask	**Time (h)**	**NADPH*int* nmol/μL**	**NADPH*ext* nmol/μL**	**Vsample*[Next(t+Δt)-Next(t)]/Δt**	**Ks**	**Ni*Vlive**	**Vdead*[Ni(t+Δt)-Ni(t)]/Δt**	**Ni*[Vdead(t+Δt)-Vdead(t)]/Δt**
Control 1	**24**	2.3159	0.1773	7.8814	3.0579	2.5729	0.0000	0.0138
Control 1	**32**	2.3625	0.2404	12.3791	1.7227	7.1787	0.0008	0.0115
Control 2	**24**	1.4989	0.1720	16.1194	4.5255	3.5596	0.0013	0.0093
Control 2	**32**	2.0606	0.2365	12.9877	1.6734	7.7526	0.0049	0.0097

Table 7-1 Discretized values for NADPH mass balance.

From Table 7-1, it is clear that values for the secretion term are significantly higher than the loss by dead cells. For these reasons and for the fluorescence measurements, it is concluded that the NADPH observed in the supernatant mostly originates from secretion most probably bound to catalase as shown by the experiments in the previous section.

7.4 ODE Model of adaptation

The results in this chapter show that NADPH plays a key role in quenching oxidative stress either as a reactant for anti-oxidative reactions (Figure 7-1) or due to its protective action for catalase. The dynamic evolution of NADPH during culture development as measured by fluorescence of the supernatant is expected to exhibit a high correlation with the evolution of oxidative species over time. Furthermore, since oxidative stress is known to have a detrimental effect on growth, a high degree of dynamic correlation was also expected among NADPH, ROS and the key cell culture parameters such as biomass and key nutrient (glutamate) depletion. To describe these expected dynamic correlations, a simple mathematical model is proposed that describes the evolution of the variables related to oxidative stress that were measured at both lab scale and production. The model is based on the main reactions that are related to oxidative stress and it only describes the evolution of the main variables measured in the experiments: glutamate, biomass, ROS and extracellular NADPH. This model not only serves to explain the dynamic sequence of events between the onset of oxidative stress (e.g. addition of hydrogen peroxide, production of NADPH in response stress and impact on cell growth) but it also serves to explain the adaptation to stress observed in the experiments.

Essential elements of the metabolic network of *B. pertussis* were considered to build an ODE model to explain the mechanism of adaptation (Figure 7-11).

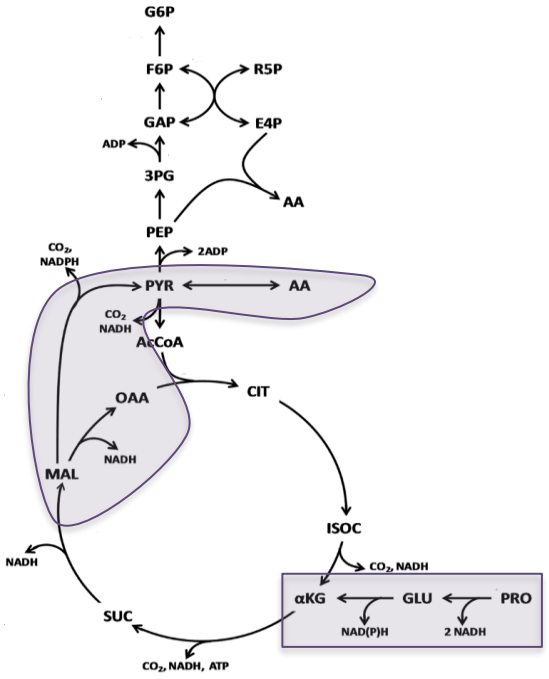

Figure 7-11 Simplified metabolic pathway in *B. pertussis*: G6P: glucose-6-phosphate; F6P: fructose-6-phosphate; R5P: ribulose-5-phosphate; E4P: erythrose-4-phosphate; GAP: glyceraldehyde-3-phosphate; 3PG: 3-phosphoglycerate; PEP: phosphoenolpyruvate; PYR: pyruvate; AcCoA: acetyl-CoA; CIT: citrate, ISOC: isocitrate; αKG: α-ketoglutarate; SUC: succinate; MAL: malate; OAA: oxaloacetate; GLU: glutamate; PRO: proline; AA: amino acids. (Adapted from Izac *et al.*, 2015).

B. pertussis uses glutamate and proline as sources of carbon. These two amino acids enter into the TCA cycle through the production of α-ketoglutarate and NADPH. NADPH is also produced in the reaction from maleate to pyruvate and oxaloacetate, which are also funneled to the production of biomass through amino acid synthesis. NADPH formed in these reactions serves in the adaption to oxidative stress. The reactions used in the model are identified in Figure 7-11. It was also assumed that catalase production is induced in response to stress as per Figure 7-1 as reported by Cabiscol *et al.*, (2000) for *E. coli*.

To model the adaptation to stress it was hypothesized that two key enzymes regulate the response to stress: E1 and E2 that accumulate overtime in response to stress. The function of E2 is to initially inhibit growth while the function of E1 is to progressively accumulate and contribute to increasing amounts of $NADP^+$ to be produced by quenching reactions of ROS (Figure 7-11). As such, E1 could correspond to catalase that is induced by ROS. The availability of increasing amounts of $NADP^+$ serve to increase the production of biomass through reaction 7 and 8 below.

Although the effect of oxidative stress has been widely reported (Imlay *et al*., 2015) the exact enzyme that is responsible for such inhibition (E1) has not been determined in this study. For example, it is known that excess stress accelerates reactions with free iron that result in mutagenesis and DNA damage.

In general, the combination of reactions 3 to 8 reflect the overall contribution of glutamate to biomass through the TCA cycle and through pyruvate formation. It should be remembered that *B. pertussis* presents a gluconeogenesis pathway by which G6P is produced from pyruvate. Then G6P feeds into the pentose phosphate pathway for biomass formation.

In summary the metabolic reactions considered for the model are as follows:

Reaction 1: GLU → amino acids (biosynthesis)

Reaction 2: GLU → biomass nucleotides

Reaction 3: GLU → α-ketoglutarate + NADPH

Reaction 4: α-ketoglutarate → malate

Reaction 5: NADPH + ROS → H_2O + $NADP^+$

Reaction 6: NADPH – catalase (protection of catalase) → $NADP^+$

Reaction 7: $NADP^+$ + malate → pyruvate + NADPH

Reaction 8: pyruvate → biomass

Reaction 9: GLU → ROS

Reaction 10: adaptive activation of enzyme (possible catalase) in response to the rate of oxidative stress and described by the time integration of the ratio ROS/biomass

Reaction 11: adaptive activation of second enzyme (possible reductase) in response to oxidative stress and is described as a time integration of the ratio of ROS/biomass

Based on the identified important metabolic reactions given above a set of 7 ODE equations were formulated as follows:

$$\frac{dGLU}{dt} = \frac{-k1*GLU*Xv}{k2+GLU+0.01*E2} \tag{7.2}$$

$$\frac{dXv}{dt} = \frac{k3*GLU*Xv}{k2+GLU+0.1*E2^{2.9}} + 0.006 * E1 * Xv * GLU \tag{7.3}$$

$$\frac{dROS}{dt} = \frac{k4*GLU*Xv}{k5+GLU} - \frac{2*k6*ROS*NADPH*Xv}{k7+ROS+NADPH} \tag{7.4}$$

$$\frac{dE1}{dt} = \frac{1600*ROS}{Xv} \quad (\text{GLU} > 1), \quad \frac{dE1}{dt} = -500 * E1 \tag{7.5}$$

$$\frac{dE2}{dt} = \frac{110*ROS}{Xv} \quad (\text{GLU} > 1), \quad \frac{dE2}{dt} = -0.1 * E2 \tag{7.6}$$

$$\frac{dNADPH}{dt} = \frac{k10*GLU*Xv}{k11+GLU} - \frac{2*k8*ROS*NADPH*Xv}{k9+ROS+NADPH} - 0.001 * (Cat\_NADPH) * Xv \tag{7.7}$$

$$\frac{dCat\_NADPH}{dt} = 0.09 * E1 * Xv - 0.03 * (Cat\_NADPH) * ROS \tag{7.8}$$

Where $k1$=1, $k2$=6, $k3$=21, $k4$=0.4, $k5$=0.0001, $k6$=0.25, $k7$=24, $k8$=2.35, $k9$=0.1, $k10$=5.5, $k11$=0.0001

The parameters where calculated using a nonlinear programming solver in Matlab, with trial and error adjustments.

GLU = extracellular glutamate concentration, *Xv* = biomass, *ROS* = reactive oxygen species (measured by cDCF by flow cytometry), *Cat_NADPH* = refers to the enzyme/NADPH complex measured in the supernatant by fluorescence where the enzyme is presumably catalase based on the findings presented in previous sections), E1 and E2 are two enzymes, where E1 is intracellular catalase and E2 is an enzyme responsible for growth inhibition which cannot be categorically identified.

The relation between the differential equations and the metabolic reactions is shown in Table 7-2.

Equation 7.2 describes the overall flux of the main nutrient (glutamate) towards biomass formation through synthesis of nucleotides, amino acids and flux through the TCA cycle.

Equation 7.3 describes the formation of biomass from consumption of nutrients. This equation also includes an additional term (second term in the RHS) that reflects enhanced growth in response to increased availability of $NADP^+$ from anti-oxidative reactions mediated by intracellular catalase. This additional term is key to explaining the adaptation to stress reflected by a rapid increase in growth observed towards the end of the fermentation.

Equation 7.4 describes the production of ROS from glutamate through the electron transport chain (first term in the RHS) and its consumption following its reaction with intracellular NADPH (second term in the RHS).

Equations 7.5 and 7.6 describe the accumulation over time of enzymes E1 and E2 and their posterior deactivation due to proteolytic activity. The deactivation is applied when the concentration of glutamate is below some threshold (GLU<1).

Equation 7.7 describes the intracellular NADPH concentration determined by the production of NADPH in the TCA cycle (first term in RHS) and the depletion of NADPH through reaction with ROS (second term in RHS) and binding with catalase and posterior secretion outside the cell (third term in RHS).

Equation 7.8 describes the accumulation of the *Cat_NADPH* complex in the supernatant that is measured by fluorescence and it is determined by the production of catalase (first term in RHS) and a depletion term possibly related to proteolytic activity (second term in RHS). This second term had to be added to explain a slight decrease in the *Cat_NADPH* fluorescence measurements that could not be explained otherwise.

Equation	Reactions
7.2	1,2,3,4,5,6,7,8
7.3	1,2,3,4,5,6,7,8
7.4	5 and 9
7.5	10
7.6	11
7.7	3,5 and 6
7.8	10

Table 7-2 Relationship between ODE system and reactions chosen from the metabolic network.

The model was assessed against experimental data for 20 L fermentations: i- control; ii- low inoculum; and iii- H_2O_2 addition at 4 h. It was only assessed for the fermenter and not in flasks because in the absence of the DO control in flasks, cells respond differently to stress, and the model does not account for these differences. Also, there was no GLU data available for the flask studies. In Figure 7-12 and Figure 7-13 are shown for both sets of experiments where connected dots indicate

experimental results and solid lines indicate model predictions. Red lines indicate control experiments, i.e. no peroxide addition and usual inoculum size used (OD 0.3), and blue lines indicate, oxidative stress conditions induced by either the addition of H_2O_2 at 4 h after the start of the batch or by the use of a low inoculum size that as shown in Chapters 5 and 6 resulted in increased ROS levels. The experimental values and time were scaled.

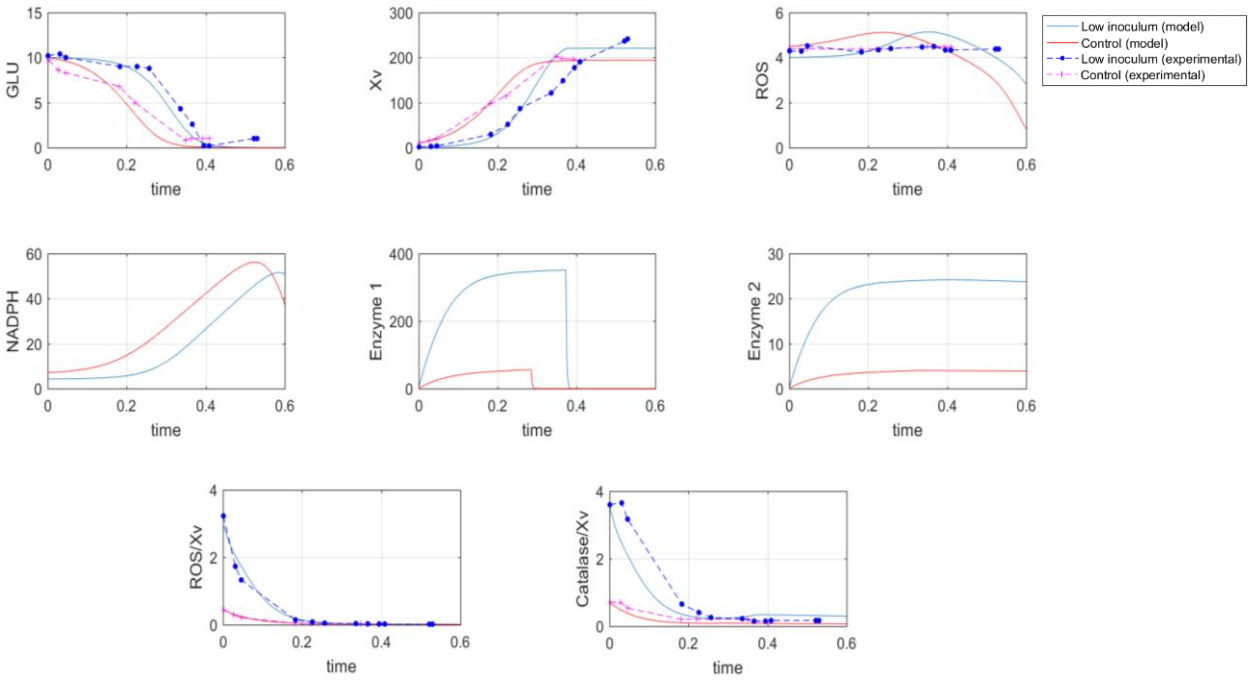

Figure 7-12 Model prediction vs. experimental data for a 20 L fermentation with a different inoculum size.

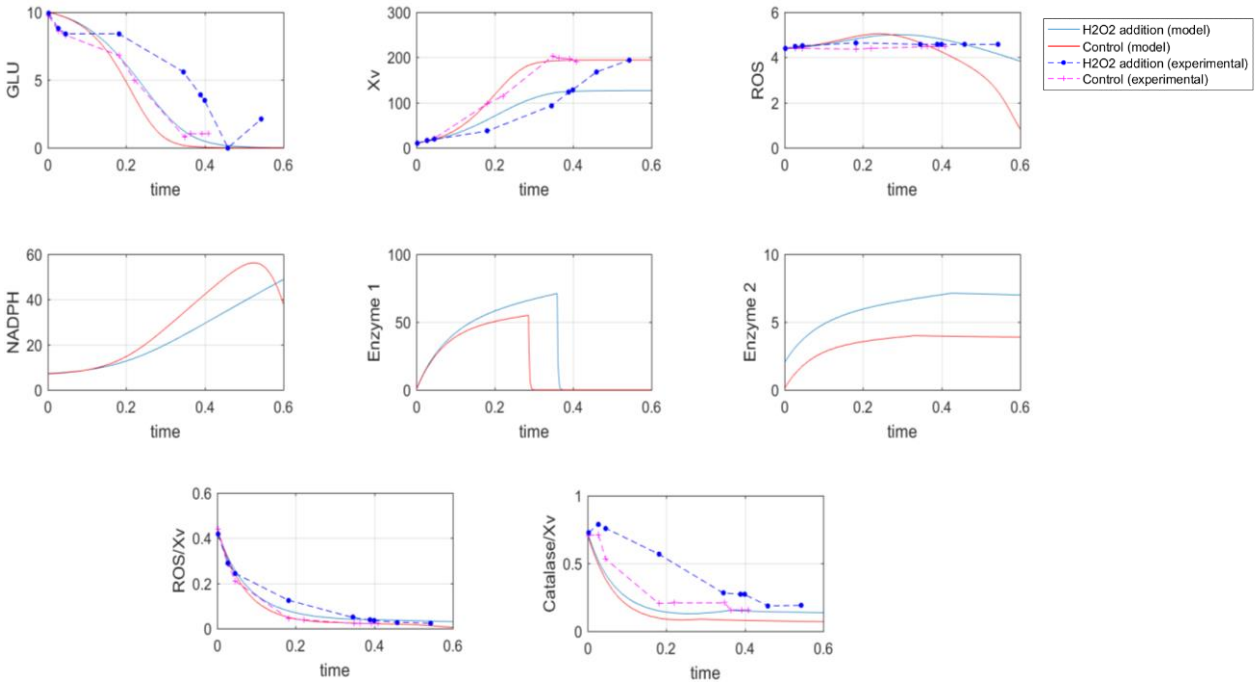

Figure 7-13 Model prediction vs. experimental data for a 20 L fermentation with addition of H_2O_2

The model simulated well the trends observed in the experiments. For the low inoculum experiment, where it was hypothesized that the cells undergo higher stress when the inoculum is small because the cells are exposed for a longer duration to higher concentrations of nutrients, adaptation to the stress towards the end of the culture is observed experimentally and it was successfully described by the model. NADPH increases because it is secreted in its bound form to catalase and accumulates in the supernatant.

The model simulated well the behavior for the H_2O_2 addition experiment, where stress was imposed by the external addition of peroxide. The indirect supply of oxygen due to the conversion of peroxide by catalase causes the reactor controller to slow down agitation bringing with it a decrease in mass transfer, which slows down the depletion of glutamate and consequently biomass growth. The behavior

observed for Enzyme 1 (E1) does not seem biologically likely, and it is assumed to be due to parameters that need to be adjusted.

The model simulated this trend. The mechanism of adaptation activated by the enzymes can be explained as the mechanism "on-off" activated by the transcription factor OxyR. In response to oxidative stress, the transcription factor OxyR triggers the synthesis of enzymes that detoxify ROS. NADPH helps to regenerate these enzymes once they are oxidized after detoxification by ROS. When the enzymes are regenerated, the OxyR is deactivated, and in this manner the process is auto-regulated (Cabiscol *et al.*, 2000). Equations 4 and 5 consider the activation and the deactivation of these enzymes.

7.5 Discussion

Following the recognition of the central role of NADPH in the current investigation, this chapter provides experimental and modelling results to interpret the NADPH measurements during cell culture and its correlation with the ROS levels, nutrients and biomass.

First, the fact that NADPH supernatant measurements by fluorescence exhibited a shift in emission-excitation wavelength as compared to the emission-excitation reported for pure NADPH hinted that the cofactor is bound to an enzyme causing the observed shift. Catalase activity determination showed that catalase activity is present in the supernatant for lab-scale and production bioreactor samples. Using NaOH it was demonstrated that the changes occur in the fluorescence spectra following induced conformational changes in the catalase-NADPH complex. A mass balance that considered viable and dead cells and intracellular and extracellular levels of measured NADPH indicates that the NADPH observed in the supernatant mostly originates from secretion rather than being released from dead cells. Finally, a dynamic metabolic model was proposed based on the main metabolic pathways related to

glutamate depletion, ROS production, biomass formation and build-up of NADPH bound to catalase in the supernatant. The importance of this model is that it provides a mechanistic understanding of the dynamic phenomena occurring in culture following exposure to stress. In particular a possible mechanistic explanation of the adaptation mechanism originating from the increased availability of $NADP^+$ that serves to promote growth through increased pyruvate formation is proposed. Furthermore, the model helps to integrate the key measurements collected from the experiments, i.e. glutamate, biomass, ROS and supernatant NADPH, and to elucidate cause and effect relations during culture growth.

Chapter 8

Flow Cytometric Analyses and Multivariate Analyses of *B. pertussis* Fermentations in the Vaccine Manufacturing Process

8.1 Introduction

Following the observations in our earlier studies (Zavatti *et al.*, 2016) that revealed a negative correlation between the levels of NADPH measured in the supernatant of Sanofi Pasteur production fermenters and level of PRN (based on Kjeldahl measurements) at the end of the process it was hypothesized that oxidative stress is the cause of the observed variability in the process. As explained in the literature review, NADPH is one of the key reactants in anti-oxidative reactions occurring in *B. pertussis* and through natural evolution bacteria have acquired the ability to upregulate pathways for generation of NADPH in response to ROS.

In addition it was observed in these earlier studies (Zavatti *et al.*, 2016) that fermentation profiles including dissolved oxygen, pH and aeration rates did not show any clear correlation to productivity levels. This led to an additional hypothesis that variability may be related to the heterogeneity of the cell populations in the fermenters that is not well captured by the fermentation profiles, since the latter reflect average properties only.

To investigate these hypotheses a cytometry study was conducted using samples collected from the production train at Sanofi Pasteur. Different markers indicative of oxidative stress and viability were investigated and correlations sought with final Kjeldahl-based productivity measurements using multivariate statistical techniques.

8.2 PCA analysis in the upstream process

Five PRN batches were analyzed from the upstream production process using flow cytometry. The variables measured were cDCF fluorescence (related to ROS), and forward and side scattering. Each batch consisted of four fermentations of 20 L, four fermentations of 200 L and four fermentations of 2000 L. The time points analyzed were 0 h, 7 h and 24 h for the 20 L and 200 L fermenters, and 0 h, 7 h, 24 h, 36 h, and 52 h for the 2000 L fermenter.

PCA was performed to reduce the number of variables in the flow cytometry data and to identify major statistically significant correlations within the original data set. The optimal number of principal components was determined based on a cross-validation procedure presented in the Chapter 3. To further assess the relevance of each of the flow cytometry variables to productivity, the data was organized into three matrices: i- a matrix with data for cDCF, forward scattering and side scattering for the 20 L fermentations; ii- a matrix with data for cDCF, forward scattering and side scattering for the 200 L fermentations; and iii- a matrix with data for cDCF, forward scattering and side scattering for the 2000 L fermentations. There were a total of 33 variables for each time point (11 variables for each parameter). The number of variables per parameter was determined by the software associated with the flow cytometer through a "binning" algorithm (i.e. summation of occurrences within bins each corresponding to a particular range of values of a particular flow cytometry parameter being tested). Accordingly, each bin will be referred heretofore as intensity bins since they correspond to different ranges of intensities for each parameter. The choice of the number of bins was done based on a trial and error procedure where different numbers were tried and for each of these choices a multivariate PCA model was determined. The number of bins that resulted in a PCA model that captured the greatest variability in the data was chosen for further analysis. The resulting number of components obtained

after pre-processing the data with auto-scaling and cross-validation, and the variance captured for each component are shown in Table 8-1.

	20 L Fermenters		**200 L Fermenters**		**2000 L Fermenters**	
PC	Variance (%)	Cumulative Variance (%)	Variance (%)	Cumulative Variance (%)	Variance (%)	Cumulative Variance (%)
1	25.50	25.50	27.19	27.19	42.18	42.18
2	13.05	38.55	19.55	46.74	16.66	58.84
3	12.05	50.60	10.87	57.61	11.45	70.29
4	9.09	59.69	7.99	65.60	7.90	78.20
5	-	-	-	-	4.28	82.47

Table 8-1 Variance captured by each principal component in the 20 L, 200 L and 2000 L fermenters.

Figure 8-1 shows the loadings related to the principal components for the set of samples from the 20 L fermenters. Variables for all the analyses are as follows: i- from 1 to 11 refer to cDCF distributions; ii- from 12 to 22 refer to forward scattering distributions; and iii- from 23 to 33 refer to side scattering distributions.

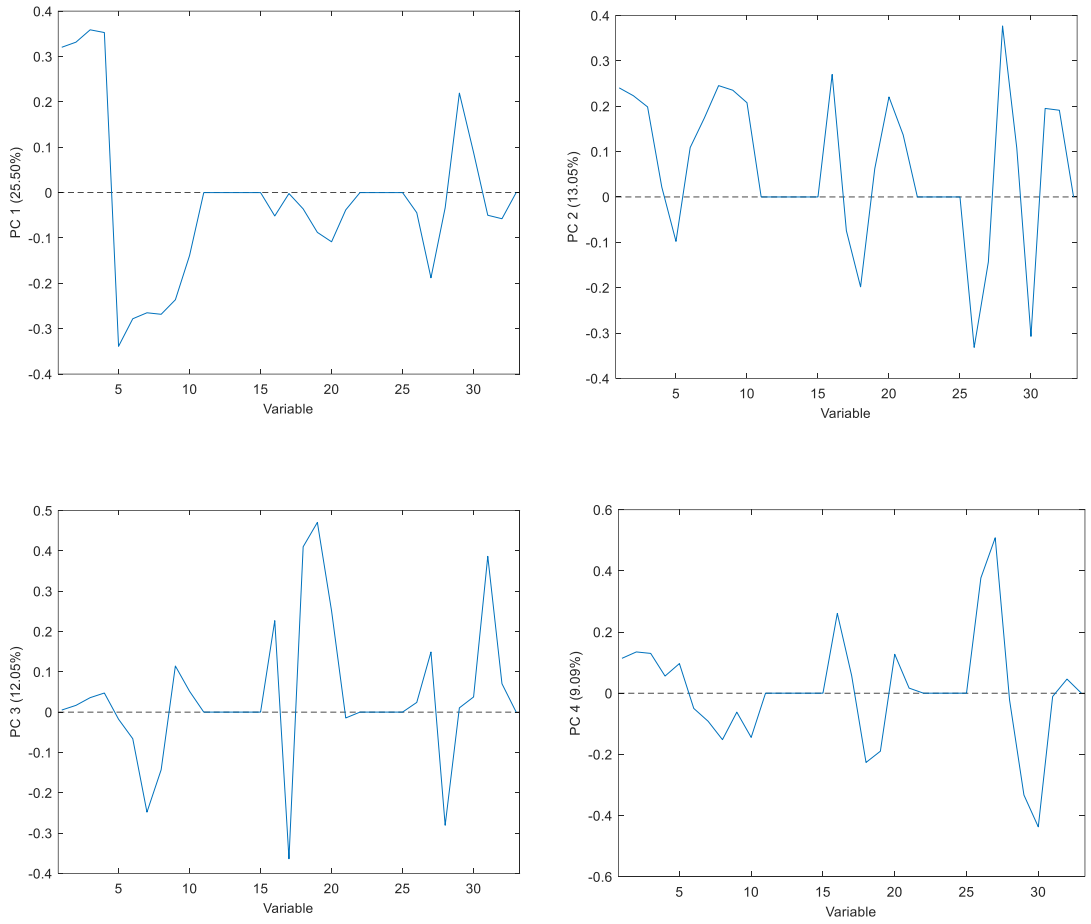

Figure 8-1 PC1, PC2, PC3 and PC4 loadings for the 20 L fermenters. Variables from 1 to 11 refer to cDCF, from 12 to 22 refer to forward scattering and from 23 to 33 refer to side scattering.

For PC1 the intensities from the intensity bins 1 to 11 present the highest values of occurrences (cells), and for this reason it is assumed that this component is primarily correlated to cDCF (ROS content). Since in PC2 and PC4, the variables that present the highest values are from 23 to 33, it is assumed that these two components are mostly correlated with side scattering. PC3 is taken to be correlated to forward scattering since variables from 12 to 22 present the highest values.

The loadings of the principal components for samples for the 200 L fermenters are shown in Figure 8-2. PC1 is taken to be related primarily to cDCF. PC2 is assumed to be correlated to cDCF and side scattering, PC3 to side scattering and PC4 to forward scattering and ROS.

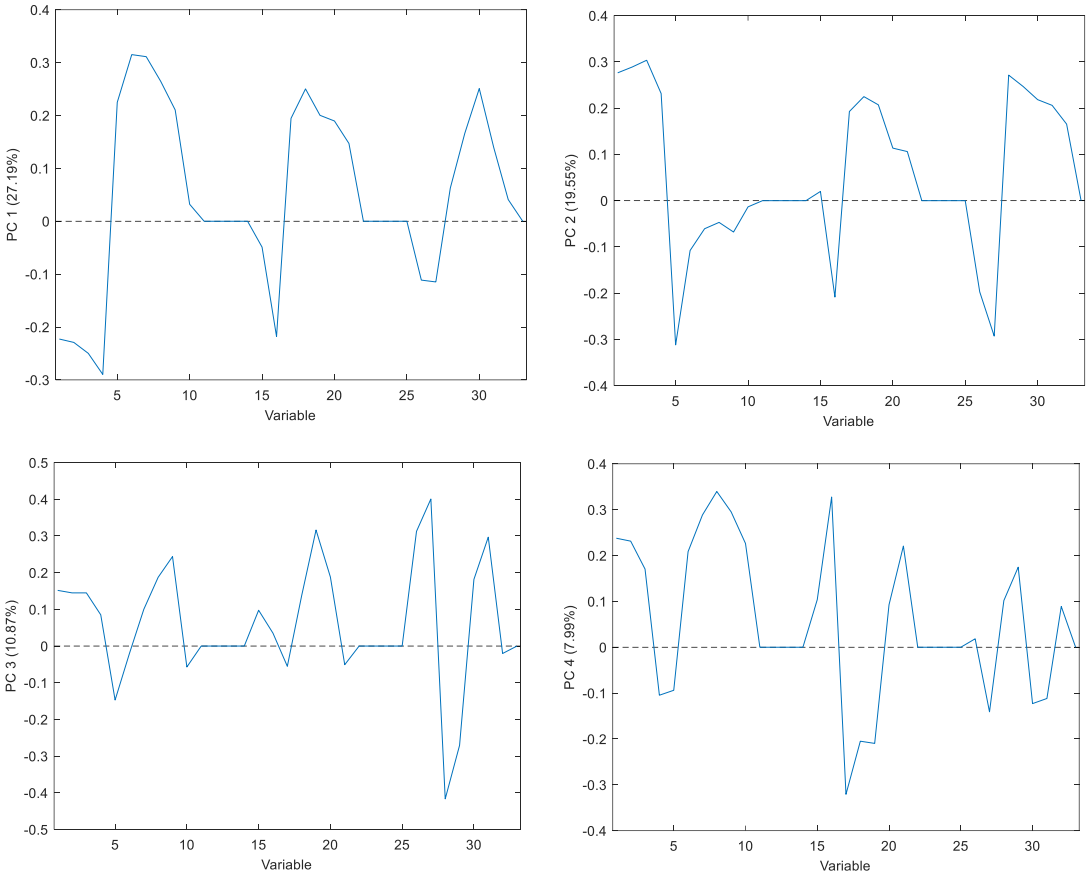

Figure 8-2 PC1, PC2, PC3 and PC4 loadings for the 200 L fermenters. Variables from 1 to 11 refer to cDCF, from 12 to 22 refer to forward scattering and from 23 to 33 refer to side scattering.

The loadings related to the principal components in the 2000 L fermentations are shown in Figure 8-3.

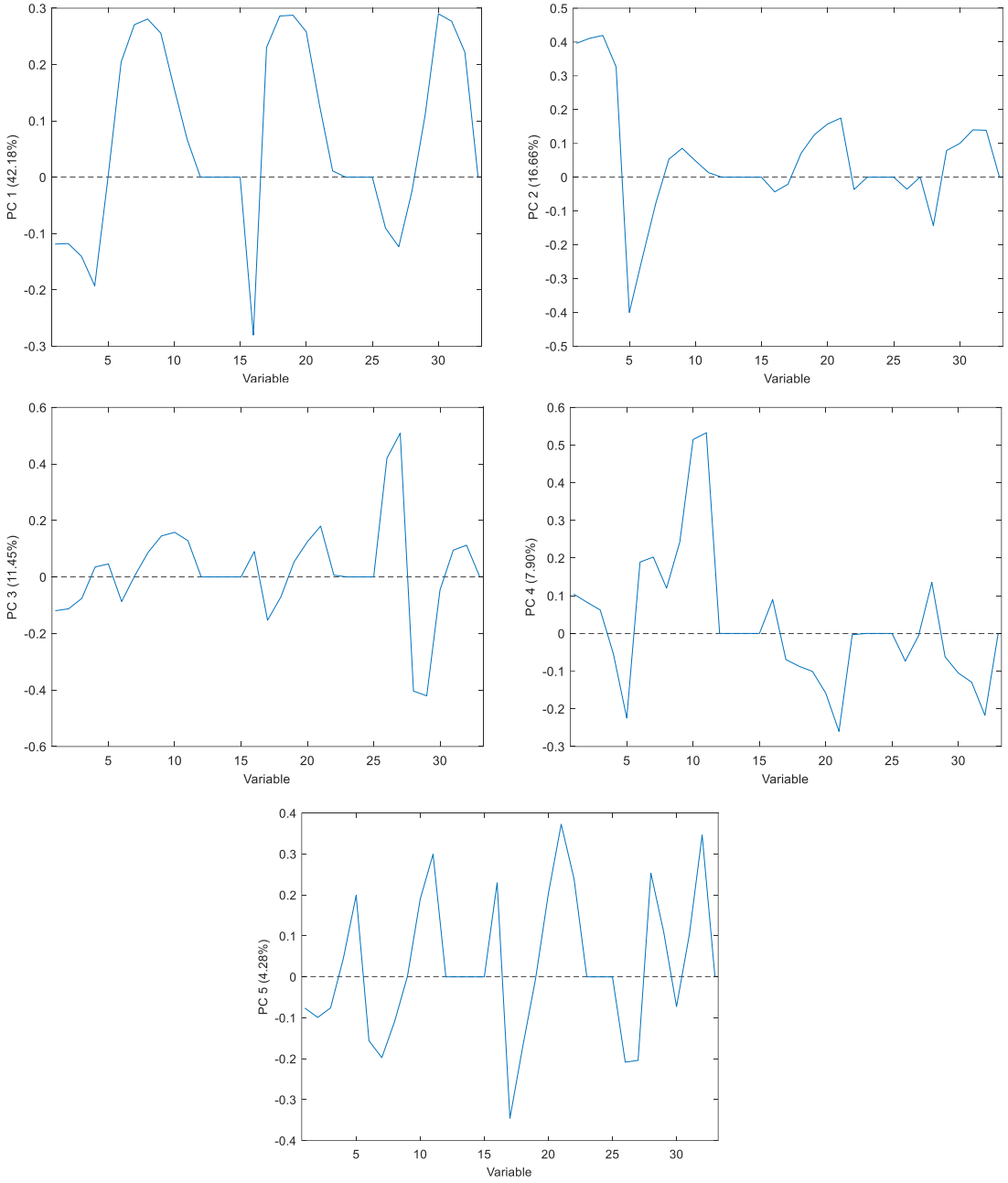

Figure 8-3 PC1, PC2, PC3, PC4 and PC5 loadings for the 2000 L fermenters. Variables from 1 to 11 refer to cDCF, from 12 to 22 refer to forward scattering and from 23 to 33 refer to side scattering.

Since for PC1 the three plots show approximately the same height, it is assumed that this component is correlated to the three parameters with similar degrees of correlation (cDCF, forward and side scattering). PC2 and PC4, appear to be correlated to cDCF, PC3 to side scattering and PC5 to forward scattering, respectively.

The fact that in all loadings there are positive and negative values indicates that there are direct and inverse correlations between the variables and the scores. For instance, if the values are positive for the loading correlated to cDCF, this indicates that when the scores are positive, there is a larger amount of intracellular cDCF in the bioreactors. On the other hand, if the values of the loadings are negative, there is an inverse correlation and thus the corresponding scores are positive, it means that there is a smaller quantity of cDCF.

The relationship among different samples can be visualized from the scores plot of the PCA multivariate model (Wise *et al*., 2007). By comparing the score of each sample for each principal component, differences and similarities can be determined among the original samples (Persson *et al*., 2001).

Score plots for the three data matrices related to the fermenters of different volume are shown in Figures Figure 8-4 to Figure 8-11. Colors indicate the final PRN yield value obtained at the end of the purification process. The main goal was to determine from these plots if a correlation between the evolution for the entire train of fermenters and the final productivity of PRN after downstream processing exists.

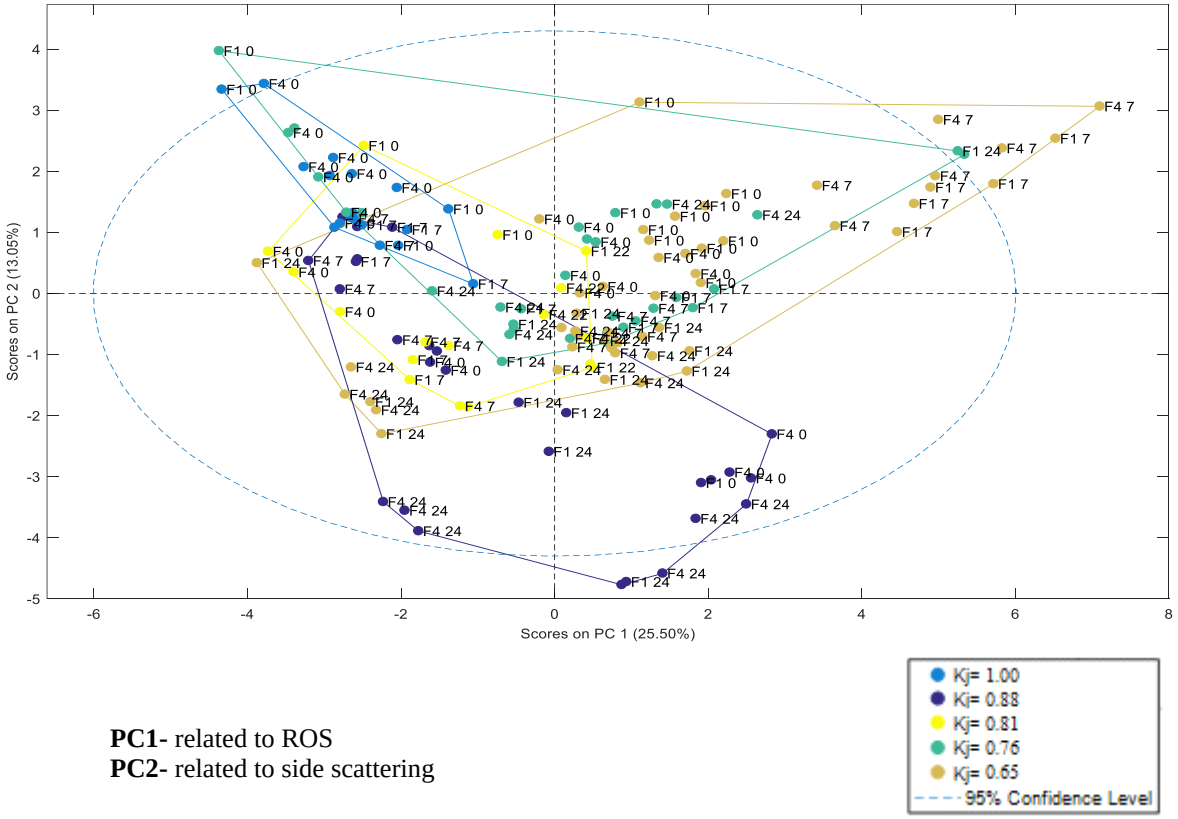

PC1- related to ROS
PC2- related to side scattering

Figure 8-4 PC1-PC2 scores plot for population distributions in the 20 L fermenter. Legend shows the PRN (Kj) for each batch. Points in the graph refer to the fermentation (F1 to F4) and the time points (0 h, 7 h, or 24 h). Kj values were normalized.

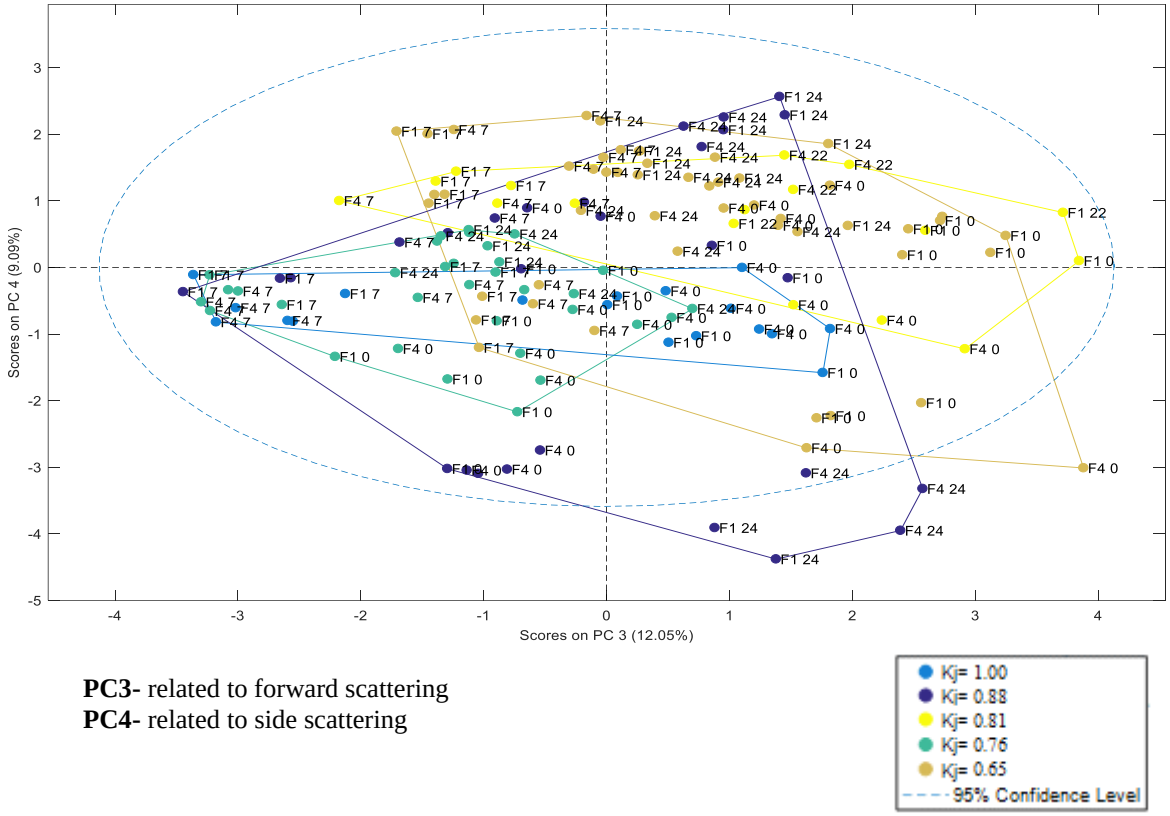

PC3- related to forward scattering
PC4- related to side scattering

Figure 8-5 PC3-PC4 scores plot for population distributions in the 20 L fermenter. Legend shows the PRN (Kj) for each batch. Points in the graph refer to the fermenter (F1 to F4) and the time points (0 h, 7 h, or 24 h). Kj values were normalized.

Figure 8-4 shows PC1 and PC2 for the 20 L fermentations. F1 and F4 refer to two different 20 L fermenters for the two trains of reactors. Numbers next to each data point refer to the time from where the sample was taken counting from the start time of the particular fermentation. PC1 appeared to be related to cDCF (ROS content) and PC2 to side scattering. Most of the points corresponding to batches

that resulted in lower yield fell in the upper right quadrant, meaning that these samples had higher quantity of ROS than the others. Also, the side scattering, which is related to the granularity or internal content of the cells, appeared to be increased mostly for time 0 h samples. This might signify that the previous flask fermentation had a different growth trend with respect to the others.

In Figure 8-5 PC3 and PC4 are shown. PC3 appeared to be related to forward scattering and PC4 to side scattering. For PC3 also most of the points related to the batch with low productivity seem to have variations in forward scattering with respect to the others. Studies in *Campylobacter jejuni* (Oh *et al.*, 2015) have shown that *C. jeuni* mutants lacking of key antioxidant genes, such as *katA* and *sodB*, presented different morphology under aerobic conditions. Since forward scattering is a measure of the size of the cell, these differences might signify a morphological change of the bacteria due to stress.

PC1 and PC2 scores, and PC3 and PC4 scores for samples from the 200 L fermentations are shown in Figure 8-6 and Figure 8-7, respectively.

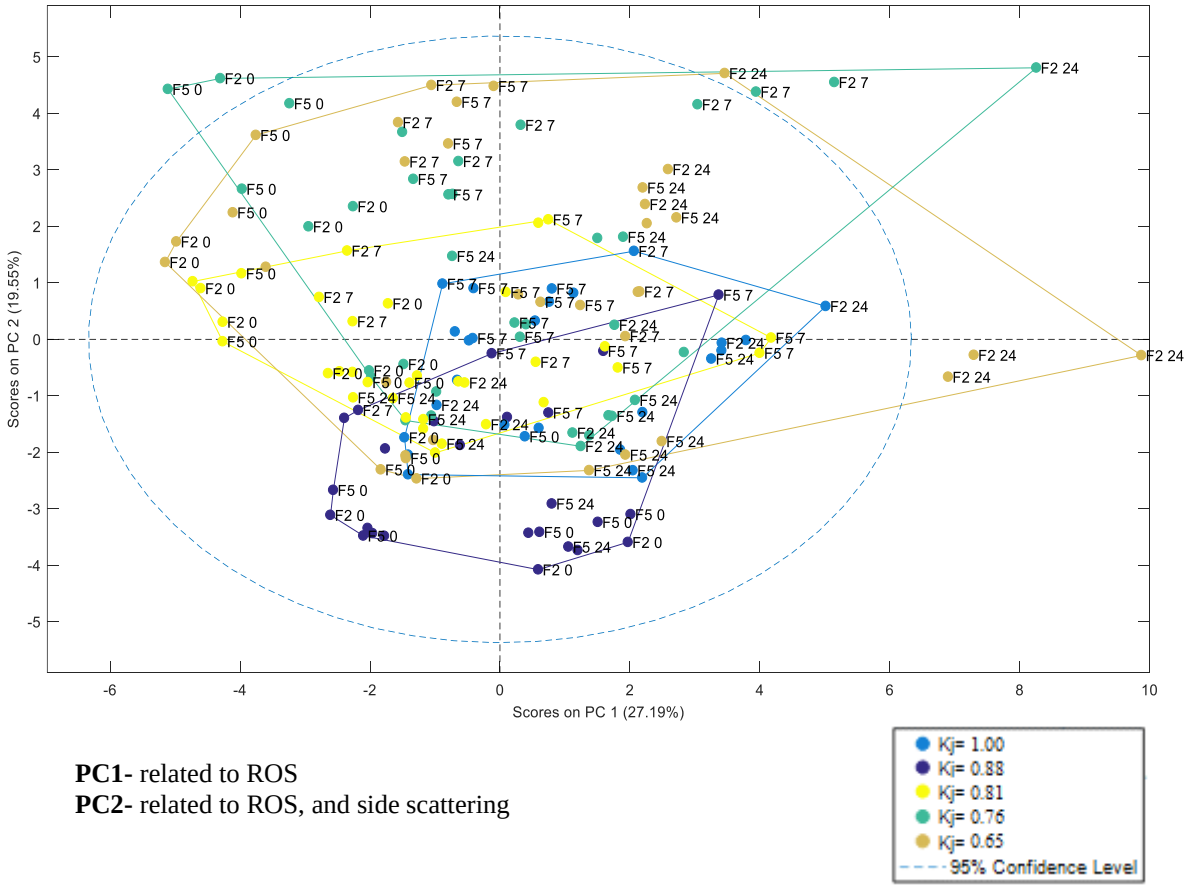

PC1- related to ROS
PC2- related to ROS, and side scattering

Figure 8-6 PC1-PC2 scores plot for population distributions in the 200 L fermenter. Legend shows the PRN (Kj) for each batch. Points in the graph refer to fermentations (F2 or F5) and time points (0 h, 7 h, or 24 h). Kj values were normalized.

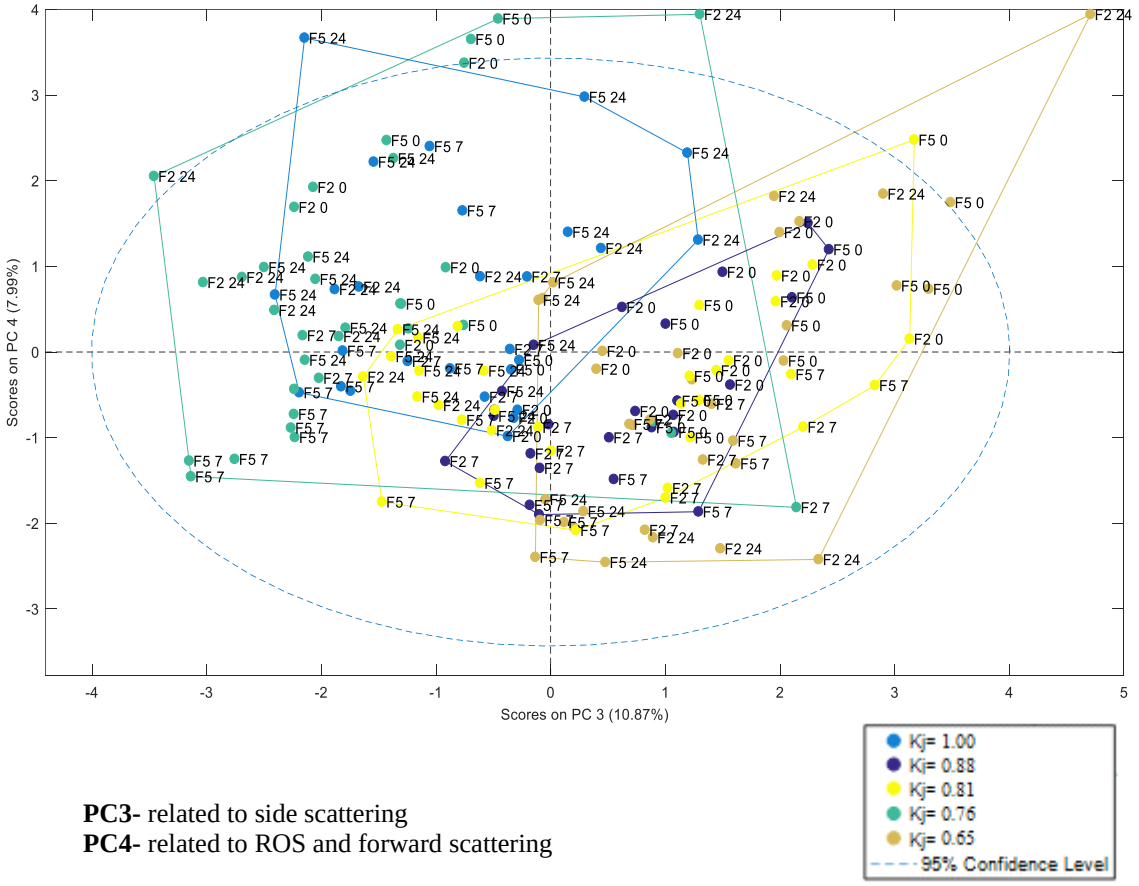

PC3- related to side scattering
PC4- related to ROS and forward scattering

Figure 8-7 PC3-PC4 scores plot for population distributions in the 200 L fermenter. Legend shows the PRN (Kj) for each batch. Points in the graph refer to fermenters (F2 or F5) and time points (0 h, 7 h, or 24 h. Kj values were normalized.

PC1 for the 200 L fermenter, which is related to ROS content, does not show a clear correlation with PRN yield, since scores from batches with low productivity and batches with high productivity fall both in the same quadrants of the plot. On the other hand, PC2 that is also related to ROS, and side scattering appeared to increase for batches with low PRN productivity.

Figure 8-7 shows the score plot for PC3 and PC4. PC3 is assumed to be related to side scattering and PC4 to ROS and forward scattering. For these components, there is no clear correlation with the PRN productivity.

The score plots for samples from 2000 L fermentations are shown in Figures from Figure 8-8 to Figure 8-11.

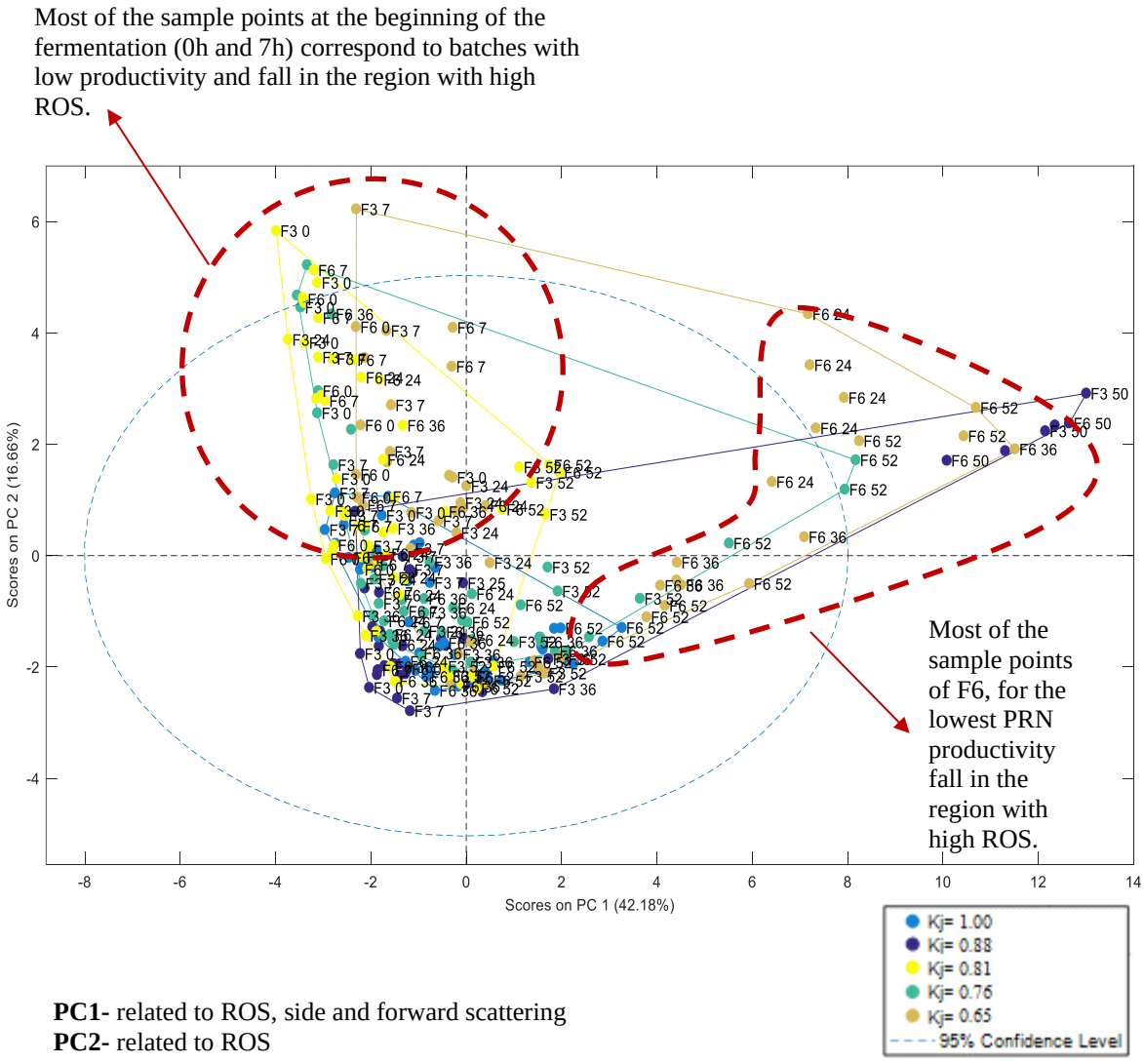

PC1- related to ROS, side and forward scattering
PC2- related to ROS

Figure 8-8 PC1-PC2 scores plot for population distributions in the 2000 L fermenter. Legend shows the PRN (Kj) for each batch. Points in the graph refer to fermenters (F3 to F6) and time points (0 h, 7 h, 24 h, 36 h, or 52 h). Kj values were normalized.

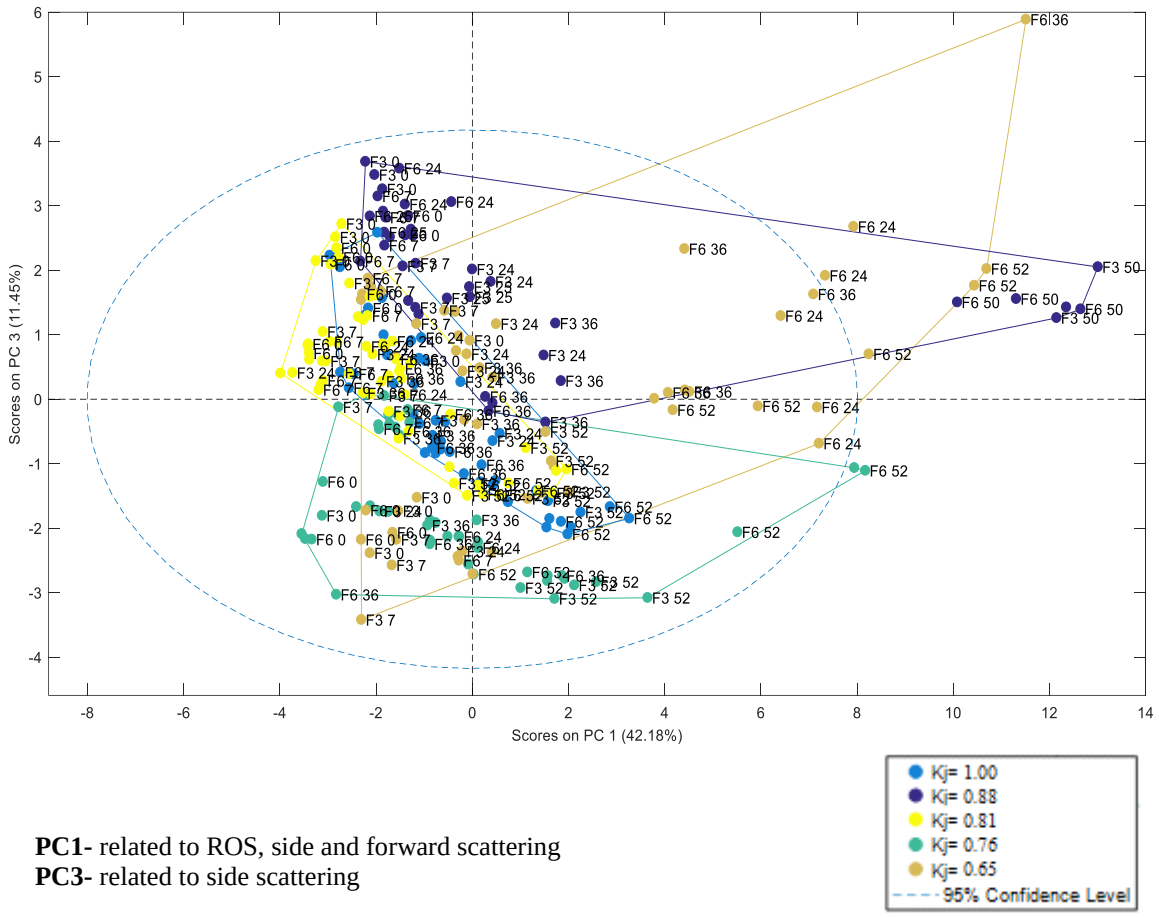

PC1- related to ROS, side and forward scattering
PC3- related to side scattering

Figure 8-9 PC1-PC3 scores plot for population distributions in the 2000 L fermenter. Legend shows the PRN (Kj) for each batch. Points in the graph refer to the fermentations (F3 to F6) and the time points (0 h, 7 h, 24 h, 36 h, or 52 h). Kj values were normalized.

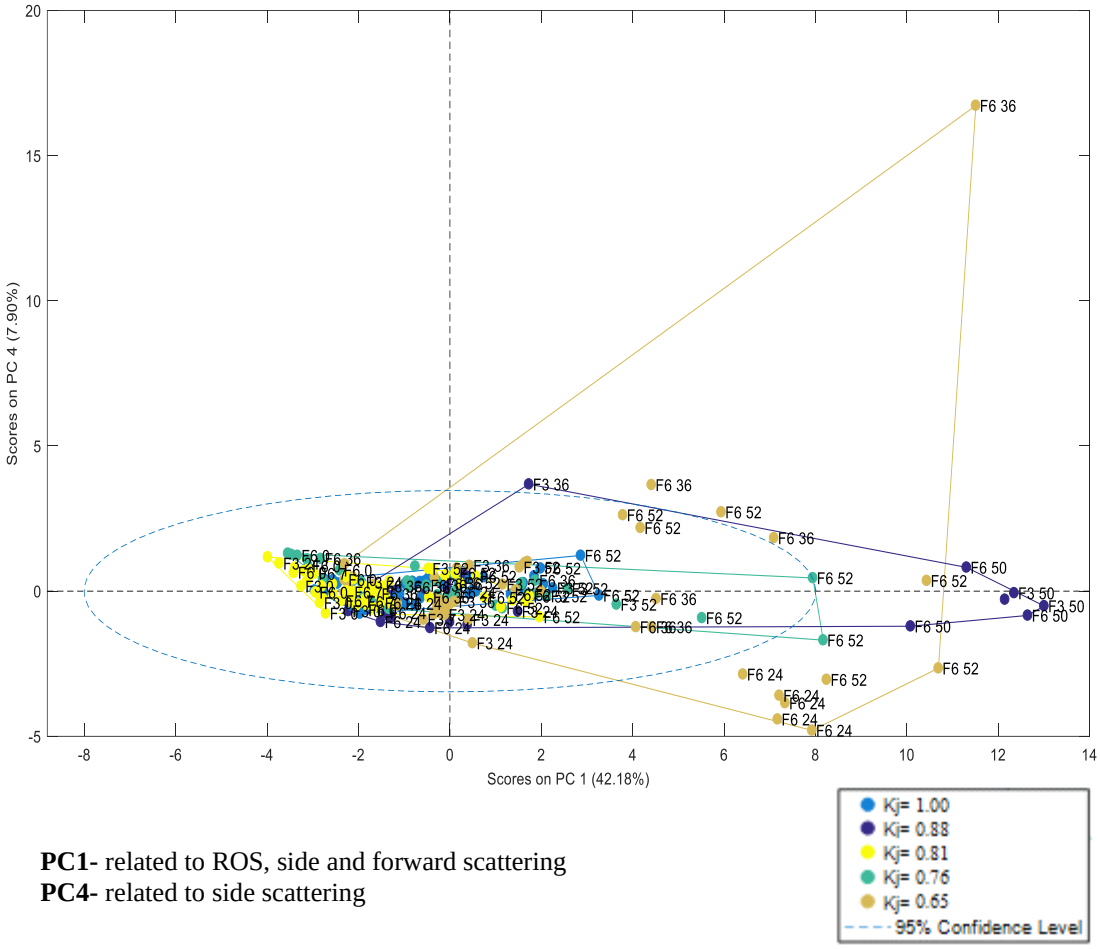

PC1- related to ROS, side and forward scattering
PC4- related to side scattering

Figure 8-10 PC1-PC4 scores plot for population distributions in the 2000 L fermenter. Legend shows the PRN (Kj) for each batch. Points in the graph refer to fermenters (F3 to F6) and time points (0 h, 7 h, 24 h, 36 h, or 52 h). Kj values were normalized.

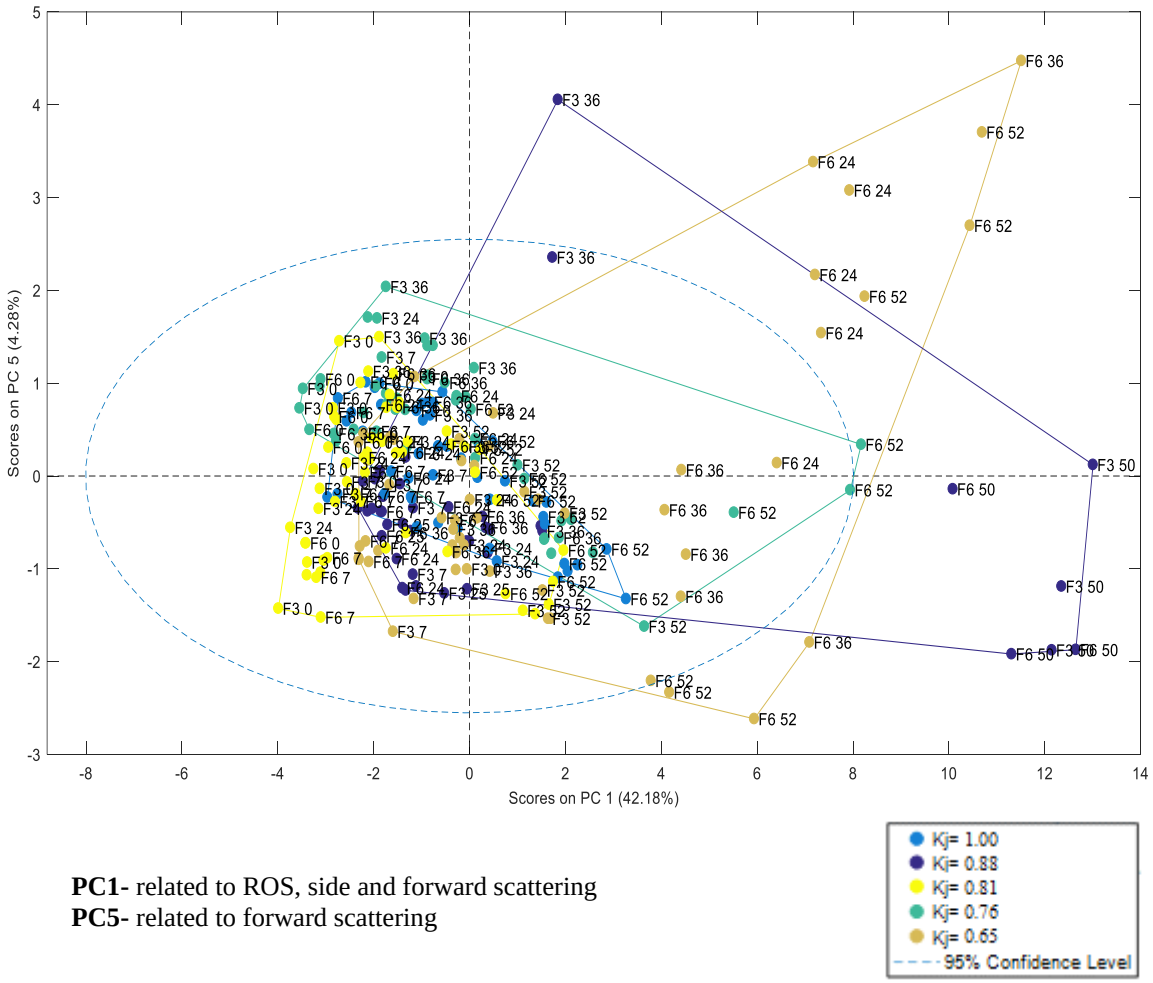

PC1- related to ROS, side and forward scattering
PC5- related to forward scattering

Figure 8-11 PC1-PC5 scores plot for population distributions in the 2000 L fermenter. Legend shows the PRN (Kj) for each batch. Points in the graph refer to fermenters (F3 or F6) and time points (0 h, 7 h, 24 h, 36 h, or 52 h). Kj values were normalized.

For the 2000 L fermentations, PC1 is correlated to ROS, forward scattering and side scattering since the curves of the loadings for this component (Figure 8-3) have the same height. PC2 and PC4 are both related to ROS, PC3 to side scattering and PC5 to forward scattering.

In Figure 8-8, it is particularly noticeable that most of the scores at the beginning of the fermentation (0 h and 7 h) for batches with low productivity fall in the upper left quadrant of the plot, which is the region corresponding to large amounts of ROS (PC2). On the other hand, for PC1 most of the scores corresponding to one of the 2000 L fermentations (F6) come from batches with the lowest productivity fall in the region with high ROS, forward scattering and side scattering for the entire duration of the batch. Also few scores for the batch with high productivity fall in this region, but these scores are for the end of the fermentation where most of the population is expected to be senescent cells. For the rest of the PC's, it is not clear whether there is correlation between the scores and productivity.

From the information extracted from the score plots of the entire train of fermentation (20 L, 200 L, 2000 L) it can be concluded that batches with low productivity presented higher amounts of ROS, and the morphology of the cells was different as shown by differences in the side and forward scattering scores. The cells were not examined microscopically.

One could argue that the inoculum in each fermenter has a decisive effect on the evolution of the fermentation and thus changes in the distribution of the cell population of the inoculum may explain the observed variability in ROS and scattering among the fermentations. However, following the observation that batches that resulted in low productivity exhibited higher ROS along the entire train of fermenters leads to the more plausible explanation that the media had a substantial repercussion on the growth and production of PRN.

For example, bench scale experiments done with autoclaved and filtered media (Figure 6-16) demonstrated that in autoclaved media bacteria grow slowly when oxidative stress is externally impose with H_2O_2. Thus, the combination of high oxidative stress and different media treatment (autoclaving) has been found to result in significant deterioration in growth and productivity.

Furthermore, since higher ROS is expected to lead to a reduced growth rate and productivity, the biomass time profiles for the 2000 L fermentations were measured to corroborate these effects. As expected, the biomass profiles of the F6 fermentation exhibited a slower growth as compared to the other fermentations (Figure 8-12). Very similar behavior was observed for the bench scale fermentations with autoclaved media and H_2O_2 addition. This also agrees with the information extracted from the PC1-PC2 score plot (Figure 8-8) where samples from the F6 fermentation seem to have more ROS, forward and side scattering than the others. Furthermore, the biomass growth profile in Figure 8-12 for the fermentation resulting in the lowest productivity (purple lines for Kjeldahl of 0.65) shows a typical pattern, also observed in the bench scale experiments, where the growth is slower during the fermentation but significantly increases towards the end. This later recovery was explained in Chapter 5 and 6 as a mechanism of adaptation to oxidative stress that has been reported in several studies (Crawford *et al*., 1994; Pickering *et al*., 2013). In fact it has been found from thorough analysis of the fermentation data available for a period of several years that the final biomass values do not differ by much among the runs while the corresponding productivity is variable. The fact that the slow growth observed in some fermentations and further recovering towards the final hours may explain this observation.

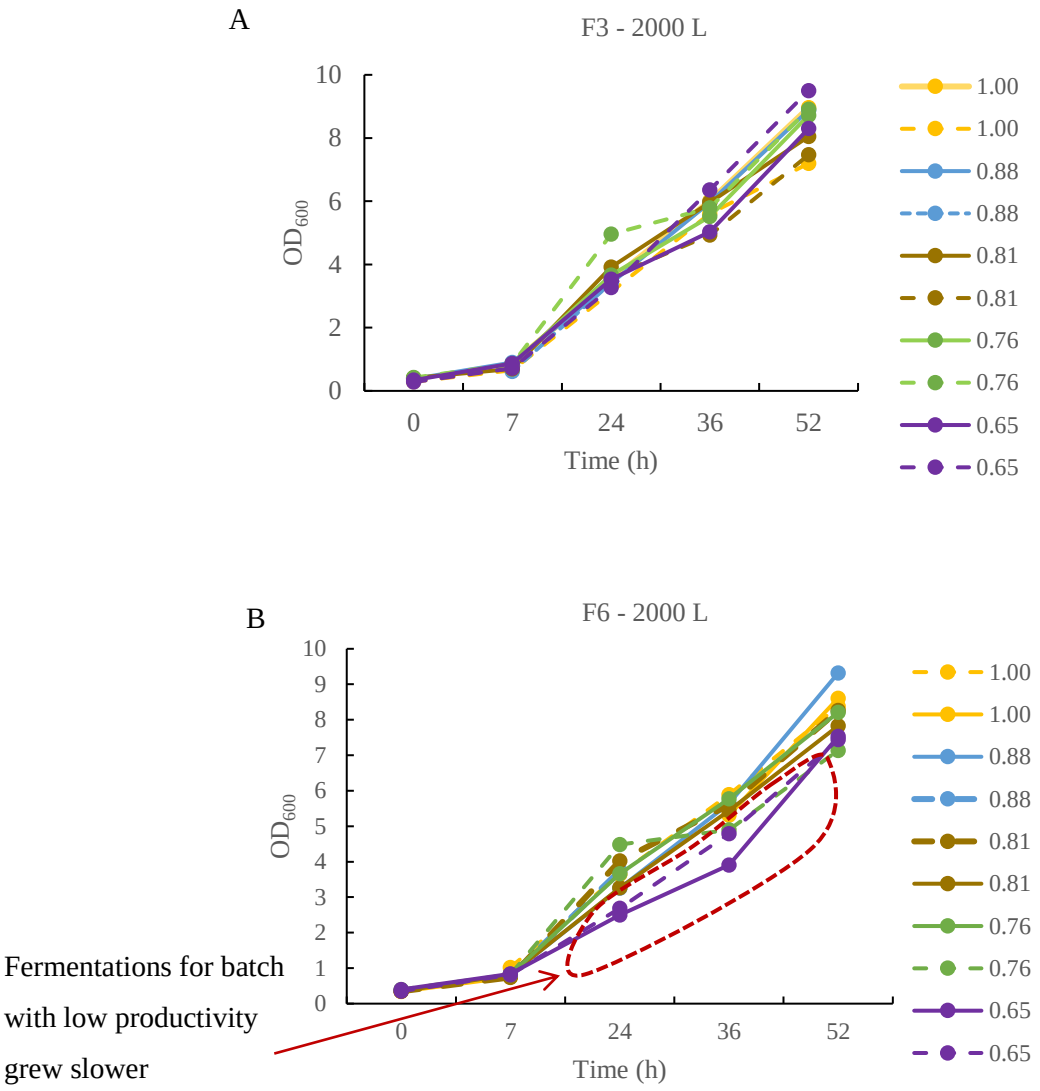

Figure 8-12 Biomass in A- F3-2000L fermentations and B- F6-2000 L fermentations. Legend shows final PRN Kjeldahl values (normalized) obtained after purification.

In summary, it is believed that there are variations in the media (e.g. concentration of constituents or time of sterilization) that cause variability in growth and PRN productivity.

8.3 PLS regression for PRN prediction

To quantify the degree of correlation between the cytometry data and the productivity (Kjeldahl values) PLS (Partial Least Squares) based regression models were obtained using the same method described in Chapter 3. These models were formulated to correlate samples in the 2000 L fermentations at each time point with PRN productivity. Only the 2000 L data were considered based on the premise that this is the last fermentation step before the downstream processing and thus it is expected to have the largest impact on the final PRN productivity. Two types of modelling approaches were pursued: i- the inputs to the model were the entire distributions of cDCF, forward and side scattering of the cells (from Figures Figure 8-13 to Figure 8-17); ii- the inputs were the weighted averages of the cytometry profiles calculated as shown in Equation 3.1 (from Figures Figure 8-18A to Figure 8-22A) and iii- the inputs were the weighted averages divided by OD for Figures from Figure 8-18B to Figure 8-22B (as explained in Chapter 5 the ROS/OD is expected to be related to the production rate of ROS rather than its concentration). In all plots, Ymeasured refers to PRN measured by Kjeldahl analysis and Ypredicted refers to the PRN values predicted. The green line represents the 1:1 correlation between the measured and predicted value, and the red line is the regression.

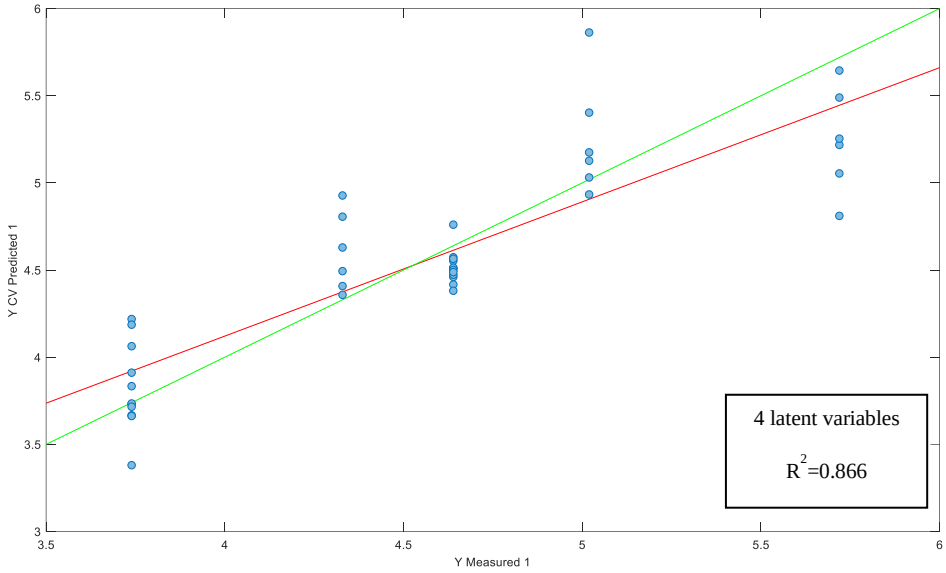

Figure 8-13 PLS for distributions of cDCF, forward and side scattering at t=0 h in the 2000 L fermenter.

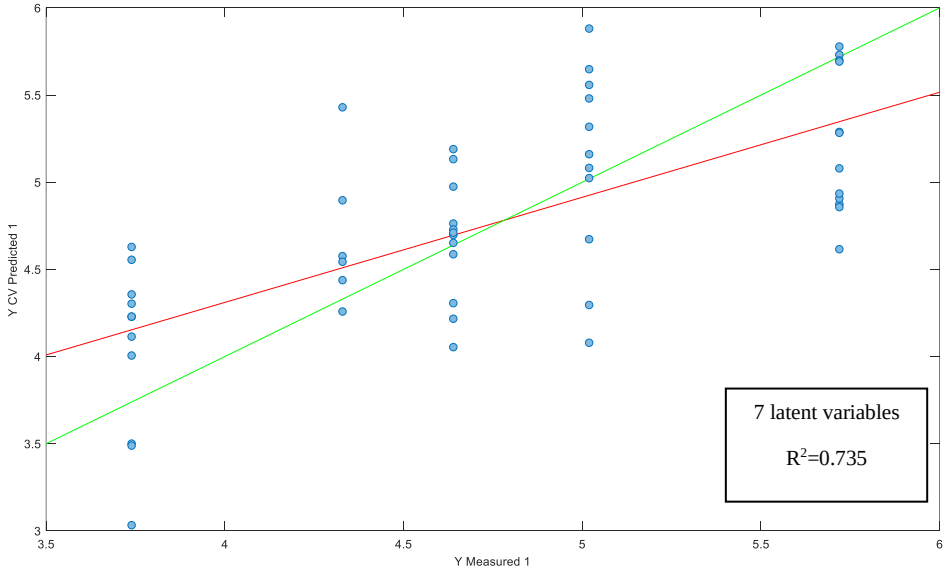

Figure 8-14 PLS for distributions of cDCF, forward and side scattering at t=7 h in 2000 L fermenter.

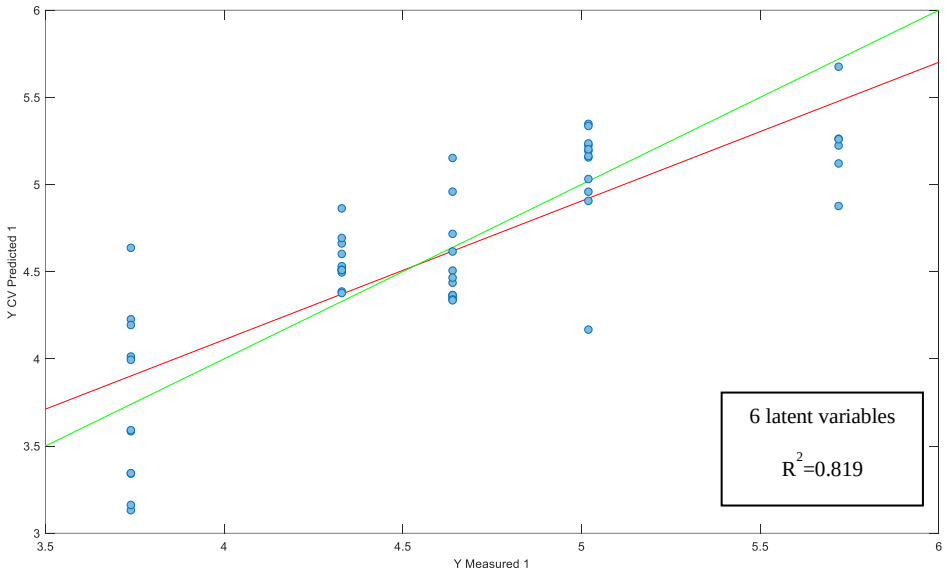

Figure 8-15 PLS for distributions of cDCF, forward and side scattering at t=24 h in 2000 L fermenter.

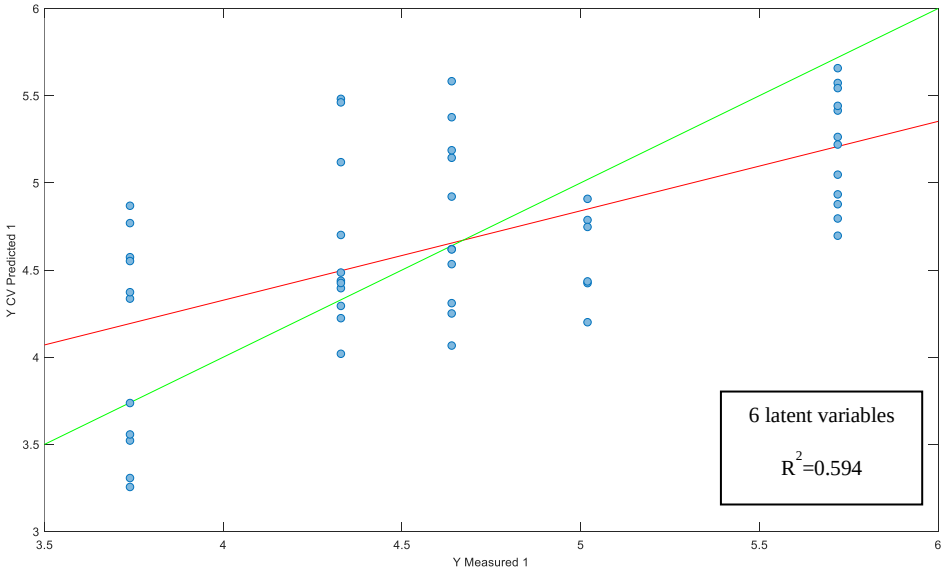

Figure 8-16 PLS for distributions of cDCF, forward and side scattering at t=36 h in 2000 L fermenter.

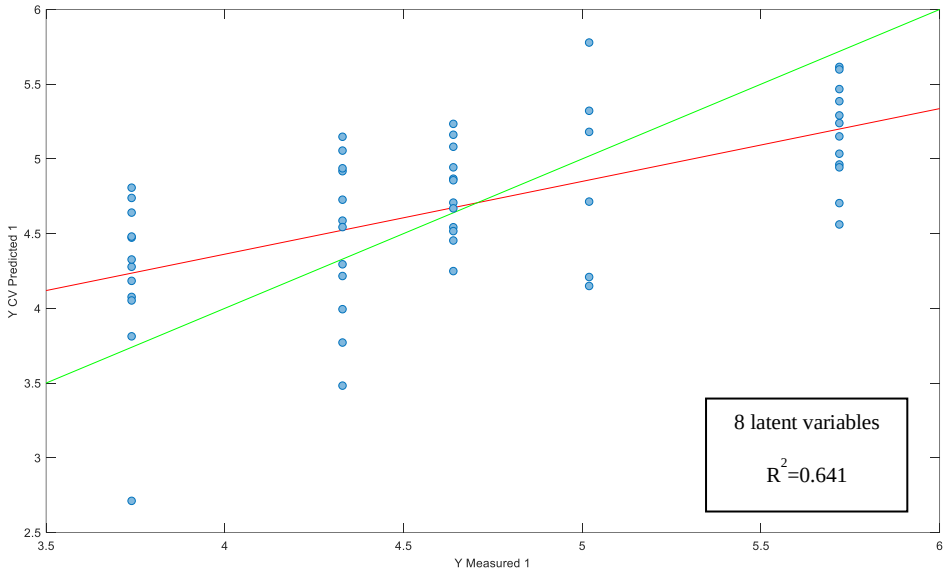

Figure 8-17 PLS for distributions of cDCF, forward and side scattering at t=52 h in 2000 L fermenter.

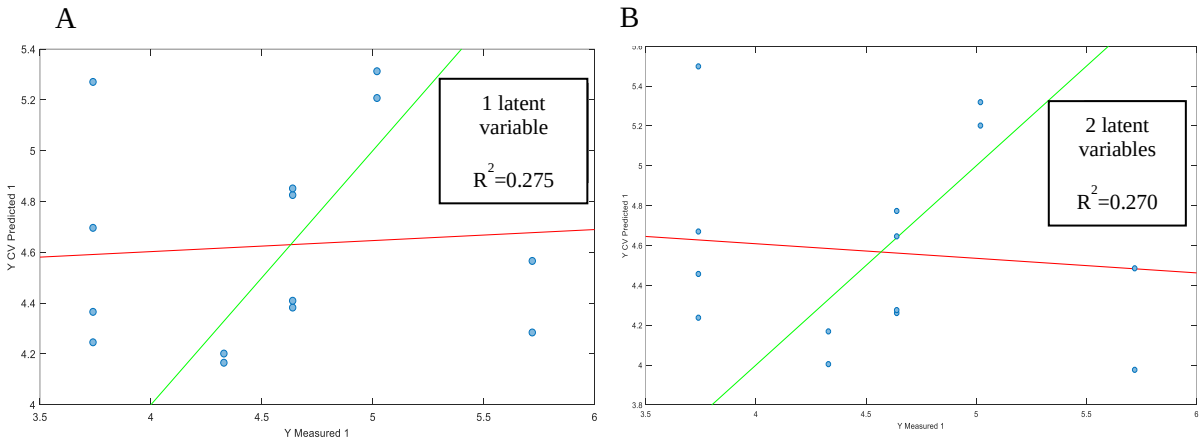

Figure 8-18 PLS for A- weighted average and B- weighted average / OD of cDCF, forward and side scattering at t=0 h in 2000 L fermenter.

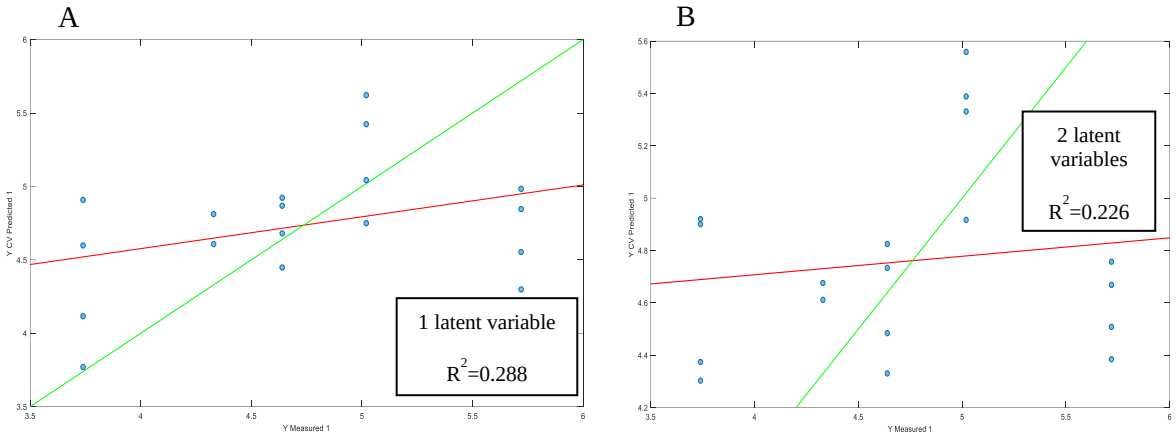

Figure 8-19 PLS for A- weighted average and B- weighted average / OD of cDCF, forward and side scattering at t=7 h in 2000 L fermenter.

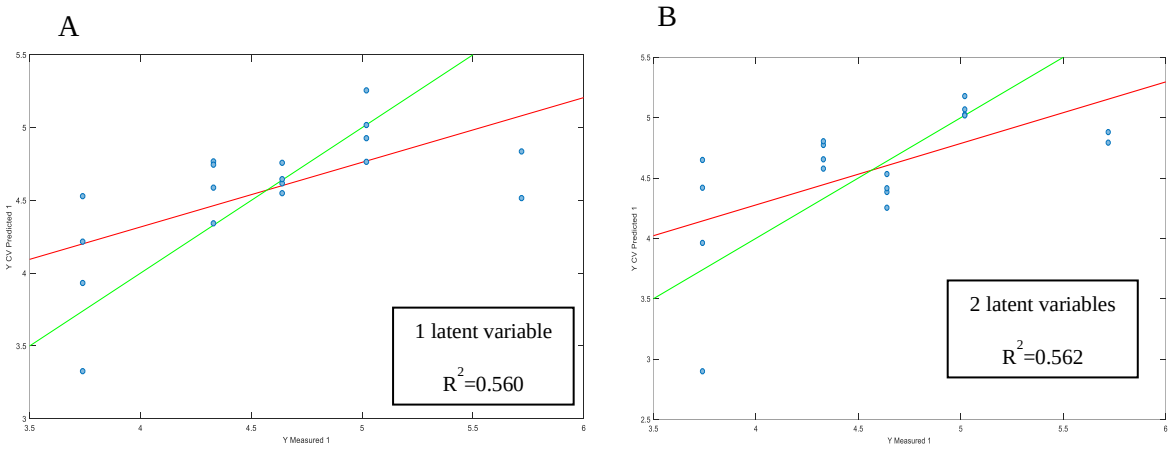

Figure 8-20 PLS for A- weighted average and B- weighted average / OD of cDCF, forward and side scattering at t=24 h in 2000 L fermenter.

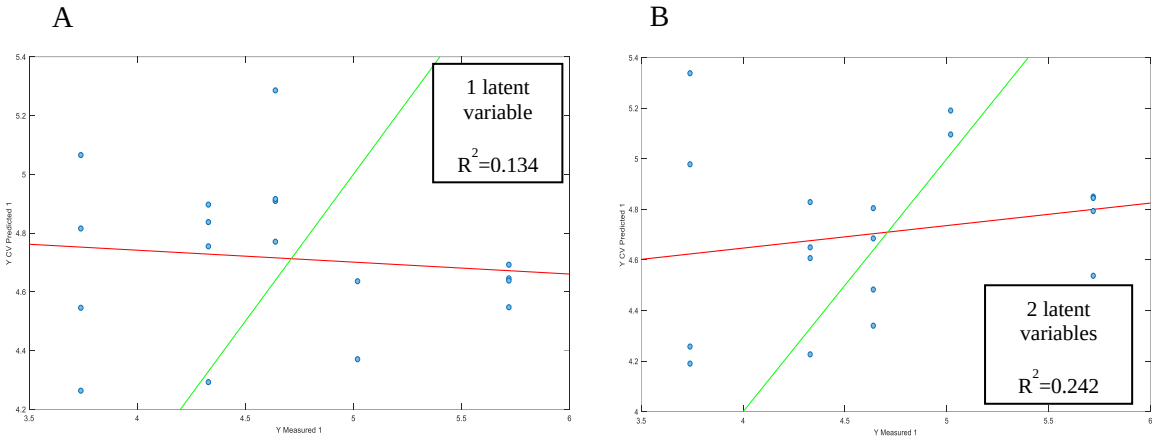

Figure 8-21 PLS for A- weighted average and B- weighted average / OD of cDCF, forward and side scattering at t=36 h in 2000 L fermenter.

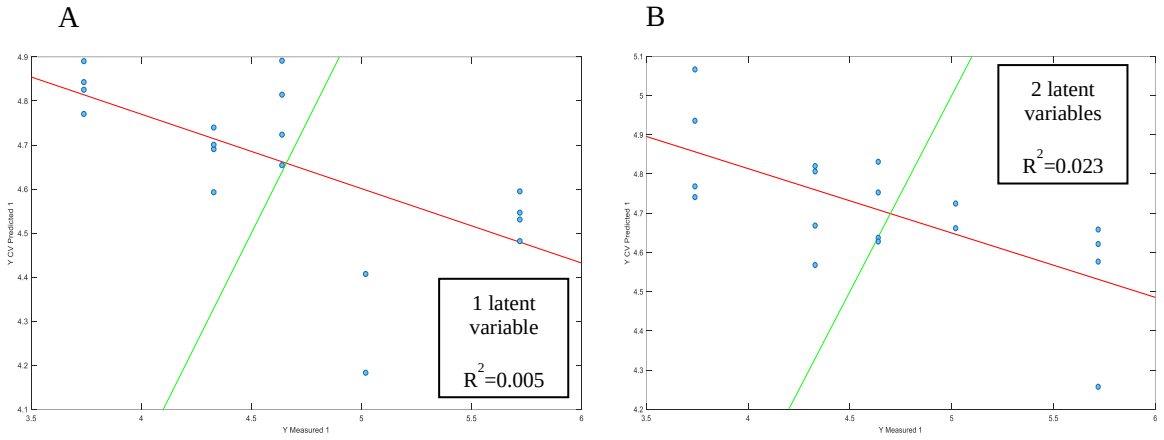

Figure 8-22 PLS for A- weighted average and B- weighted average / OD of cDCF, forward and side scattering at t=52 h in 2000 L fermenter.

For the two types of modelling approaches that were considered the errors between measured Kjeldahl values and predicted value were calculated. Table 2 shows the goodness of fit (R^2) for each regression.

Time point	R^2 for PLS using distributions	R^2 for PLS using Weighted Average	R^2 for PLS using Weighted Average / OD
0 h	0.866	0.275	0.270
7 h	0.735	0.288	0.226
24 h	0.819	0.560	0.562
36 h	0.594	0.134	0.242
52 h	0.641	0.005	0.023

Table 8-2 Goodness of fit for PLS regressions.

From Table 8-2 it is clear that PLS regression models done using the distributions of the population instead of a weighted average as inputs, which will represent an average measurement of the whole sample, resulted in significantly better fit. These results show that measurements of population distributions appear, as initially hypothesized, to be a better indicator of the fermentation state rather than average measurements.

Measurements at earlier stages (e.g. 0 h or 7 h) were found to be particularly informative in terms of PRN yield at the end of the fermentation.

8.4 Discussion

The key findings of this chapter are:

- Higher levels of ROS as quantified by flow cytometry correlate with the final PRN productivity.

- Scattering appears also to be different among the cultures, which might be indicative of conformational changes in the cells.
- The cultures with higher ROS levels correlate with slower growth and lower PRN productivity.
- The degree of correlation with flow cytometry distributions shows higher correlation with final productivity as compared to the weighted averages of the same distributions.
- The batches that resulted in lower productivity exhibited generally higher ROS levels across the entire train of fermentations.

These findings appear to coincide with some of the observations for the bench scale experiments presented in Chapters 5 and 6 where the oxidative stress was artificially induced by addition of H_2O_2 or by using smaller size inocula. For example, higher levels of stress resulted in significantly slower growth and lower productivity. Also, the growth profiles exhibited a similar pattern of adaptation to stress where following the imposition of stress the biomass growth rate recovered towards the latter stages of the batch. The fact that the distribution was correlated to the productivity rather than the average of the distribution may also explain, as shown in past studies (Zavatti *et al.*, 2016), that fermentation profiles that are expected to capture only average properties are not significantly correlated to productivity. Finally, the fact that the levels of ROS for batches that resulted in low productivity are consistently higher across the entire train of fermenters seems to indicate that changes in media among different batches or its pre-treatment may explain the observed changes in oxidative stress and resulting variability in productivity.

Chapter 9
Conclusions and Future Work

This thesis presents a comprehensive investigation of the sources of variability in productivity of a key antigen in an industrial vaccine manufacturing process. The research involved parallel investigation of the phenomena in lab scale experiments as well as analysis of samples collected from production fermenters. Different experimental analytical techniques were developed and applied in order to measure different aspects of the problem including fluorescence and flow cytometry. The lab scale experiments were instrumental for several reasons: to validate the correlation between NADPH, ROS, growth and productivity, to understand the effect of oxidative stress under externally induced oxidative conditions and to find parallelisms between the effect of stress in lab-scale tests and production tests.

The application of flow cytometry in conjunction with multivariate statistical analysis for monitoring and forecasting the sources of variability in an industrial process is a key contribution of the work. While flow cytometry is generally used in research settings, the current work opens the possibility of using cytometry as an additional standard tool for regular monitoring of the industrial process. A key finding of the work is that there is a significant correlation between oxidative stress distributions of the cell population and productivity. Moreover, the fact that such correlation could not be clearly found between the average of the cell population distribution and productivity explains why the fermentation profiles of key quantities (DO, pH, temperature), that are regularly monitored and controlled, do not correlate with productivity since they only represent average culture properties. Finally, a mathematical model was developed to explain the possible mechanisms of adaptation to oxidative stress observed for bench scale fermentations and the dynamic correlations between the key properties measured in the work: ROS, nutrient (glutamate), biomass and NADPH.

9.1 Comparison between flow cytometry and fluorescence spectroscopy in ROS detection

To assess the reliability of ROS measurements done with fluorescein based probes (DCFDA, H_2DCFDA and carboxy-H_2DCFDA), fluorescence was measured with two different techniques: flow cytometry and fluorescence spectroscopy. The aim was to observe the same trends with both techniques in samples stressed with different levels of H_2O_2.

The first experiments done using DCFDA in samples from flasks treated with different concentrations of H_2O_2 did not show a consistent trending between both techniques. This differences are attributed to the effect of quenching that can be caused by high concentration of the sample, collisions among molecules, formation of a complex between the fluorophore and the quencher and resonance energy transfer. For this reason, experiments testing different dilutions were done using fluorescence, and indicated that DCFDA and H_2DCFDA appeared to be less stable than carboxy-H_2DCFDA, since the fluorescence emission increased with increasing dilution. Fluorescence was expected to decrease since less quantity of cells and fluorophores were present as dilution was increased. On the other hand, the fluorescence of carboxy-H_2DCFDA showed decreasing emission values with increasing dilution thus ruling out the occurrence of quenching

Since fluorescence measurements are average measurements of fluorophores in the samples, it was necessary to calculate a weighted average of the measured distributions, which showed to be better correlated with fluorometric values than the median values of the distributions.

The results with carboxy-H_2DCFDA for both techniques appeared to be well correlated to each other showing similar consistent trends, and for this reason this probe was used for further ROS analyses.

9.2 Impact of oxidative stress externally imposed on antigen production and growth of *B. pertussis*

External imposition of oxidative stress had a dramatic detrimental effect on PRN production and growth. Fermentations with 600 μM of H_2O_2 added at either 4 h or 24 h appeared to grow slowly compared to control cultures. On the other hand, this initial inhibition of growth was overcome in the cell culture through a mechanism of adaptation were NADPH seems to have a key role. This mechanism of adaptation has been reported for *E. coli* but it has not been reported previously for *B. pertussis*. Furthermore, cells in flask fermentations seem to overcome inhibition faster than cells grown in 2 L and 20 L fermenters. This is attributed to the presence of a closed-loop control in the fermenters that seems to exacerbate the exposure to oxidative stress. Dissolved oxygen (DO) is maintained to target through the manipulation of aeration and agitation rate. When H_2O_2 is added, catalase acts to convert it into water and oxygen. In response to the production of this extra amount of oxygen, the agitation decreases to maintain the DO at target, resulting in a decrease of mass transfer and metabolism. This effect is not seen on flasks, since DO is not closed-loop controlled in flasks. The specific productivity of PRN for cells treated with H_2O_2 at 4 h for flasks, 2 L fermenter and 20 L fermenter were 0.0366, 0.0199, 0.0177 μg/mL/OD-hour respectively as compared to productivities in the control fermenters without addition of peroxide: 0.0421, 0.0235 and 0.0218 μg/mL/OD-hour respectively.

Cells treated with 600 μM rotenone at 4 h did not adapt or recover after the addition. On the other hand, cells treated at 23 h adapted and continued growing. It has been reported that when growth changes to iron-limited conditions, cells can lose sensitivity to rotenone. The remaining iron in the media was not tested in this experiment but its presence seems to be a plausible explanation of this effect since $FeSO_4$ is added at the beginning of the fermentation and it is possible that at 23 h it can be depleted. The averages of the specific productivity for PRN were 0.0635, 0.0819, and 0.0561

μg/mL/OD-hour, for control and for rotenone added at 4 h and 23 h, respectively. The specific productivity at 4 h appears to be higher than the control. Since this culture did not recover, it is possible that the increased quantity in the specific productivity is due to release of pertactin from disintegrating cells due to lysis.

Increased DO did not have a significant impact on growth, since the final optical density was similar to control cultures, but it had an impact on PRN productivity (0.0193 μg/mL/OD-hour compared to 0.0235 μg/mL/OD-hour for control). This can be explained in that energy is redirected to build enzymes to cope with the stress, which will result in less antigen production. Also, it is believed that the increase in agitation for maintaining the DO at target, increased shear stress thus possibly causing PRN fragmentation.

Inoculation with a smaller inoculum size was found to be another source of oxidative stress since cells remain exposed to large quantities of nutrients for a longer time, and this will result in a greater production of electrons that will overwhelm cell defense mechanisms to stress (Wellen *et al*., 2010). In this experiments, a similar behavior was observed as in the experiments where H_2O_2 was added: cells grew slower than the control, but at some time in the fermentation, cells recovered and end up having an OD even higher than the control. Adaptation in flasks occurred over a shorter period of time compared to the 2 L and 20 L fermentations. This fact is also attributed to the existence of the closed-loop control. Since at the beginning of the fermentation there is a smaller quantity of cells, the oxygen requirements are lower, so the agitation required to maintain the DO at target is lower, which leads to a decrease of mass transfer, cell metabolism and nutrient consumption. Due to this reduced nutrient consumption the nutrient concentrations remain higher for longer time period as compared to the control cultures thus causing higher oxidative stress. PRN productivity also decreased for batches that started with a small inoculum size.

Autoclaved media and filtered media also appeared to have a significant impact on growth and productivity when stressed is imposed with H_2O_2. Cells in filtered media and treated with H_2O_2 had a similar growth than control cells (no H_2O_2 addition). On the other hand, cells in autoclaved media treated with H_2O_2 exhibited reduced inhibition but eventually recovered after 24 h possibly due to the adaptation mechanism explained above. Specific productivity of PRN in fermentation with autoclaved media and filtered media were 0.0680 and 0.0713 μl/ml/OD-hour respectively. Thus, differences in treatment of the media may explain part of the variability in productivity observed in the manufacturing process at Sanofi Pasteur.

9.3 The role of NADPH in anti-oxidative mechanisms in *B. Pertussis*: Experimental and Modelling Studies

Fluorescence spectra of denatured catalase showed a peak around Ex/Em 340/440 nm, which is related to NADPH. The spectra is similar to the one observed in the supernatant from production fermentation samples. Also, qualitative determinations of catalase by foaming experiments showed that this enzyme is present in the supernatant of flask fermentations. It is believed that the observed NADPH fluorescence in the supernatant comes from NADPH molecules bound to catalase.

Intracellular and extracellular NADPH measurements in combination with a mass balance showed that NADPH in the supernatant originates from secretion rather than release from dead cells.

A novel mathematical model was developed based on key metabolic pathways related to glutamate depletion, ROS production, biomass formation and build-up of NADPH bound to catalase. The model is important to mechanistically explain the observed adaptation of cells in fermentations under control conditions, stress imposed with H_2O_2 and a smaller inoculum size. The model also was used to explain

the dynamic interactions between the key variables related to the occurrence of oxidative stress, i.e. ROS, NADPH, glutamate (main carbon source), biomass and catalase.

9.4 Flow cytometric analysis on production samples

PCA was found to be effective in recognizing correlations between cell distributions from fermentation steps and productivity. A clear correlation was found between ROS quantities, and scattering with PRN and this correlation is seen for the fermentations analyzed for each batch: two seed fermenters of 20 L, two intermediate fermenters of 200 L, and two production fermenters of 2000 L.

For the 20 L fermenters, samples belonging to the batches with the lowest productivity of PRN appeared to have larger quantities of cDCF (related to ROS). Also, samples collected during the first half of the fermentation appeared to exhibit more side scattering as compared to the second half, which might indicate that the initial flask fermentation, preceding the 20 L fermenter, had significant variability in growth. Also, forward scattering seems to be highly variable among the 20 L fermentations, which could signify morphological changes in the bacteria due to stress in the initial flask fermentations, as reported in the literature (Oh *et al.*, 2015).

For the 200 L, there is also correlation between ROS and side scattering with productivity, but no correlation was found with forward scattering.

For the 2000 L, most of the sample points at 0 h and 7 h that correspond to batches with low productivity fall in the region with high ROS, and also sample points of one of the fermenters (F6) that correspond to the lowest PRN productivity, fall in the region with high ROS, and high side and forward scattering.

Since the common factor for the whole train of fermenters seems to be higher quantities of ROS for batches with the lowest productivity, it is believed that media can play an important role in these variations. From the small scale experiments with autoclaved media and filtered media, it is clear that the biomass evolution was different and cells in autoclaved media grew slowly when stress was imposed with H_2O_2. These differences in growth also were seen in the biomass profiles of the F6-2000 L fermenter thus indicating the possibility of differences in operation between the two F3 and F6, 2000 L fermenters. It is known that the duration of sterilization in the production process is not identical for all fermenters, and this might be affecting the final yield of PRN.

PLS regression was used to find correlations and predict the PRN content at the end of the purification from data collected from production samples. Using PLS models, significantly better correlations were found using the distribution measurements rather than average values. This is an indication that the heterogeneity of the cell population in terms of ROS and scattering is a better index of the state of the fermentation as compared to average parameters of the population.

9.5 Future Work

While flow cytometry in combination with multivariate statistical analysis showed a correlation with the state of the fermentations with the final protein content, the causes of variability are still in question. Since it was shown that inoculum variations can lead to variations in productivity, it is proposed:

- More extensive research about the correlation between ROS and scattering. The idea is to find methods that allow to perform flow cytometric analysis without the need of using extrinsic dyes (e.g. to find a correlation between cDCFDA and scattering, so in future analysis only the

use of scattering will be sufficient as a measure of stress). That would speed the analysis where time is valuable especially in a production facility.

- The use of flow cytometry cell sorting in order to sort cells that show morphological differences, based on scattering measurements. The goal is to select cells that appear to be healthier based on their size (e.g. from PCA it seems that stressed cells have increased side and forward scattering) to be used as inocula and to demonstrate how these initially sorted distributions affect the evolution of the fermentation and the final productivity.

- Additional investigations need to be done regarding the evolution of extracellular metabolites during fermentation. In this research it was suggested that the NADPH peak is secreted and is bound to catalase. On the other hand, there are studies in eukaryotic cells that confirm that cells can efficiently release NAD (Billington *et al*., 2006). Even though, fluorometric analysis show that NADPH is bound to an enzyme, the release of this cofactor by itself cannot be ruled out and it must be further studied.

- The PCA analysis done in this thesis only used data collected from ROS and scattering. Data from viability analysis was excluded because it appeared to introduce more noise causing the variance captured by the PC's to decrease. It is proposed to use a more robust predictive model such as deep learning, which is an artificial intelligence tool that will allow processing of large amounts of data from different tests through the recognition of patterns in order to predict the evolution of the fermentations.

Appendix A

Monitoring of an antigen manufacturing process

Vanessa Zavatti[1], Hector Budman[1], Raymond Legge[1], Melih Tamer[2]

Received: 21 October 2015 / Accepted: 4 February 2016

Abstract: Fluorescence spectroscopy in combination with multivariate statistical methods was employed as a tool for monitoring the manufacturing process of pertactin (PRN), one of the virulence factors of *Bordetella pertussis* utilized in whooping cough vaccines. Fluorophores such as amino acids and co-enzymes were detected throughout the process. The fluorescence data collected at different stages of the fermentation and purification process were treated employing principal component analysis (PCA). Through PCA, it was feasible to identify sources of variability in PRN production. Then, partial least squares (PLS) was employed to correlate the fluorescence spectra obtained from pure PRN samples and the final protein content measured by a Kjeldahl test from these samples. In view that a statistically significant correlation was found between fluorescence and PRN levels, this approach could be further used as a method to predict the final protein content.

Keywords: Principal component analysis, Partial least squares, Fluorescence spectroscopy, Antigen manufacturing, Vaccines, Bioprocess monitoring, *Bordetella pertussis*

& Hector Budman
hbudman@uwaterloo.ca

[1] Department of Chemical Engineering, University of Waterloo, Waterloo, ON, Canada

[2] Sanofi Pasteur, Toronto, ON, Canada

Published online: 16 February 2016

Introduction

Whooping cough is a bacterial infection of the lungs characterized by severe coughing fits. *Bordetella pertussis* is the major causative agent of this condition. To prevent this disease, both whole-cell and acellular pertussis vaccines have been developed. The acellular vaccines are clearly less reactogenic, but have immunological limitations that are the subject of considerable discussion [1]. Current acellular vaccines are based on the following virulence factors: pertussis toxin (PT), filamentous hemagglutinin (FHA), pertactin (PRN), and fimbriae (FIM). Not all acellular vaccines contain the four listed virulence factors; some of them are based on just PT and FHA, or on PT alone.

The manufacturing process of a whooping cough vaccine is mainly composed of two phases: the upstream fermentation process and the downstream purification process. The upstream fermentation process involves fermentations in a series of bioreactors of increasing volume where the microorganism is grown under controlled conditions. Subsequently, the antigens of interest are separated from the cells and isolated from the proteins and other parts of the growth medium. This separation process include different techniques of purification that aim to produce a high purity product. The pellet is collected by centrifugation and dissolved in a buffer solution followed by chromatographic separation. The run-through material is then ultra-filtered and diafiltered in two separate steps. The resulting concentrate is dissolved in water and subjected to another chromatographic step and diafiltration. In the PRN purification process, this antigen is precipitated in three steps with ammonium sulphate at three different concentrations. The final filtration of PRN involves a pre-filtration and sterile filtration. Finally, the samples are collected for quality control.

A wide variety of techniques have been developed for bioprocess monitoring. Depending on the location where the samples are analyzed, methods for analysis can be classified in on-line monitoring (when a sample is automatically withdrawn and analyzed), in-line monitoring (when the sensor is directly positioned in the vessel or in the flow line), and off-line monitoring (when samples are withdrawn from the process and analyzed in a suitable device). Spectroscopy where spectral information is acquired from fluorescence, UV–Vis (ultraviolet–visible), NIR (near infrared), MIR (mid-infrared), FIR (far-infrared) and Raman spectroscopy are some of the techniques used for process monitoring in conjunction with multivariate data analysis [2–4].

In this project, the upstream fermentation process and the downstream purification of PRN were monitored and evaluated using spectro-fluorescence in combination with multivariate statistical based models. Samples were collected from a large scale industrial manufacturing process. The goal of the current study was to monitor the different steps of the manufacturing process for identifying the sources of variability in productivity observed for this system. Having an appropriate insight into the bio-process is expected to provide opportunities for optimizing and increasing productivity [5]. The use of fluorescence spectroscopy also referred to as spectrofluorometry has been reported for biomass detection, characterization of reactors and bioprocess monitoring [5–8]. Since a wide range of excitation-emission wavelength can be monitored using fluorescence spectroscopy, several fluorophores, such as amino acids, vitamins and coenzymes, can be detected simultaneously [5]. Some amino acids, such as tryptophan, tyrosine and phenylalanine are intrinsically fluorescent. Tryptophan is particularly useful in fluorescence analysis since, due to its high quantum yield and high sensitivity to its local environment, can be used for inferring conformational transitions, protein–protein interactions and/or denaturation [9, 10]. Enzymes cofactors, such as NAD(P)H and FAD, are also fluorescent. Since their quantum yields change upon binding to proteins, fluorescence from these two fluorophores has been extensively used to study their interaction with enzymes [12].

The key characteristic of fluorescence spectrometry is its high sensitivity in comparison to light absorption measurements because of the zero background of the signal [2]. Spectrofluorometry may achieve limits of detection several orders of magnitude lower than those achieved by other techniques. Limits of detection of 10^{-10} M or lower are possible for intensely fluorescent molecules. Because of the low detection limits, fluorescence is widely used for quantification of trace constituents of biological and environmental samples [11]. Fluorescence spectrometry is also highly selective since not only intrinsic fluorophores (naturally fluorescent) can be detected, but also specific non-fluorescent structures can be labeled with appropriate fluorescent probes [10].

Fluorescence intensities are typically directly proportional to concentration. There are, however, variables that affect this linearity such as: (1) quenching occurring due to high concentration that impedes the passing of light, collisions with other molecules, formation of a complex with the quencher and energy transfer when one fluorophores excites another molecule without emitting light, (2) the molecular environment of fluorophores (the more exposed to the environment the fluorophore is, the emission shifts towards higher wavelengths) and (3) light scattering [12].

On the other hand, spectral overlap, noise, strong correlations among data and complex interferences make difficult data interpretation [13]. Correlations in data such as the ones occurring with fluorescence data result in almost singularity of the data matrices that must be inverted to calculate least squares regressions [14] thus resulting in high sensitivity to sensor noise. For these reasons, multivariate analysis was used in this work to extract the most important information associated with the properties of the system being studied. First, principal component analysis (PCA) was used to compress the data. The resulting compressed data for different stages of the process was analyzed for identifying sources of variability in productivity. Variability in productivity of antigens was observed from batch to batch. Hence, we were interested to identify which steps of the manufacturing process are most responsible for this variability. Then, the partial least squares' approach (PLS) was used for correlating the fluorescence spectra and the final protein content of PRN as measured by a Kjeldahl test. Although fluorescence has been applied for measuring monoclonal antibody concentration it has not been used before for measuring an antigen such as PRN as done in this study [15, 16]. In this latter case the objective was to have an independent method to cross-validate the measurements obtained by the Kjeldahl approach.

The application of fluorescence to monitor an entire vaccine manufacturing process using fluorescence measurements from several points along the process is novel and it has not been reported in the literature. Hence, this work presents a novel approach for diagnosing and monitoring biotechnological processes by the combination of multivariate statistics and fluorescence spectra from different locations along the manufacturing process.

Materials and methods

Samples

Samples were provided by Sanofi Pasteur (Toronto, Ontario, Canada) collected from upstream and downstream

processing stages for different batches (Table 1). Figure 1 presents a schematic description of the manufacturing process. In the upstream part of the process, there are two parallel fermenters, referred to as F3 and F6 in Fig. 1, which total contents are combined together before down-stream processing. For the fluorescence analysis, a total of four samples were collected for each upstream fermentation step, referred to as F3-S, F6-S, CPS-B2-(F3), CPS-B2-(F6) in Fig. 1, that correspond to samples from each fer-enter and their corresponding centrifuged samples. Samples were collected twice per week.

As shown in the process flow diagram (Fig. 1), CPS-B2-(F3) and CPS-B2-(F6) samples are combined and filtered. The two resulting batches of broth are combined together and sent to the downstream purification process. From the ultrafiltration step, there are four samples [two for CPS-Conc and two for CPS-Conc-PW (permeate waste)]. From the perlite chromatography column, four samples are collected, two for SPEP-R-Conc and two for SPEP-R-Conc-PW (permeate waste). After the first ammonium sulphate precipitation (two SKA-S1 samples and two SKA-P1-R samples), the two pellets (SKA-P1-R) are combined and precipitated again with ammonium sulphate at 10 % w/v. After the third ammonium sulphate precipitation at 20 % w/v, the samples analyzed by fluorescence were: SKA-S3, SKA-P4, SKA-CH1, UF/D1, SKA-UF/D2, and SKA-CH2. In total, 25 samples for each batch were analyzed as summarized in Table 1.

Nine different batches were analyzed: A–I (Table 2) with a total of 225 samples (9 9 25). These samples were initially stored in a freezer at -20 LC. After thawing, all samples were diluted prior to fluorescence analysis. The upstream fermentation samples, CPS-Conc, and CPS-Conc-PW, were diluted with 0.9 % saline buffer (0.15 mM NaCl). SPEP-R-Conc and SPEP-R-Conc-PW were diluted with 50 mM Tris–HCl buffer, and the rest of the samples with 10 mM Tris–HCl buffer. Tris–HCl buffer was pre-pared with Trizma base [Tris-(hydroxymethyl)-amino-methane] with pH adjusted to 8.0 using HCl. The dilution factor was 0.05.

Table 2 shows the final normalized Kjeldahl values for each batch in the last step of the PRN purification (SKA-F) (no showed in the flow-diagram of the process). The samples referred to as ‘‘Pass-thru’’ are samples from CPS-Conc to SKA-S1 (Table 1).

Acquisition of fluorescence spectra

Fluorescence excitation-emission spectra were acquired with a Cary Eclipse Fluorescence Spectrophotometer from Agilent Technologies. The samples were analyzed with quartz cuvettes using a slit width of 5 nm and PMT (photomultiplier tube) of 600 V. These parameters were chosen based on the spectra acquired from samples at different dilutions and at different values of slit widths and PMT. Good signal, reproducibility, lack of signal quenching due to high concentrations were the aspects taken into account for selecting those parameters. The excitation and emission ranges were 210–470 and 260–550 nm, respectively. A wide range of Ex/Em values was used to ensure that all fluorophores expected to be contained within the samples were observed. The ranges of Ex/Em values for different common fluorophores that were expected to occur in the samples are reported in the literature.

Table 1 Steps in the upstream and downstream process along with step ID and number of samples per batch

Step	Step ID	Number of samples
Production fermentation	F3-S	2
	F6-S	2
Centrate	CPS-B2-(F3)	2
	CPS-B2-(F6)	2
First concentration/ultrafiltration	CPS-Conc	2
	CPS-Conc-PW	2
Second concentration/ultrafiltration	SPEP-R-Conc	2
	SPEP-R-Conc-PW	2
First fractionation	SKA-S1	2
	SKA-P1-R	1
Third fractionation	SKA-S3	1
	SKA-P4	1
Chromatography column	SKA-CH1	1
First ultrafiltration/diafiltration	UF/D1	1
Second ultrafiltration/diafiltration	SKA-UF/D2	1
Chromatography column	SKA-CH2	1
Total		25

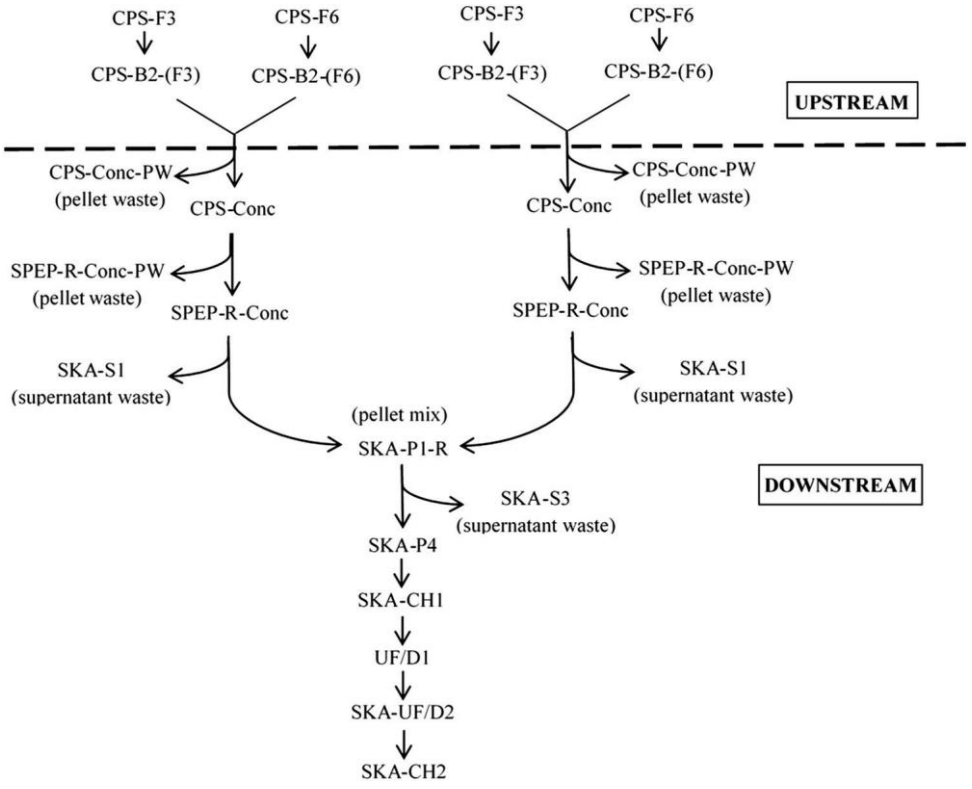

Fig. 1 Flow-diagram of the upstream and downstream PRN purification process. Samples' notation refer to different processing steps according to Table 1

Table 2 Normalized Kjeldahl values per batch

Batch	Fermenters	Pass-thru	Kjeldahl (g N/batch) in SKA-F
A	A1	A3	0.41
	A2	A4	
B	B1	B3	0.45
	B2	B4	
C	C1	C3	0.51
	C2	C4	
D	D1	D3	0.59
	D2	D4	
E	E1	E3	0.66
	E2	E4	
F	F1	F3	0.73
	F2	F4	
G	G1	G3	0.76
	G2	G4	
H	H1	H3	0.92
	H2	H4	
I	I1	I3	1.00
	I2	I4	

PCA and PLS analysis

The fluorescence spectra acquired for each sample consisted of 8148 intensities obtained for different excitation/emission combinations (28 9 291 data matrix). The intensity values for each sample were rearranged into one single row and then, the rows corresponding to all samples were appended one above the other to generate one single data matrix for PCA and PLS analysis.

To identify whether the variability in productivity originates from a specific set of steps of the manufacturing process, the data was grouped into four main data matrices as follows: (1) Upstream [with samples from CPS-F3, CPS-F6, CPS-B2-(F3), CPS-B2-(F6), CPS-Conc, CPS-Conc-PW], (2) Downstream 1 (with samples from SPEP-R-Conc, SPEP-R-Conc-PW, SKA-S1, SKA-P1-R, SKA-S3, SKA-P4, SKA-CH1, UF/D1, SKA-UF/D2, SKA-CH2), (3) Downstream 2 (with samples from SPEP-R-Conc, SKA-P1-R, SKA-P4, SKA-CH1, UF/D1, SKA-UF/D2, SKA-CH2) and (4) Downstream 3 (with samples from SPEP-R-Conc-PW, SKA-S1, SKA-S3). Downstream 1 matrix, which contains all the spectra obtained from samples in the downstream, was separated into two matrices: Downstream 2, which excludes waste samples, and Downstream 3 which only includes waste samples (Table 3).

Even though CPS-Conc and CPS-Conc-PW belong to the downstream process, they were considered together with samples from the upstream data matrix for PCA because up to the centrifugation step, from which CPS samples are obtained, there is a significant amount of antigens and co-enzymes in the samples. Thus, it was

Table 3 Matrices for PCA

	Upstream		Downstream 1	
			Downstream 2	Downstream 3
Samples	CPS-F3	CPS-B2-(F3)	SPEP-R-Conc	SPEP-R-Conc-PW
	CPS-F6	CPS-B2-(F6)	SKA-P1-R	SKA-S1
	CPS-Conc	CPS-Conc-PW	SKA-P4	SKA-S3
			SKA-CH1, UF/D1, SKA-UF/D2, SKA-CH2	

expected that by tracking samples where proteins are abundant, higher sensitivity to variability in fermentations outcomes might be assessed.

The four data matrices defined above were analyzed using PCA in order to compress the original variables into a lower number of orthogonal (non-correlated) principal variables referred to as principal components (PC). These PC's are linear combinations of the original variables (fluorescence intensities) that capture the variability in the data. Only a subset of the PC's that describe a significant percentage of the variability is kept for further analysis whereas the remaining PC's are discarded on the assumption that they are not informative since they capture variability arising from noise.

PCA decomposes a set of data (matrix X) as the sum of the products of vectors s_i and p_i, plus a residual matrix E (Eq. 1).

$$X = \sum_{i=1}^{n} s_i \times p_i + E \quad (1)$$

where n is the number of samples. The s_i vectors are known as scores and contain information on how the samples relate to the principal components. The p_i, vectors are known as loadings and contain information on how the original variables relate to each other along the principal components.

Before performing this analysis, the data were pre-treated by means of mean centering and scaling to unit variance. By performing mean centering, the average is subtracted from every column, so the new mean of each column is zero. The data is scaled to have unit variance by dividing each column by the standard deviation of the values in that particular column. Without normalization by the variance, the PCA model could wrongly focus on few variables with the largest absolute variances [17]. Cross-validation by random subset method was performed to choose the number of components [17]. This method consists of dividing the data into a number of subsets (N) randomly selected. Then, the model is built based on N - 1 subsets, leaving one out. The model is then used to predict the subset left out. The resulting prediction error is then plotted against the number of principal components (PC's), and the number with less error is chosen. Generally, and in particular for the current study, the error is the root mean square error of cross-validation (RMSECV), which is defined as:

$$\mathrm{RMSECV} = \sqrt{\frac{\sum_{i=1}^{n} (y_i - \hat{y}_i)^2}{n}} \quad (2)$$

where y_i is the measured value, $y\hat{}_i$ is the predicted variable and n is the number of calibration samples [14].

PLS was used to obtain a regression model between the fluorescence spectra of pure PRN (matrix X) corresponding to samples of SKA-CH2 (Fig. 1) and the final protein content measured by a Kjeldahl test (matrix Y). This method performs data compression and extracts a small number of latent variables (LVs) that best describes the observed or measured data. For PLS, the data mean centered and auto-scaled, as for PCA, and a cross-validation was implemented as well for selecting the number of latent variables.

PLS performs data compression and extracts a small number of latent (not directly measured) variables (LVs) that describes the observed or measured data. In contrast to PCA, PLS not only finds the major variations in X and Y, but identifies the latent variables that better correlate the scores in the X matrix with the scores in the Y matrix such as to obtain maximum covariance. Accordingly, PLS decomposes X and Y matrix as follows:

$$X = TQ + E = \sum_{i=1}^{m} t_i \times q_i + E \quad (3)$$

$$Y = UC + F = \sum_{i=1}^{m} u_i \times c_i + F \quad (4)$$

where m is the number of latent variables. The t_i and u_i vectors are the scores and contain information on how the samples relate to the latent variables. Scores in T are the projections of the input data X, i.e. fluorescence intensities to a LV in the X space, and scores in U are the projections of the response data, i.e. protein content to a LV in the Y space. The q_i and c_i vectors are known as loadings and represent the relationship between T and X space, and U and Y space, respectively. E and F contain the residuals left unexplained by the model.

The inner relation between U and T is given by the following equation

$$U = WT \quad (5)$$

where W is the weight matrix. From Eq. (5), it is possible to predict the scores in Y from scores in X, and then the new response data from Eq. (4).

To predict the response (Yr) from a new set of data (Xnew), the T score matrix can be calculated by multiplying Xnew by the known loadings (Q) from the calibration model. Subsequently, U can be calculated using Eq. (5). The new response (Yr) is then calculated by multiplying U by the known loading value C (Eq. 4).

In this project, both PCA and PLS regressions were performed using the PLS_Matlab Toolbox (Eigenvector Research Inc., Manson,WA). Data collection, analysis and plotting were conducted using the MATLAB R2012b software (The Mathworks Inc., Natick, MA).

Results and discussion

Fluorescence analysis

To monitor the PRN manufacturing process, reproducible fluorescence spectra were obtained in order to track changes of intrinsic fluorophores, mainly tryptophan, NAD(P)H and FAD that could elucidate possible causes of variability in the final product yield. The reproducibility of the fluorescence measurement was assessed by repeating the analysis of specific samples randomly chosen from the available data (10 % of error).

The most significant features in the spectra for all analyzed samples were two peaks related to tryptophan (Trp) at excitation wavelengths of (Ex) 230 and 280 nm, and emission wavelengths (Em) from 330 to 350 nm. Previous studies have shown [18] that the wavelengths where tryptophan exhibits significant emission intensities depend on the location of the amino acid residue in the protein. When the Trp residues are buried in non-polar regions of the protein, a blue-shift is observed. As the residues are located closer to the surface and thus more exposed to the environment, the emission intensities occur at higher wavelengths (red-shift) [18]. Emissions for free tryptophan in solution are observed around 350–360 nm. The ability of Trp to be excited at 230 nm is due to absorbance of its carboxylic moiety and its excitation at 280 nm is due to absorbance by the indole ring. In addition, all the spectra collected in the current work exhibits two peaks associated with NAD(P)H at excitations' wavelengths of 280 and 340 nm, and emission wavelength of 460 nm. Typical excitations wavelengths for NAD(P)H occur at 260 and 340–360 nm, corresponding to the absorption by the adenine and pyridine rings, respectively [19]. Binding of NAD(P)H to other proteins has been reported to cause a shift in its excitation wavelength from 260 to 280 nm. Such shift has been observed in the spectra obtained from early steps in the manufacturing process depicted in Fig. 1, and based on literature it is believed to be due to the binding of NAD(P)H to a dehydrogenase [10, 20].

First order Rayleigh scattering (FORS) and second order Rayleigh scattering (SORS) observed in the spectra have been reported to be indicative of protein aggregation [21]. Raman scattering (RS) emerges from the interaction of light with solvent molecules, and it is noticeable at low concentrations of fluorophores [22]. Similar patterns have been observed in the spectra among the nine batches analyzed in this work, but there are differences among samples collected from different process steps shown in Fig. 1 and from different batches that resulted in different final protein content as determined for each batch by Kjeldahl analysis. Such differences are manifested in the emissions wavelengths, in the intensities at a particular excitation wavelengths and shifts in significant excitation wavelengths. The latter shifts are for example related to the fact that tryptophan can emit at an excitation wavelength of 230 and 280 nm (peaks for both excitations are observed in all steps). For native PRN, emission of tryptophan arises at 335 nm, but when present in solution it occurs at 350 nm [23].

For the upstream fermentation steps [F3-S, F6-S, CPS-B2-(F3), CPS-B2-(F6)], the intensities were relatively low despite the expected abundance of proteins in the samples since at this point of the manufacturing process all antigens are present. The overall low fluorescence intensity observed for the samples collected from the upstream step it is believed to be due to quenching resulting from the presence of suspended particles where the latter are mostly cells' debris. A shift in the emission of Trp to *340 nm for the upstream samples is observed suggesting that Trp residues may be exposed on the surface due to unfolding of proteins.

As stated before, an excitation shift from 260 to 280 nm for NAD(P)H is observed in the spectra, suggesting a binding with a dehydrogenase. The typical emission of this cofactor at excitation 340 nm is also observed.

Another peak generally associated to FAD occurs at a region adjacent to the peak observed at Ex/Em = 450/ 530 nm. FAD is a product of the TCA cycle which activity is expected to be significant for aerobic fermentations. At this point, it is not possible to determine with fluorescence whether the emissions related to tryptophan solely originated from the content of this antigen in PRN since PT, FHA, FIM among other proteins are also present in the samples collected from the upstream step. Since FIM does not contain tryptophan, the fluorescence from this protein

would originate mainly from the presence of tyrosine [24]. Figure 2 shows the common spectra obtained for the fermenters.

In the fluorescence spectra of CPS-Conc samples, a shift in the emission of Trp is still observed while emissions for the remaining fluorophores appear without a significant variation. On the other hand, in the excitation-emission matrix (EEM) for the permeate waste (CPS-Conc-PW), a prominent emission for NAD(P)H-dehydrogenase complex is observed. This peak appears with higher intensity in batches where the final protein content for PRN, measured by Kjeldahl, is low thus possibly suggesting a correlation between the abundance of this complex in the samples collected from the fermentations and the final productivity of PRN for that particular batch (Fig. 3).

In the EEM of the sample referred to as SPEP-R-Conc, the emission peaks for fluorophores other than tryptophan start to become less evident. On the other hand, fluorescence signals corresponding to NAD(P)H, FAD and tryptophan appear in a lesser amount in the permeate waste (SPEP-R-Conc-PW). These observations seem to indicate that as the purification proceeds, the peak of Trp becomes more intense possibly correlating this increase with the expected progressive increase in concentration of the protein in the sample.

For the EEM of the sample referred to as SKA-R-P1, the most intense peak as expected is the one corresponding to tryptophan since the sample contains mostly protein. At this point, the two parallel manufacturing lines of the process are combined together to obtain a higher concentration of protein, as compared to the protein levels observed in samples collected at a point prior to the combination of the two streams. In contrast, lower intensities of Trp are observed for the SKA-S1 waste indicating a rela-tively small loss of protein from the system at this step of the purification process. The Trp in the waste stream could be related to the presence of other antigens and to some wasted PRN. Also, some traces of NAD(P)H and/or NAD(P)H-dehydrogenase complex are also present in these two samples.

A large Trp peak is present in the supernatant waste originated from the third ammonium sulphate precipitation (SKA-S3). The Em at *340 nm suggests that the Trp residues may be increasingly exposed to the solvent due to unfolding, but it is not possible to ascertain whether this emission comes from PRN since other antigens could still be present in the sample. For the resulting concentrate from this step (SKA-P4), only the Trp peak is present, and the dominant emission wavelength starts to resemble the characteristic value for PRN at 335 nm as reported in literature [23].

From this point in the process, i.e. the third ammonium sulphate precipitation step, until the last step (SKA-CH2 sample), only the Trp peak is observed in the EEM as expected for samples with increasingly pure protein. There is still a slight decrease in the tryptophan intensities which may be a result from the elimination of traces of other antigens during the later stages of the PRN purification process.

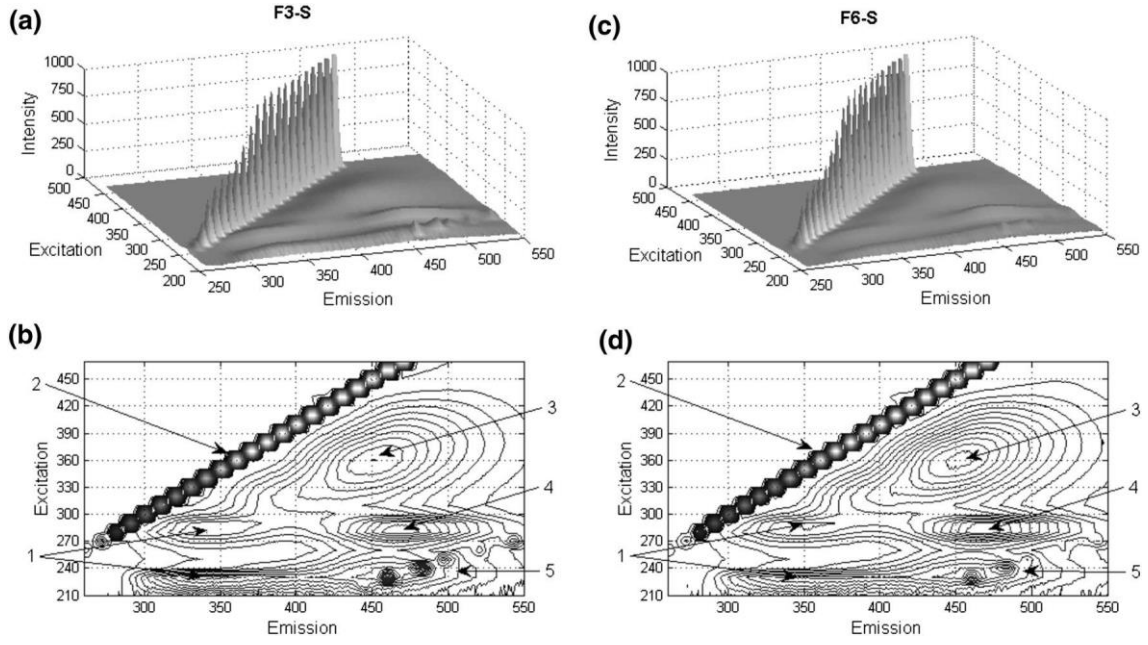

Fig. 2 Excitation–Emission Matrices for fermenters F3 (a, b), and F6 (c, d). 1-Trp, 2-FORS, 3-NAD(P)H, 4-NAD(P)H-enzyme complex, 5-SORS

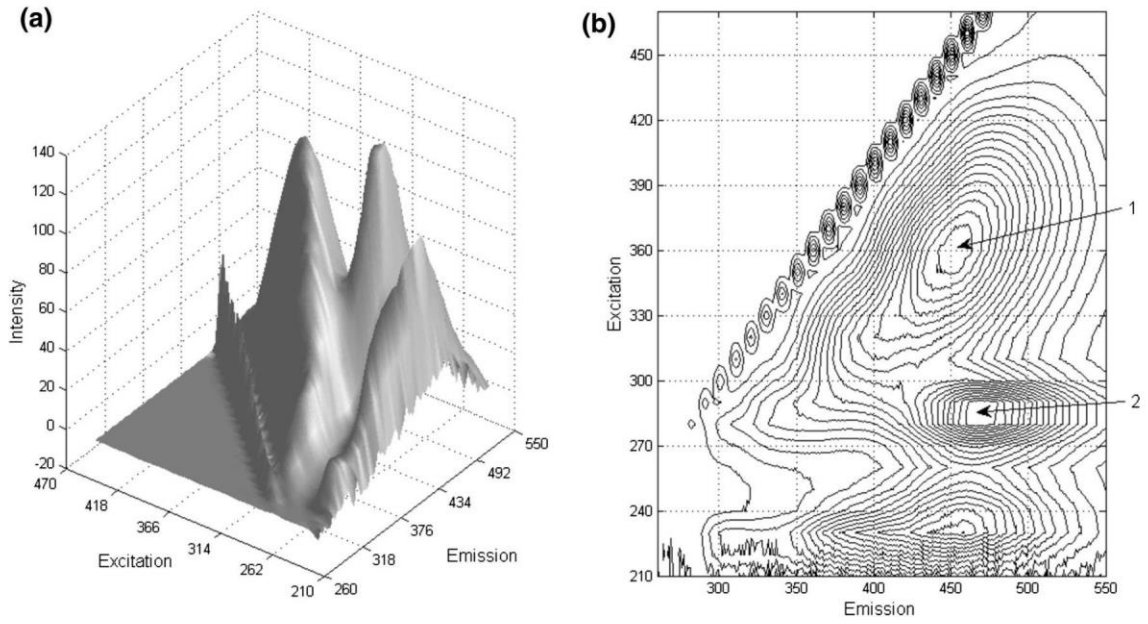

Fig. 3 EEM for CPS-Conc-PW sample. 1-NAD(P)H, 2-NAD(P)H-enzyme complex

PCA analysis

As described before in the ''Materials and methods'' section, four data matrices, where one is associated to the upstream stage and the other three to the downstream stages were analyzed using PCA (see Table 3 indicating these groupings). This analysis was performed in order to compress the originally large variables' space resulting from EEM spectra into a smaller variables' space where such data compression is possible due to the occurrence of major correlations in the original data. After performing cross-validation, and calculating the RMSECV, the number of components that explained most of the variability in the data resulted to be 3.

To identify possible differences between the upstream and downstream phases, the loadings from the spectra measured for the upstream and downstream samples were individually calculated. The sign of the PC loadings are important for interpreting the direction of the correlation between a particular fluorophore and changes in the scores corresponding to a particular loading. For example, if the PC loadings are positive, increases in the scores corresponding to this loading will indicate an increase in a fluorophore emitting at that particular loading as given by corresponding EEM values. On the other hand when the PC loadings are negative, increases in the corresponding fluorophore will drive the scores to be more and more negative.

For the upstream process, the loadings calculated for the principal component (PC1) were mostly related to Trp and scattering (Fig. 4). Because the intensities are large for what is attributed to Trp, it is hypothesized that PC1 is most likely related to the concentration of this amino acid into protein. It should be noticed that although the fluorescence intensities were positive, negative PCA loadings occur because of the mean centering and scaling procedure applied to the data before building the PCA model. It should be noticed that negative values of the loading vector indicate an inverse correlation, i.e. when the score value is negative, protein content is high, and vice versa. On the other hand, the loading vector for the second principal component (PC2) possesses higher positive intensities for the peak attributed to the NAD(P)H-enzyme complex, indicating a direct correlation with this fluorophore, i.e. higher values of this fluorophore will result in higher t2 scores. For the third principal component (PC3), the excitation-emission matrix (EEM) showed a ''shoulder'' to a peak with positive intensity values where Trp emission is characteristic, but the maximum emission presents a red-shift. This could be indicative of conformational changes in the proteins, since it has been reported that when tryptophan is more exposed to the environment, the emission is shifted to higher wavelength [18, 23, 25].

For the three remaining data matrices constructed from samples collected from different groupings of downstream processing steps (Table 3), the loadings related to PC1 and PC2 showed an inverse correlation to scattering (FORS) and a proportional correlation to protein content, respectively. For these matrices, the number of PC's obtained from cross-validation was two.

Comparing the loadings calculated for the downstream samples with those calculated for the upstream samples, the NAD(P)H-enzyme binding peak was not significant or was absent in the downstream loadings.

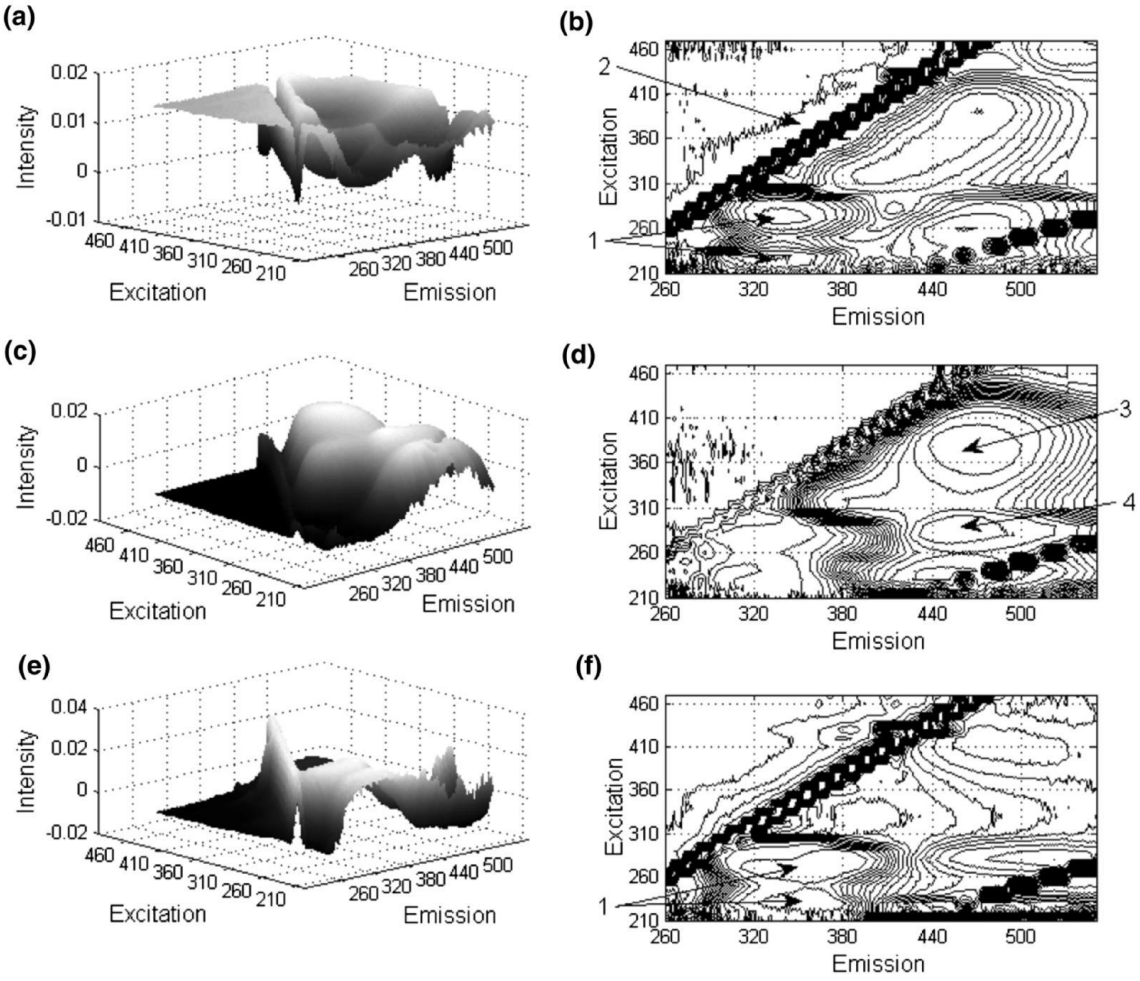

Fig. 4 Loadings for upstream samples: PC1 with variance 43.69 % (a, b), PC2 with variance 26.27 % (c, d), and PC3 with variance 15.71 % (e, f). 1-Trp, 2-FORS, 3-NAD(P)H, 4-NAD(P)H-enzyme complex

The relationship among different samples can be extracted from the score plots [16]. By comparing the score of each sample for each principal component, similarities and differences can be estimated among the samples [26].

The scores plot for the upstream data matrix in the plane of the first principal components PC1 and PC2 is shown in Fig. 5 where each subplot corresponds to a different batch.

Each point in these score plots represents the score for a particular sample. As previously discussed, for the upstream data PC1 was inversely correlated to protein content, whereas PC2 and PC3 were directly correlated to NAD(P)H-enzyme complex concentration and protein content, respectively. The main objective of this analysis was to find a possible correlation between the fluorescence corresponding to different steps of the production process and the final PRN concentration in the final stage of the purification in order to identify possible causes of low productivity for this product.

For the PC1–PC2 score plot, the batches with low final Kjeldahl (Table 2) have the largest positive values for PC2, indicating that the quantity of NAD(P)H-enzyme complex in the samples was higher in the batches with low final Kjeldahl as compared to those lots with high final Kjeldahl. This fact hints at the possibility that certain metabolic pathways related to the consumption of NAD(P)H are proceeding at different rates in different fermentations and these differences might be a source of variability in the final yield of PRN.

It has been reported that under oxidative stress, the production of NADPH increases, since the latter provides the reductive environment to quench the potential of reactive oxygen species (ROS) [27, 29]. ROS are produced during normal cellular metabolism, but if their concentration increases to a level that exceeds the cell's defense capacity, cellular damage may lead to cellular death [28, 29]. The major targets of ROS are DNA, RNA, proteins and lipids [30].

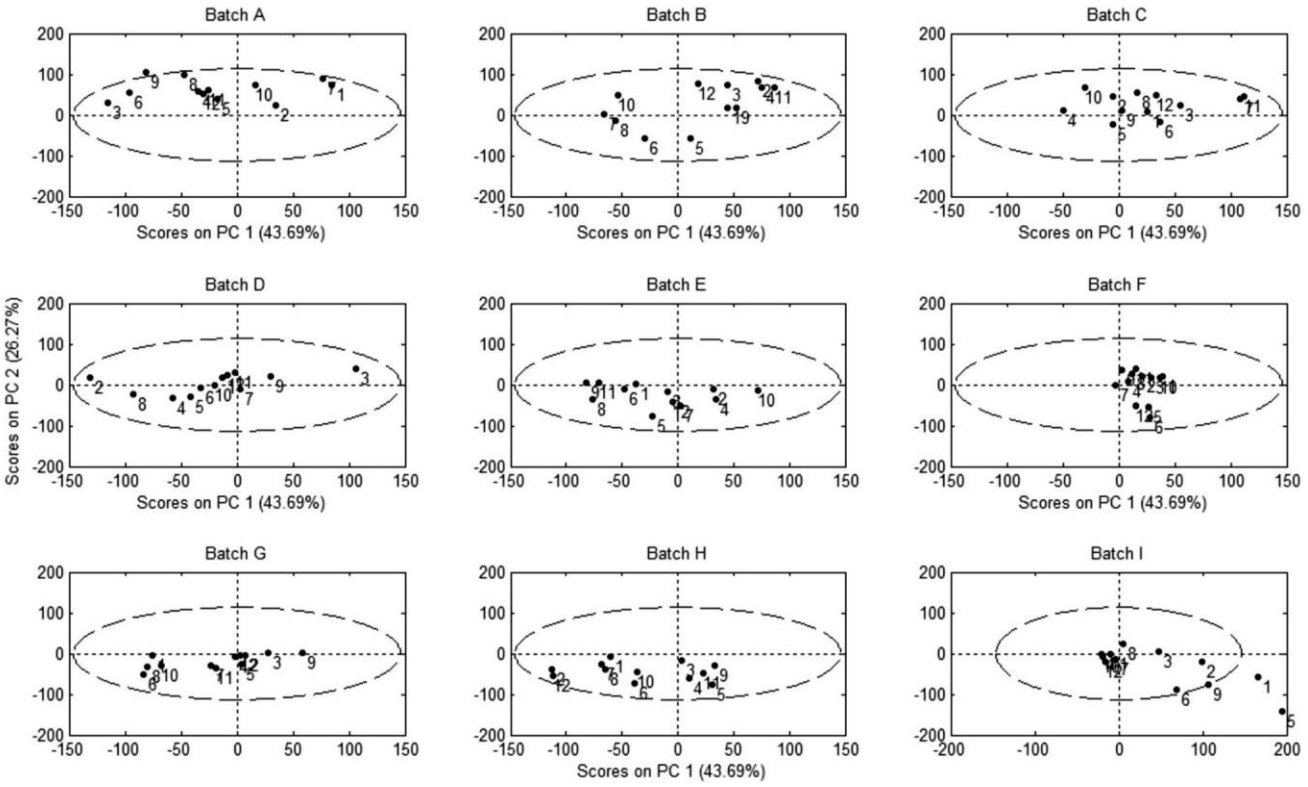

Fig. 5 PC1-PC2 scores plots for the upstream matrix. Numbers refer to the step in the process for each batch: 1 CPS-B2-(F3), 2 CPS-B2-(F3), 3 CPS-B2-(F6), 4 CPS-B2-(F6), 5 CPS-CONC, 6 CPS-CONC, 7 CPS-CONC-PW, 8 CPS-CONC-PW, 9 F3-S, 10 F3-S, 11 F6-S and 12 F6-S. X axis corresponds to PC1 with 43.69 % of variance and Y axis corresponds to PC2 with 26.27 % of variance. Batches A–D resulted in low final Kjeldahl, and batches E–I in high final Kjeldahl (as indicated in Table 2)

Some score points for batches with high productivity according to their Kjeldahl values fall in the low protein content area of the plot. This suggests that for these batches, not all the four fermentations proceeded to completion (final PRN comes from four fermenters, it might be possible that in a high yield batch not all four fermenters produced high quantity of protein). Score plots for the groups of downstream data (total downstream, downstream without waste and downstream waste are shown in Figs. 6, 7 and 8, respectively.

From these plots, it is not possible to identify any pattern that differentiates batches with low final Kjeldahl from batches with high final Kjeldahl. Samples that belong either to batches with high Kjeldahl or low Kjeldahl are dispersed in the plots thus exhibiting a lack of correlation between scores and productivity. For this reason, downstream purification protocols were dismissed as a cause of low productivity.

Regressions between PCA scores obtained from fermentation samples and PRN concentration

While fluorescence data was used above to draw qualitative observations regarding the variability of the process, the data can be also used for quantification by building regression models. Two regressions were built between PCA scores obtained from fermentation samples and final PRN concentration to assess whether there is a statistical significant correlation between fluorescence fingerprints in the fermenters and final PRN productivity. One regression was made between the average of PC1 scores (inversely correlated to protein content), the average of PC2 scores (directly correlated to NAD(P)H-enzyme content) in the fermenters and the final content of PRN measured by Kjeldahl analysis (in the last step of the purification). The resulting equation is

$$f(x,y) = a + b \times x + c \times y \quad (6)$$

where, a = 0.6697 (0.5967, 0.7428), b = 0.0001096 (-0.0001151, 0.0003343), c = -0.0004559 (-0.0006453, -0.0002665) (coefficients with 95 % confidence bounds), x = average of PC1 Scores (protein content in the fermenters), y = average of PC2 Scores (NAD(P)H-enzyme content in the fermenters), *f(x,y)*= protein content measured by Kjeldahl (PRN in the final purification step).

The goodness of fit was $R^2 = 0.8561$. Figure 9 shows a graphical representation of the model.

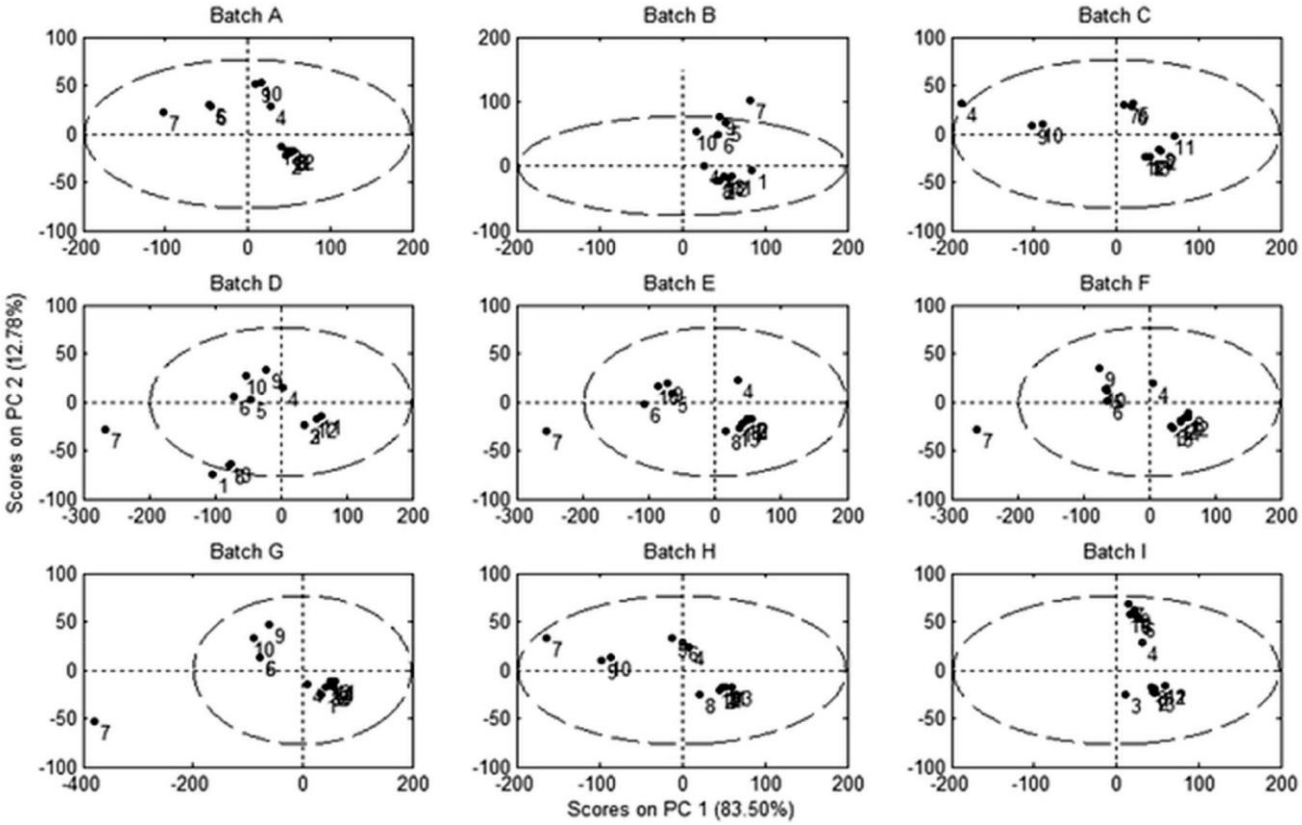

Fig. 6 PC1-PC2 scores plots for the downstream matrix. Numbers refer to the step in the process for each batch: 1 SKA-CH1, 2 SKA-CH2, 3 SKA-P4, 4 SKA-S1, 5 SKA-S1, 6 SKA-S3, 7 SKA-UF/D2, 8 SPEP-R-CONC, 9 SPEP-R-CONC, 10 SPEP-R-CONC-PW, 11 SPEP-R-CONC-PW, 12 UF/D1. X axis corresponds to PC1 with 83.50 % of variance and Y axis corresponds to PC2 with 12.78 % of variance. Batches A–D resulted in low final Kjeldahl, and batches E– I in high final Kjeldahl (as indicated in Table 2)

From the regression model, one can conclude that when NAD(P)H content is high, y (average of PC2 scores) is positive, therefore *f(x,y)* decreases. On the other hand, for the average of PC1, the 95 % confident bounds for this coefficient are -0.0001151 and 0.0003343, allowing zero as a possible value, which means that in some cases the final protein content as measured by Kjeldahl (*f(x,y)*) can be independent of the scores x. One feasible explanation for this is since in the fermenters not only PRN is present, other antigens such as FIM, FHA and PT contribute to the fluorescence emission of tryptophan making difficult to find a correlation between the protein content in the fermenters and the PRN content at the end of the process.

A PLS regression model was also built between the averages of the PC2 scores, that are related to NAD(P)H-complex, and the measured Kjeldahl values. PLS generally provides better prediction accuracy for regression models that correlate noisy input data (fluorescence) to noisy output data (Kjeldahl). Besides capturing the variance, PLS tries to describe the data with a small number of latent variables (LV) that maximize covariance to achieve a correlation between two sets of data [16]. Figure 10 shows the plot of the regression. The goodness of fit was 0.78.

We also attempted to build a PLS regression model between EEMs in different locations of the upstream process and final PRN but the regression results were not better ($R^2 = 0.65$) than for the regression presented above between the PC's scores and Kjeldahl measurements because there are several proteins present in the upstream and downstream locations other than PRN. Using a regression based on the PCs obtained from PCA was effective because we knew a priori the particular EEM regions that will strongly correlate with the fluorophores of interest, i.e. tryptophan and NAD(P)H.

PLS for predicting PRN concentration

An additional regression model was developed using partial least squares (PLS) for predicting the final PRN concentration based on fluorescence measurements obtained from samples collected in the final step of the purification process. The objective was to see whether fluorescence can be used to predict the PRN concentration in pure samples

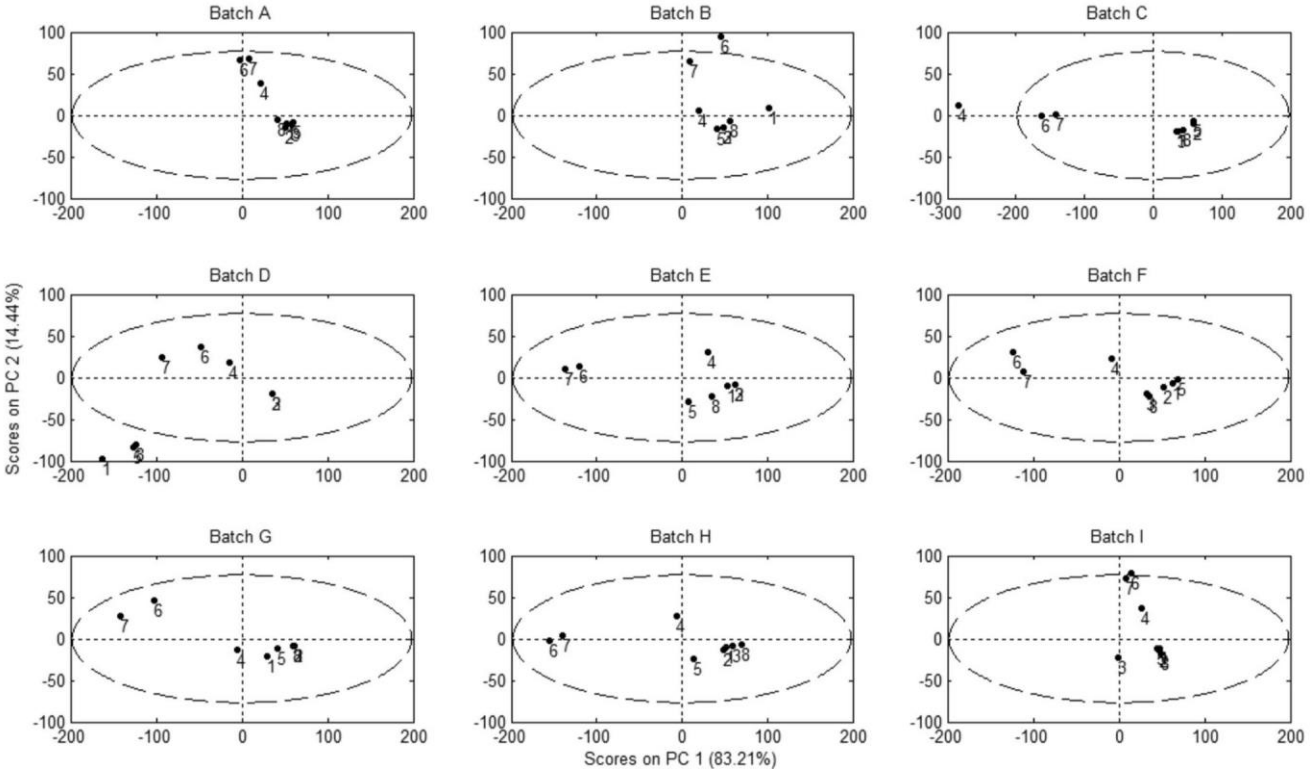

Fig. 7 PC1-PC2 scores plots for the downstream without waste matrix. Numbers refer to the step in the process for each batch: 1 SKA-CH1, 2 SKA-CH2, 3 SKA-P4, 4 SKA-UF/D2, 5 SPEP-R-CONC, 6 SPEP-R-CONC, and 7 UF/D1. X axis corresponds to PC1 with 83.21 % of variance and Y axis corresponds to PC2 with 14.44 % of variance. Batches A–D resulted in low final Kjeldahl, and batches E–I in high final Kjeldahl (as indicated in Table 2)

where there are no additional proteins or species in the sample which may interfere with the PRN-related fluorescence.

Specifically, a PLS regression was developed to capture a correlation between SKA-CH2 samples (matrix X) and final Kjeldahl values (matrix Y). The PLS model (Fig. 11) for this set of data was expressed as a linear combination of four latent variables (LV).

The R^2 value was 0.745 showing a positive linear correlation, between fluorescence intensities and PRN content. Thus fluorescence in combination with a PLS regression model is shown as an effective approach to predict Kjel-dahl values from fluorescence measurements.

Conclusions

This work presents a novel application of fluorescence spectroscopy in combination with multivariate analysis for diagnosing and identifying the sources of variability in a vaccine manufacturing process. By means of fluorescence, it was possible to identify fluorescent compounds, such as amino acids and cofactors, which allow for rapid qualitative analysis and off-line monitoring. The work also proposes the use of fluorescence for quantifying the amount of protein product in the final stages of the process by using data collected in the early stages of the process in conjunction with multivariate statistical techniques, such as PCA and PLS.

PCA was found to be effective for recognizing correlations between conditions at different steps of the manufacturing process with the PRN concentration at the end of the process. From this analysis, it was noticed that the amount of NAD(P)H-enzyme complex was high in the fermenters of the batches with low productivity, suggesting that certain types of metabolic reactions related to the production of NAD(P)H are taking place in the fermentation steps that might be causing variability in the final yield of PRN. NADPH accumulation has been reported for other bacteria to be related to oxidative stress with resulting production of ROS and reduced protein productivity. It was not possible to find a correlation between protein content in the fermenters with the PRN content at the end of the process. This might be due to the fact that in the fermenters not only PRN is present; also other proteins contribute to the emission tryptophan.

In the analysis of the three matrices containing only downstream data, it was not possible to find any pattern

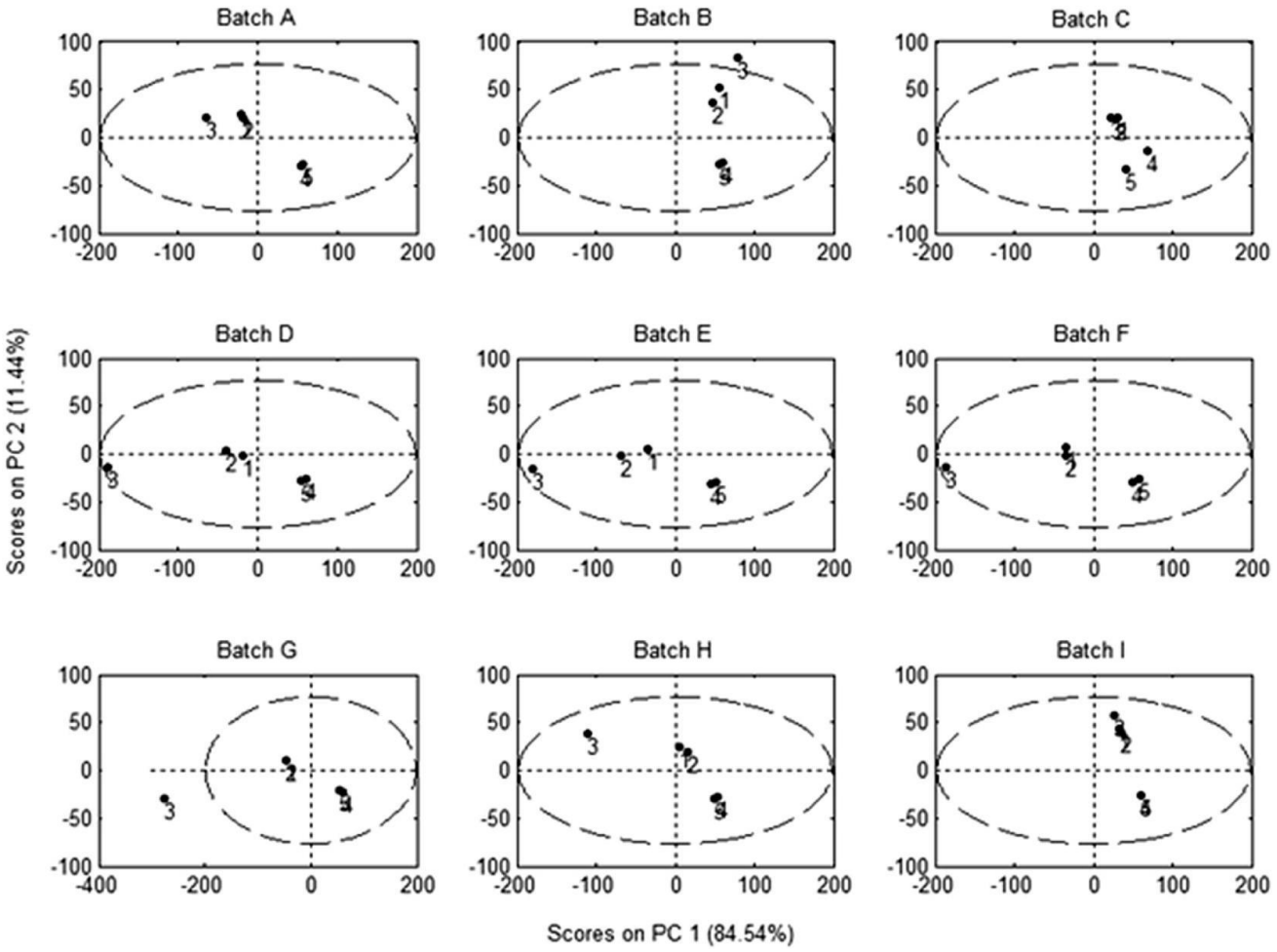

Fig. 8 PC1-PC2 scores plots for the downstream waste matrix. Numbers refer to the step in the process for each batch: 1 SKA-S1, 2 SKA-S1, 3 SKA-S3, 4 SPEP-R-CONC-PW, and 5 SPEP-R-CONC-PW. X axis corresponds to PC1 with 84.54 % of variance and Y axis corresponds to PC2 with 11.44 % of variance. Batches A–D resulted in low final Kjeldahl, and batches E–I in high final Kjeldahl (as indicated in Table 2)

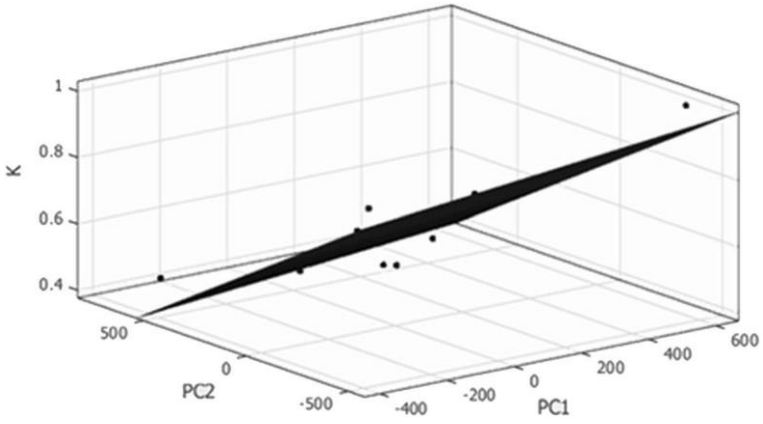

Fig. 9 Regression among PC1 scores average and PC2 score average in the fermenters, and final Kjeldahl values

that differentiates batches with low final Kjeldahl from batches with high final Kjeldahl thus hinting that the source of variability in the final protein content is in the upstream stages.

The two regression models built between PCA scores obtained from fermentation samples and PRN concentration, demonstrated that there is a statistical significant correlation between fluorescence information and PRN

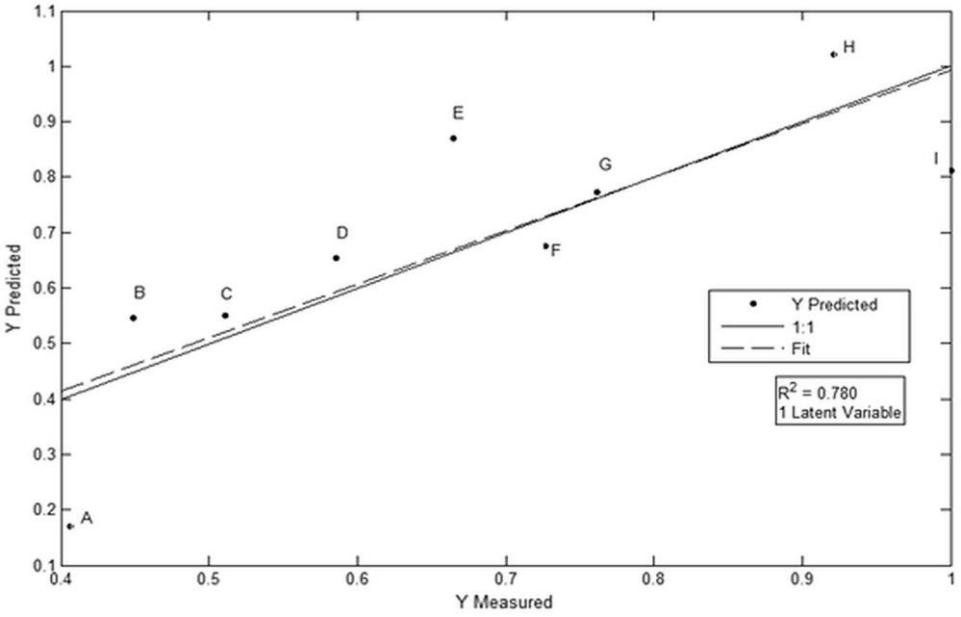

Fig. 10 PLS regression between PC2 scores [NAD(P)H complex] and Kjeldahl values

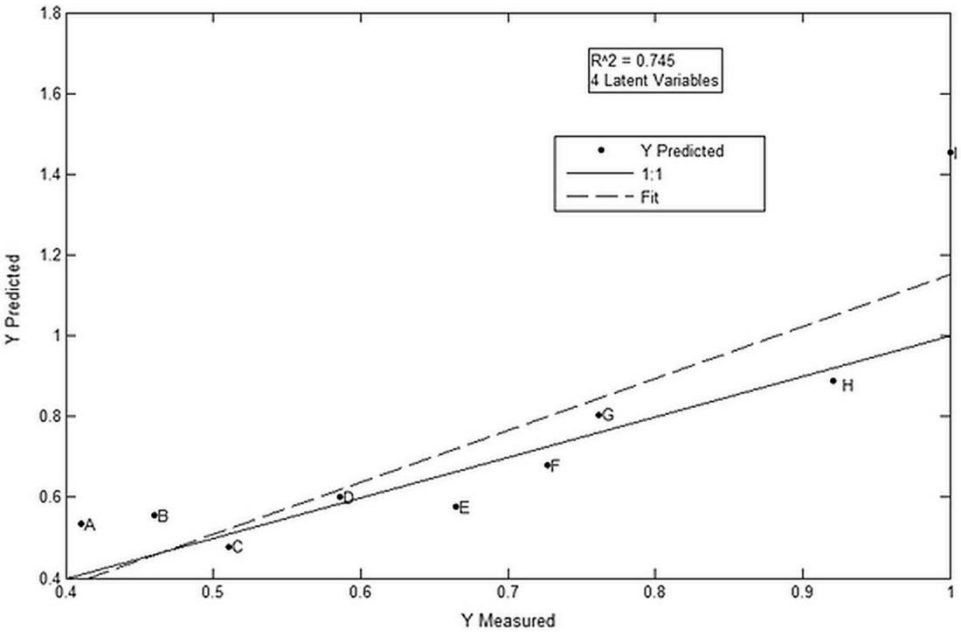

Fig. 11 PLS regression between SKA-CH2 and Kjeldahl values

levels. A good correlation was achieved when using PLS to predict the final PRN concentration from fluorescence measurements obtained from samples collected in the final step of the purification process, demonstrating the feasibility of using fluorescence as a rapid method to predict protein concentration.

Acknowledgments The authors would like to thank NSERC (National Science and Engineering Research Council of Canada) and Sanofi Pasteur for the financial support.

References

1. Warfel JM, Edwards KM (2015) Pertussis vaccines and the challenge of inducing durable immunity. Curr Opin Immunol 35:48–54
2. Lourenc¸o N, Lopes D, Almeida J, Sarraguc¸a A, Pinheiro C (2012) Bioreactor monitoring with spectroscopy and chemometrics: a review. Anal Bioanal Chem 404(4):1211–1237
3. Oh Se-Kyu, Yoo Sung Jin, Jeong Dong Hwi, Lee Jong Min (2013) Real-time estimation of glucose concentration in algae cultivation system using Raman spectroscopy. Bioresour Technol 142:131–137

4. Carrondo M, Alves P, Carinhas N, Glassey J, Hesse F, Merten O, Micheletti M, Noll T, Oliveira R, Reichl U, Staby A, Teixeira A, Weichert H, Mandenius C (2012) How can measurement, monitoring, modeling and control advance cell culture in industrial biotechnology? Biotechnol J 7(12):1522–1529
5. Lindemann C, Marose S, Nielsen H, Scheper T (1998) Two-dimensional fluorescence spectroscopy for on-line bioprocess monitoring. Sens Actuators B Chem 51(1):273–277
6. Marose S, Lindemann C, Ulber R, Scheper T (1999) Optical sensor systems for bioprocess monitoring. Trends Biotechnol 17(1):30–34
7. Skibsted E, Lindemann C, Roca C, Olsson L (2001) On-line bioprocess monitoring with a multiwavelength fluorescence sensor using multivariate calibration. J Biotechnol 88(1):47–57
8. Hagedorn A, Legge RL, Budman H (2003) Evaluation of spectrofluorometry as a tool for estimation in fed-batch fermentations. Biotechnol Bioeng 83(1):104–111
9. Royer CA (2006) Probing protein folding and conformational transitions with fluorescence. Chem Rev 106(5):1769–1784
10. Lakowicz JR (2007) Principles of fluorescence spectroscopy. Springer, NY
11. Wehry EL (1997) Molecular fluorescence and phosphorescence spectrometry. Handbook of instrumental techniques for analytical chemistry, pp 507–539
12. Christensen J, Norgaard L, Bro R, Engelsen SB (2006) Multivariate autofluorescence of intact food systems. Chem Rev 106:1979–1993
13. Harms P, Kostov Y, Rao G (2002) Bioprocess monitoring. Curr Opin Biotechnol 13(2):124–127
14. Wise BM, Gallagher N, Bro R, Shaver J, Windig W, Koch RS (2007) PLS-Toolbox Version 3.5 for use with MATLAB^{TM}, Manual. Eigenvector Research, Inc., Manson
15. Ohadi K, Legge RL, Budman HM (2015) Intrinsic fluorescence-based at situ soft sensor for monitoring monoclonal antibody aggregation. Biotechnol Prog 31(5):1423–1432
16. Ohadi K, Legge RL, Budman HM (2015) Development of a soft-sensor based on multi-wavelength fluorescence spectroscopy and a dynamic metabolic model for monitoring mammalian cell cultures. Biotechnol Bioeng 112(1):197–208
17. Wise BM, Gallagher NB (1996) The process chemometrics approach to process monitoring and fault detection. J Process Control 6(6):329–348
18. Burstein EA, Vedenkina NS, Ivkova MN (1973) Fluorescence and the location of tryptophan residues in protein molecules. Photochem Photobiol 18(4):263–279
19. Rover L Jr, Fernandes JC, Neto GdO, Kubota LT, Katekawa E, Serrano SH (1998) Study of NADH stability using ultraviolet–visible spectrophotometric analysis and factorial design. Anal Biochem 260(1):50–55
20. Gazzotti P, Bock H, Fleischer S (1974) Role of lecithin in D-b-hydroxybutyrate dehydrogenase function. Biochem Biophys Res Commun 58(1):309–315
21. Militello V, Vetri V, Leone M (2003) Conformational changes involved in thermal aggregation processes of bovine serum albumin. Biophys Chem 105(1):133–141
22. Deshpande SS (2001) Principles and applications of luminescence spectroscopy. Crit Rev Food Sci Nutr 41(3):155–224
23. Junker M, Schuster CC, McDonnell AV, Sorg KA, Finn MC, Berger B, Clark PL (2006) Pertactin beta-helix folding mechanism suggests common themes for the secretion and folding of autotransporter proteins. Proc Natl Acad Sci USA 103(13): 4918–4923
24. Crowley-Luke A, Reddin K, Gorringe A, Hudson MJ, Robinson A (2001) Formulation and characterization of Bordetella pertussis fimbriae as novel carrier proteins for Hib conjugate vaccines. Vaccine 19(25–26):3399–3407
25. Seabrook RN, Atkinson T, Irons LI (1991) A spectroscopic and conformational study of pertussis toxin. Eur J Biochem 198(3):741–747
26. Persson T, Wedborg M (2001) Multivariate evaluation of the fluorescence of aquatic organic matter. Anal Chim Acta 434(2):179–192
27. Singh RM (2007) Oxidative stress evokes a metabolic adaptation that favors increased NADPH synthesis and decreased NADH production in Pseudomonas fluorescens. J Bacteriol 189(18): 6665–6675
28. Sigler KC (1999) Oxidative stress in microorganisms—I. Folia Microbiol 44(6):587–624
29. Beriault RH (2007) The overexpression of NADPH-producing enzymes counters the oxidative stress evoked by gallium, an iron mimetic. Biometals 20(2):165–176
30. Cabiscol ET (2000) Oxidative stress in bacteria and protein damage by reactive oxygen species. Int Microbiol 3(1).

References

Abdi, H., & Williams, L. J. (2010). Principal component analysis. *Wiley Interdisciplinary Reviews: Computational Statistics*, 2(4), 433-459.

Abrashev, R., Krumova, E., Dishliska, V., Eneva, R., Engibarov, S., Abrashev, I., & Angelova, M. (2011). Differential effect of paraquat and hydrogen peroxide on the oxidative stress response in *Vibrio cholerae* Non O1 26/06. *Biotechnology & Biotechnological Equipment*, 25(sup1), 72-76.

Augustin, J. C., Brouillaud-Delattre, A., Rosso, L., & Carlier, V. (2000). Significance of Inoculum Size in the Lag Time of *Listeria monocytogenes*. *Applied and Environmental Microbiology*, 66(4), 1706-1710.

Aldsworth, T. G., Sharman, R. L., & Dodd, C. E. R. (1999). Bacterial suicide through stress. *Cellular and Molecular Life Sciences CMLS*, 56(5-6), 378-383.

Álvarez-Barrientos, A., Arroyo, J., Cantón, R., Nombela, C., & Sánchez-Pérez, M. (2000). Applications of flow cytometry to clinical microbiology. *Clinical Microbiology Reviews*, 13(2), 167-195.

Anjem, A., Varghese, S., & Imlay, J. A. (2009). Manganese import is a key element of the OxyR response to hydrogen peroxide in *Escherichia coli*. *Molecular Microbiology*, 72(4), 844-858.

Babu, M. M., Bhargavi, J., Saund, R. S., & Singh, S. K. (2001). Virulence factors of *Bordetella pertussis*. *Current Science*, 80(12), 1512-1522.

Bai, Z., Harvey, L. M., & McNeil, B. (2003). Physiological responses of chemostat cultures of *Aspergillus niger* (B1-D) to simulated and actual oxidative stress. *Biotechnology and Bioengineering*, 82(6), 691-701.

Baez, A., & Shiloach, J. (2013). *Escherichia coli* avoids high dissolved oxygen stress by activation of SoxRS and manganese-superoxide dismutase. *Microbial Cell Factories*, 12(1), 23.

Baez, A., & Shiloach, J. (2014). Effect of elevated oxygen concentration on bacteria, yeasts, and cells propagated for production of biological compounds. *Microbial Cell Factories*, 13(1), 181.

Barrière, C., Brückner, R., Centeno, D., & Talon, R. (2002). Characterisation of the katA gene encoding a catalase and evidence for at least a second catalase activity in *Staphylococcus xylosus*, bacteria used in food fermentation. *FEMS Microbiology Letters*, 216(2), 277-283.

Benov, L. (2001). How superoxide radical damages the cell. *Protoplasma*, 217(1-3), 33-36.

Bériault, R., Hamel, R., Chenier, D., Mailloux, R. J., Joly, H., & Appanna, V. D. (2007). The overexpression of NADPH-producing enzymes counters the oxidative stress evoked by gallium, an iron mimetic. *Biometals*, 20(2), 165-176.

Berney, M., Hammes, F., Bosshard, F., Weilenmann, H. U., & Egli, T. (2007). Assessment and interpretation of bacterial viability by using the LIVE/DEAD BacLight Kit in combination with flow cytometry. *Applied and Environmental Microbiology*, 73(10), 3283-3290.

Betteridge, D. J. (2000). What is oxidative stress?. *Metabolism*, 49(2), 3-8.

Billington, R. A., Bruzzone, S., De Flora, A., Genazzani, A. A., Koch-Nolte, F., Ziegler, M., & Zocchi, E. (2006). Emerging functions of extracellular pyridine nucleotides. *Molecular Medicine*, 12(11-12), 324.

Biosciences, B. D. (2000). Introduction to Flow Cytometry: A learning guide. *Manual Part, 1*.

Birtwistle, M. (2014). Experimental Methods in Systems Biology [PowerPoint slides]. Retrieved December, 2015, from https://www.coursera.org/learn/experimental-methods.

Boulos, L., Prevost, M., Barbeau, B., Coallier, J., & Desjardins, R. (1999). LIVE/DEAD® BacLight™: application of a new rapid staining method for direct enumeration of viable and total bacteria in drinking water. *Journal of Microbiological Methods*, 37(1), 77-86.

Breeuwer, P., & Abee, T. (2000). Assessment of viability of microorganisms employing fluorescence techniques. *International Journal of Food Microbiology*, 55(1), 193-200.

Broger, T., Odermatt, R. P., Huber, P., & Sonnleitner, B. (2011). Real-time on-line flow cytometry for bioprocess monitoring. *Journal of Biotechnology*, 154(4), 240-247.

Brumaghim, J. L., Li, Y., Henle, E., & Linn, S. (2003). Effects of hydrogen peroxide upon nicotinamide nucleotide metabolism in *Escherichia coli* changes in enzyme levels and nicotinamide nucleotide pools and studies of the oxidation of NAD(P)H by Fe(III). *Journal of Biological Chemistry*, 278(43), 42495-42504.

Budman, H., Patel, N., Tamer, M., & Al-Gherwi, W. (2013). A dynamic metabolic flux balance based model of fed-batch fermentation of *Bordetella pertussis*. *Biotechnology Progress*, 29(2), 520-531.

Burstein, E. A., Vedenkina, N. S., & Ivkova, M. N. (1973). Fluorescence and the location of tryptophan residues in protein molecules. *Photochemistry and Photobiology*, 18(4), 263-279.

Cabiscol Català, E., Tamarit Sumalla, J., & Ros Salvador, J. (2000). Oxidative stress in bacteria and protein damage by reactive oxygen species. *International Microbiology*, 3(1), 3-8.

Carrondo, M. J., Alves, P. M., Carinhas, N., Glassey, J., Hesse, F., Merten, O. W., Micheletti, M., Noll, T., Oliveira, R., Reichl, U., Staby, A., Teixeira, A., Weichert, H. & Mandenius, C. (2012). How can measurement, monitoring, modeling and control advance cell culture in industrial biotechnology?. *Biotechnology Journal*, 7(12), 1522-1529.

Cattelan, N., Dubey, P., Arnal, L., Yantorno, O. M., & Deora, R. (2016). *Bordetella* biofilms: a lifestyle leading to persistent infections. *Pathogens and Disease*, 74(1), ftv108.

Charles, I., Fairweather, N., Pickard, D., Beesley, J., Anderson, R., Dougan, G., & Roberts, M. (1994). Expression of the *Bordetella pertussis* P. 69 pertactin adhesin in *Escherichia coli*: fate of the carboxy-terminal domain. *Microbiology*, 140(12), 3301-3308.

Chelikani, P., Fita, I., & Loewen, P. C. (2004). Diversity of structures and properties among catalases. *Cellular and Molecular Life Sciences* CMLS, 61(2), 192-208.

Cohen, S. M., & Wheeler, M. W. (1946). Pertussis vaccine prepared with phase-I cultures grown in fluid medium. *American Journal of Public Health and the Nation's Health*, 36(4), 371-376.

Crawford, D. R., & Davies, K. J. (1994). Adaptive response and oxidative stress. *Environmental Health Perspectives*, 102(Suppl 10), 25.

Czechowska, K., Johnson, D. R., & van der Meer, J. R. (2008). Use of flow cytometric methods for single-cell analysis in environmental microbiology. *Current Opinion in Microbiology*, 11(3), 205-212.

Dalle-Donne, I., Rossi, R., Giustarini, D., Milzani, A., & Colombo, R. (2003). Protein carbonyl groups as biomarkers of oxidative stress. *Clinica Chimica Acta*, 329(1), 23-38.

Dartnell, L. R., Roberts, T. A., Moore, G., Ward, J. M., & Muller, J. P. (2013). Fluorescence characterization of clinically-important bacteria. *PloS One*, 8(9), e75270.

Darzynkiewicz, Z., & Juan, G. (2001). Analysis of DNA content and BrdU incorporation. *Current Protocols in Cytometry*, 7-7.

Davey, H. M., & Kell, D. B. (1996). Flow cytometry and cell sorting of heterogeneous microbial populations: the importance of single-cell analyses. *Microbiological Reviews*, 60(4), 641-696.

Degelau, A., Freitag, R., Linz, F., Middendorf, C., Scheper, T., Bley, T., Müller, S., Stoll, P. & Reardon, K. F. (1992). Immuno- and flow cytometric analytical methods for biotechnological research and process monitoring. *Journal of Biotechnology*, 25(1), 115-144.

DeShazer, D., Barnnan, J. D., Moran, M. J., & Friedman, R. L. (1994). Characterization of the gene encoding superoxide dismutase of *Bordetella pertussis* and construction of a SOD-deficient mutant. *Gene*, 142(1), 85-89.

Díaz, M., Herrero, M., García, L. A., & Quirós, C. (2010). Application of flow cytometry to industrial microbial bioprocesses. *Biochemical Engineering Journal*, 48(3), 385-407.

Diwan, J. J., *Electron Transfer Chain. Biochemistry of Metabolism*. Retrieved from https://www.rpi.edu/dept/bcbp/molbiochem/MBWeb/mb1/part2/redox. htm

Dugan, L. L., & Choi, D. W. (1999). Hypoxic-Ischemic Brain Injury and Oxidative Stress. Siegel, G.J., Agranoff, B.W., Albers, R.W., Fisher, S.K., Uhler, M.D., (Eds.), *Basic neurochemistry: Molecular, cellular and medical aspect*s. Lippincott-Raven Publishers, Philadelphia, New York, Chapter 34.

Dutton, R. L., Scharer, J. M., & Moo-Young, M. (1998). Descriptive parameter evaluation in mammalian cell culture. *Cytotechnology*, 26(2), 139-152.

Elshereef, R. (2009). Application of multi-wavelength fluorometry to monitoring protein ultrafiltration. Doctoral dissertation. University of Waterloo, Waterloo, Canada.

Esterházy, D., King, M. S., Yakovlev, G., & Hirst, J. (2008). Production of Reactive Oxygen Species by Complex I (NADH: Ubiquinone Oxidoreductase) from *Escherichia coli* and Comparison to the Enzyme from Mitochondria. *Biochemistry*, 47(12), 3964-3971.

Eruslanov, E., & Kusmartsev, S. (2010). Identification of ROS using oxidized DCFDA and flow-cytometry. In *Advanced Protocols in Oxidative Stress II* (pp. 57-72). Humana Press, Totowa, NJ.

Farr, S. B., & Kogoma, T. O. K. I. O. (1991). Oxidative stress responses in *Escherichia coli* and Salmonella typhimurium. *Microbiological reviews*, 55(4), 561-585.

Frank, J., Pompella, A., & Biesalski, H. K. (2000). Histochemical visualization of oxidant stress. *Free Radical Biology and Medicine*, 29(11), 1096-1105.

Frisard, M., & Ravussin, E. (2006). Energy metabolism and oxidative stress. *Endocrine*, 29(1), 27-32.

Gaillard, M. E. (2009). Genómica funcional de *Bordetella pertussis*, implicancias sobre una enfermedad considerada reemergente (Doctoral dissertation, Facultad de Ciencias Exactas).

Gant, V. A., Warnes, G., Phillips, I., & Savidge, G. F. (1993). The application of flow cytometry to the study of bacterial responses to antibiotics. *Journal of Medical Microbiology*, 39(2), 147-154.

Gay, M., Cerf, O., & Davey, K. R. (1996). Significance of pre-incubation temperature and inoculum concentration on subsequent growth of Listeria monocytogenes at 14° C. *Journal of Applied Bacteriology*, 81(4), 433-438.

Gazzotti, P., Bock, H., & Fleischer, S. (1974). Role of lecithin in d-β-hydroxybutyrate dehydrogenase function. *Biochemical and Biophysical Research Communications*, 58(1), 309-315.

Givan, A. L. (2000). The basics of staining for cell surface proteins. In *In Living Color* (pp. 142-164). Springer Berlin, Heidelberg.

Gomes, A., Fernandes, E., & Lima, J. L. (2005). Fluorescence probes used for detection of reactive oxygen species. *Journal of Biochemical and Biophysical Methods*, 65(2), 45-80.

Gordon, K. M., Duckett, L., Daul, B., & Petrie, H. T. (2003). A simple method for detecting up to five immunofluorescent parameters together with DNA staining for cell cycle or viability on a benchtop flow cytometer. *Journal of Immunological Methods*, 275(1), 113-121.

Graeff-Wohlleben, H., Killat, S., Banemann, A., Guiso, N., & Gross, R. (1997). Cloning and characterization of a Mn-containing superoxide dismutase (SodA) of *Bordetella pertussis*. *Journal of Bacteriology*, 179(7), 2194-2201.

Grose, J. H., Joss, L., Velick, S. F., & Roth, J. R. (2006). Evidence that feedback inhibition of NAD kinase controls responses to oxidative stress. *Proceedings of the National Academy of Sciences*, 103(20), 7601-7606.

Guo, F. X., Shi-Jin, E., Liu, S. A., Chen, J., & Li, D. C. (2008). Purification and characterization of a thermostable MnSOD from the thermophilic fungus *Chaetomium thermophilum*. *Mycologia*, 100(3), 375-380.

Gupta RC, Milatovic D. (2014). Insecticides. In Gupta RC, (Eds). *Biomarkers in Toxicology*. Amsterdam: Academic Press/Elsevier. p. 389–407.

Hairston, P. P., Ho, J., & Quant, F. R. (1997). Design of an instrument for real-time detection of bioaerosols using simultaneous measurement of particle aerodynamic size and intrinsic fluorescence. *Journal of Aerosol Science*, 28(3), 471-482.

Halliwell, B., & Whiteman, M. (2004). Measuring reactive species and oxidative damage in vivo and in cell culture: how should you do it and what do the results mean?. *British Journal of Pharmacology*, 142(2), 231-255.

Hansson, L., & Häggström, M. H. (1984). Effects of growth conditions on the activities of superoxide dismutase and NADH-oxidase/NADH-peroxidase in *Streptococcus lactis*. *Current Microbiology*, 10(6), 345-351.

Heikal, A., Nakatani, Y., Dunn, E., Weimar, M. R., Day, C. L., Baker, E. N., Lott, J. S., Sazanov, L.A., & Cook, G. M. (2014). Structure of the bacterial type II NADH dehydrogenase: a monotopic membrane protein with an essential role in energy generation. *Molecular Microbiology*, 91(5), 950-964.

Henderson, I. R., Navarro-Garcia, F., & Nataro, J. P. (1998). The great escape: structure and function of the autotransporter proteins. *Trends in Microbiology*, 6(9), 370-378.

Hijnen, M. (2006). The *Bordetella pertussis* protein Pertactin: role in immunity and immune evasion. Doctoral dissertation. Utrecht University. Utrecht, Netherlands (p. 200).

Hijnen, M., He, Q., Schepp, R., Van Gageldonk, P., Mertsola, J., Mooi, F. R., & Berbers, G. A. (2008). Antibody responses to defined regions of the *Bordetella pertussis* virulence factor pertactin. *Scandinavian Journal of Infectious Diseases*, 40(2), 94-104.

Ho, J., Spence, M., & Hairston, P. (1999). Measurement of biological aerosol with a fluorescent aerodynamic particle sizer (FLAPS): correlation of optical data with biological data. *Aerobiologia*, 15(4), 281-291.

Imaizumi, A., Suzuki, Y., Ono, S., Sato, H., & Sato, Y. (1983). Heptakis (2, 6-O-dimethyl) beta-cyclodextrin: a novel growth stimulant for *Bordetella pertussis* phase I. *Journal of Clinical Microbiology*, 17(5), 781-786.

Imlay, J. A. (2013). The molecular mechanisms and physiological consequences of oxidative stress: lessons from a model bacterium. *Nature Reviews Microbiology*, 11(7), 443.

Imlay, J. A. (2015). Diagnosing oxidative stress in bacteria: not as easy as you might think. *Current Opinion in Microbiology*, 24, 124-131.

Iwase, T., Tajima, A., Sugimoto, S., Okuda, K. I., Hironaka, I., Kamata, Y., Takada, K. & Mizunoe, Y. (2013). A simple assay for measuring catalase activity: a visual approach. *Scientific Reports*, 3, 3081.

Jacobberger, J. W., Sramkoski, R. M., & Stefan, T. (2011). Multiparameter cell cycle analysis. Flow *Cytometry Protocols*, 229-249

Jiskoot, W., Westdijk, J., Reubsaet, C. H. K., & Beuvery, E. C. (1996). Analysis of *Bordetella pertussis* Suspensions by ELISA and Flow Cytometry. In *Novel Strategies in the Design and Production of Vaccines* (pp. 153-157). Springer US.

Junker, M., Schuster, C. C., McDonnell, A. V., Sorg, K. A., Finn, M. C., Berger, B., & Clark, P. L. (2006). Pertactin beta-helix folding mechanism suggests common themes for the secretion and

folding of autotransporter proteins. *Proceedings of the National Academy of Sciences of the United States of America*, 103(13), 4918-4923.

Keyer, K., Gort, A. S., & Imlay, J. A. (1995). Superoxide and the production of oxidative DNA damage. *Journal of Bacteriology*, 177(23), 6782-6790.

Keyer, K., & Imlay, J. A. (1996). Superoxide accelerates DNA damage by elevating free-iron levels. *Proceedings of the National Academy of Sciences*, 93(24), 13635-13640.

Khelef, N., DeShazer, D., Friedman, R. L., & Guiso, N. (1996). In vivo and in vitro analysis of *Bordetella pertussis* catalase and Fe-superoxide dismutase mutants. *FEMS Microbiology Letters*, 142(2-3), 231-235.

Kimoto-Nira, H., Moriya, N., Ohmori, H., & Suzuki, C. (2014). Altered superoxide dismutase activity by carbohydrate utilization in a *Lactococcus lactis* strain. *Journal of Food Protection*, 77(7), 1161-1167.

Kirkman, H. N., & Gaetani, G. F. (1984). Catalase: a tetrameric enzyme with four tightly bound molecules of NADPH. *Proceedings of the National Academy of Sciences*, 81(14), 4343-4347.

Kirkman, H. N., Galiano, S., & Gaetani, G. F. (1987). The function of catalase-bound NADPH. *Journal of Biological Chemistry*, 262(2), 660-666.

Kneeshaw, S., Keyani, R., Delorme-Hinoux, V., Imrie, L., Loake, G. J., Le Bihan, T., Reichheld, J. & Spoel, S. H. (2017). Nucleoredoxin guards against oxidative stress by protecting antioxidant enzymes. *Proceedings of the National Academy of Sciences*, 114(31), 8414-8419.

Korshunov, S., & Imlay, J. A. (2006). Detection and quantification of superoxide formed within the periplasm of *Escherichia coli*. *Journal of Bacteriology*, 188(17), 6326-6334.

Kostakioti, M., Newman, C. L., Thanassi, D. G., & Stathopoulos, C. (2005). Mechanisms of protein export across the bacterial outer membrane. *Journal of Bacteriology*, 187(13), 4306-4314.

Kotogány, E., Dudits, D., Horváth, G. V., & Ayaydin, F. (2010). A rapid and robust assay for detection of S-phase cell cycle progression in plant cells and tissues by using ethynyl deoxyuridine. *Plant Methods*, 6(1),5.

Kumar, N., & Borth, N. (2012). Flow-cytometry and cell sorting: An efficient approach to investigate productivity and cell physiology in mammalian cell factories. *Methods*, 56(3), 366-374.

Lakowicz, J. R. (2006). Principles of fluorescence spectroscopy. Springer, NY.

Lee, B. S., & Kim, E. K. (2004). Lipopeptide production from Bacillus sp. GB16 using a novel oxygenation method. *Enzyme and Microbial Technology*, 35(6-7), 639-647.

Li, G. (2013). The positive and negative aspects of reactive oxygen species in sports performance. In *Current Issues in Sports and Exercise Medicine*. InTech.

Li, N., Ragheb, K., Lawler, G., Sturgis, J., Rajwa, B., Melendez, J. A., & Robinson, J. P. (2003). Mitochondrial complex I inhibitor rotenone induces apoptosis through enhancing mitochondrial reactive oxygen species production. *Journal of Biological Chemistry*, 278(10), 8516-8525.

Li, Q., Bai, Z., O'Donnell, A., Harvey, L. M., Hoskisson, P. A., & McNeil, B. (2011). Oxidative stress in fungal fermentation processes: the roles of alternative respiration. *Biotechnology Letters*, 33(3), 457-467.

Light, P. A., Ragan, C. I., Clegg, R. A., & Garland, P. B. (1968). Iron-limited growth of *Torulopsis utilis*, and the reversible loss of mitochondrial energy conservation at site 1 and of sensitivity to rotenone and piericidin A. *FEBS letters*, 1(1), 4-8.

Liu, Z., & Liu, S. (2015). High phosphate concentrations accelerate bacterial peptide decomposition in hypoxic bottom waters of the northern Gulf of Mexico. *Environmental Science & Technology*, 50(2), 676-684.

Locht, C. (1999). Molecular aspects of *Bordetella pertussis* pathogenesis. *International Microbiology*, 2(3), 137-144.

López-Sánchez, N., & Frade, J. M. (2013). Genetic evidence for p75NTR-dependent tetraploidy in cortical projection neurons from adult mice. *The Journal of Neuroscience*, 33(17), 7488-7500.

Lourenço, N. D., Lopes, J. A., Almeida, C. F., Sarraguça, M. C., & Pinheiro, H. M. (2012). Bioreactor monitoring with spectroscopy and chemometrics: a review. *Analytical and Bioanalytical Chemistry*, 404(4), 1211-1237.

Lowry, O. H., & Passoneau, J. V. (1972). *A flexible system of enzymatic analysis*, Acad. Press, New York.

Lukaszewicz-Hussain, A., & Moniuszko-Jakoniuk, J. (2004). Liver catalase, glutathione peroxidase and reductase activity, reduced glutathione and hydrogen peroxide levels in acute intoxication with chlorfenvinphos, an organophosphate insecticide introduction. *Polish Journal of Environmental Studies*, 13(3), 303-309.

Lushchak, V. I., Bagnyukova, T. V., Husak, V. V., Luzhna, L. I., Lushchak, V., & Storey, K. B. (2005). Hyperoxia results in transient oxidative stress and an adaptive response by antioxidant enzymes in goldfish tissues. *The International Journal of Biochemistry & Cell Biology*, 37(8), 1670-1680.

Lushchak, V. I. (2011). Adaptive response to oxidative stress: Bacteria, fungi, plants and animals. *Comparative Biochemistry and Physiology Part C: Toxicology & Pharmacology*, 153(2), 175-190.

Luttmann, R., Bracewell, D. G., Cornelissen, G., Gernaey, K. V., Glassey, J., Hass, V. C., Kaiser, C., Preusse, C., Striedner, G., & Mandenius, C. F. (2012). Soft sensors in bioprocessing: a status report and recommendations. *Biotechnology Journal*, 7(8), 1040-1048.

Lynch, M., & Kuramitsu, H. (2000). Expression and role of superoxide dismutases (SOD) in pathogenic bacteria. *Microbes and Infection*, 2(10), 1245-1255.

Mailloux, R. J., Bériault, R., Lemire, J., Singh, R., Chénier, D. R., Hamel, R. D., & Appanna, V. D. (2007). The tricarboxylic acid cycle, an ancient metabolic network with a novel twist. *PloS One*, 2(8), e690.

Mailloux, R. J., Singh, R., Brewer, G., Auger, C., Lemire, J., & Appanna, V. D. (2009). α-Ketoglutarate dehydrogenase and glutamate dehydrogenase work in tandem to modulate the antioxidant α-ketoglutarate during oxidative stress in *Pseudomonas fluorescens*. *Journal of Bacteriology*, 191(12), 3804-3810.

Maringanti, S., & Imlay, J. A. (1999). An intracellular iron chelator pleiotropically suppresses enzymatic and growth defects of superoxide dismutase-deficient *Escherichia coli*. *Journal of Bacteriology*, 181(12), 3792-3802.

Meade, B. D., Plotkin, S. A., & Locht, C. (2014). Possible options for new pertussis vaccines. The *Journal of Infectious Diseases*, 209(suppl_1), S24-S27.

Messner, K. R., & Imlay, J. A. (2002). Mechanism of superoxide and hydrogen peroxide formation by fumarate reductase, succinate dehydrogenase, and aspartate oxidase. *Journal of Biological Chemistry*, 277(45), 42563-42571.

Middaugh, J., Hamel, R., Jean-Baptiste, G., Beriault, R., Chenier, D., & Appanna, V. D. (2005). Aluminum triggers decreased aconitase activity via Fe-S cluster disruption and the overexpression of isocitrate dehydrogenase and isocitrate lyase: a metabolic network mediating cellular survival. *Journal of Biological Chemistry*, 280(5), 3159-3165.

Miller, A. F. (2001). Fe-superoxide dismutase. In *Handbook of Metalloproteins, vol. 1*. Wieghardt K, Huber R, Poulos TL, Messerschmidt A (Eds): Chichester, New York, Weinheim, Brisbane, Singapore and Toronto: Wiley and Sons. 668-682.

Miller, M. B., & Bassler, B. L. (2001). Quorum sensing in bacteria. *Annual Reviews in Microbiology*, 55(1), 165-199.

Müller, S., Harms, H., & Bley, T. (2010). Origin and analysis of microbial population heterogeneity in bioprocesses. *Current Opinion in Biotechnology*, 21(1), 100-113.

Munna, M. S., Nur, I. T., Rahman, T., & Noor, R. (2013). Influence of exogenous oxidative stress on *Escherichia coli* cell growth, viability and morphology. *American Journal of Bioscience*, 1, 59-62.

Munna, M. S., Tamanna, S., Afrin, M. R., Sharif, G. A., Mazumder, C., Kana, K. S., Urmi, N. J., Uddin, M. A., Rahman, T. & Noor, R. (2014). Influence of aeration speed on bacterial colony forming unit (CFU) formation capacity. *American Journal of Microbiology Research*, 2(1), 47-51.

Mustacich, D., & Powis, G. (2000). Thioredoxin reductase. *Biochemical Journal*, 346(1), 1-8.

Nakamura, M. M., Liew, S. Y., Cummings, C. A., Brinig, M. M., Dieterich, C., & Relman, D. A. (2006). Growth phase-and nutrient limitation-associated transcript abundance regulation in *Bordetella pertussis*. *Infection and immunity*, 74(10), 5537-5548.

Nakamura, M., Bhatnagar, A., & Sadoshima, J. (2012). Overview of pyridine nucleotides review series. *Circulation Research*, 111(5), 604-610.

Naviaux, R. K. (2012). Oxidative shielding or oxidative stress?. *Journal of Pharmacology and Experimental Therapeutics*, 342(3), 608-618.

Nielsen, T. H., Sjøholm, O. R., & Sørensen, J. (2009). Multiple physiological states of a *Pseudomonas fluorescens* DR54 biocontrol inoculant monitored by a new flow cytometry protocol. *FEMS Microbiology Ecology*, 67(3), 479-490.

Nolan, J. P., & Yang, L. (2007). The flow of cytometry into systems biology. *Briefings in Functional Genomics & Proteomics*, 6(2), 81-90.

Noofeli, M. (2008). Genetic analysis and characterisation of the BapC autotransporter of *Bordetella pertussis*. Doctoral dissertation. University of Glasgow.

Nunez, R. (2001). DNA measurement and cell cycle analysis by flow cytometry. *Current Issues in Molecular Biology*, 3, 67-70.

Oh, E., McMullen, L., & Jeon, B. (2015). Impact of oxidative stress defense on bacterial survival and morphological change in *Campylobacter jejuni* under aerobic conditions. *Frontiers in Microbiology*, 295(6), 1-8.

Oh, S. K., Yoo, S. J., Jeong, D. H., & Lee, J. M. (2013). Real-time estimation of glucose concentration in algae cultivation system using Raman spectroscopy. *Bioresource Technology*, 142, 131-137.

Qiu, P., Simonds, E. F., Bendall, S. C., Gibbs Jr, K. D., Bruggner, R. V., Linderman, M. D., Sachs, K., Nolan, G. P., & Plevritis, S. K. (2011). Extracting a cellular hierarchy from high-dimensional cytometry data with SPADE. *Nature Biotechnology*, 29(10), 886-891.

Pandolfi, P. P., Sonati, F., Rivi, R., Mason, P., Grosveld, F., & Luzzatto, L. (1995). Targeted disruption of the housekeeping gene encoding glucose 6-phosphate dehydrogenase (G6PD): G6PD is dispensable for pentose synthesis but essential for defense against oxidative stress. *The EMBO Journal*, 14(21), 5209-5215.

Pannala, V. R., & Dash, R. K. (2015). Mechanistic characterization of the thioredoxin system in the removal of hydrogen peroxide. *Free Radical Biology and Medicine*, 78, 42-55.

Persson, T., & Wedborg, M. (2001) Multivariate evaluation of the fluorescence of aquatic organic matter. *Analytica Chimica Acta*, 434(2), 179–192

Pickering, A. M., Vojtovich, L., Tower, J., & Davies, K. J. (2013). Oxidative stress adaptation with acute, chronic, and repeated stress. *Free Radical Biology and Medicine*, 55, 109-118.

Pile, J., & Dougherty, H. W. (1977). Ferrisuperoxide dismutase distribution in several bacteria. *The Journal of General and Applied Microbiology*, 23(6), 303-310.

Peiris, R. H. (2010). Development of fluorescence-based tools for characterization of natural organic matter and development of membrane fouling monitoring strategies for drinking water treatment systems. Doctoral dissertation. University of Waterloo, Waterloo, Canada.

Pohlscheidt, M., Charaniya, S., Bork, C., Jenzsch, M., Noetzel, T. L., & Luebbert, A. (2013). Bioprocess and fermentation monitoring. *Encyclopedia of Industrial Biotechnology*.

Prajapati, S., Bhakuni, V., Babu, K. R., & Jain, S. K. (1998). Alkaline unfolding and salt-induced folding of bovine liver catalase at high pH. *European Journal of Biochemistry*, 255(1), 178-184.

Public Health Agency of Canada, Pertussis (whooping cough), Canada. Last Date Modified: 21 February 2014. Retrieved from http://www.phac-aspc.gc.ca/im/vpd-mev/pertussiseng.php.

Puri, D. (2011). *Textbook of medical biochemistry*, 3rd Edn. New Delhi. Elsevier Health Sciences.

Raghavan, P. S., Rajaram, H., & Apte, S. K. (2011). Nitrogen status dependent oxidative stress tolerance conferred by overexpression of MnSOD and FeSOD proteins in *Anabaena sp*. strain PCC7120. *Plant Molecular Biology*, 77(4-5), 407-417.

Rieseberg, M., Kasper, C., Reardon, K. F., & Scheper, T. (2001). Flow cytometry in biotechnology. *Applied Microbiology and Biotechnology*, 56(3-4), 350-360.

Rinnan, Å., Booksh, K. S., & Bro, R. (2005). First order Rayleigh scatter as a separate component in the decomposition of fluorescence landscapes. *Analytica Chimica Acta*, 537(1), 349-358.

Robinson, T. P., Aboaba, O. O., Kaloti, A., Ocio, M. J., Baranyi, J., & Mackey, B. M. (2001). The effect of inoculum size on the lag phase of *Listeria monocytogenes*. *International Journal of Food Microbiology*, 70(1-2), 163-173.

Roederer, M., Brenchley, J. M., Betts, M. R., & De Rosa, S. C. (2004). Flow cytometric analysis of vaccine responses: how many colors are enough?. *Clinical Immunology*, 110(3), 199-205.

Rodriguez, M. E., Samo, A. L., Hozbor, D. F., & Yantorno, O. M. (1993). Effect of hydromechanical forces on the production of filamentous haemagglutinin and pertussis toxin of *Bordetella pertussis*. *Journal of Industrial Microbiology*, 12(2), 103-108.

Rolfe, M. D., Rice, C. J., Lucchini, S., Pin, C., Thompson, A., Cameron, A. D., Alston, M., Stringer, M. F., Betts, R. P., Baranyi, J., Peck, M. W., & Hinton, J. (2012). Lag phase is a distinct growth phase that prepares bacteria for exponential growth and involves transient metal accumulation. *Journal of Bacteriology*, 194(3), 686-701.

Ross, D., Kepa, J. K., Winski, S. L., Beall, H. D., Anwar, A., & Siegel, D. (2000). NAD(P)H: quinone oxidoreductase 1 (NQO1): chemoprotection, bioactivation, gene regulation and genetic polymorphisms. *Chemico-biological Interactions*, 129(1-2), 77-97.

Rover Jr, L., Fernandes, J. C., de Oliveira Neto, G., Kubota, L. T., Katekawa, E., & Serrano, S. H. (1998). Study of NADH stability using ultraviolet–visible spectrophotometric analysis and factorial design. *Analytical Biochemistry*, 260(1), 50-55.

Rowatt, E. (1957). Some factors affecting the growth of *Bordetella pertussis*. *Microbiology*, 17(2), 279-296.

Rui, B., Shen, T., Zhou, H., Liu, J., Chen, J., Pan, X., Liu, H., Wu, J., Zheng, H., & Shi, Y. (2010). A systematic investigation of *Escherichia coli* central carbon metabolism in response to superoxide stress. *BMC Systems Biology*, 122(4), 1-12.

Sachidanandham, R., & Gin, K. Y. H. (2009). Flow cytometric analysis of prolonged stress-dependent heterogeneity in bacterial cells. *FEMS Microbiology Letters*, 290(2), 143-148.

Schweder, T., & Hecker, M. (2004). Monitoring of stress responses. In *Physiological Stress Responses in Bioprocesses* (pp. 47-71). Springer Berlin, Heidelberg.

Shacter, E. (2000). Quantification and Significance of Protein Oxidation in Biological Samples. *Drug metabolism reviews*, 32(3-4), 307-326.

Shapiro, H. M. (2005). *Practical flow cytometry*. John Wiley & Sons. New Jersey.

Shi, L., Günther, S., Hübschmann, T., Wick, L. Y., Harms, H., & Müller, S. (2007). Limits of propidium iodide as a cell viability indicator for environmental bacteria. *Cytometry Part A*, 71(8), 592-598.

Sincock, S. A., & Robinson, J. P. (2001). Flow cytometric analysis of microorganisms. *Methods in Cell Biology*, 64, 511-538.

Singh, R., Mailloux, R. J., Puiseux-Dao, S., & Appanna, V. D. (2007). Oxidative stress evokes a metabolic adaptation that favors increased NADPH synthesis and decreased NADH production in *Pseudomonas fluorescens*. *Journal of Bacteriology*, 189(18), 6665-6675.

Sklar, L. A. (2005). *Flow cytometry for biotechnology*. Oxford University Press. New York.

Smart, J. B., & Thomas, T. D. (1987). Effect of oxygen on lactose metabolism in *Lactic streptococci*. *Applied and Environmental Microbiology*, 53(3), 533-541.

Soh, N. (2006). Recent advances in fluorescent probes for the detection of reactive oxygen species. *Analytical and Bioanalytical Chemistry*, 386(3), 532-543.

Spaans, S. K., Weusthuis, R. A., Van Der Oost, J., & Kengen, S. W. (2015). NADPH-generating systems in bacteria and archaea. *Frontiers in Microbiology*, 742(6), 1-27.

Spence, M. T., & Johnson, I. D. (Eds.). (2010). *The molecular probes handbook: a guide to fluorescent probes and labeling technologies*. Live Technologies Corporation.

Srienc, F. (1999). Cytometric data as the basis for rigorous models of cell population dynamics. *Journal of Biotechnology*, 71(1), 233-238.

Stamatakis, M. (2010). Cell population balance, ensemble and continuum modeling frameworks: conditional equivalence and hybrid approaches. *Chemical Engineering Science*, 65(2), 1008-1015.

Stiefel, P., Schmidt-Emrich, S., Maniura-Weber, K., & Ren, Q. (2015). Critical aspects of using bacterial cell viability assays with the fluorophores SYTO9 and propidium iodide. *BMC microbiology*, 15(1), 36.

Stocks, S. M. (2004). Mechanism and use of the commercially available viability stain, BacLight. *Cytometry Part A*, 61(2), 189-195.

Storey, B. T. (1980). Inhibitors of energy-coupling site 1 of the mitochondrial respiratory chain. *Pharmacology & therapeutics*, 10(2), 399-406.

Sugisaki, K., Hanawa, T., Yonezawa, H., Osaki, T., Fukutomi, T., Kawakami, H., Yamamoto. T., & Kamiya, S. (2013). Role of (p) ppGpp in biofilm formation and expression of filamentous structures in *Bordetella pertussis*. *Microbiology*, 159(7), 1379-1389.

Thalen, M. (2008). Whooping cough vaccines: production of virulent *B. pertussis* (p. 149). Doctoral dissertation. Wageningen University.

ThermoFisher (2006). Reactive Oxygen Species (ROS) Detection Reagents. Retrieved from https://assets.thermofisher.com/TFS-Assets/LSG/manuals/mp36103.pdf).

Touati, D. (2000). Iron and oxidative stress in bacteria. *Archives of Biochemistry and Biophysics*, 373(1), 1-6.

Tretter, L., & Adam-Vizi, V. (2004). Generation of reactive oxygen species in the reaction catalyzed by α-ketoglutarate dehydrogenase. *Journal of Neuroscience*, 24(36), 7771-7778.

Tretter, L., & Adam-Vizi, V. (2005). Alpha-ketoglutarate dehydrogenase: a target and generator of oxidative stress. *Philosophical Transactions of the Royal Society B: Biological Sciences*, 360(1464), 2335-2345.

Vaughan, T. E., Pratt, C. B., Sealey, K., Preston, A., Fry, N. K., & Gorringe, A. R. (2014). Plasticity of fimbrial genotype and serotype within populations of *Bordetella pertussis*: analysis by paired flow cytometry and genome sequencing. *Microbiology*, 160(9), 2030-2044

Veal, D. A., Deere, D., Ferrari, B., Piper, J., & Attfield, P. V. (2000). Fluorescence staining and flow cytometry for monitoring microbial cells. *Journal of Immunological Methods*, 243(1), 191-210.

Vojinović, V., Cabral, J., & Fonseca, L. (2006). Real-time bioprocess monitoring: Part I: In situ sensors. *Sensors and Actuators B: Chemical*, 114(2), 1083-1091.

Wan, B., Zhang, Q., Ni, J., Li, S., Wen, D., Li, J., Xiao, H., He, P., Ou, H., Tao, J., Teng, Q., Lu, J., W, W. & Yao, Y. (2017). Type VI secretion system contributes to *Enterohemorrhagic Escherichia coli* virulence by secreting catalase against host reactive oxygen species (ROS). *PLoS Pathogens*, 13(3), e1006246.

Wang, J. D., & Levin, P. A. (2009). Metabolism, cell growth and the bacterial cell cycle. *Nature Reviews Microbiology*, 7(11), 822-827.

Warfel, J. M., & Edwards, K. M. (2015). Pertussis vaccines and the challenge of inducing durable immunity. *Current Opinion in Immunology*, 35, 48-54.

Wehry, E. L. (1997). Molecular fluorescence and phosphorescence spectrometry. *Handbook of Instrumental Techniques for Analytical Chemistry*; Settle, F. A., Ed.; Prentice Hall: Upper Saddle River, NJ, 1997; pp 507−539.

Wellen, K. E., & Thompson, C. B. (2010). Cellular metabolic stress: considering how cells respond to nutrient excess. *Molecular Cell*, 40(2), 323-332.

Wersto, R. P., Chrest, F. J., Leary, J. F., Morris, C., Stetler-Stevenson, M., & Gabrielson, E. (2001). Doublet discrimination in DNA cell-cycle analysis. *Cytometry*, 46(5), 296-306.

Williams, S. C., Hong, Y., Danavall, D. C. A., Howard-Jones, M. H., Gibson, D., Frischer, M. E., & Verity, P. G. (1998). Distinguishing between living and nonliving bacteria: evaluation of the vital stain propidium iodide and its combined use with molecular probes in aquatic samples. *Journal of Microbiological Methods*, 32(3), 225-236.

Wiederschain, G. Y. (2011). The Molecular Probes handbook. A guide to fluorescent probes and labeling technologies. *Biochemistry* (Moscow), 76(11), p.1276.

Winson, M. K., & Davey, H. M. (2000). Flow cytometric analysis of microorganisms. *Methods*, 21(3), 231-240.

Wise, B. M., Gallagher, N., Bro, R., Shaver, J., Windig, W., & Koch, R. S. (2007). PLS-Toolbox Version 3.5 for use with MATLAB™, Manual. Eigenvector Research, Inc. Manson, WA, USA.

Wulff, S., Martin, K., Vandergaw, A., Boenisch, T., Brotherick, I., Hoy, T., Hudson, J., Jespersgaard, C., Lopez, P., Orfao, A., & Overton, W. R. (2006). *Guide to flow cytometry*. Dako Cytomation.

Yao, D., Liu, L., Li, J., Hua, Z., Du, G., & Chen, J. (2009). Overproduction of catalase by oxidative stress on *Bacillus subtilis* WSHDZ-01. *Chinese Journal of Biotechnology*, 25(5), 786-792.

Zámocký, M., & Koller, F. (1999). Understanding the structure and function of catalases: clues from molecular evolution and in vitro mutagenesis. *Progress in Biophysics and Molecular Biology*, 72(1), 19-66.

Zavatti, V., Budman, H., Legge, R., & Tamer, M. (2016). Monitoring of an antigen manufacturing process. *Bioprocess and Biosystems Engineering*, 39(6), 855-869.

Zheng, W., Zhao, Y., Zhang, M., Wei, Z., Miao, K., & Sun, W. (2009). Oxidative stress response of *Inonotus obliquus* induced by hydrogen peroxide. *Medical Mycology*, 47(8), 814-823.

Zhu, G. Y., Zamamiri, A., Henson, M. A., & Hjortsø, M. A. (2000). Model predictive control of continuous yeast bioreactors using cell population balance models. *Chemical Engineering Science*, 55(24), 6155-6167.